Bio-inks for 3D Printing of Cartilage Implants

**Tailoring gelMA and polyHPMA-lac-PEG hydrogels for
the fabrication of spatially organized constructs**

Vivian H. M. Mouser

Bio-inks for 3D printing of Cartilage Implants

Tailoring gelMA and polyHPMA-lac-PEG hydrogels for the fabrication of spatially organized constructs

Bio-inkten voor het 3D printen van kraakbeenimplantaten
Modificatie van gelMA en polyHPMA-lac-PEG hydrogelen voor de productie van gelaagde constructen

(met een samenvatting in het Nederlands)

Proefschrift

ter verkrijging van de graad van doctor aan de Universiteit Utrecht
op gezag van de rector magnificus, prof. dr. G. J. van der Zwaan,
ingevolge het besluit van het college voor promoties
in het openbaar te verdedigen op donderdag 15 juni 2017
des middags te 12.45 uur

door

Vivian Hilda Maria Mouser
geboren op 17 november 1988 te Eindhoven

Promotor: Prof. dr. ir. J. Malda
                     Prof. dr. W. J. A. Dhert

Co-promotoren: Dr. ir. D. Gawlitta
                     Dr. R. Levato

This thesis is based upon the following publications:

Mouser, V.H.M., Levato, R., Bonassar, L.J., D'Lima D.D., Klein, T.J., Grande, D.A., Saris, D.B.F., Zenobi-Wong, M., Gawlitta, D., Malda, J. Three-Dimensional Bioprinting and Its Potential in the Field of Articular Cartilage Regeneration. *Cartilage* (2016). doi:10.1177/1947603516665445

Mouser, V.H.M., Melchels, F.P.W., Visser, J., Dhert, W.J.A., Gawlitta, D., Malda, J. Yield stress determines bioprintability of hydrogels based on gelatin-methacryloyl and gellan gum for cartilage bioprinting. *Biofabrication* **8**, 035003 (2016)

*Abbadessa, A., *Mouser, V.H.M., Blokzijl, M.M., Gawlitta, D., Dhert, W.J.A., Hennink, W.E., Malda, J., Vermonden, T. A Synthetic Thermosensitive Hydrogel for Cartilage Bioprinting and Its Biofunctionalization with Polysaccharides. *Biomacromolecules* **17**, 2137–2147 (2016)

*Mouser, V.H.M., *Abbadessa, A., Levato, R., Hennink, W.E., Vermonden, T., Gawlitta, D., Malda, J. Development of a thermosensitive HAMA-containing bio-ink for the fabrication of composite cartilage repair constructs. Biofabrication 9, 15026 (2017)

Mouser, V.H.M., Dautzenberg, N.M.M., Levato, R., van Rijen, M.H.P., Dhert, W.J.A., Malda, J., Gawlitta, D. The spatial distribution of chondrocytes in a hydrogel construct dictates cartilage defect repair. *Submitted for publication*

* both authors contributed equally

Table of Content

Chapter 1

General introduction and research aims

1. Articular cartilage and regenerative medicine

Articular cartilage is the tissue layer that covers the bone inside joints, and consists predominantly of proteoglycans, collagen type II, and water. In addition, it contains a limited number of cells, the so-called chondrocytes. The matrix composition and orientation is depth dependent and can be divided into three zones: the superficial, the middle or intermediate, and the deep zone (Figure 1). The deep zone protrudes into a calcified layer, which forms the transition region from cartilage to bone tissue[1–3]. The superficial zone is defined as the 10-20% of the cartilage thickness closest to the joint-space. It has the highest cell density and collagen type II content, and the lowest proteoglycan content, biosynthetic activity, and compressive modulus[4–7], compared to the other zones. The collagen fibers are orientated parallel to the cartilage surface and the chondrocytes are relatively small and flattened[4,8]. The deep zone is defined as the 30-40% of the cartilage thickness closest to the calcified layer. It has the lowest cell density and the highest proteoglycan content, biosynthetic activity, and compressive modulus[4–6]. The collagen fibers are orientated perpendicular to the cartilage surface and the chondrocytes are rounded, relatively large, and columnar organized[4,8]. The middle zone forms the transition between the superficial and deep zone and has intermediate cell density, proteoglycan content, compressive modulus, cell size, and location. The collagen fiber orientation is angled, as the fibers change from the perpendicular orientation in the deep zone to the parallel orientation in the superficial zone, to form the characteristic arch-like structures[9]. Various zone specific proteins have been identified. Proteoglycan 4 (PRG4, or lubricin)[10–12], clusterin[13,14], and collagen type I[12] are mostly expressed in the superficial layer, whereas cartilage intermediate layer protein (CILP)[15] is mostly found in the middle zone. Cartilage oligomeric protein (COMP)[16,17] and collagen type X[12] are localized in both the middle and deep zone.

Articular cartilage has two main functions to allow smooth movement of the joint: absorbing impact forces and reducing surface friction. To perform as a shock absorber, a high osmotic pressure is required. This is generated by the negatively charged proteoglycans that attract ions, which at their turn attract water and induce swelling. However, the swelling is restricted by the arch-like collagen fibers resulting in a high osmotic pressure. Minimal surface friction is obtained with a combination of the parallel-orientated collagen fibers, flattened chondrocytes, and PRG4 secretion in the superficial zone. To maintain these functions, the balance in matrix content, location, and spatial organization is crucial. Articular cartilage has only limited cell numbers and no vasculature or innervation, thus, the tissue has a limited regenerative capacity. Therefore, a disruption of the tissue balance due to *e.g.* a cartilage tear, will induce a cascade of degradation, which eventually results in an arthritic joint if no interventions are made. Current therapies used in the clinic to repair chondral defects are based on marrow stimulation *e.g.* microfracture, or cell delivery *e.g.* (matrix-induced) autologous chondrocyte implantation ((M)ACI)[18–21]. Although these techniques result in immediate pain relieve for the patient, the newly formed tissue has a fibrous character and often fails over time, making new surgeries and eventually a total joint replacement necessary. Regenerative medicine aims to restore damaged tissue using a combination of cells, scaffolding materials, and biological cues
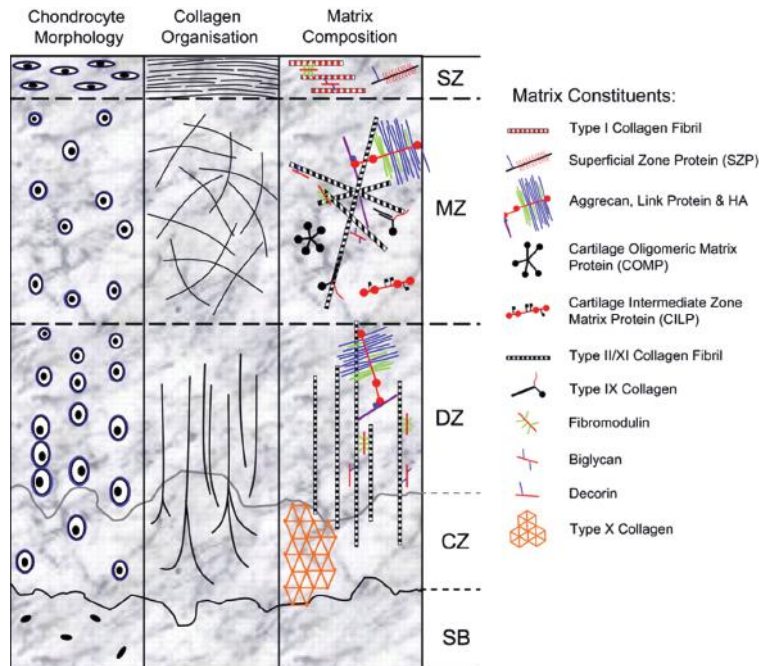
1

Figure 1. Schematic overview of the depth-dependent characteristics of articular cartilage. *From top to bottom: the superficial zone (SZ), middle zone (MZ), deep zone (DZ), calcified cartilage (CZ), and the subchondral bone (SB). In each cartilage zone, the chondrocyte morphology and organization (left), collagen fiber orientation (middle), and biochemical composition of the matrix (right) differs. Reproduced from Hayes et al. (2007)[12] with permission of SAGE Publications, Inc.. Copyright © (2007) The Histochemical Society, Inc..*

(e.g. growth factors, peptides, or matrix particles) and thus, forms a new approach to restore articular cartilage defects. Ideally, the damaged cartilage would be replaced by a cartilage-like construct that can temporarily take over the function of the native cartilage while allowing cells, either from the surrounding tissue or embedded in the construct, to gradually replace the biomaterial with new functional cartilage tissue.

2. Three-dimensional bioprinting
Three-dimensional (3D) bioprinting is a relatively new and promising approach to create personalized regenerative cartilage constructs, as it allows accurate positioning of (cell-laden) biomaterials in a layer-by-layer fashion, based on a 3D computer model[22]. However, the search for printable biomaterials is challenging, as these so called 'bio-inks' must support encapsulation of cells and/or bioactive proteins, and should thus be printable under cell-friendly conditions, while obtaining constructs with high shape-fidelity. The specific bio-ink requirements differ for the different dispensing methods, which include extrusion, ink-jet, and laser dispensing. Of these, extrusion printing is the most suitable option for the fabrication of the relatively large constructs with high cell densities necessary for the fabrication of tissue constructs. Further, bioprinting with multiple bio-inks, allows the fabrication of constructs with complex organizations *e.g.* the

depth dependent organization of articular cartilage (Figure 2). A detailed overview of the advantages and challenges of 3D bioprinting techniques for the field of articular cartilage regeneration may be found in Chapter 2.
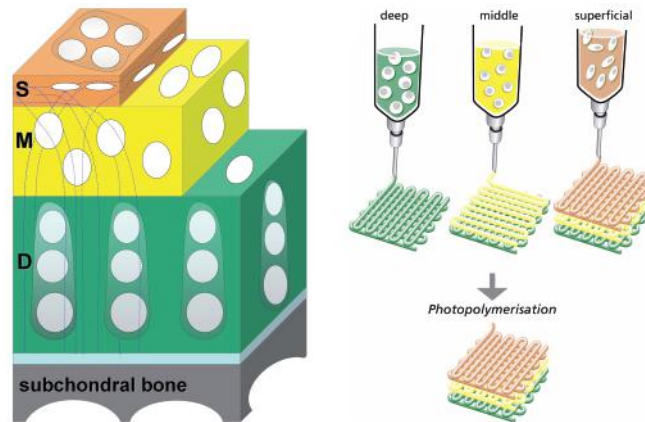
Figure 2. Schematic overview of the 3D bioprinting strategy for the fabrication of zonally organized cartilage regenerative constructs. s = superficial zone, m = middle zone, d = deep zone, dotted lines indicate collagen fiber alignment. Reproduced from Klein et al. (2009)[23] with permission. Copyright © (2009) Wiley-VCH Verlag GmbH & Co. KGaA.

3. Bio-inks

The most commonly used bio-inks for extrusion 3D printing are hydrogels. Hydrogels facilitate homogeneous cell encapsulation in an environment with a high water-content that can mimic the natural cell habitat, and thus supports cell survival. Additionally, biological and chemical cues can relatively easy be incorporated to support matrix production by embedded cells[24]. Although hydrogel bio-inks are promising, optimizing their mechanical and biological properties remains challenging, as an optimal bio-ink needs to meet an array of requirements, which sometimes contradict each other: printable at cell friendly conditions (*e.g.* temperature, pressure, and printing speed), shape-stable during printing, cross-linkable for stability after printing, degradable over time, and supportive for cell encapsulation, survival, proliferation, and (zonal) differentiation. Especially, the printing with high shape-fidelity and high cell survival and differentiation requires opposite material properties[25]. Thus, it is almost unavoidable to compromise on some of the listed bio-ink requirements. This highlights the need for further evaluation and development of hydrogel bio-inks, to obtain a bio-ink with all desired physical, mechanical, and biological properties.

3.1. Physical properties of a bio-ink

Multiple physical properties beneficial for 3D extrusion printing have been identified[25,26]. The viscosity of a bio-ink plays an important role, as a certain viscosity is required to allow filament instead of droplet formation at the nozzle of the bioprinter[27]. The viscosity of a hydrogel is mainly dependent on the polymer concentration and its molecular weight[25,26].

In thermo-sensitive hydrogels, the viscosity can also be influenced by adjusting the temperature. Thermo-gelation of a hydrogel allows 3D printing with a liquid polymer solution by heating/cooling the cartridge, while collecting a viscous hydrogel on the cooled/heated baseplate. However, thermo-gelation alone is usually not enough to generate constructs with high shape-fidelity, as the gelation process is relatively slow[28]. An additional material property favorable for 3D printing is shear thinning[29], meaning that with increasing pressure the viscosity decreases due to the alignment of the polymer chains (Figure 3A)[25,28]. Shear thinning materials form physical gels in the cartridge, become fluid upon dispensing due to the increased shear stresses, and solidify again after extrusion when the shear forces are no longer present. The minimal stress necessary to induce flow in a physical hydrogel is called the yield stress[26,28]. The yield stress increases when reversible interactions occur between polymer chains *e.g.* hydrogen or ionic bonds. As hydrogen and ionic bonds are rapidly formed, they increase the immediate stability of extruded filaments and thus of the whole construct[25,26,28].

3.2. Stability and mechanical performance of a printed construct

To improve the final construct stiffness and to guarantee construct stability after printing, chemical cross-linking can be used. Chemical cross-linking introduces irreversible bonds between the polymer chains and thus permanently fix the printed construct. Multiple approaches facilitate chemical cross-linking, however they all require the presence of specific chemical groups on the polymer chains of the bio-ink. A common approach involves reactions with complementary chemical groups such as Michael addition reactions[30], click chemistry[31], or enzymatic reactions[32]. Another technique involves the incorporation of photo-polymerizable groups *e.g.* methacrylate groups, on the precursors, which can form covalent bonds after irradiation with (UV) light (Figure 3B)[26].

Although chemical cross-linking significantly increases the construct stiffness, the maximum stiffness reachable for any hydrogel remains much lower compared to native articular cartilage. In order to reach construct stiffness in the range of that of cartilage tissue, reinforcement strategies provide an outcome. Thermoplastic polymers are often used for this purpose, including poly-ε-caprolactone (PCL)[33–36], which can be printed and infused with a hydrogel or co-printed with a hydrogel bio-ink, to fabricate two-component constructs with sufficient mechanical properties. Overall, the reinforcement skeleton dominates the construct stiffness, while the hydrogel component provides the biological requirements[33]. The mechanical properties of the final construct can be tailored by changing the molecular weight of the PCL or by altering the architecture of the reinforcement skeleton[37].

3.3. Biological characteristics of a bio-ink

Multiple cell types have been explored for cartilage tissue-engineering purposes *e.g.* chondrocytes/chondrons[38–40], articular cartilage progenitor cells (ACPCs, or chondroprogenitor cells)[41], and multipotent mesenchymal stromal cells (MSCs)[42]. A detailed description of these cells and their potential for cartilage bioprinting is included in Chapter 2, section 3.1. Although printing with cell-laden hydrogels is feasible without
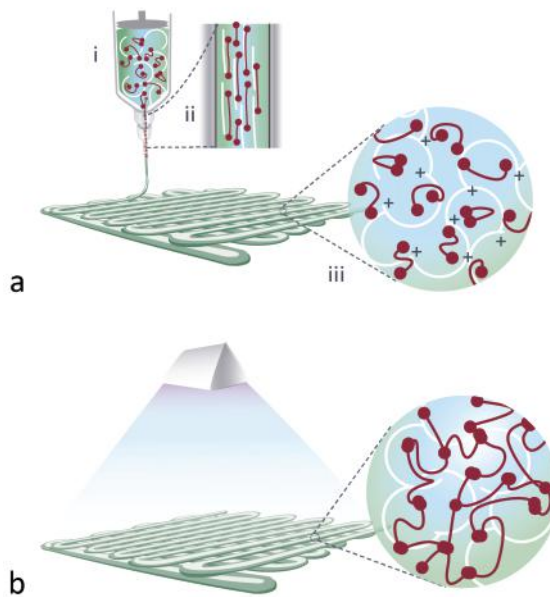
Figure 3. Schematic representation of 3D printing with a shear thinning, two-component hydrogel (gelMA/ gellan gum, A), followed by UV curing to induce covalent polymer bounds (B). *In the syringe a temporary network is formed due to the temperature and ionic interactions (i). When the hydrogel is extruded through a nozzle, the temporary network is broken by the increased shear forces (ii). This causes alignment of the polymer chains, which results in a decrease of viscosity. Upon leaving the nozzle, the filament no longer experiences shear stresses and the temporary network is restored, causing the extruded filament to solidify instantly (iii). After this, the slower thermo-gelation process further increases the construct stability until the network is permanently fixed via UV curing (B). Panel 1A reproduced from Malda et al. (2013)[25] with permission. Copyright © (2013) John Wiley and Sons. Panel 1B reproduced from Melchels et al. (2014)[28] with permission. Copyright © (2014) The Royal Society of Chemistry.*

compromising cell viability, the inclusion of cells restricts some of the bio-ink properties. Hydrogels with high polymer concentrations, high viscosities, and high cross-linking densities are favorable for the printing procedure, however, when going too high, these properties hamper cell differentiation and/or matrix production and distribution[25,43]. Additionally, printing temperatures are restricted to cell-friendly temperatures (4-40˚C) and shear stresses in the nozzle of the printer should be limited (*e.g*. ≤ 5 kPa for human MSCs printed with a microvalve-based printhead)[44].

Also, biological cues *e.g.* growth factors, bioactive proteins, peptides, chemicals, and matrix components, are incorporable in hydrogel bio-inks to attract and/or instruct cells from the surrounding tissue or to stimulate embedded cells. Multiple cues have been explored for the bioprinting of cartilage constructs including chondroitin sulfate (CS) and hyaluronic acid (HA). Both CS and HA are large polysaccharides that are present in native cartilage. The presence of CS in several hydrogel systems was demonstrated to increase the formation of cartilage-like tissue by embedded chondrocytes[45–48]. However, CS has also been associated with fibrocartilage formation[46]. HA is known to influences

1

multiple biological processes including cell proliferation, migration, attachment, and differentiation[49,50]. Consequently, the presence of HA can stimulate anabolic processes of chondrocytes[46,51–57]. However, also for the incorporation of HA some studies reported a negative influence of HA on cartilage matrix synthesis by chondrocytes[54–57]. Both CS and HA can be methracrylated (CSMA and HAMA, respectively) to allow photo cross-linking after printing, preventing the molecules from leaching out of the construct[58,59]. In addition, the incorporation of HA in a bio-ink increases the viscosity, which is beneficial for especially extrusion-based bioprinting[27], making both CSMA and HAMA interesting candidates for the enhancement of cartilage bio-inks.

3.4. Bio-inks for cartilage repair

Several hydrogels are under investigation for their use as bio-inks including hydrogels based on collagen[60], gelatin[27,36,46,61–63], hyaluronic acid[64], chitosan[65], alginate[66], poly(ethylene glycol)[67], hydroxyethyl-methacrylate-derivatized dextran[68], and poly(N-hydroxypropyl-methacrylacrylamide lactate)[69]. Each hydrogel system has its own advantages and challenges. A big debate is whether to use natural or synthetic polymers, as natural polymers are usually relatively easy to obtain in larger quantities, they are biodegradable, and can resemble the native environment of the target tissue. Contrarily, synthetic polymers often require complex synthesis and biological components need to be added in order for the hydrogel to resemble the native environment. However, as they are designed at a molecular level, the final hydrogel properties can be accurately tailored with limited batch to batch variations, which is a major challenge for natural polymers. This thesis focusses on two different hydrogel systems for cartilage bioprinting. Firstly on gelatin-methacryloyl (gelMA) based on natural collagens and, secondly on the synthetic triblock copolymers of polyethylene glycol (PEG) and partially methacrylated poly(N-(2-hydroxypropyl) methacrylamide mono/dilactate (polyHPMA-lac).

3.4.1. GelMA for cartilage bioprinting

The feasibility of using gelMA for cartilage tissue-engineering purposes, is already widely being explored. GelMA is made from denatured collagens, mainly collagen type I. Therefore, it is enzymatically degradable, contains inherent cell adhesion domains, and has low immunogenicity[61,70]. Both chondrocytes and MSCs can be stimulated to produce cartilage-like tissue when grown in gelMA hydrogels[27,46,71,72]. Additionally, due to its thermo-sensitive properties, gelMA is compatible with bioprinting techniques, however only when precise control of the bio-ink and nozzle temperatures is accomplished[63]. After printing, the presence of methacrylate groups allows chemical cross-linking upon UV curing to permanently fix the construct[73]. The printability of gelMA was demonstrated to increase with the addition of the polysaccharide gellan gum, which significantly increases the viscosity and gelation speed of the blend via the introduction of ionic interactions[28]. Thus, gelMA, especially when combined with gellan gum, forms a promising bio-ink to further evaluate and develop for the bioprinting of organized cartilage implants.

3.4.2. PolyHPMA-lac-PEG triblock copolymers for cartilage bioprinting

The second hydrogel system this thesis focusses on, consist of tailorable copolymers based on a PEG mid-block flanked by two polyHPMA-lac outer blocks[69,74–77]. Similar to gelMA, the polyHPMA-lac-PEG polymers are methacrylated to allow UV cross-linking. In addition, polyHPMA-lac-PEG hydrogels display lower critical solution temperature, meaning that they have low viscosities at low temperatures and form physical gels at higher temperatures[78]. The opportunity to tailor the molecular architecture, provides accurate control over the degradation rates and mechanical properties of cross-linked polyHPMA-lac-PEG hydrogels[74,75,78]. Also, the feasibility of 3D printing with polyHPMA-lac-PEG hydrogels has been demonstrated, but only with relatively high polymer concentrations and degrees of methacrylation. Finally, chondrocytes embedded in polyHPMA-lac-PEG hydrogels remained viable up to at least 3 days of culture[69]. For these reasons, polyHPMA-lac-PEG hydrogel forms an interesting candidate for the bioprinting of cartilage implants. However, matrix deposition by chondrocytes has not been evaluated in this hydrogel system yet. Also, the optimal concentration for printing, mechanical stability, and chondrogenic potential of embedded cells, has not been investigated so far. Further evaluation is thus required to determine the suitability polyHPMA-lac-PEG hydrogels for cartilage bioprinting.

4. Evaluation of novel regenerative implants

Bio-ink development is an important step for the creation of personalized regenerative cartilage constructs. However, in order to use such constructs for the treatment of cartilage defects in patients, the functioning of the constructs needs to be evaluated *in vivo*[79]. Usually, a new biomaterial is first tested subcutaneously or intramuscularly in rodent models for safety and mechanistic studies. When safety is established in these models, larger animal models *e.g.* lapine, canine, porcine, or equine, are required to evaluate construct functioning and cartilage repair at orthotopic locations. However, animal models are low-volume throughput, cost-intensive, and have multiple ethical considerations. It is therefore important to replace, reduce, and refine the need for animal models as much as possible (three Rs guiding principle for animal testing). *Ex vivo* models are interesting tools to accomplish this, as they can be used to pre-screen new therapies before moving forwards to animal models.

Several *ex vivo* models have been proposed for the evaluation of new cartilage repair strategies. A relatively straightforward model encompasses the culture of cartilage explants from cadaveric joints. In the cartilage explants, artificial damage is created which can be 'treated' with the therapy under evaluation[80,81]. However, during culture the matrix composition of the explants and the chondrocyte gene expression patterns change[82–84]. These changes have two main causes. Firstly the collagen network is severely damaged during harvest. As a result, the osmotic pressure within native cartilage is lost during culture and GAGs, no longer restrained by the collagen fibers, diffuse out of the explant[83]. Secondly, the subchondral bone is missing in this model, while the subchondral bone provides structural support to the cartilage and is known to influence cartilage disease processes[85–88]. Therefore, the osteochondral culture model was introduced[82]. This

1

model requires the harvest of osteochondral plugs from cadaveric joints. In the cartilage layer of the plugs, defects are created and filled with cartilage repair constructs, in order to evaluate repair mechanisms during *in vitro* culture of the plugs[82,89–91]. During the course of this PhD project, a culture platform with separate cartilage and bone medium compartments was developed in collaboration with LifeTec Group (Eindhoven, The Netherlands). With this approach, both tissue types are provided with their optimized medium compositions, without compromising the cartilage-bone interface of the plug itself[92].
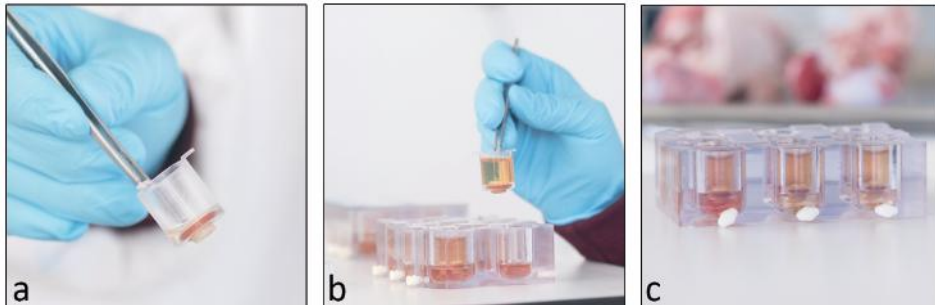

Figure 4. Culture platform containing separate medium compartments for the cartilage and bone tissue of osteochondral plugs. The osteochondral plug is placed in a special insert, with the cartilage surface on the inside of the insert and the bone part below the insert (a). Medium with specific supplements for the cartilage tissue is pipetted into the insert, covering the cartilage surface (b). Subsequently, the insert is placed in a custom-made wells plate with the bone part pointing towards the bottom (c). In the wells plate, medium containing supplements for the bone tissue is pipetted to provide the bone tissue with nutrients. (Photos with courtesy of L. M. Kock, LifeTec Group B.V., Eindhoven, The Netherlands).

5. Research aims and thesis outline

A new, promising approach to treat cartilage defects is the implantation of regenerative constructs. It is hypothesized that the performance and integration in the defect of such constructs may be improved by the incorporation of the spatial organization that is found in native cartilage[93,94]. 3D extrusion bioprinting facilitates the fabrication of biological active constructs with specific shapes and architectures. Therefore, the main aim of this thesis is **to investigate the application of gelMA and polyHPMA-lac-PEG based hydrogels, as bio-ink platforms for the 3D bioprinting of cell-laden organized cartilage implants** (Table 1).

In order to successfully bioprint organized cartilage implants, some challenges need to be overcome. First, a bio-ink is required that is printable under cell-friendly conditions with a high resolution, mechanically strong enough to withstand the mechanical forces present in the joint, and that supports chondrogenesis of the embedded cells. For this purpose two hydrogel systems are evaluated: gelMA and polyHPMA-lac-PEG. Second, optimal cell sources, as well as the optimal spatial cell distribution in a hydrogel construct for cartilage regeneration, need to be identified. As there are currently no guidelines

for the material properties necessary to allow bioprinting, the first specific aim of this thesis is to identify the rheological properties of gelMA/gellan hydrogels that allow bioprinting with encapsulated cells and high shape-fidelity. The second specific aim is to further develop gelMA and polyHPMA-lac PEG hydrogel systems for their printability, mechanical properties, and chondrogenic potential via the incorporation of gellan gum or HAMA in gelMA hydrogels, and CSMA, HAMA, or PCL reinforcement in polyHPMA-lac-PEG hydrogels. The third specific aim of this thesis is to evaluate zone-specific cartilage matrix production of chondrocytes, MSCs, and ACPCs, in gelMA/gellan hydrogels. Finally, this thesis aims to identify the optimal spatial positioning of chondrocytes in gelMA/gellan hydrogel constructs for cartilage repair, using the osteochondral plug model. Accomplishing these aims will give us deeper understanding of the required material properties (mechanical and biological) for cartilage extrusion bioprinting and of the required construct design. Hence, it will bring us closer to the fabrication of spatially organized cartilage constructs for clinical practice.

Table 1. Summary of the research aims.

Main aim:	
To investigate the application of gelMA and polyHPMA-lac-PEG based hydrogels, as bio-ink platforms for the 3D bioprinting of cell-laden organized cartilage implants.	
Specific-aims:	**Chapter**
1. To identify the rheological properties of gelMA/gellan hydrogels that allow bioprinting of cell-laden hydrogels with a high shape-fidelity.	3
2. To further develop gelMA and polyHPMA-lac-PEG hydrogel systems for their printability, mechanical properties, and chondrogenic potential.	3-6
3. To evaluate zone-specific cartilage-matrix deposition of chondrocytes, articular cartilage progenitor cells, and multipotent mesenchymal stromal cells in gelMA/gellan hydrogels with or without HAMA.	6
4. To identify the optimal spatial positing of chondrocytes in gelMA/gellan constructs, cultured in cartilage defects in osteochondral plugs, for cartilage repair.	7

1

Chapter 2 provides an overview of the potential and opportunities of 3D bioprinting techniques for the fabrication of regenerative cartilage constructs. **Chapter 3** aims to identify the rheological properties that govern the printing process (aim 1). Additionally, multiple gelMA/gellan concentrations and ratios are evaluated for their printability (filament formation and deposition), mechanical properties, and chondrogenesis of embedded chondrocytes (aim 2). **Chapter 4** focusses on the characterization of methacrylated polyHPMA-lac-PEG triblock copolymer-based hydrogels in terms of chondrogenesis, mechanical behavior, degradation kinetics, and printability. Further, the effect on the mechanical properties, degradation rate, and printability of incorporating CSMA and HAMA is also explored (aim 2). Subsequently, in **Chapter 5,** the potential of HAMA to improve chondrogenesis of chondrocytes embedded in polyHPMA-lac-PEG hydrogels is further evaluated for multiple concentrations. In addition, the feasibility of co-printing polyHPMA-lac-PEG hydrogels with PCL reinforcement to enhance the mechanical stiffness of the final constructs is investigated in this Chapter (aim 2). For the generation constructs with spatial variations, **Chapter 6** evaluates zone-specific cartilage matrix synthesis of chondrocytes, ACPCs, and MSCs in gelMA/gellan hydrogels with or without HAMA. Sequentially, cell-laden zonal constructs were bioprinted with the optimal bio-inks to explore long-term differentiation (aim 3). Finally, in **Chapter 7** the effect of spatial variations of chondrocytes in gelMA/gellan hydrogels on cartilage repair in a full thickness cartilage defect is studied using the osteochondral plug model (aim 4).

References

1. Buckley, M. R., Gleghorn, J. P., Bonassar, L. J. & Cohen, I. Mapping the depth dependence of shear properties in articular cartilage. *J. Biomech.* **41,** 2430–2437 (2008).
2. Silverberg, J. L. *et al.* Structure-Function Relations and Rigidity Percolation in the Shear Properties of Articular Cartilage. *Biophys. J.* **107,** 1721–1730 (2014).
3. Schuurman, W. *et al.* Cartilage regeneration using zonal chondrocyte subpopulations: a promising approach or an overcomplicated strategy? *J. Tissue Eng. Regen. Med.* **9,** 669–678 (2015).
4. Wong, M., Wuethrich, P., Eggli, P. & Hunziker, E. Zone-specific cell biosynthetic activity in mature bovine articular cartilage: A new method using confocal microscopic stereology and quantitative autoradiography. *J. Orthop. Res.* **14,** 424–432 (1996).
5. Schinagl, R. M., Gurskis, D., Chen, A. C. & Sah, R. L. Depth-dependent confined compression modulus of full-thickness bovine articular cartilage. *J. Orthop. Res.* **15,** 499–506 (1997).
6. Buckwalter, J. A. & Mankin, H. J. Articular cartilage: tissue design and chondrocyte-matrix interactions. *Instr. Course Lect.* **47,** 477–486 (1998).
7. Muir, H., Bullough, P. & Maroudas, A. The distribution of collagen in human articular cartilage with some of its physiological implications. *J. Bone Joint Surg. Br.* **52,** 554–563 (1970).
8. Siczkowski, M. & Watt, F. M. Subpopulations of chondrocytes from different zones of pig articular cartilage. Isolation, growth and proteoglycan synthesis in culture. *J. Cell Sci.* **97 (Pt 2),** 349–60 (1990).
9. Benninghoff, A. Form und Bau der Gelenkknorpel in ihren Beziehungen zur Funktion. *Z. Anat. Entwicklungsgesch.* **76,** 43–63 (1925).
10. Li, Z., Yao, S., Alini, M. & Grad, S. Different response of articular chondrocyte subpopulations to surface motion. *Osteoarthr. Cartil.* **15,** 1034–1041 (2007).
11. Schumacher, B. L., Hughes, C. E., Kuettner, K. E., Caterson, B. & Aydelotte, M. B. Immunodetection and partial cDNA sequence of the proteoglycan, superficial zone protein, synthesized by cells lining synovial joints. *J. Orthop. Res.* **17,** 110–120 (1999).
12. Hayes, A. J., Hall, A., Brown, L., Tubo, R. & Caterson, B. Macromolecular Organization and In Vitro Growth Characteristics of Scaffold-free Neocartilage Grafts. *J. Histochem. Cytochem.* **55,** 853–866 (2007).
13. Malda, J. *et al.* Localization of the potential zonal marker clusterin in native cartilage and in tissue-engineered constructs. *Tissue Eng. Part A* **16,** 897–904 (2010).
14. Khan, I. M., Salter, D. M., Bayliss, M. T., Thomson, B. M. & Archer, C. W. Expression of clusterin in the superficial zone of bovine articular cartilage. *Arthritis Rheum.* **44,** 1795–1799 (2001).
15. Lorenzo, P., Bayliss, M. T., Heinegårdt, D. & Heinegard, D. A Novel Cartilage Protein (CILP) Present in the Mid-zone of Human Articular Cartilage Increases with Age. *J. Biol. Chem.* **273,** 23463–23468 (1998).
16. DiCesare, P. E., Mörgelin, M., Carlson, C. S., Pasumarti, S. & Paulsson, M. Cartilage oligomeric matrix protein: Isolation and characterization from human articular cartilage. *J. Orthop. Res.* **13,** 422–428 (1995).
17. Murray, R. C., Smith, R. K., Henson, F. M. & Goodship, A. The distribution of cartilage oligomeric matrix protein (COMP) in equine carpal articular cartilage and its variation with exercise and cartilage deterioration. *Vet. J.* **162,** 121–128 (2001).
18. Mandelbaum, B. *et al.* Treatment outcomes of autologous chondrocyte implantation for full-thickness articular cartilage defects of the trochlea. *Am. J. Sports Med.* **35,** 915–921 (2007).
19. Marlovits, S., Zeller, P., Singer, P., Resinger, C. & Vécsei, V. Cartilage repair: Generations of autologous chondrocyte transplantation. *Eur. J. Radiol.* **57,** 24–31 (2006).
20. Brittberg, M. Cell Carriers as the Next Generation of Cell Therapy for Cartilage Repair: A Review of the Matrix-Induced Autologous Chondrocyte Implantation Procedure. *Am. J. Sports Med.* **38,** 1259–1271 (2010).
21. Steadman, J. R., Rodkey, W. G. & Rodrigo, J. J. Microfracture: surgical technique and rehabilitation to treat chondral defects. *Clin Orthop Relat Res* S362–9 (2001). doi:10.1097/00003086-200110001-00033
22. Melchels, F. P. W. *et al.* Additive manufacturing of tissues and organs. *Prog. Polym. Sci.* **37,** 1079–1104 (2012).
23. Klein, T. J. *et al.* Strategies for Zonal Cartilage Repair using Hydrogels. *Macromol. Biosci.* **9,** 1049–1058 (2009).
24. Seliktar, D. Designing cell-compatible hydrogels for biomedical applications. *Science* **336,** 1124–8 (2012).
25. Malda, J. *et al.* 25th Anniversary Article: Engineering Hydrogels for Biofabrication. *Adv. Mater.* **25,** 5011–5028 (2013).
26. Jungst, T., Smolan, W., Schacht, K., Scheibel, T. & Groll, J. Strategies and Molecular Design Criteria for 3D Printable Hydrogels. *Chem. Rev.* **116,** 1496–1539 (2016).
27. Schuurman, W. *et al.* Gelatin-methacrylamide hydrogels as potential biomaterials for fabrication of tissue-engineered cartilage constructs. *Macromol. Biosci.* **13,** 551–561 (2013).
28. Melchels, F. P. W., Dhert, W. J. A., Hutmacher, D. W. & Malda, J. Development and characterisation of a new bioink for additive tissue manufacturing. *J. Mater. Chem. B* **2,** 2282–2289 (2014).
29. Guvendiren, M., Lu, H. D. & Burdick, J. a. Shear-thinning hydrogels for biomedical applications. *Soft Matter* **8,** 260–272 (2012).
30. Censi, R., Fieten, P. J., Di Martino, P., Hennink, W. E. & Vermonden, T. In-situ forming hydrogels by simultaneous thermal gelling and Michael addition reaction between methacrylate bearing

thermosensitive triblock copolymers and thiolated hyaluronan. *J. Control. Release* **148,** e28–e29 (2010).

31. Lallana, E., Sousa-Herves, A., Fernandez-Trillo, F., Riguera, R. & Fernandez-Megia, E. Click Chemistry for Drug Delivery Nanosystems. *Pharm. Res.* **29,** 1–34 (2012).

32. Moreira Teixeira, L. S., Feijen, J., van Blitterswijk, C. A., Dijkstra, P. J. & Karperien, M. Enzyme-catalyzed crosslinkable hydrogels: Emerging strategies for tissue engineering. *Biomaterials* **33,** 1281–1290 (2012).

33. Schuurman, W. *et al.* Bioprinting of hybrid tissue constructs with tailorable mechanical properties. *Biofabrication* **3,** 021001 (2011).

34. Lee, J.-S. *et al.* 3D printing of composite tissue with complex shape applied to ear regeneration. *Biofabrication* **6,** 024103 (2014).

35. Kundu, J., Shim, J.-H. H., Jang, J., Kim, S.-W. W. & Cho, D.-W. W. An additive manufacturing-based PCL-alginate-chondrocyte bioprinted scaffold for cartilage tissue engineering. *J. Tissue Eng. Regen. Med.* **9,** 1286–1297 (2015).

36. Visser, J. *et al.* Biofabrication of multi-material anatomically shaped tissue constructs. *Biofabrication* **5,** 035007 (2013).

37. Olubamiji, A. D. *et al.* Modulating mechanical behaviour of 3D-printed cartilage-mimetic PCL scaffolds: influence of molecular weight and pore geometry. *Biofabrication* **8,** 025020 (2016).

38. Bekkers, J. E. J. *et al.* Single-Stage Cell-Based Cartilage Regeneration Using a Combination of Chondrons and Mesenchymal Stromal Cells: Comparison With Microfracture. *Am. J. Sports Med.* **41,** 2158–2166 (2013).

39. Poole, C. A., Ayad, S. & Schofield, J. R. Chondrons from articular cartilage: I. Immunolocalization of type VI collagen in the pericellular capsule of isolated canine tibial chondrons. *J. Cell Sci.* **90 (Pt 4),** 635–643 (1988).

40. Zhang, Z. Chondrons and the Pericellular Matrix of Chondrocytes. *Tissue Eng. Part B Rev.* **21,** 267–277 (2015).

41. Jiang, Y. & Tuan, R. S. Origin and function of cartilage stem/progenitor cells in osteoarthritis. *Nat. Rev. Rheumatol.* **11,** 206–12 (2015).

42. Dominici, M. *et al.* Minimal criteria for defining multipotent mesenchymal stromal cells. The International Society for Cellular Therapy position statement. *Cytotherapy* **8,** 315–317 (2006).

43. Bryant, S. J. & Anseth, K. S. Hydrogel properties influence ECM production by chondrocytes photoencapsulated in poly(ethylene glycol) hydrogels. *J. Biomed. Mater. Res.* **59,** 63–72 (2002).

44. Blaeser, A. *et al.* Controlling Shear Stress in 3D Bioprinting is a Key Factor to Balance Printing Resolution and Stem Cell Integrity. *Adv. Healthc. Mater.* **5,** 326–333 (2016).

45. Ko, C. S., Huang, J. P., Huang, C. W. & Chu, I. M. Type II collagen-chondroitin sulfate-hyaluronan scaffold cross-linked by genipin for cartilage tissue engineering. *J. Biosci. Bioeng.* **107,** 177–182 (2009).

46. Levett, P. A. *et al.* A biomimetic extracellular matrix for cartilage tissue engineering centered on photocurable gelatin, hyaluronic acid and chondroitin sulfate. *Acta Biomater.* **10,** 214–223 (2014).

47. Hwang, N. S. *et al.* Response of zonal chondrocytes to extracellular matrix-hydrogels. *FEBS Lett.* **581,** 4172–4178 (2007).

48. Villanueva, I., Weigel, C. a & Bryant, S. J. Cell-matrix interactions and dynamic mechanical loading influence chondrocyte gene expression and bioactivity in PEG-RGD hydrogels. *Acta Biomater.* **5,** 2832–2846 (2009).

49. Ponta, H., Sherman, L. & Herrlich, P. A. CD44: From adhesion molecules to signalling regulators. *Nat. Rev. Mol. Cell Biol.* **4,** 33–45 (2003).

50. Lesley, J. Hyaluronan Binding by Cell Surface CD44. *J. Biol. Chem.* **275,** 26967–26975 (2000).

51. Chung, C., Erickson, I. E., Mauck, R. L. & Burdick, J. A. Differential Behavior of Auricular and Articular Chondrocytes in Hyaluronic Acid Hydrogels. *Tissue Eng. Part A* **14,** 1121–1131 (2008).

52. Park, H., Choi, B., Hu, J. & Lee, M. Injectable chitosan hyaluronic acid hydrogels for cartilage tissue engineering. *Acta Biomater.* **9,** 4779–4786 (2013).

53. Liao, E., Yaszemski, M., Krebsbach, P. & Hollister, S. Tissue-Engineered Cartilage Constructs Using Composite Hyaluronic Acid/Collagen I Hydrogels and Designed Poly(Propylene Fumarate) Scaffolds. *Tissue Eng.* **13,** 537–550 (2007).

54. Allemann, F. *et al.* Effects of hyaluronan on engineered articular cartilage extracellular matrix gene expression in 3-dimensional collagen scaffolds. *J. Biomed. Mater. Res.* **55,** 13–19 (2001).

55. Akmal, M. *et al.* The effects of hyaluronic acid on articular chondrocytes. *J. Bone Jt. Surg. - Br. Vol.* **87-B,** 1143–1149 (2005).

56. Levett, P. A., Hutmacher, D. W., Malda, J. & Klein, T. J. Hyaluronic acid enhances the mechanical properties of tissue-engineered cartilage constructs. *PLoS One* **9,** e113216 (2014).

57. Kawasaki, K., Ochi, M., Uchio, Y., Adachi, N. & Matsusaki, M. Hyaluronic acid enhances proliferation and chondroitin sulfate synthesis in cultured chondrocytes embedded in collagen gels. *J. Cell. Physiol.* **179,** 142–148 (1999).

58. Oudshoorn, M. H. M., Rissmann, R., Bouwstra, J. A. & Hennink, W. E. Synthesis of methacrylated hyaluronic acid with tailored degree of substitution. *Polymer.* **48,** 1915–1920 (2007).

59. Hachet, E., Van Den Berghe, H., Bayma, E., Block, M. R. & Auzély-Velty, R. Design of biomimetic cell-interactive substrates using hyaluronic acid hydrogels with tunable mechanical properties. *Biomacromolecules* **13,** 1818–27 (2012).

60. Smith, C. M. *et al.* Three-dimensional bioassembly tool for generating viable tissue-engineered constructs. *Tissue Eng.* **10,** 1566–1576 (2004).

1

61.   Nichol, J. W. *et al.* Cell-laden microengineered gelatin methacrylate hydrogels. *Biomaterials* **31,** 5536–44 (2010).

62.   Levato, R. *et al.* Biofabrication of tissue constructs by 3D bioprinting of cell-laden microcarriers. *Biofabrication* **6,** 035020 (2014).

63.   Billiet, T., Gevaert, E., De Schryver, T., Cornelissen, M. & Dubruel, P. The 3D printing of gelatin methacrylamide cell-laden tissue-engineered constructs with high cell viability. *Biomaterials* **35,** 49–62 (2014).

64.   Skardal, A. *et al.* Photocrosslinkable hyaluronan-gelatin hydrogels for two-step bioprinting. *Tissue Eng. Part A* **16,** 2675–85 (2010).

65.   Yan, Y. *et al.* Fabrication of viable tissue-engineered constructs with 3D cell-assembly technique. *Biomaterials* **26,** 5864–71 (2005).

66.   Cohen, D. L., Malone, E., Lipson, H. & Bonassar, L. J. Direct freeform fabrication of seeded hydrogels in arbitrary geometries. *Tissue Eng.* **12,** 1325–1335 (2006).

67.   Fedorovich, N. E. *et al.* Evaluation of photocrosslinked Lutrol hydrogel for tissue printing applications. *Biomacromolecules* **10,** 1689–96 (2009).

68.   Pescosolido, L. *et al.* Hyaluronic acid and dextran-based semi-IPN hydrogels as biomaterials for bioprinting. *Biomacromolecules* **12,** 1831–1838 (2011).

69.   Censi, R. *et al.* A Printable Photopolymerizable Thermosensitive p(HPMAm-lactate)-PEG Hydrogel for Tissue Engineering. *Adv. Funct. Mater.* **21,** 1833–1842 (2011).

70.   Dang, J. M. & Leong, K. W. Natural polymers for gene delivery and tissue engineering. *Adv. Drug Deliv. Rev.* **58,** 487–99 (2006).

71.   Yue, K. *et al.* Synthesis, properties, and biomedical applications of gelatin methacryloyl (GelMA) hydrogels. *Biomaterials* **73,** 254–271 (2015).

72.   Gao, G. *et al.* Improved properties of bone and cartilage tissue from 3D inkjet-bioprinted human mesenchymal stem cells by simultaneous deposition and photocrosslinking in PEG-GelMA. *Biotechnol. Lett.* **37,** 2349–2355 (2015).

73.   Van Den Bulcke, A. I. *et al.* Structural and Rheological Properties of Methacrylamide Modified Gelatin Hydrogels. *Biomacromolecules* **1,** 31–38 (2000).

74.   Censi, R. *et al.* Photopolymerized thermosensitive hydrogels for tailorable diffusion-controlled protein delivery. *J. Control. Release* **140,** 230–236 (2009).

75.   Censi, R. *et al.* Photopolymerized thermosensitive poly(HPMAlactate)-PEG-based hydrogels: Effect of network design on mechanical properties, degradation, and release behavior. *Biomacromolecules* **11,** 2143–2151 (2010).

76.   Vermonden, T. *et al.* Macromolecular diffusion in self-assembling biodegradable thermosensitive hydrogels. *Macromolecules* **43,** 782–789 (2010).

77.   Censi, R. *et al.* The tissue response to photopolymerized PEG-p(HPMAm-lactate)-based hydrogels. *J. Biomed. Mater. Res. A* **97,** 219–29 (2011).

78.   Vermonden, T. *et al.* Photopolymerized thermosensitive hydrogels: Synthesis, degradation, and cytocompatibility. *Biomacromolecules* **9,** 919–926 (2008).

79.   Chu, C. R., Szczodry, M. & Bruno, S. Animal Models for Cartilage Regeneration and Repair. *Tissue Eng. Part B Rev.* **16,** 105–115 (2010).

80.   Khansai, M., Boonmaleerat, K., Pothacharoen, P., Phitak, T. & Kongtawelert, P. Ex vivo model exhibits protective effects of sesamin against destruction of cartilage induced with a combination of tumor necrosis factor-alpha and oncostatin M. *BMC Complement. Altern. Med.* **16,** 205 (2016).

81.   Sharma, S., Vazquez-Portalatin, N., Calve, S. & Panitch, A. Biomimetic Molecules Lower Catabolic Expression and Prevent Chondroitin Sulfate Degradation in an Osteoarthritic ex Vivo Model. *ACS Biomater. Sci. Eng.* **2,** 241–250 (2016).

82.   De Vries-van Melle, M. L. *et al.* An osteochondral culture model to study mechanisms involved in articular cartilage repair. *Tissue Eng. Part C. Methods* **18,** 45–53 (2012).

83.   Bolis, S., Handley, C. J. & Cornper, W. D. Passive loss of proteoglycan from articular cartilage explants. *Biochim. Biophys. Acta - Gen. Subj.* **993,** 157–167 (1989).

84.   Bos, P. K., Kops, N., Verhaar, J. A. N. & van Osch, G. J. V. M. Cellular origin of neocartilage formed at wound edges of articular cartilage in a tissue culture experiment. *Osteoarthr. Cartil.* **16,** 204–211 (2008).

85.   Botter, S. M. *et al.* Cartilage damage pattern in relation to subchondral plate thickness in a collagenase-induced model of osteoarthritis. *Osteoarthr. Cartil.* **16,** 506–514 (2008).

86.   Botter, S. M. *et al.* ADAMTS5-/- mice have less subchondral bone changes after induction of osteoarthritis through surgical instability: implications for a link between cartilage and subchondral bone changes. *Osteoarthr. Cartil.* **17,** 636–645 (2009).

87.   Sniekers, Y. H. *et al.* Development of osteoarthritic features in estrogen receptor knockout mice. *Osteoarthr. Cartil.* **17,** 1356–1361 (2009).

88.   Zhang, L., Hu, H., Tian, F., Song, H. & Zhang, Y. Enhancement of subchondral bone quality by alendronate administration for the reduction of cartilage degeneration in the early phase of experimental osteoarthritis. *Clin. Exp. Med.* **11,** 235–243 (2011).

89.   De Vries-van Melle, M. L. *et al.* Chondrogenesis of Mesenchymal Stem Cells in an Osteochondral Environment Is Mediated by the Subchondral Bone. *Tissue Eng. Part A* **20,** 23–33 (2014).

90.   De Vries-van Melle, M. L. *et al.* Chondrogenic differentiation of human bone marrow-derived mesenchymal stem cells in a simulated osteochondral environment is hydrogel dependent. *Eur. Cell. Mater.* **27,** 112–23; discussion 123 (2014).

1

91.   Elson, K. M. *et al.* Non-Destructive Monitoring of Viability in an Ex Vivo Organ Culture Model of Osteochondral Tissue. **29,** 356–369 (2015).
92.   Schwab, A. Ex vivo culture platform for assessment of cartilage repair treatment strategies. *ALTEX* (2016). doi:10.14573/altex.1607111
93.   Klein, T. J., Malda, J., Sah, R. L. & Hutmacher, D. W. Tissue Engineering of Articular Cartilage with Biomimetic Zones. *Tissue Eng. Part B Rev.* **15,** 143–157 (2009).
94.   Hollander, A. P., Dickinson, S. C. & Kafienah, W. Stem Cells and Cartilage Development: Complexities of a Simple Tissue. *Stem Cells* **28,** 1992–1996 (2010).

Chapter 2

Three-dimensional bioprinting and its potential in the field of articular cartilage regeneration

Vivian H. M. Mouser
Riccardo Levato
Lawrence J. Bonassar
Darryl D. D'Lima
Daniel A. Grande
Travis J. Klein
Daniël B. F. Saris
Marcy Zenobi-Wong
Debby Gawlitta
Jos Malda

Abstract

Three-dimensional (3D) bioprinting techniques can be used for the fabrication of personalized, regenerative constructs for tissue repair. The current article provides insight into the potential and opportunities of 3D bioprinting for the fabrication of cartilage regenerative constructs.

Although 3D printing is already used in the orthopedic clinic, the shift towards 3D *bio*printing has not yet occurred. We believe that this shift will provide an important step forward in the field of cartilage regeneration. Three-dimensional bioprinting techniques allow incorporation of cells and biological cues during the manufacturing process, to generate biologically active implants. The outer shape of the construct can be personalized based on clinical images of the patients defect. Additionally, by printing with multiple bio-inks osteochondral or zonally organized constructs can be generated. Relevant mechanical properties can be obtained by hybrid printing with thermoplastic polymers and hydrogels, as well as by the incorporation of electrospun meshes in hydrogels. Finally, bioprinting techniques contribute to the automation of the implant production process, reducing the infection risk.

To prompt the shift from non-living implants towards living 3D bioprinted cartilage constructs in the clinic some challenges need to be addressed. The bio-inks and required cartilage construct architecture need to be further optimized. The bio-ink and printing process need to meet the sterility requirements for implantation. Finally, standards are essential in order to ensure a reproducible quality of the 3D printed constructs. Once these challenges are addressed, 3D bioprinted living articular cartilage implants may find their way into daily clinical practice.

1. Introduction

Three-dimensional bioprinting, one of the main approaches within the field of biofabrication[1], is an emerging technology that allows for the fabrication of constructs with control over spatial resolution, shape, and mechanical properties. Bioprinting facilitates the accurate positioning of biomaterials, cells, and biological cues in a layer-by-layer fashion and can, thus, be applied for the generation of personalized regenerative implants. Articular cartilage is a thin, avascular, structural organ, and is therefore an easier potential target for treatment with bioprinted regenerative constructs compared to vascularized organs, like the liver and kidney. Cartilage contains predominantly proteoglycans, water, collagen type II, and low numbers of chondrocytes. Due to this low cell number and the absence of vascularization, the tissue has a limited regenerative capacity[2]. Consequently, most articular cartilage injuries will progress towards osteoarthritis if no interventions are taken[3]. Significant improvements in reparative cartilage treatments have been achieved over the last few decades (Figure 1). However, full cartilage restoration remains a significant challenge. It is generally accepted that for stable long-term reconstruction, function repair, or even regeneration, the therapy should not only address the cartilage, but also focus on reconstructing the underlying bone and re-establishing joint homeostasis. Therefore, bioprinted, personalized, regenerative constructs may provide a solution for cartilage injuries.

Although, bioprinting technology is rapidly gaining interest in the field of regenerative medicine, it is still in its infancy (Figure 1). Consequently, significant steps will have to be taken before this technology can be translated to wide-spread clinical applications. The International Cartilage Repair Society (ICRS) has adopted a leading role in analyzing the current state of scientific developments for cartilage regeneration in order to, for example, provide recommendations for the execution of preclinical and clinical studies[4]. The present position article can be regarded as an extension to this previous initiative and summarizes the current status of 3D bioprinting in the field of cartilage regeneration. More specifically, this article aims to address the potential and opportunities of 3D bioprinting for the fabrication of personalized regenerative articular cartilage constructs with tailored biological properties, architecture, and mechanical properties.

2. Current status of 3D printing in the orthopedic clinic

Three-dimensional printing technologies use 3D computer models to determine the final shape of the printed construct. Imaging techniques currently used in the clinic *e.g.* x-rays, magnetic resonance imaging (MRI), and computed tomography (CT), provide macroscopically detailed sequences of 2D images of patients. These sequences can relatively easily be translated into 3D images, which can serve as blueprints for 3D printing *e.g.,* upon conversion into stereolithography (STL) and additive manufacturing (AMF) files[5]. Currently, 3D printing technologies are already part of a number of clinical routines. Three-dimensional models of complex abnormalities are, for example, printed for educational purposes and to help surgeons in preoperative planning for challenging surgeries[6–8]. Moreover, patient-specific drilling and sawing guides are printed to assist orthopedic surgeons with the placement of pedicle screws and total joint replacements
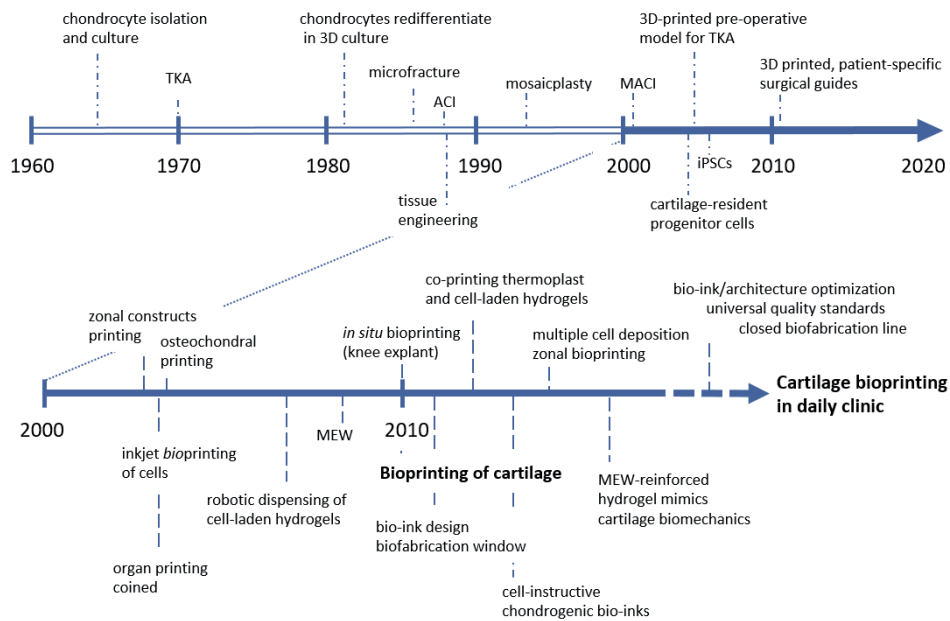
Figure 1: Evolution of cartilage repair and bioprinting of cartilage. *Additive manufacturing techniques and in particular bioprinting are enabling to produce patient-specific, complex architectures that mimic the composition of articular cartilage. With the development of novel bioactive bio-inks and the combination of different 3D bioprinting techniques, functional cartilage constructs will be obtained. Optimized and mature bioprinted grafts will have to meet high quality standards in order to be used as clinical devices for cartilage and joint healing. TKA = total knee arthroplasty; ACI = autologous chondrocyte implantation; MACI = matrix induced autologous chondrocyte implantation; iPSC = induced pluripotent stem cell; MEW = melt electrospinning writing.*

respectively[9,10]. Additionally, customized 3D printed implants are already commercially available *e.g.* for calvarial reconstruction[11]. These examples indicate that the current 3D printing technologies have the capability to provide personalized implants for orthopedic defects. However, the transition from 3D printing of polymers, ceramics, and metals towards 3D *bio*printing of living and biologically active constructs has not taken place in the clinical practice yet. In this research field, however, several steps have already been performed to demonstrate the possibilities and the feasibility of the clinical transition (Table 1-3).

3. The potential of 3D bioprinting for regenerative cartilage constructs

3.1. Cell laden and bioactive inks

Bioprinting techniques provide many possibilities for the fabrication of personalized cartilage constructs. A key factor for the success of these regenerative constructs is to make them biologically active. One strategy to accomplish this is by incorporating cells. It has been widely demonstrated that the bioprinting process when using extrusion, inkjet, or laser-based printing technologies, does not hamper the viability or long-term performance of the deposited cells[12–19]. Extrusion-based printing allows the

deposition of cell-laden filaments and is regarded as the most suitable technique for the 3D bioprinting of viable constructs of several centimeters in size and with high cell densities[20]. Consequently, for the printing of cartilage constructs, extrusion-based printing techniques are most often considered (85% of the publications, Table 1-3). However, the resolution of the fiber thickness is limited by the extrusion process to ~100 micrometer. In contrast, inkjet and laser-based printing allow the deposition of smaller volumes and are, thus, more suitable for the accurate deposition of micropatterns, down to the level of single cells. Currently, the most promising carrier materials, or 'bio-inks', for cell-based 3D bioprinting are based on hydrogels, as they facilitate homogeneous cell encapsulation in a highly hydrated and mechanically supportive 3D environment.

Multiple cell types have been explored for their application in bioactive cartilage implants. Autologous chondrocytes or chondrons, chondrocytes with their pericellular matrix, can be harvested form a non-loadbearing cartilage surface or the perimeter of a cartilage defect in the patient[21–23]. So far, in cartilage bioprinting research, the focus has predominantly been on the use of chondrocytes (Table 1-3). Nevertheless, when using autologous chondrocytes, obtaining sufficient cell numbers remains a challenge, especially since expansion in monolayer culture causes dedifferentiation of the cells towards a more fibroblastic phenotype[24]. Additionally, complications such as donor site morbidity are likely to occur. An alternative cell type is the multipotent mesenchymal stromal cell (MSC) population, which can be derived from multiple tissues *e.g.* bone marrow, adipose tissues, and muscles[25]. These cells can be differentiated into chondrocyte-like cells in the presence of specific growth factors, such as the transforming growth factor beta family. However, adequate cues to control MSC fate have to be provided, as these cells have the tendency to progress into hypertrophic chondrogenesis and to give rise to bone formation via the endochondral pathway once implanted *in vivo*[26]. Combining MSCs with chondrocytes or chondrons has shown promising results both *in vitro* and *in vivo*, in which it seems that the MSCs stimulate and direct the chondrocytes/chondrons to synthesize new cartilage-like tissue[27–29]. Furthermore, alternative cell populations with regenerative potential are being investigated, including sub-populations of chondroprogenitor cells, which can be harvested from mature cartilage and can be expanded in mono-layer culture without losing their interface between chondrogenic phenotype[30]. Also the induced pluripotent stem cells that show unlimited self-renewal and can be generated from numerous, easily accessible cell types, (*i.e.* keratinocytes), constitute an interesting cell source for cartilage regeneration, provided that the safety concerns about their usage are cleared[31,32]. Multiple research groups are focusing on these different cell populations for cartilage regeneration purposes and on enhancing the cell performance by *e.g.* culturing with specific growth factors, biological cues, and mechanical loading regimes, however, these detailed strategies are not within the scope of the present opinion article and have been reviewed elsewere[33–35].

An alternative strategy to generate bioactive constructs based on 3D printing technologies involves the embedding of biological cues that stimulate encapsulated cells or attracts and/or stimulates cells from the host. Hydrogel-based bio-inks allow for the incorporation of growth factors, bioactive proteins, peptides, chemicals, and matrix

2

components[36], and printing procedures have so far not shown any negative effects on the activity of these biological cues[17,37–39] (Table 1). Large molecules that are constituents of the native cartilage matrix, such as hyaluronic acid[40,41], can be used as promising biological cues for cartilage regeneration. Addition of these components also impact on the overall rheological properties, often increasing the printability of a hydrogel bio-ink for extrusion printing[17,42]. When printing with thermoplastic polymers, on the other hand, biological molecules are exposed to relatively high temperatures during the extrusion process. Therefore, while thermostable compounds can be loaded during printing, labile compounds need to be incorporated afterwards. For example, dexamethasone still exhibits osteoinductive properties *in vitro* after being printed in a polycaprolactone (PCL)/poloxamine polymer blend at 110°C[43]. Contrarily, transforming growth factor beta cannot be heated to this temperature but can be coated on printed PCL scaffolds and was demonstrated to attract and stimulate cells from surrounding tissues *in vivo* when incorporated with this approach[44]. Furthermore, other recently developed regenerative strategies, that include *e.g.* the incorporation of cell-secreted exosomes[45] or microRNAs, can easily be combined with bioprinting technologies, since all these moieties can be preserved in the highly hydrated environment provided by hydrogel bio-inks.

3.2. Shape, architecture, and multiphasic organization

For the generation of personalized regenerative implants, precise control over shape and internal architecture is essential. As discussed above, the outer shape of a construct can be personalized by using medical imaging as the foundation of the print template. Additionally, multiple 'inks' consisting of different biomaterials, bioactive factors, and/or cells, can be loaded in a bioprinter to fabricate complex anatomical architectures with multiple tissue types. Irregular shapes and overhangs can also be obtained via the printing of support structures with a sacrificial material, such as alginate, agarose, PCL, polyvinyl alcohol (PVA), poly-ethylene glycol (PEG), and pluronics[12–14,46,47].

Printing with multiple bio-inks also allows for the inclusion of multiple tissues and tissue interfaces in a single construct. This is of particular importance in the orthopedic field, where tissue interfaces play a significant role in the underlying (patho)biology. Osteochondral constructs have, for example, been successfully generated with either osteoblasts in the bone part and chondrocytes in the cartilage part[48], or stem cells in both layers with additional biological cues to induce bone differentiation in the one part and cartilage formation in the other[26,49]. However, in the latter study further evaluation of biological cues is necessary, as the MSCs generated bone via the endochondral pathway in the cartilage layer after *in vivo* implantation[26]. Further, to mimic the bone compartment, bio-inks that can both carry cells and harden over time have been developed, to achieve a stiffness within the same range of those of cancellous bone[38]. Such bio-inks could be combined with hydrogels described above to obtain fully printed, cellular composites with mechanical properties that appropriately match bone and cartilage regions. Additionally, vessel-like structures can be printed in the bone compartment to support vascularization by using sacrificial materials[13,14,46].

Printing with multiple bio-inks also provides a platform to mimic the zonal

organization of articular cartilage. Articular cartilage exhibits distinct depth dependence in composition and mechanical performance[50,51], which have been notably difficult to reproduce with conventional approaches to cartilage repair[52]. It is believed that restoration of this zonal organization will improve integration and performance of the construct at the defect site[53,54]. Three-dimensional bioprinting may be a unique tool to achieve the appropriate zone-specific compositional and mechanical heterogeneity present in articular cartilage. Increasing resolution of 3D bioprinters might even allow for imitation of the specific fiber arrangement of the split line patterns found at the articular surface, as well as, the more complex Benninghoff arcade orientation of collagen fibers emanating from the subchondral bone[55]. Additionally, depth-dependent differences in cell densities can be replicated via gradient bioprinting, in which a cell-free and a cell-laden bio-ink are mixed at the nozzle of the bioprinter to accurately change the final cell density during printing[56]. The zonal cellular phenotypes of embedded/seeded cells can be stimulated by the incorporation of biological cues and matrix components[57,58]. For example, it was demonstrated that the incorporation of chondroitin sulfate and matrix metalloproteinase-sensitive peptides in a PEG-based hydrogel stimulates MSCs to produce superficial zone specific matrix components, while incorporating chondroitin sulfate alone or hyaluronic acid stimulates intermediate and deep zone matrix production, respectively[59]. Another option for the fabrication of zonally organized constructs is to incorporate zonally harvested chondrocytes, which have been shown to maintain their zone specific biosynthetic activities during culture in PEG-based hydrogels[60].

3.3. Mechanical properties

Finally, 3D bioprinting can generate constructs composed of both hydrogels and thermoplastic polymers with mechanical properties that suit the challenging mechanical environment of the joint. It has been demonstrated that these hybrid constructs exhibit mechanical characteristics similar to the thermoplastic polymer frame without the hydrogel[47,61]. Therefore, by changing the architecture of the thermoplastic polymer frame, the mechanical properties of the construct can be tailored[62,63]. To prevent disruption of the interface between the two materials during mechanical loading, covalent binding of the thermoplastic polymer and the hydrogel was shown feasible and effective[64]. Additionally, the hybrid printing and covalent binding of both materials did not affect the viability of cells incorporated in the hydrogel[47,61].

An alternative approach to reinforce hydrogel constructs is using melt electrospun meshes. Melt electrospinning writing allows for the controlled deposition of thermoplastic polymer filaments with a thickness in the order of 1-20 micrometer, while bioprinting generates filaments with a thickness in the order of 100 micrometer[65]. By incorporating electrospun meshes in a cast hydrogel construct, the mechanical behavior of the hybrid construct can approach the bulk mechanical properties of native articular cartilage[66]. Therefore, if accurate melt electrospinning writing could be combined with 3D bioprinting technologies, organized constructs with heterogeneous mechanical characteristics similar to native articular cartilage could be fabricated. The first set-ups to combine melt electrospinning with bioprinting are already being developed. For example

2

2

the feasibility of generating constructs with alternating layers of inkjet printed hydrogels and random electrospun thermoplastic polymer meshes has already been demonstrated, emphasizing the prospect of the fabrication of organized, custom made constructs with native mechanical characteristics[67].

3.4. Automation of implant production process

Bioprinting can also contribute to the automation of the implant production process. Besides printing into a wells-plate, constructs could also be printed directly into a bioreactor, minimizing handling and, thus, infection risks. Also, successful co-printing of a bioreactor simultaneously with a construct has been demonstrated[68]. Constructs fabricated with these approaches require a two-step surgical procedure for clinical implantation. During a first surgery autologous cells are harvested, which then need to be bioprinted and pre-cultured in a laboratory. Later, during a second surgery, the bioprinted construct can be implanted into the patient's cartilage defect. As bioprinting is a relatively fast process (minutes), a one-step surgical approach might also be feasible, in which the cell-laden construct is fabricated in the operation theater and directly implanted. Potentially, cartilage defects could also be filled *in situ*, by printing the implant directly into the lesion. This approach has been exemplified by the direct *ex vivo* printing into osteochondral plugs or femurs[69,70]. In line with this, steps exploring the feasibility of *in situ* bioprinting for other tissues have been taken, *e.g.* for calvarial defects in living mice[16]. Additionally, a bio-pen is being developed to simplify the *in situ* print procedure[71]. Although one-step surgical procedures and printing directly into a defect are exciting concepts and foster the idea of further automation in surgery, it would add the challenge to initiate the neo-cartilage formation within the harsh environment of a diseased joint.

4. Current challenges in bringing 3D bioprinting to clinical applications

Bioprinting requires the combination of multiple elements in a bio-ink *e.g.* printability, shape stability after printing, cell therapies, biological cues, and mechanical strength. Taking all these aspects into account often results in a trade-off, in which the separate elements are suboptimal in the bio-ink or final construct[20]. Future research should for example focus on new methods to improve the printability of hydrogel-based bio-inks without negatively influencing the cell behavior[17,72]. Additional, research should focus on new methods for the formulation and processing of bio-inks prior to printing[73], in order to generate a larger range of biomaterials that can successfully be employed in bioprinting technologies. Besides optimizing the printing procedures and bio-inks, there is still a need for deeper understanding of cartilage regeneration in general, in order to determine *e.g.* what cell types, biological cues, and organization are required in the final construct for successful cartilage regeneration.

For the clinical translation of bioprinted living cartilage implants, the bio-ink has to meet the same regulations and safety requirements, concerning *e.g.* sterility, (endo)toxin content, reproducibility, and if cell-laden Advanced Therapy Medicinal Product (ATMP) regulations as biomaterials used for other implantable devices[74]. To ensure sterility after 3D printing, the printing process needs to be incorporated in a Good Manufacturing

Practice (GMP) facility, and the printer itself and all its components should be sterile and able to operate in a sterile environment. Further, the whole fabrication process should preferably involve minimal manual handling and post-processing steps in closed systems. Bioprinters that can fulfill these requirements are already commercially available. Ideally, these systems also would have an integrated bioreactor system to allow for *in vitro* culture prior to implantation without extra handling of the construct. During this culture the constructs can relatively easily be stimulated with *e.g.* growth factors or mechanical loading, to stimulate the encapsulated cells to differentiate into the desired lineage. Additionally, cartilage-like tissue formation is stimulated in this period to provide an initial matrix, which will increase the construct stiffness and might improve integration in the defect. A bioprinter-bioreactor setup, or closed biofabrication line, is not commercially available yet, however the first steps towards these kind of setups are currently being taken[75].

To ensure safety of 3D bioprinted living medical implants for clinical use and to help organizations qualify and validate the printing process and bio-inks, standards are required. Standards are already available for additive manufacturing in general, under American Society for Testing and Materials (ASTM) F2792. Additionally, standards for tissue-engineered constructs have been published by the ASTM international committee F04, the International Organization for Standardization (ISO) technical committee 150/SCZ, and the British Standards Institute (BSI). However, currently no such standard is available for *bio*printing technologies[76,77]. There are a number of attempts to develop validation protocols for relatively simple bioprint-related analyses, such as the quantification of the shape-fidelity of a 3D printed construct. Such analysis are based on the length, width, and height of a printed filament compared to the nozzle diameter[78,79], the shape of the pores in a 3D construct compared to the theoretical shape[80], or on the deviation between the printed construct and the 3D computer model[39,81]. Notably, multiple studies have demonstrated that optical scanning for validation can be incorporated in 3D bioprinters[69,82]. This offers the prospect of real-time assessment of print fidelity and immediate quality control/quality analysis that may be useful for regulatory compliance. Ultimate clinical translation will also have to include strategies and regulations for cell sourcing, whether autologous or allogeneic, cell incorporation in the bio-ink or seeding on the printed construct, and implantation techniques to implant and fix the printed construct into the defect side. One universal standard to assess the quality of a 3D printed living construct in terms of sterility, shape-fidelity, biological properties, cell incorporation, surgical implantation techniques, and safety, is still lacking and needs to be set up in order to smoothen the transition from bench to bed-side.

5. Conclusions

The 3D printing techniques that are currently used in the orthopedic clinic are just a glimpse of how this technology might contribute to future patient treatments, especially for articular cartilage regenerative therapies. Bioprinting techniques allow for the fabrication of personalized constructs with accurately positioned cells and biological cues to mimic the osteochondral interface and/or the zonal organization of articular cartilage.

2

Mechanical properties can be tailored by hybrid printing or reinforcement strategies to match those of the cartilage area which needs replacement. Finally, bioprinting fosters the prospect of automation of the implant production process.

Although bioprinting provides many opportunities to generate cartilage regenerative constructs, which closely resemble the native tissue, there are still multiple challenges that need to be overcome. The main challenge is to make the transition in the clinic from non-living personalized 3D printed implants towards biologically active and living implants. In order to accomplish this, some additional challenges need to be overcome first. Bio-inks have to be further optimized and the required construct architecture and mechanical properties need to be established. Additionally, the printing process, as well as the bio-inks, need to meet the specific sterility requirements to allow for implantation. Finally, universal quality standards are necessary to smoothen the clinical translation of new bio-inks and printing technologies. Tackling these challenges will foster the shift of biologically active and living bioprinted implants from the laboratory towards the daily clinical practice.

Table 1. Overview of Publications on the (Bio)fabrication of (Articular) Cartilage Regenerative Constructs.

Reference	Printing technique	Bio-ink		(Bio)printed constructs		Remarks
		Material(s)	Cells and/or biological cues	Mechanical properties	Tissue formation	
Cohen et al. (2006)[18]	Extrusion bio-printing	Alginate	- Full thickness bovine articular chondrocytes	- Compressive modulus (unconfined) ~1.8±0.1 kPa.	In vitro - Viability, ~94% - Cartilage-like tissue formation similar in printed constructs as in casted alginate or alginate beads.	- Printed meniscus and intervertebral disk shapes.* - Demonstrated that viability and differentiation behavior of chondrocytes were not influenced by the printing procedure.
Schuurman et al. (2012)[61]	Extrusion printing	Alginate reinforced with PCL[I]	- C20A4 cell-line*	- Compressive modulus (unconfined) ~6000 kPa.	In vitro - Viability, ~70-90%	- First demonstration of simultaneous deposition of thermoplastic polymer and hydrogel for the fabrication of reinforced constructs.
Cui et al. (2012)[19]	Inkjet bio-printing	PEGDMA[II]	- Full thickness human articular chondrocytes - TGF-β1[III] and FGF-2[IV] in medium during culture	- Compressive modulus (unconfined) ~30-37 kPa.	In vitro - More cell proliferation and more total cartilage-like tissue formation in constructs cultured with both TGF-β1[III] and FGF-2[IV] after 4 weeks of differentiation.	- Demonstrated that culturing printed constructs with both TGF-β1[III] and FGF-2[IV] increases proliferation and on longer term (21 days) cartilage-like tissue formation.

2

2

Cui et al. (2012)[70]	Inkjet bio-printing	PEGDMA[II]	- Full thickness human articular chondrocytes	- Compressive modulus (unconfined) ~38-320 kPa	*Ex vivo* - Viability, ~89% - Cartilage-like tissue formation increased during the first 4 weeks of culture and remained stable after (6 weeks total). - Stable construct integration in the defect after 6 weeks.	- Printing directly into defects in porcine osteochondral plugs. - Demonstrated the importance of rapid gelation for maintaining initial cell distribution.
Schuurman et al. (2013)[17]	Extrusion bio-printing	GelMA[V] with hyaluronic acid PCL[I] reinforcement*	- Full thickness equine articular chondrocytes - Hyaluronic acid	- Compressive modulus (unconfined) for gelMA[V] constructs: ~10-175 kPa (dependent on concentration).	*In vitro* - Viability, ~73-83% - Similar cartilage-like tissue formation in constructs with and without hyaluronic acid after 4 weeks differentiation.	- Addition of hyaluronic acid increased the printability.
Boere et al. (2014)[64]	Extrusion printing	GelMA[V] (cast) reinforced with pHMGCL/PCL[VI] (printed)	- Full thickness human articular chondrocytes	- Construct failure (unconfined compression) ~2.7 N (~7.7 N when covalent bonds between gelMA[V] and pHMGCL/ PCL[VI]).	*In vitro* - Interconnected cartilage-like tissue network after 6 weeks of differentiation. *In vivo* - Rats, subcutaneous; more collagen type II but less GAGs after 8 weeks compared to *in vitro* study.	- Covalent bonds between hydrogel and reinforcement to increase construct stability and mechanical strength.

2

Kundu *et al.* (2015)[83]	Extrusion bio-printing	Alginate reinforced with PCL[I]	- Nasal human chondrocytes - TGF-β[III]	- Not reported	*In vitro* - Viability, ~85% - More cartilage-like tissue formation in constructs with TGF-β[III] after 4 weeks of differentiation. *In vivo* - Immunodeficient mice, subcutaneous; moderate cartilage-like tissue formation in constructs with TGF-β[III] after 4 weeks.	- Printed constructs with a cell and growth factor-laden bio-ink, reinforced with a printed thermoplastic polymer.
Kesti *et al.* (2015)[84]	Extrusion bio-printing	HAMA[VII] with HA-pNIPAAM[VIII]	- Full thickness bovine articular chondrocytes	- Not reported	*In vitro* - Viability, low when HA-pNIPAAM[VIII] remains in the culture, high when HA-pNIPAAM[VIII] was eluted.	- HA-pNIPAAM[VIII] supports printing and can be eluted from the final construct after printing and crosslinking.
Kesti *et al.* (2015)[39]	Extrusion bio-printing	Gellan with alginate	- Full thickness bovine articular chondrocytes - Hydroxyapatite particles - Cartilage extracellular matrix particles	- Tensile modulus ~116–230 kPa.	*In vitro* - Viability, ~80-96% (60% in the center of large constructs) - Cartilage extracellular matrix particles increased cartilage-like tissue formation during 8 weeks of differentiation. However, constructs cultured in TGF-β3[III] supplemented medium contained most cartilage matrix.	- Printed ear, nose, meniscus, and vertebral disk shapes by using support structures.*

2

Markstedt et al. (2015)[85]	Extrusion bio printing	Nanofibrillated cellulose with alginate	- Nasal human chondrocytes	- Compressive modulus (unconfined) ~75-250 kPa (depending on the ratio of both components).	*In vitro* - Viability, ~73-86%	- Printed ear and meniscus shapes.*
Visser et al. (2015)[66]	Melt electro-spinning	Electrospun PCL[I] infused with gelMA[V]	- Human articular chondrocytes in gelMA[V] - Hyaluronic acid - Mechanical stimulation (14 days without followed by 14 days with)	- Compressive modulus (unconfined) ~80-400 kPa for hybrid construct depending on mesh porosity. - Similar stress/strain curve for gelMA[V] reinforced with a 93% porous mesh as for native articular cartilage.	*In vitro* - Viability, ~73-86% - Expression of chondrogenic genes increased in mechanical stimulated constructs during 4 weeks of culture. No differences were found at protein level.	- With low content of thermoplastic polymer fibers (7%), mechanical properties could be achieved within the range of articular cartilage.

2

Izadifar et al. (2016)[86]	Extrusion bio-printing	Alginate reinforced with PCL[I]	- Full thickness embryonic chick chondrocytes ('rounded' and 'fibroblastic' sub-populations)	- Not reported	*In vitro* - Viability, ~77-85% - More proliferation and cartilage-like tissue formation in constructs with the 'fibroblastic' chondrocyte sub-population compared to the 'rounded' sub-population.	- Printed constructs with a cell-laden bio-ink, reinforced with a printed thermoplastic polymer. - Demonstrated rapid cooling of PCL[I] strands after printing. - Different chondrocyte sub-populations give differences in cartilage-like tissue formation.
Abbadessa et al. (2016)[87]	Extrusion bio-printing	polyHPMA-lac-PEG[IX]	- Full thickness equine articular chondrocytes - HAMA[VII] or CSMA[X]	- Compressive modulus (unconfined) ~13-16 kPa for all combinations.	*In vitro* - Viability, ~85-95% (printed) - Similar levels of cartilage-like tissue formation in polyHPMA-lac-PEG[IX] hydrogels as in fibrin controls after 4 weeks of culture (cast).	- Incorporation of HAMA[VII] and to a lesser extent CSMA[X] decreased the degradation rate and improved the thermosensitive profile and printability.

2

| Mouser et al. (2016)[88] | Extrusion bio-printing | gelMA[V] with gellan gum | - Full thickness equine articular chondrocytes | - Compressive modulus (unconfined) ~2.7-186 kPa depending on concentration and ratio of gelMA[V] and gellan gum. | In vitro
- All evaluated concentrations supported cartilage-like tissue formation during 6 weeks of culture. Relatively high gellan gum concentrations compromised chondrogenesis and high total polymer concentrations hampered matrix distribution. | - Identified yield stress as dominant factor for bioprintability.
- Addition of gellan gum improved filament deposition, increased construct stiffness, and supported chondrogenesis. |

*Proof of concept study
[I] PCL = polycaprolactone
[II] PEGDMA = Poly(ethylene) glycol dimethacrylate
[III] TGF = transforming growth factor
[IV] FGF = Fibroblast growth factor
[V] GelMA = Gelatin-methacryloyl
[VI] pHMGCL/PCL = poly(hydroxylmethylglycolide-co-ε-caprolactone)/poly(ε-caprolactone)
[VII] HAMA = methacrylated hyaluronic acid
[VIII] HA-pNIPAAM = poly(N-isopropylacrylamide) grafted hyaluronan
[IX] polyHPMA-lac-PEG = polyethylene glycol midblock flanked by two poly[N-(2-hydroxypropyl) methacrylamide mono/dilactate]
[X] CSMA = methacrylated chondroitin sulfate

Table 2. Overview of Publications on the (Bio)fabrication of Zonally Organized Cartilage Regenerative Constructs.

Reference	Printing technique	Bio-ink		(Bio)printed constructs		Remarks
		Material(s)	Cells and/or biological cues	Mechanical properties	Tissue formation	
Woodfield et al. (2004)[89] Woodfield et al. (2005)[90]	Extrusion printing	PEGT/PBT[I]	- Full thickness human articular chondrocytes (seeded after printing) - Differences in pore size	- Equilibrium compressive modulus (unconfined) ~200-2500 kPa. - Dynamic compressive modulus (unconfined) ~200-4300 kPa.	*In vitro* - Viability, no quantification - Cartilage-like tissue formation after 3 weeks of differentiation. *In vivo* (homogenous pore size) - Immunodeficient mice, subcutaneous; more cartilage-like tissue formation after 3 weeks compared to *in vitro*. Fibrous capsule around construct.	- Goal was to study zonal differentiation. - Demonstrated that pore size gradients promote inhomogeneous cell distribution. However no differences in cartilage-like tissue formation was found when normalized to the cell density.
Schuurman et al. (2013)[91]	Extrusion printing	PEGT-PBT[XI]	- Superficial zone equine articular chondrocyte pellets - Deep zone equine articular chondrocyte pellets	- Not reported	*In vitro* - Abundant cartilage-like tissue formation during 1 month of differentiation. However, zonal characteristics could not be maintained.	- Demonstrated the feasibility of placing aggregates based on cells in a printed scaffold.

[I] PCL = polycaprolactone

[XI] PEGT-PBT = poly(ethylene glycol)-terephthalate-poly(butylene terephthalate)

2

Table 3. Overview of Publications on the (Bio)fabrication of Osteochondral Regenerative Constructs.

Reference	Printing technique	Bio-ink		(Bio)printed constructs		Remarks
		Material(s)	Cells and/or biological cues	Mechanical properties	Tissue formation	
*Lee et al. (2010)[44]	Extrusion printing	PCL[I] with hydroxyapatite	- Cell free - PCL[I] network infused with a TGF-β3[III] laden collagen type I hydrogel (cartilage) - Different pore size for bone and cartilage	- Not reported for the construct prior to implantation. - Compressive modulus (unconfined) ~5500 kPa at explanation.	*In vivo* - Rabbits, orthotopic; cells migrated into the scaffolds and produced cartilage-like tissue after 4 months in the presence of TGF-β3[III].	- Demonstrated the feasibility of cartilage regeneration via cell-free scaffolds that attract host cells.
*Cohen et al. (2010)[69]	Extrusion printing	Alginate (cartilage) Gelatin (bone)	- Cell free - Demineralized bone matrix (bone)	- Not reported	*Ex vivo* - Printing directly into an (osteo)chondral defect in a bovine femur.	- First demonstration of printing directly into a defect with automatic geometric feedback during printing.
*Shim et al. (2012)[92]	Extrusion bio-printing	Alginate reinforced with PCL[I]	- Nasal human chondrocytes (cartilage) - Human osteoblast cell-line (MG63, bone)	- Not reported	*In vitro* - Viability, ~90-95% - Cells proliferated during 7 days of culture.	- Proof of concept for printing with multiple cell types that remain in their separate compartments during culture.

2

| Fedorovich et al. (2012)[48] | Extrusion bio-printing | alginate | - Full thickness human articular chondrocytes (cartilage)
- Human mesenchymal stromal cells (bone)
- Biphasic calcium phosphate particles (bone) | - Compressive modulus (unconfined) ~4-15 kPa (dependent on construct porosity). | *In vitro*
- Viability, ~89%
- Bone-like and cartilage-like tissue formation in the separate regions of the constructs after 3 weeks of differentiation.
In vivo
- Immunodeficient mice, subcutaneous; bone-like and cartilage-like tissue formation in the separate regions after 6 weeks. | - Demonstrated the feasibility of printing heterogeneous tissue constructs with distinctive tissue formation in osteo and chondral regions. |
| Levato et al. (2014)[49] | Extrusion bio-printing | GelMA[V] with gellan gum | - Murine mesenchymal stromal cells (cartilage/bone)
- Polylactic acid microcarriers (bone) | - Compressive modulus (unconfined) ~25-50 kPa (dependent on concentration of microcarriers). | *In vitro*
- Viability, ~60-90% | - Demonstrated the feasibility to extrude larger aggregates (cells on microcarriers).
- Focus paper on bone compartment, osteochondral constructs as proof of concept. |

*Proof of concept study
[I] PCL = polycaprolactone
[III] TGF = transforming growth factor
[V] GelMA = Gelatin-methacryloyl

43

References

1. Groll, J. *et al.* Biofabrication: reappraising the definition of an evolving field. *Biofabrication* **8,** 013001 (2016).
2. Almarza, A. J. & Athanasiou, K. A. Design characteristics for the tissue engineering of cartilaginous tissues. *Ann. Biomed. Eng.* **32,** 2–17 (2004).
3. Prakash, D. & Learmonth, D. Natural progression of osteo-chondral defect in the femoral condyle. *Knee* **9,** 7–10 (2002).
4. Buschmann, M. D. & Saris, D. B. F. Introduction to the International Cartilage Repair Society Recommendation Papers. *Cartilage* **2,** 99–99 (2011).
5. Ventola, C. L. Medical Applications for 3D Printing: Current and Projected Uses. *P T* **39,** 704–11 (2014).
6. Spottiswoode, B. S. *et al.* Preoperative three-dimensional model creation of magnetic resonance brain images as a tool to assist neurosurgical planning. *Stereotact. Funct. Neurosurg.* **91,** 162–169 (2013).
7. Windisch, G. *et al.* A model for clubfoot based on micro-CT data. *J. Anat.* **210,** 761–766 (2007).
8. Cohen, J. & Reyes, S. A. Creation of a 3D printed temporal bone model from clinical CT data. *Am. J. Otolaryngol.* **36,** 619–624 (2015).
9. Noble, J. W., Moore, C. A. & Liu, N. The Value of Patient-Matched Instrumentation in Total Knee Arthroplasty. *J. Arthroplasty* **27,** 153–155 (2012).
10. Lu, S. *et al.* A novel computer-assisted drill guide template for thoracic pedicle screw placement: A cadaveric and clinical study. *Int. J. Med. Robot. Comput. Assist. Surg.* **5,** 184–191 (2009).
11. Probst, F. A., Hutmacher, D. W., Müller, D. F., Machens, H.-G. & Schantz, J.-T. Rekonstruktion der Kalvaria durch ein präfabriziertes bioaktives Implantat. *Handchirurgie · Mikrochirurgie · Plast. Chir.* **42,** 369–373 (2010).
12. Visser, J. *et al.* Biofabrication of multi-material anatomically shaped tissue constructs. *Biofabrication* **5,** 035007 (2013).
13. Skardal, A., Zhang, J. & Prestwich, G. D. Bioprinting vessel-like constructs using hyaluronan hydrogels crosslinked with tetrahedral polyethylene glycol tetracrylates. *Biomaterials* **31,** 6173–6181 (2010).
14. Lee, W. *et al.* On-demand three-dimensional freeform fabrication of multi-layered hydrogel scaffold with fluidic channels. *Biotechnol. Bioeng.* **105,** 1178–1186 (2010).
15. Koch, L., Gruene, M., Unger, C. & Chichkov, B. Laser assisted cell printing. *Curr. Pharm. Biotechnol.* **14,** 91–7 (2013).
16. Keriquel, V. *et al.* In vivo bioprinting for computer- and robotic-assisted medical intervention: preliminary study in mice. *Biofabrication* **2,** 014101 (2010).
17. Schuurman, W. *et al.* Gelatin-methacrylamide hydrogels as potential biomaterials for fabrication of tissue-engineered cartilage constructs. *Macromol. Biosci.* **13,** 551–561 (2013).
18. Cohen, D. L., Malone, E., Lipson, H. & Bonassar, L. J. Direct freeform fabrication of seeded hydrogels in arbitrary geometries. *Tissue Eng.* **12,** 1325–1335 (2006).
19. Cui, X., Breitenkamp, K., Lotz, M. & D'Lima, D. Synergistic action of fibroblast growth factor-2 and transforming growth factor-beta1 enhances bioprinted human neocartilage formation. *Biotechnol. Bioeng.* **109,** 2357–2368 (2012).
20. Malda, J. *et al.* 25th anniversary article: Engineering hydrogels for biofabrication. *Adv. Mater.* **25,** 5011–28 (2013).
21. Bekkers, J. E. J. *et al.* Single-Stage Cell-Based Cartilage Regeneration Using a Combination of Chondrons and Mesenchymal Stromal Cells: Comparison With Microfracture. *Am. J. Sports Med.* **41,** 2158–2166 (2013).
22. Poole, C. A., Ayad, S. & Schofield, J. R. Chondrons from articular cartilage: I. Immunolocalization of type VI collagen in the pericellular capsule of isolated canine tibial chondrons. *J. Cell Sci.* **90 (Pt 4),** 635–643 (1988).
23. Zhang, Z. Chondrons and the Pericellular Matrix of Chondrocytes. *Tissue Eng. Part B Rev.* **21,** 267–277 (2015).
24. Ma, B. *et al.* Gene expression profiling of dedifferentiated human articular chondrocytes in monolayer culture. *Osteoarthr. Cartil.* **21,** 599–603 (2013).
25. Dominici, M. *et al.* Minimal criteria for defining multipotent mesenchymal stromal cells. The International Society for Cellular Therapy position statement. *Cytotherapy* **8,** 315–317 (2006).
26. Visser, J. *et al.* Endochondral bone formation in gelatin methacrylamide hydrogel with embedded cartilage-derived matrix particles. *Biomaterials* **37,** 174–182 (2015).
27. Acharya, C. *et al.* Enhanced chondrocyte proliferation and mesenchymal stromal cells chondrogenesis in coculture pellets mediate improved cartilage formation. *J. Cell. Physiol.* **227,** 88–97 (2012).
28. Mo, X. *et al.* Variations in the ratios of co-cultured mesenchymal stem cells and chondrocytes regulate the expression of cartilaginous and osseous phenotype in alginate constructs. *Bone* **45,** 42–51 (2009).
29. Windt, T. S. De *et al.* Direct Cell – Cell Contact with Chondrocytes Is a Key Mechanism in Multipotent Mesenchymal. *Tissue Eng. Part A* **21,** 2536–2547 (2015).
30. Jiang, Y. & Tuan, R. S. Origin and function of cartilage stem/progenitor cells in osteoarthritis. *Nat. Rev. Rheumatol.* **11,** 206–12 (2015).
31. Medvedev, S. P. *et al.* Human Induced Pluripotent Stem Cells Derived from Fetal Neural Stem Cells Successfully Undergo Directed Differentiation into Cartilage. *Stem Cells Dev.* **20,** 1099–1112 (2011).
32. Wei, Y. *et al.* Chondrogenic differentiation of induced pluripotent stem cells from osteoarthritic chondrocytes in alginate matrix. *Eur. Cell. Mater.* **23,** 1–12 (2012).
33. Vonk, L. A., de Windt, T. S., Slaper-Cortenbach, I. C. M. & Saris, D. B. F. Autologous, allogeneic, induced

pluripotent stem cell or a combination stem cell therapy? Where are we headed in cartilage repair and why: a concise review. *Stem Cell Res. Ther.* **6,** 94 (2015).

34. Panadero, J. A., Lanceros-Mendez, S. & Ribelles, J. L. G. Differentiation of mesenchymal stem cells for cartilage tissue engineering: Individual and synergetic effects of three-dimensional environment and mechanical loading. *Acta Biomater.* (2016). doi:10.1016/j.actbio.2016.01.037

35. Mardones, R., Jofré, C. M. & Minguell, J. J. Cell Therapy and Tissue Engineering Approaches for Cartilage Repair and/or Regeneration. *Int. J. Stem Cells* **8,** 48–53 (2015).

36. Vermonden, T., Censi, R. & Hennink, W. E. Hydrogels for Protein Delivery. *Chem. Rev.* **112,** 2853–2888 (2012).

37. Poldervaart, M. T. *et al.* Sustained release of BMP-2 in bioprinted alginate for osteogenicity in mice and rats. *PLoS One* **8,** e72610 (2013).

38. Sawkins, M. J. *et al.* Cell and protein compatible 3D bioprinting of mechanically strong constructs for bone repair. *Biofabrication* **7,** 035004 (2015).

39. Kesti, M. *et al.* Bioprinting Complex Cartilaginous Structures with Clinically Compliant Biomaterials. *Adv. Funct. Mater.* **25,** 7406–7417 (2015).

40. Ishida, O., Tanaka, Y., Morimoto, I., Takigawa, M. & Eto, S. Chondrocytes are regulated by cellular adhesion through CD44 and hyaluronic acid pathway. *J. Bone Miner. Res.* **12,** 1657–1663 (1997).

41. Levett, P. A. *et al.* A biomimetic extracellular matrix for cartilage tissue engineering centered on photocurable gelatin, hyaluronic acid and chondroitin sulfate. *Acta Biomater.* **10,** 214–223 (2014).

42. Levett, P. A., Hutmacher, D. W., Malda, J. & Klein, T. J. Hyaluronic acid enhances the mechanical properties of tissue-engineered cartilage constructs. *PLoS One* **9,** e113216 (2014).

43. Costa, P. F. *et al.* Additive manufacturing of scaffolds with dexamethasone controlled release for enhanced bone regeneration. *Int. J. Pharm.* (2015). doi:10.1016/j.ijpharm.2015.10.055

44. Lee, C. H. *et al.* Regeneration of the articular surface of the rabbit synovial joint by cell homing: a proof of concept study. *Lancet* **376,** 440–448 (2010).

45. Malda, J., Boere, J., van de Lest, C. H. A., van Weeren, R. P. & Wauben, M. H. M. Extracellular vesicles - new tool for joint repair and regeneration - IN PRESS. *Nat. Rev. Rheumatol.* (2016). doi:10.1038/nrrheum.2015.170

46. Miller, J. S. *et al.* Rapid casting of patterned vascular networks for perfusable engineered three-dimensional tissues. *Nature Materials* **11,** 768–774 (2012).

47. Lee, J.-S. *et al.* 3D printing of composite tissue with complex shape applied to ear regeneration. *Biofabrication* **6,** 024103 (2014).

48. Fedorovich, N. E. *et al.* Biofabrication of Osteochondral Tissue Equivalents by Printing Topologically Defined, Cell-Laden Hydrogel Scaffolds. *Tissue Eng. Part C Methods* **18,** 33–44 (2012).

49. Levato, R. *et al.* Biofabrication of tissue constructs by 3D bioprinting of cell-laden microcarriers. *Biofabrication* **6,** 035020 (2014).

50. Buckley, M. R., Gleghorn, J. P., Bonassar, L. J. & Cohen, I. Mapping the depth dependence of shear properties in articular cartilage. *J. Biomech.* **41,** 2430–2437 (2008).

51. Silverberg, J. L. *et al.* Structure-Function Relations and Rigidity Percolation in the Shear Properties of Articular Cartilage. *Biophys. J.* **107,** 1721–1730 (2014).

52. Griffin, D. J. *et al.* Mechanical characterization of matrix-induced autologous chondrocyte implantation (MACI®) grafts in an equine model at 53 weeks. *J. Biomech.* **48,** 1944–1949 (2015).

53. Klein, T. J., Malda, J., Sah, R. L. & Hutmacher, D. W. Tissue Engineering of Articular Cartilage with Biomimetic Zones. *Tissue Eng. Part B Rev.* **15,** 143–157 (2009).

54. Hollander, A. P., Dickinson, S. C. & Kafienah, W. Stem Cells and Cartilage Development: Complexities of a Simple Tissue. *Stem Cells* **28,** 1992–1996 (2010).

55. Benninghoff, A. Form und Bau der Gelenkknorpel in ihren Beziehungen zur Funktion. *Z. Anat. Entwicklungsgesch.* **76,** 43–63 (1925).

56. Carlier, A. *et al.* Computational model-informed design and bioprinting of cell-patterned constructs for bone tissue engineering. *Biofabrication* **8,** 025009 (2016).

57. Klein, T. J. *et al.* Strategies for Zonal Cartilage Repair using Hydrogels. *Macromol. Biosci.* **9,** 1049–1058 (2009).

58. Tatman, P. D. *et al.* Multiscale Biofabrication of Articular Cartilage: Bioinspired and Biomimetic Approaches. *Tissue Eng. Part B Rev.* **21,** 543–559 (2015).

59. Nguyen, L. H., Kudva, A. K., Saxena, N. S. & Roy, K. Engineering articular cartilage with spatially-varying matrix composition and mechanical properties from a single stem cell population using a multi-layered hydrogel. *Biomaterials* **32,** 6946–6952 (2011).

60. Kim, T.-K. *et al.* Experimental Model for Cartilage Tissue Engineering to Regenerate the Zonal Organization of Articular Cartilage. *Osteoarthr. Cartil.* **11,** 653–664 (2003).

61. Schuurman, W. *et al.* Bioprinting of hybrid tissue constructs with tailorable mechanical properties. *Biofabrication* **3,** 021001 (2011).

62. Moroni, L., de Wijn, J. R. & van Blitterswijk, C. A. Three-dimensional fiber-deposited PEOT/PBT copolymer scaffolds for tissue engineering: Influence of porosity, molecular network mesh size, and swelling in aqueous media on dynamic mechanical properties. *J. Biomed. Mater. Res. Part A* **75A,** 957–965 (2005).

63. Moroni, L., de Wijn, J. R. & van Blitterswijk, C. A. 3D fiber-deposited scaffolds for tissue engineering: Influence of pores geometry and architecture on dynamic mechanical properties. *Biomaterials* **27,** 974–985 (2006).

64. Boere, K. W. M. *et al.* Covalent attachment of a three-dimensionally printed thermoplast to a gelatin

2

hydrogel for mechanically enhanced cartilage constructs. *Acta Biomater.* **10,** 2602–2611 (2014).

65.   Hochleitner, G. *et al.* Additive manufacturing of scaffolds with sub-micron filaments via melt electrospinning writing. *Biofabrication* **7,** 035002 (2015).

66.   Visser, J. *et al.* Reinforcement of hydrogels using three-dimensionally printed microfibres. *Nat. Commun.* **6,** 6933 (2015).

67.   Xu, T. *et al.* Hybrid printing of mechanically and biologically improved constructs for cartilage tissue engineering applications. *Biofabrication* **5,** 015001 (2013).

68.   Costa, P. F. *et al.* Biofabrication of customized bone grafts by combination of additive manufacturing and bioreactor knowhow. *Biofabrication* **6,** 035006 (2014).

69.   Cohen, D. L., Lipton, J. I., Bonassar, L. J. & Lipson, H. Additive manufacturing for in situ repair of osteochondral defects. *Biofabrication* **2,** 035004 (2010).

70.   Cui, X., Breitenkamp, K., Finn, M. G. G., Lotz, M. & D'Lima, D. D. Direct human cartilage repair using three-dimensional bioprinting technology. *Tissue Eng. Part A* **18,** 1304–1312 (2012).

71.   O'Connell, C. D. *et al.* Development of the Biopen: a handheld device for surgical printing of adipose stem cells at a chondral wound site. *Biofabrication* **8,** 015019 (2016).

72.   Melchels, F. P. W., Dhert, W. J. A., Hutmacher, D. W. & Malda, J. Development and characterisation of a new bioink for additive tissue manufacturing. *J. Mater. Chem. B* **2,** 2282–2289 (2014).

73.   Cohen, D. L. *et al.* Increased Mixing Improves Hydrogel Homogeneity and Quality of Three-Dimensional Printed Constructs. *Tissue Eng. Part C Methods* **17,** 239–248 (2011).

74.   Halme, D. G. & Kessler, D. A. FDA Regulation of Stem-Cell–Based Therapies. *N. Engl. J. Med.* **355,** 1730–1735 (2006).

75.   Mironov, V., Kasyanov, V. & Markwald, R. R. Organ printing: from bioprinter to organ biofabrication line. *Curr. Opin. Biotechnol.* **22,** 667–673 (2011).

76.   Hutmacher, D. W. Bioprinting, biofabrication, biomanufacturing? The need for definitions and norms in additive manufacturing in the biomedical sciences. *MRS Bull.* **40,** (2015).

77.   Chhaya, M. P. *et al.* Additive manufacturing in biomedical sciences and the need for definitions and norms. *Expert Rev Med Devices* **12,** 537–43 (2015).

78.   Kang, K. H., Hockaday, L. A. & Butcher, J. T. Quantitative optimization of solid freeform deposition of aqueous hydrogels. *Biofabrication* **5,** 035001 (2013).

79.   Wüst, S., Godla, M. E., Müller, R. & Hofmann, S. Tunable hydrogel composite with two-step processing in combination with innovative hardware upgrade for cell-based three-dimensional bioprinting. *Acta Biomater.* **10,** 630–640 (2014).

80.   Billiet, T., Gevaert, E., De Schryver, T., Cornelissen, M. & Dubruel, P. The 3D printing of gelatin methacrylamide cell-laden tissue-engineered constructs with high cell viability. *Biomaterials* **35,** 49–62 (2014).

81.   Murphy, S. V, Skardal, A. & Atala, A. Evaluation of hydrogels for bio-printing applications. *J. Biomed. Mater. Res. - Part A* **101 A,** 272–284 (2013).

82.   Ballyns, J. J. *et al.* An Optical Method for Evaluation of Geometric Fidelity for Anatomically Shaped Tissue-Engineered Constructs. *Tissue Eng. Part C Methods* **16,** 693–703 (2010).

83.   Kundu, J., Shim, J.-H. H., Jang, J., Kim, S.-W. W. & Cho, D.-W. W. An additive manufacturing-based PCL-alginate-chondrocyte bioprinted scaffold for cartilage tissue engineering. *J. Tissue Eng. Regen. Med.* **9,** 1286–1297 (2015).

84.   Kesti, M. *et al.* A versatile bioink for three-dimensional printing of cellular scaffolds based on thermally and photo-triggered tandem gelation. *Acta Biomater.* **11,** 162–172 (2015).

85.   Markstedt, K. *et al.* 3D Bioprinting Human Chondrocytes with Nanocellulose–Alginate Bioink for Cartilage Tissue Engineering Applications. *Biomacromolecules* **16,** 1489–1496 (2015).

86.   Izadifar, Z., Chang, T., Kulyk, W., Chen, X. & Eames, B. F. Analyzing Biological Performance of 3D-Printed, Cell-Impregnated Hybrid Constructs for Cartilage Tissue Engineering. *Tissue Eng. Part C Methods* **22,** 173–188 (2016).

87.   Abbadessa, A. *et al.* A Synthetic Thermosensitive Hydrogel for Cartilage Bioprinting and Its Biofunctionalization with Polysaccharides. *Biomacromolecules* **17,** 2137–2147 (2016).

88.   Mouser, V. H. M. *et al.* Yield stress determines bioprintability of hydrogels based on gelatin-methacryloyl and gellan gum for cartilage bioprinting. *Biofabrication* **8,** 035003 (2016).

89.   Woodfield, T. B. F. *et al.* Design of porous scaffolds for cartilage tissue engineering using a three-dimensional fiber-deposition technique. *Biomaterials* **25,** 4149–4161 (2004).

90.   Woodfield, T. B. F. *et al.* Polymer scaffolds fabricated with pore-size gradients as a model for studying the zonal organization within tissue-engineered cartilage constructs. *Tissue Eng.* **11,** 1297–1311 (2005).

91.   Schuurman, W. *et al.* Three-dimensional assembly of tissue-engineered cartilage constructs results in cartilaginous tissue formation without retainment of zonal characteristics. *J. Tissue Eng. Regen. Med.* n/a–n/a (2013). doi:10.1002/term.1726

92.   Shim, J.-H., Lee, J.-S., Kim, J. Y. & Cho, D.-W. Bioprinting of a mechanically enhanced three-dimensional dual cell-laden construct for osteochondral tissue engineering using a multi-head tissue/organ building system. *J. Micromechanics Microengineering* **22,** 085014 (2012).

Chapter 3

Yield stress determines bioprintability of hydrogels based on gelatin-methacryloyl and gellan gum for cartilage bioprinting

Vivian H. M. Mouser
Ferry P. W. Melchels
Jetze Visser
Wouter J. A. Dhert
Debby Gawlitta
Jos Malda

Abstract

Bioprinting of chondrocyte-laden hydrogels facilitates the fabrication of constructs with controlled organization and shape *e.g.* articular cartilage implants. Gelatin-methacryloyl (gelMA) supplemented with gellan gum is a promising bio-ink. However, the rheological properties governing the printing process, and the influence of gellan gum on the mechanical properties and chondrogenesis of the blend, are still unknown. Here, we investigated the suitability of gelMA/gellan for cartilage bioprinting.

Multiple concentrations, ranging from 3-20% gelMA with 0-1.5% gellan gum, were evaluated for their printability, defined as the ability to form filaments and to incorporate cells at 15-37°C. To support the printability assessment, yield stress and viscosity of the hydrogels were measured. Stiffness of UV-cured constructs, as well as cartilage-like tissue formation by embedded chondrocytes, were determined *in vitro*.

A large range of gelMA/gellan concentrations were printable with inclusion of cells and formed the bioprinting window. Addition of gellan gum improved filament deposition by inducing yielding behavior, increased construct stiffness, and supported chondrogenesis. High gellan gum concentrations, however, did compromise cartilage matrix production and distribution, and even higher concentrations resulted in too high yield stresses to allow cell encapsulation.

This study demonstrates the high potential of gelMA/gellan blends for cartilage bioprinting and identifies yield stress as a dominant factor for bioprintability.

1. Introduction

Additive manufacturing techniques *e.g.* bioprinting, melt electrospinning, and stereolithography, allow the fabrication of organized three-dimensional (3D) constructs to regenerated or replace damaged tissues[1–3]. Especially, bioprinting is a promising technique to create such tissue-engineered constructs, as it allows accurate positioning of cells and biomaterials in a layered fashion[1,4]. As a result, constructs with controlled porosity to provide optimal diffusion of nutrients, oxygen, and waste products for embedded cells can be fabricated.

Bioprinting techniques are rapidly advancing, yet, the search for suitable bioprinting materials, the so-called 'bio-inks', remains challenging[2,5]. Multiple physicochemical material properties that are favorable for printing have been identified *e.g.* fast gelation after extrusion (thermo-gelation and/or cross-linking), high viscosity, yielding behavior, and shear thinning[4,6]. However, it is not clear what the most dominant properties are and in what range these parameters should be to ensure printing with high shape-fidelity. Additionally, a bio-ink should allow the incorporation of cells and should have biological properties to support cell survival, differentiation, and tissue formation.

Hydrogels seem to be the most promising basis for bio-inks, as they can mimic the natural cell habitat and have a high water content, which supports cell survival and facilitates a homogeneous cell distribution inside the 3D structure. Additionally, hydrogels allow the formation of constructs with various shapes and mechanical properties, and relevant biological and chemical cues can be easily incorporated. Nonetheless, it is difficult to unite the appropriate physicochemical and biological material properties in one hydrogel system. Highly viscous hydrogels with high cross-linking densities are favorable to fabricate constructs with high shape-fidelity. Contrarily, liquid hydrogels with low crosslinking densities are more favorable for the differentiation of cells[7,8].

Several hydrogel systems have been explored for their potential as a bio-ink, including hydrogels based on collagen[9], gelatin[10–12], hyaluronic acid[13], chitosan[14], alginate[15], poly(ethylene glycol)[16], hydroxyethyl-methacrylate-derivatized dextran[17], and poly(N-hydroxypropyl-methacrylacrylamide lactate)[18]. Of these, gelatin has great potential for bioprinting as it exhibits thermo-gelation to support the printing process and it contains inherent cell adhesion domains, low immunogenicity, and can be degraded enzymatically to support cells in their tissue formation[19,20]. Furthermore, gelatin can be functionalized with methacrylamide and (to a lesser extent) methacrylate groups to enable cross-linking with UV light, which can permanently fix the shape of a printed construct and thus generates mechanical stability[21].

Important targets for the implantation of 3D printed, tissue-engineered constructs, are articular cartilage defects. As, articular cartilage lacks vasculature and innervation, and contains only few chondrocytes, it has low self-renewal capacity[22,23]. Additionally, bioprinting provides the opportunity to replicate the zonal organization of articular cartilage, by combining multiple biomaterials and/or cells in a single construct[11,24]. Recent studies have shown that gelatin-methacryloyl (gelMA) supports cartilage-like tissue formation of both mesenchymal stem cells and chondrocytes *in vitro*[10,25–27]. Hence, gelMA-based hydrogels are extremely interesting for the treatment of cartilage defects.

The suitability of gelMA as a bio-ink for the printing of 3D structures has also been demonstrated[12]. However, printing gelMA on its own requires relatively high polymer concentrations, ultra-precise control of ink and nozzle temperatures, and cooling of the building platform, as gelMA has low viscosity and relatively slow thermal gelation[12].

Recently, Melchels et al. (2014)[28] demonstrated that the addition of gellan gum to a gelMA hydrogel can significantly increase the viscosity and speed of gelation of the hydrogel blend. This effect is due to the ionic cross-links that gellan gum can form with gelMA and itself, which induces pseudo-plasticity (a form of shear thinning) and yield stress[28]. Additionally, gellan gum is known to support the chondrogenic potential of mesenchymal stem cells and chondrocytes *in vivo*[29].

The demonstration of the beneficial effect of gellan gum on the printablity of gelMA is a promising step forward for the 3D bioprinting of gelMA-based cartilage repair constructs. However, further evaluation is essential as this effect was only demonstrated for one gelMA/gellan concentration. Additionally, the influence of gellan gum on the mechanical properties of the UV cross-linked blends and on the chondrogenic potential of embedded cells is yet unknown. Therefore, the aim of this study is to relate different concentrations and ratios of gelMA/gellan to the hydrogel's printability (filament formation and deposition), mechanical properties, and chondrogenic potential. We expect not only to find the optimal compositions for cartilage bioprinting, but also to identify the rheological property or properties that dictate bioprinting behavior. Consequently, this paper reveals the cartilage bioprinting window for gelMA/gellan blends.

2. Materials and methods

2.1. Preparation of polymer solution

GelMA was synthesized by reacting gelatin (Sigma Aldrich, type A from porcine skin, 175g Bloom; Zwijndrecht, the Netherlands) with methacrylic anhydride (Sigma Aldrich) as previously described[28]. The polymer was freeze-dried and stored at -20°C until further use.

Irgacure 2959 (gift from BASF, Ludwigshafen, Germany) was dissolved in MilliQ with 10% PBS v/v (optimal salt concentration for the ionic interaction of gelMA with gellan gum[28]) at 70°C for 20 minutes, to a final concentration of 0.1% w/v. To generate an isotonic solution, 4.86% D-(+)-mannose (Sigma Aldrich) was added. The solution was filter-sterilized and used to dissolve gelMA and low-acyl gellan gum (Gelzan™ CM, Gelrite®; Sigma Aldrich) at different concentrations, as shown in Figure 1.

2.2. Screening of filament formation

Multiple polymer concentrations and ratios (Figure 1) were prepared, aspirated in a 3 ml Luer Lock syringe with a 23 gauge metal needle (Precision Tip PN 7018302, Nordson EFD, Bedfordshire, England), and loaded into the BioScaffolder dispensing system (SYS+ENG, Salzgitter-Bad, Germany). The BioScaffolder fabricates 3D structures by coordinated motion of, in this case, a piston-driven dispensing head while depositing on a stationary platform. The syringe temperature was varied from 37°C to 15°C in the
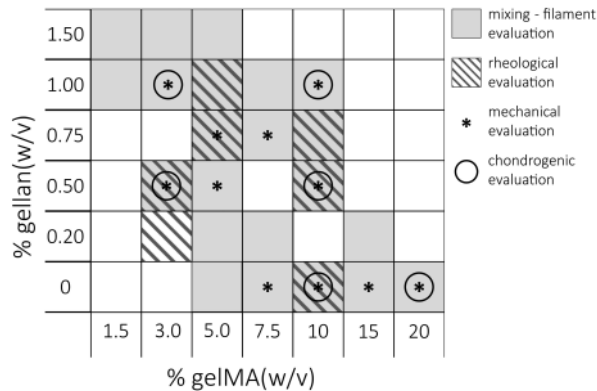
Figure 1. A schematic overview of all evaluated gelMA/gellan concentrations. *Hydrogel formulations were evaluated for their printability at 15-37°C, and the ability to mix them with a cell pellet at 37°C (grey), rheological properties (hatched grey), mechanical properties after UV cross-linking (*), and for cartilage-like tissue formation of embedded chondrocytes (◯).*

dispensing head and the ability to deposit a filament was evaluated. First, the shape of the polymer solution at the nozzle was observed. When a droplet formed, as described by Schuurman *et al.* (2013)[10], the print temperature was considered too high and would be reduced until a continuous filament was formed at the nozzle. When a filament could be formed, *Π*-shaped lines were printed. A polymer solution was considered printable if a *Π*-shape could be printed without corrugation, droplet formation or interruptions in the final structure. If corrugations occurred the printing temperature was considered too low and if droplets formed the printing temperature was considered too high (Figure 2). Images of the deposited filaments were made with a stereomicroscope (Olympus SZ61, SZ2-ILST, Olympus DP70 camera, Hamburg, Germany). Furthermore, the possibility to mix cell into the polymer solution using a gel pipette was assessed at 37°C. The mixing was considered successful if the cells were completely resuspended and no air bubbles or lumps appeared in the cell-laden polymer solution.

2.3. Rheometry
To support the filament printing observations, rheological measurements were performed on selected hydrogel compositions (Figure 1) using an AR G-2 rheometer (TA-Instruments, Etten-Leur, the Netherlands) equipped with a cone-plate geometry (cone diameter: 20 mm; angle: 1°; gap: 300 µm). For a selection of printable gels (3/0.5%; 10/0%; 10/0.5% gelMA/gellan), yield stress was measured in duplicate at the observed optimal temperatures for filament deposition (logarithmic flow ramp, loading temperature: 80°C, after loading the temperature was reduced to the measuring temperature and an additional 120 seconds was waited to ensure the whole sample contained the proper temperature, stress: 0.1-1000 Pa; duration of measurement: 5 minutes). To explore the lower boundary of the bioprinting window, the yield stress was measured at 15°C for the 3/0.2% gelMA/gellan formulation, which did not form a filament between 15°C and 37°C. To explore the upper boundary of the bioprinting window, the yield stress was
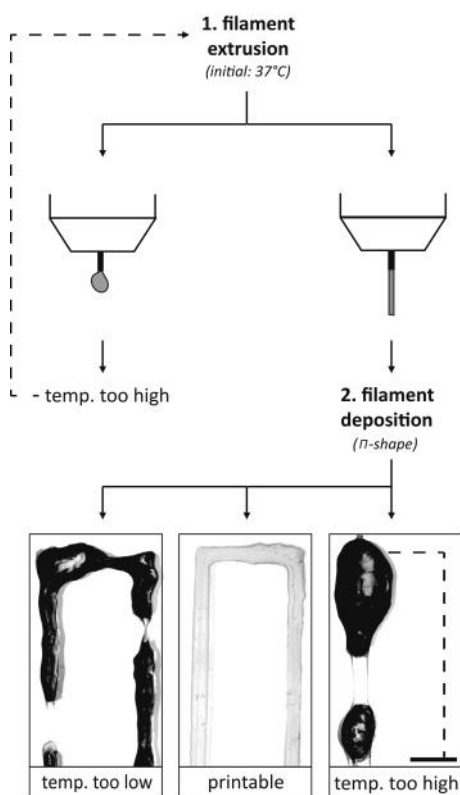
3

Figure 2. A schematic overview of the iterative hydrogel filament screening process. *First filament extrusion was evaluated (1), when the temperature was too high (droplet formation) it was lowered and evaluated again, and when a certain temperature allowed filament extrusion, the appearance of the deposited filament was evaluated by printing a Π-shape (2). The print temperature was adjusted until a smooth filament was formed or until an endless loop occurred which meant that the hydrogel formulation was unprintable at a temperature of 15 - 37°C. The irregularities of the filament surface cause light scatter, which turns black on the pictures. Scale bar represents 2 mm and the dotted line in the printed structures represents the missing part of the Π-shape.*

measured for multiple gel formulations just below and above this boundary (5/0.75%, 5/1%, 10/0.5% and 10/0.75% gelMA/gellan) at 37°C (flow ramp, loading temperature: 80°C, when measuring temperature is reached wait 10 minutes, stress: 10-10,000 Pa; duration: 5 minutes). In addition, the viscosity of these four formulations was measured in flow in triplicate at 37°C (flow peak hold, wait for temperature, shear rate: 300/s, duration: 20 minutes). All polymer solutions were freshly prepared as described in the section 'preparation of polymer solution' before the measurements. The yield stress was defined as the stress at which the polymer solution first started to flow, indicated as the first read-out of shear rate and viscosity on the rheometer. The corresponding viscosity drop was determined by the difference in viscosity at the yield stress and at a ten times higher stress. When the graph reached a plateau before it reached a ten times higher stress, the difference between the viscosity at the yield stress and the viscosity at the plateau was reported for the viscosity drop. The hydrogel viscosity was defined as the average viscosity of the final 10 minutes of the viscosity measurement.

2.4. Construct stiffness
Cell-free samples (n = 3) were prepared by injecting the different polymer solutions (Figure 1) into custom-made cylindrical Teflon molds (diameter: 6 mm; height 2 mm). Next, samples were UV cross-linked by exposure to 365 nm UV light (2.6 mW/cm^2, UVP CL-

1000) for 15 minutes. After removing the hydrogels from the molds, they were incubated in DMEM/F-12+GlutaMax-1 (Dulbecco's Modified Eagle Medium, 31331, Invitrogen, Carlsbad, California, USA) supplemented with 5% heat-inactivated fetal bovine serum (FBS, Biowhittaker, Breda, the Netherlands) and pen/strep (final concentration 100 units/ml penicillin and 100 μg/ml streptomycin, Gibco) for 24 hours at 37°C. A stress/strain curve was obtained for each hydrogel construct under unconfined compression using a Dynamic Mechanical Analyzer (DMA, Q800 TA-Instrument) to determine the Young's modulus. The hydrogel constructs (three for each condition) were subjected to a preload force of 0.001 N and subsequently compressed with a force ramp rate of 0.5 N/min and an upper force limit of 1.5 N. The Young's modulus was calculated as the initial slope (around 2% strain) of the stress/strain curve.

2.5. Cell isolation

To obtain primary chondrocytes, full-thickness cartilage was harvested under sterile conditions from the stifle joints of fresh equine cadavers (3 donors; 3–10 years old; with consent of the owners). The horses had macroscopically healthy cartilage. Cartilage samples were digested overnight at 37°C in DMEM (61965, Invitrogen) supplemented with 0.15% collagenase type II (Worthington Biochemical Corp, Vollenhove, the Netherlands). After incubation, the suspension was filtered through a 100 μm cell strainer and the chondrocytes were washed and stored at passage 0 in liquid nitrogen until further use.

2.6. Chondrocyte culture and construct preparation

To evaluate chondrogenesis, primary chondrocytes (passage 0) were expanded for ~14 days (seeding density of $5*10^3$ cells/cm^2) in monolayer culture with chondrocyte expansion medium, consisting of DMEM (61965, Sigma Aldrich), 10% heat-inactivated FBS (Biowhittaker), 2.5% HEPES buffer solution (1M, final concentration 25mM, 15630, Gibco), pen/strep, and 10 ng/ml FGF-2 (R&D Systems, Abingdon, UK). Cells were trypsinized and used when they reached a confluence of 80-90%.

Equine chondrocytes (3 donors, passage 1) were resuspended in the different gelMA/gellan polymer solutions at 37°C, with a cell density of $10\text{-}20*10^6$ cells/ml (differences in cell density were between cell donors; for each donor, all hydrogel formulations were prepared with the same cell density). Exceptions were the 20% gelMA and 10/1% gelMA/gellan groups, which were mixed with the cells at 40°C since thermo-gelation occurred at 37°C. Cell-laden hydrogels were cast in rectangular custom-made Teflon molds with a glass microscope slide on top and cross-linked by exposure to UV light as described above. After cross-linking, the hydrogel strips were cut into pieces of ca. 4 x 4 x 2 mm. The separate pieces were cultured in chondrogenic differentiation medium consisting of DMEM with 0.4 mM ascorbic acid (A8960, Sigma Aldrich), 1% Insulin-Transferrin-Selenium-X (31500, Gibco), 2.5% HEPES buffer solution (1M, final concentration 25mM, Gibco), 2% human serum albumin (Albuman 200g/L, final concentration 4g/L, Sanquin, the Netherlands), pen/strep, and 5 ng/mL TGF-β2 (302-B2, R&D Systems). Culture medium was refreshed twice a week and three samples for each gel formulation were harvested per cell donor at days 0, 14, 28, and 42.

2.7. Evaluation of chondrogenesis

2.7.1. Histology & Immunohistochemistry
At days 0, 14, 28, and 42, the cell-laden samples were harvested and half of each sample was fixed in formalin, dehydrated through a graded ethanol series, cleared in xylene and embedded in paraffin. Subsequently, 10 μm thick sections were cut from the embedded samples. Sections were stained with safranin-O to visualize glycosaminoglycans (GAGs), fast green to visualize collagen, and hematoxylin to stain cell nuclei[30].

Immunohistochemistry was used to visualize collagen type II distribution. Samples were deparaffinized with xylene and hydrated through graded ethanol series. After blocking for 10 minutes with H_2O_2 (0.3% in PBS), antigens were retrieved with pronase (1 mg/ml PBS, Roche life science, 11459643001, Indiana, USA) and hyaluronidase (10 mg/ml PBS, H2126, Sigma Aldrich) for 30 minutes at 37°C each. The primary antibody (DSHB, II-II6B3, dilution 1/100) was incubated overnight at 4°C. Mouse IgG (DAKO, X0931, same dilution as the primary antibody) was used as a negative control. The sections were incubated with the secondary antibody (final concentration: 1 μg/ml, IgG HRP, DAKO, P0447) for 60 minutes at room temperature. Next, the staining was developed with DAB peroxidase substrate solution (Sigma Aldrich) for 5-10 minutes. Counterstaining was performed with Mayer's Hematoxylin and after dehydration and clearing with xylene, the sections were mounted with DPX (100579, Merck Millipore, Billerica, MA, USA). All stained sections were evaluated and photographed using a light microscope (Olympus BX51 microscope, Olympus DP70 camera, Hamburg, Germany).

2.7.2. Biochemical assays
The remaining halves of the harvested cell-laden hydrogels were used for biochemical analysis. The samples were weighted (wet weight), freeze dried overnight and weighed again (dry weight). To determine the GAG and DNA contents, the samples were digested overnight at 56°C in 200 μL papain digestion buffer (0.2 M NaH_2PO_4 + 0.01 M EDTA*2 H_2O in milliQ, pH = 6.0) supplemented with 250 μL/mL papain solution (16-40 units/mg protein, P3125, Sigma Aldrich) and 0.01 M cysteine (C9768, Sigma Aldrich). The amount of sulfated GAGs, as a measure of proteoglycans, was determined with a dimethylmethylene blue (DMMB, pH = 3.0) assay[31] using known concentrations of chondroitin sulfate C (Sigma Aldrich) as a reference. In short, samples were diluted in PBS-EDTA and mixed with the DMMB solution. Excitation was measured directly after mixing, at 525 nm and 595 nm with a versa max plate reader (Molecular devices, Wokingham, UK). The measurement at 525 nm was divided by the measurement at 595 nm and the GAG concentration of the samples was calculated from a quadratic fit of the standard curve and were corrected for the dilution. Quantification of DNA was performed with a Quant-iT PicoGreen dsDNA kit (Molecular Probes, Invitrogen) using a spectrofluorometer (Biorad, Veenendaal, the Netherlands).

2.8. Statistics
Statistical analyses were performed using SPSS software (version 20, IBM Corporation,

USA). The Young's moduli of the different gelMA/gellan concentrations were compared with a one-way ANOVA. To compare GAG production normalized to DNA in the different chondrocyte laden hydrogels per time point, a Randomized Block Design ANOVA was used (to correct for donor variability). The same test was used to compare DNA content normalized to the sample wet weight at the different time points per hydrogel formulation. For all tests, normality and homogeneity were assumed and, when significant differences were detected (significance level of 0.05), a Bonferroni post-hoc test was performed.

3. Results

3.1. Hydrogel filament screening

Multiple gelMA/gellan concentrations were evaluated for their ability to form a filament at cell-friendly temperatures (15-37°C). A well-defined filament of gelMA could be printed with a concentration of 7.5% w/v or higher, but only at specific, precise temperatures (Figure 3). By adding small amounts of gellan gum (0.5-1%) the minimally required gelMA concentration for filament formation could be reduced to 3% w/v and defined filaments could be formed at a wider temperature range compared to gelMA only solutions. The lowest evaluated polymer concentrations formed droplets at the nozzle and were, therefore, not considered suitable for printing. Additionally, it was investigated whether a cell pellet could be resuspended at 37°C. Hydrogels with the highest evaluated total polymer concentrations gelled at or above 37°C, disallowing the suspension of a cell pellet. Hydrogel compositions that met both criteria of forming defined filaments at a temperature in the range of 15-37°C, and being sufficiently fluid at 37°C to allow cell encapsulation, define the bioprinting window (red outline in Figure 3). With these formulations, 3D constructs with high shape-fidelity could be printed (Figure 3B-D).
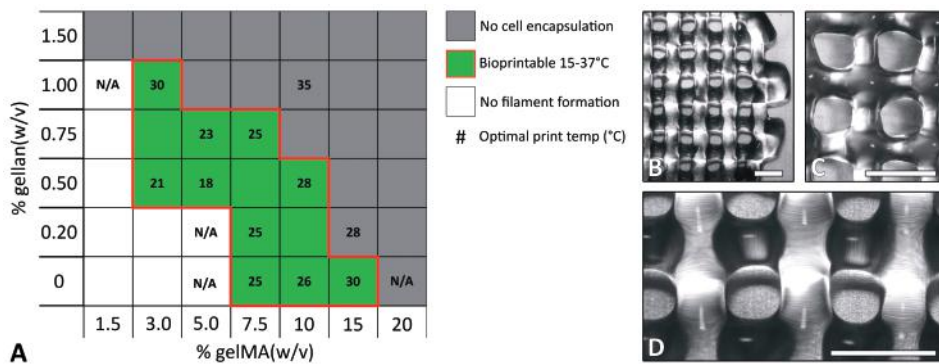
Figure 3. The bioprinting window for gelMA and gellan gum hydrogels (bordered by red line) and examples of printed constructs. A) Low polymer concentrations were too fluid to form a defined filament at 15 - 37°C (white), while high polymer concentrations formed too strong physical gels at 37°C to allow mixing with cells (dark grey). The middle range of polymer concentrations was suitable for bioprinting (green) although different optimal print temperatures were found (numbers in °C, for some formulations no optimal (cell-friendly) temperature could be found (N/A)). B) Image of a 3/1% gelMA/gellan construct printed at 30°C. C) Image of a 10/0.5% gelMA/gellan construct printed at 28°C. D) magnification of figure B. Scale bars represent 2 mm.

Stress ramps were performed for a selected number of gelMA/gellan hydrogels (3/0.2%, 3/0.5%, 10/0% and 10/0.5%) at the observed optimal temperature for filament deposition or at 15°C for 3/0.2% gelMA/gellan, which did not form a filament between 15-37°C. All evaluated formulations showed a decrease in viscosity with increasing shear rate (Figure 4A). The yield stress, defined as the minimal stress necessary to induce flow in the polymer solution, was found to strongly correlate to the gellan gum concentration and was further increased by increasing the amount of gelMA (Figure 4B). The 3/0.2% gelMA/gellan formulation showed a gradual decrease in viscosity with increasing stress. A slightly steeper curve was observed for the 3/0.5% gelMA/gellan formulation and an even steeper curve was observed for the 10% gelMA formulation. An almost vertical curve was observed for the 10/0.5% gelMA/gellan formulation. For all measured formulations the viscosity drop (over the first decade of stress) after the yield point was calculated and was found to be largest for the formulation with 0.5% gellan gum. Finally, the yield stress and viscosity were measured at 37°C for 5/0.75%, 5/1%, 10/0.5% and 10/0.75% gelMA/gellan hydrogels to investigate what determined the ability to mix in cells (Figure 5). No difference in viscosity was observed between the groups, however, the yield stress and correlated viscosity was lower for 5/0.75% and 10/0.5% gelMA/gellan hydrogels compared to 5/1% and 10/0.75% gelMA/gellan formulations, which agreed with qualitative observations on the ability to resuspend cells in the hydrogels.
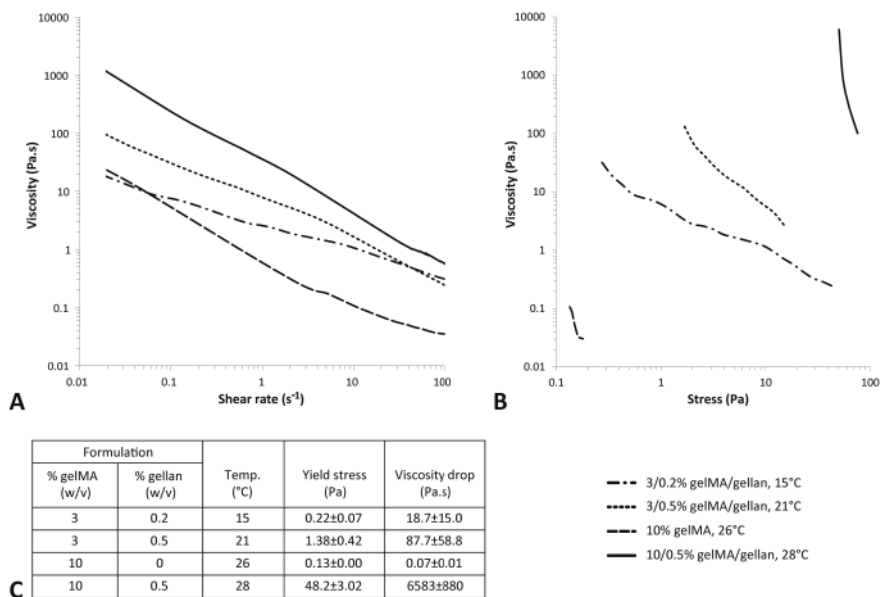

Formulation		Temp. (°C)	Yield stress (Pa)	Viscosity drop (Pa.s)
% gelMA (w/v)	% gellan (w/v)			
3	0.2	15	0.22±0.07	18.7±15.0
3	0.5	21	1.38±0.42	87.7±58.8
10	0	26	0.13±0.00	0.07±0.01
10	0.5	28	48.2±3.02	6583±880

Legend:
−·− 3/0.2% gelMA/gellan, 15°C
····· 3/0.5% gelMA/gellan, 21°C
−·− 10% gelMA, 26°C
─── 10/0.5% gelMA/gellan, 28°C

Figure 4. Rheological measurements to support filament printing observations. *The viscosity decreased for increasing shear rates for all formulations (A). Yield stress and corresponding viscosity drop differed between formulations (B, C). Measurements were performed at the optimal bioprinting temperatures or at 15°C when no filament could be printed (C). Please note the logarithmic axes and that the viscosity drop was measured over 1 decade of stress starting from the yield stress, except for 10% gelMA which reached a plateau before one decade difference.*
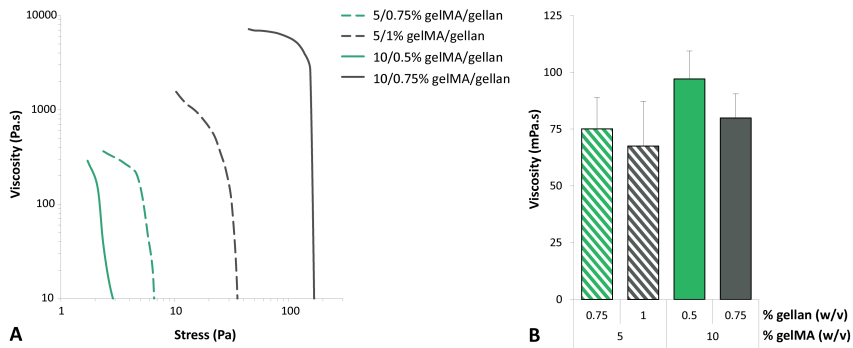
Figure 5. Quantitation of rheological parameters that determine the ability to mix in cells. *In green the formulations inside the bioprinting window and in grey the corresponding formulations above the bioprinting window. Yield stress and initial viscosity were relatively high for the formulation in which no cells could be resuspended (grey lines in A) while the viscosity, in flow, was similar for all the formulations (B, shear rate = 300/s). All measurements were performed at 37°C. Please note the logarithmic scales in figure A.*

3

3.2. Mechanical evaluation

The Young's moduli were determined for multiple gelMA/gellan concentrations in unconfined compression. For each concentration, cell-free constructs were measured at equilibrium swelling on day 1 (Figure 6). Young's moduli varied between the different groups in a range of 2.7-186 kPa. Three smaller ranges in Young's moduli could be determined; 3/0.5%, 5/0.5% gelMA/gellan and 7.5% gelMA hydrogels had Young's moduli between 10-20 kPa, 3/1%, 5/0.75%, 1.5/0.75% gelMA/gellan and 10% gelMA formulations exhibited Young's moduli between 20-30 kPa and hydrogel formulations with higher total polymer concentrations showed Young's moduli in a range of 40-186 kPa.
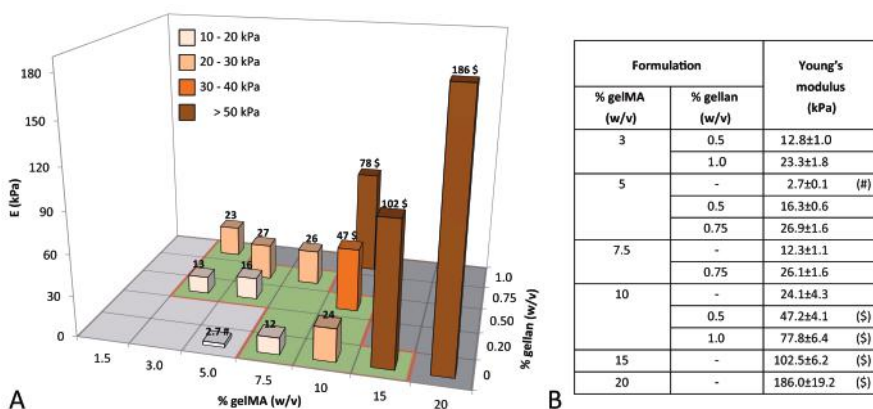

Figure 6. A grafical representation (A) and the absolute values (B) of the compressive Young's moduli (kPa) of UV cross-linked hydrogels for all evaluated concentrations. *(#) Significantly different from the Young's modulus of 3/1%, 5/0.75%, 7.5/0.75% gelMA/gellan and 10% gelMA. ($) Significantly different from all other groups.*

3.3. Matrix production and accumulation

All gelMA/gellan formulations that were evaluated for supporting chondrogenesis allowed the deposition of cartilaginous matrix by the embedded chondrocytes. For samples from all formulations, the presence of GAGs was confirmed by safranin-O staining after 28 days of culture (data not shown). This staining was more intense and more homogeneous in the samples of day 42 (Figure 7). A similar pattern was found for the deposition of collagen type II. The distribution of cell-secreted matrix varied, depending on the polymer concentrations. Safranin-O and collagen type II stainings revealed homogeneous matrix deposition in the samples with low total polymer concentrations (3-10% gelMA with 0-1% gellan), while matrix clusters were visible around the cells in the 20% gelMA constructs and to a lesser extent in the 10/1% gelMA/gellan constructs.
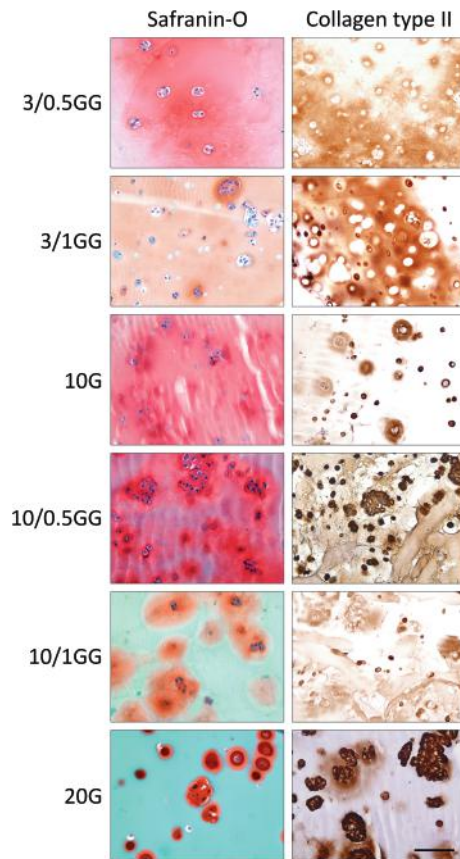
Figure 7. Extracellular cartilage matrix production after 42 days of differentiation culture. All hydrogel formulations supported GAG (column 1, in red) and collagen type II (column 2, in brown) formation of chondrocytes. Scale bar represents 100 µm for all images, G = gelMA, GG = gelMA/gellan. As gelMA is generated from denatured collagens it stains green with the Fast Green staining.

For all cultured formulations, quantitative GAG and DNA measurements were performed at days 0, 14, 28, and 42 (Figure 8). All hydrogel formulations showed an increase in GAG/DNA content during the culture period. However, after 14 days of culture the 3/0.5% and 3/1% gelMA/gellan groups had significantly lower GAG/DNA values than

the other hydrogel formulations. This trend remained visible during the final weeks of culture. At day 28, significantly higher GAG/DNA values were measured in 10% gelMA gels compared to all other groups. However, after 42 days of culture no significant differences were observed between the 10% gelMA, 10/0.5% gelMA/gellan and 20% gelMA groups. GAG normalized to the sample's wet weight showed an increase over time for all hydrogel formulations (data not shown). DNA normalized to the sample's wet weight showed a significant decrease over time for the 3/1% gelMA/gellan samples. The 3/0.5% gelMA/gellan hydrogels showed an increase in the first 14 days of culture and a decrease in the remaining culture period, while the DNA content increased during the first 28 days of culture in the 10% and 20% gelMA and 10/0.5% gelMA/gellan hydrogels. In the 10/1% gelMA/gellan hydrogels, no significant change in DNA per wet weight was observed over time.

3
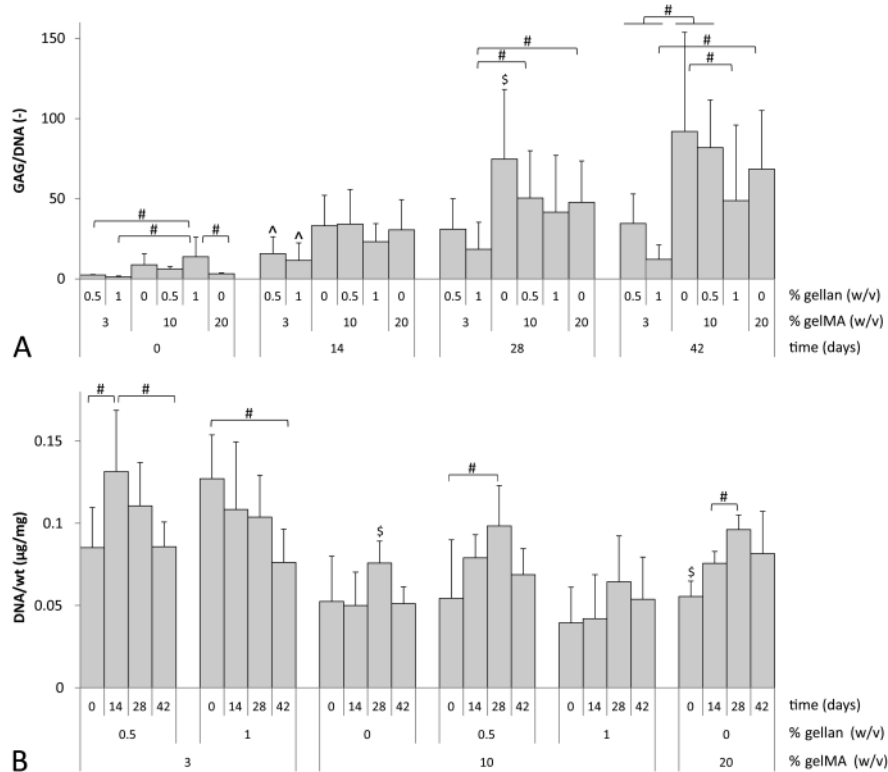
Figure 8. GAG and DNA content for all hydrogel formulations at days 0, 14, 28, and 42 of differentiation culture. A) For all groups GAG normalized to DNA increased during the culture period. Highest levels were reached in the 10% gelMA and 10/0.5% gelMA/gellan hydrogels. B) DNA content normalized to the sample's wet weight (wt) decreased for the 3/0.5% and 3/1% gelMA/gellan hydrogels during culture. The other hydrogels showed an increase of DNA during the culture period. #) significant difference between both indicated groups (p<0.05), ^) significantly different from all other groups at the time point but equal to each other, $) significantly different from all other groups at that time point (A) or gel formulation (B).

3

4. Discussion

The findings of this study reveal the bioprinting window of gelMA/gellan hydrogel blends. The lowest evaluated total polymer concentrations were too fluid for filament deposition and formed droplets at the printer nozzle, while the highest evaluated concentrations formed physical gels that appeared too solid to allow cell incorporation at 37°C. The bioprinting window of gelMA/gellan is defined as the intermediate area, in which both requirements of filament formation and miscibility with cells are met.

Although all evaluated gelMA/gellan compositions within the bioprinting window met both requirements and thus are suitable for bioprinting, different compositions possessed different material properties. Polymer solutions containing gellan gum allowed the deposition of filaments with less fine-tuning and optimization of print temperatures and printer settings, compared to their respective gelMA-only controls. This effect can be explained by the ionic cross-links that gellan gum forms with gelMA and itself, which induce pseudo-plastic behavior (a form of shear thinning)[28] and an increase in yield stress, whereas gelMA-only gels rely mostly on thermal gelation to occur during and directly after deposition[12,28]. Indeed, increased shear rate significantly reduced the viscosity for all evaluated formations. Even the 3/0.2% gelMA/gellan formulation, which could not form filaments at the nozzle of the bioprinter, showed shear thinning at 15°C. This demonstrates that shear thinning behavior is not the material property dictating filament formation and deposition. Instead, the polymer solutions that appeared printable within a broad range of conditions, exhibited relatively high yield stresses at the optimal print temperature (*e.g.* 48.2±3.0 Pa for 10/0.5% gelMA/gellan gum). At this stress, the yielding of the polymer solutions resulted in a steep viscosity drop (*e.g.* by 6.58±0.88 kPa·s for 10/0.5% gelMA/gellan). In contrast, the polymer solutions that could not form a filament within the 15-37°C range (*e.g.* 3/0.2% gelMA/gellan) did not exhibit clear yield behavior. These findings demonstrate that high yield stresses at which the viscosity reduces rapidly result in high printability of the polymer solution.

To better understand the upper boundary of the bioprinting window, two formulations below the boundary (5/0.75% and 10/0.5% gelMA/gellan) and the two corresponding concentrations above the boundary (5/1% and 10/0.75% gelMA/gellan) were evaluated for their viscosity and yield stress. Strikingly, the viscosity, when measured in flow, was the same for all four hydrogel formulations. Additionally, the measured values were within the range of previously reported viscosities for 10% gelMA and 20% gelMA polymer solutions[12]. However, the yield stresses and initial viscosities were higher in the formulations above the bioprinting window compared to their corresponding formulation in the bioprinting window. This implies that in gelMA/gellan blends, it is not the viscosity of the polymer solution that limits the miscibility with cells. Instead, the miscibility thus depends on the strength of the physical gel, which must be overcome in order to pipette the polymer solution. The transition from a gelMA/gellan formulation that can be mixed with a cell pellet to a formulation that cannot be mixed, lies in the yield stress range of 2-10 Pa.

This role of yield stress on the printability (filament formation and deposition) and miscibility with cells of a hydrogel has rarely been acknowledged in literature. Usually

other rheological properties such as viscosity and shear thinning are stated as the most important parameters governing printability, while the viscosity is stated as the limiting factor for miscibility with cells[1,2,4,26,32–38]. Our observations demonstrate a crucial role of yield stress in both cell miscibility and filament formation and deposition. We highly recommend evaluating yield behavior in future bio-ink research and development, which will validate the universality of our observations for other gel systems.

The addition of gellan gum increased the stiffness of UV cured constructs. By changing the concentrations of gelMA and/or gellan gum, the construct stiffness could be tailored over a range from 2.7-186 kPa. The stiffness depended more strongly on the gellan gum concentration than on that of gelMA. Adding only 1% gellan gum to any of the evaluated gelMA concentrations, increased the Young's modulus with approximately ~30-40 kPa. By varying the gelMA and gellan concentrations, constructs with similar Young's moduli but with different compositions could be generated. The stiffest hydrogel constructs within the bioprinting window contained 15% gelMA and had a stiffness of 102.5±6.2 kPa. Even stiffer hydrogel constructs could be generated (*e.g.* 186.0±19.2 kPa for 20% gelMA). However, these hydrogels are not suitable for the incorporation of cells but may have other potential applications.

Besides gellan gum also hyaluronic acid is a viscosity enhancer that has been applied in bioprinting[10,39]. Similar increases in Young's moduli were observed for 10% gelMA hydrogels supplemented with hyaluronic acid as obtained in the current study with the gellan gum[25,40]. Although significant increases in the construct stiffness can be achieved with the addition of gellan gum, this is obviously not within the range of the reported stiffness of native cartilage, *i.e.* 400 − 800 kPa[41–43]. In addition, cell encapsulation in a hydrogel system is known to reduce the initial construct stiffness, dependent on the cell number[44,45]. This can be explained by the decrease in absolute polymer content per construct, due to the additional volume of the cells. Also the cells might interfere with the polymer network formation via physical hindrance. In order to create hydrogel-based load-bearing cartilage constructs additional strategies are required, such as *in vitro* pre-culture. It is well known that construct stiffness significantly increases when matrix is deposited by embedded cells[40,46–48]. Secondly, hydrogels can be reinforced with printed[49,50] or electrospun[51] thermoplastic polymers to increase their stiffness.

This study shows that all evaluated gelMA/gellan hydrogels support cartilage matrix production by embedded equine chondrocytes. However, the quantity and localization of the matrix production differed considerably between the various polymer blends. An important factor that can influence cell behavior is the stiffness of the surrounding matrix[52,53]. However, no clear correlation between cell performance and construct stiffness was found for this hydrogel system. Chondrocytes were cultured inside constructs with a Young's modulus ranging from 13 to 186 kPa. The softest constructs with a stiffness 13 and 23 kPa (3/0.5% gelMA/gellan and 3/1% gelMA/gellan, respectively) contained significantly less GAG/DNA compared to the stiffer constructs with a stiffness ranging from 24-186 kPa. In addition, considerable differences in matrix production and DNA

3

3

content were found between gel formulations with similar Young's moduli. For example, significantly more GAG/DNA was present in the 10% gelMA constructs compared to the 3/1% gelMA/gellan constructs while both have a Young's modulus of 23-24 kPa.

Hydrogel constructs with relatively high gellan gum concentrations (≥ 9% of the total polymer concentration) exhibited a decreased overall GAG production and the lowest proliferation rates. As previous studies showed excellent viability and cartilage-like matrix deposition by chondrocytes in hydrogels consisting of 0.7-5% gellan gum *in vitro* and *in vivo*[29,54,55], a toxic effect of the gellan gum appears to be unlikely. The presence of gellan gum, however, may inhibit the supportive effect that gelMA has on the matrix production of embedded cells. GelMA, which is produced from denatured collagens, stimulates chondrocytes in producing cartilage-like matrix[20,56–58]. The presence of relatively high gellan gum concentrations could inhibit this stimulatory effect. Likely, the cell performance is influenced by an interplay of the availability of cell adhesion sites and the mechanical environment[59,60].

In general, high polymer concentrations can inhibit matrix formation of embedded cells[7,8,61]. This was, however not found for the concentrations evaluated in the present study. Chondrocytes in the hydrogels with the lowest total polymer concentrations (3/0.5% gelMA/gellan and 3/1% gelMA/gellan) produced the least cartilage-like matrix and showed lower DNA content compared to hydrogels with higher total polymer concentrations. This is in contradiction to the study of Schuh *et al.* (2011)[62] who observed a negative effect of high polymer concentrations for cultured porcine chondrocytes in 0.75% and 3.5% agarose. On the other hand, when calf chondrocytes were embedded in 10%, 20% or 30% poly(ethylene glycol)-based (PEG-based) hydrogels, no difference was found in GAG production. This underscores that the inhibitory effect of high polymer concentrations on matrix production, observed in other studies, may also depend on other hydrogel properties *e.g.* cell adhesion sites and local construct stiffness, than purely on the polymer concentration.

Although no quantitative inhibitory effect based on the total polymer concentration was found in this study, differences in matrix distribution were observed. The newly formed matrix in hydrogel constructs with relatively high total polymer concentrations (≥ 11%) was confined in pericellular regions. Contrarily, newly formed matrix in hydrogel constructs with lower total polymer concentrations was evenly distributed after 42 days of culture. This suggests that high total polymer concentrations not necessarily inhibit matrix formation of chondrocytes, but do hamper the distribution of the newly formed matrix. This phenomenon was, for example, also observed in PEG[8]- and agarose[63]-based hydrogels. For an adequate increase in construct stiffness due to matrix production of embedded cells, the formation of a homogeneous interconnected tissue is required. Although the addition of gellan gum to gelMA hydrogels increased the initial construct stiffness with limited increase in the total polymer concentration, the maximum initial stiffness is restricted by the homogeneous matrix deposition and the bioprinting requirements (≤ 47.2±4.1, 10/0.5% gelMA/gellan).

5. Conclusions

The bioprinting window for gelMA/gellan hydrogels was determined, designating a range of hydrogel compositions that allow printing of defined structures with encapsulated cells. This study showed that the addition of gellan gum to gelMA hydrogels (1) improves filament formation and deposition by inducing yielding behavior, (2) increases the overall construct stiffness, and (3) supports matrix production of embedded chondrocytes. However, too high yield stresses hinder cell incorporation, while relatively high gellan gum concentrations compromise cartilage matrix production by embedded chondrocytes. Additionally, high total polymer concentrations hamper the distribution of newly formed matrix. Of the studied hydrogel compositions, 10/0.5% gelMA/gellan hydrogels seemed most suited for the generation of chondrocyte-laden 3D printed cartilage equivalents. This formulation is relatively easy to process (printing and incorporating cells), and cross-linked hydrogel constructs have an appreciable Young's modulus of 47.2±4.1 kPa, while supporting cartilage tissue formation by chondrocytes and allowing for homogeneous matrix deposition. A generic requirement for filament formation appeared to be the combination of high yield stress with a large viscosity drop. However, yield stress also affected cell miscibility for gelMA/gellan hydrogels. This critical yield stress dependence may have important implications for future bio-ink development.

6. Acknowledgements

3

Reference

1. Murphy, S. V & Atala, A. 3D bioprinting of tissues and organs. Nat. Biotechnol. 32, 773–785 (2014).
2. Malda, J. et al. 25th anniversary article: Engineering hydrogels for biofabrication. Adv. Mater. 25, 5011–28 (2013).
3. Zhao, G., Zhang, X., Lu, T. J. & Xu, F. Recent Advances in Electrospun Nanofibrous Scaffolds for Cardiac Tissue Engineering. Adv. Funct. Mater. 25, 5726–5738 (2015).
4. Jungst, T., Smolan, W., Schacht, K., Scheibel, T. & Groll, J. Strategies and Molecular Design Criteria for 3D Printable Hydrogels. Chem. Rev. 116, 1496–1539 (2016).
5. Gao, B. et al. 4D Bioprinting for Biomedical Applications. Trends Biotechnol. xx, 1–11 (2016).
6. Møller, P. C. F., Fall, A. & Bonn, D. Origin of apparent viscosity in yield stress fluids below yielding. EPL (Europhysics Lett.) 87, 38004 (2009).
7. Seliktar, D. Designing cell-compatible hydrogels for biomedical applications. Science 336, 1124–8 (2012).
8. Bryant, S. J. & Anseth, K. S. Hydrogel properties influence ECM production by chondrocytes photoencapsulated in poly (ethylene glycol) hydrogels. J. Biomed. Mater. Res. 59, 63–71 (2001).
9. Smith, C. M. et al. Three-dimensional bioassembly tool for generating viable tissue-engineered constructs. Tissue Eng. 10, 1566–1576 (2004).
10. Schuurman, W. et al. Gelatin-methacrylamide hydrogels as potential biomaterials for fabrication of tissue-engineered cartilage constructs. Macromol. Biosci. 13, 551–561 (2013).
11. Visser, J. et al. Biofabrication of multi-material anatomically shaped tissue constructs. Biofabrication 5, 035007 (2013).
12. Billiet, T., Gevaert, E., De Schryver, T., Cornelissen, M. & Dubruel, P. The 3D printing of gelatin methacrylamide cell-laden tissue-engineered constructs with high cell viability. Biomaterials 35, 49–62 (2014).
13. Skardal, A. et al. Photocrosslinkable hyaluronan-gelatin hydrogels for two-step bioprinting. Tissue Eng. Part A 16, 2675–85 (2010).
14. Yan, Y. et al. Fabrication of viable tissue-engineered constructs with 3D cell-assembly technique. Biomaterials 26, 5864–71 (2005).
15. Cohen, D. L., Malone, E., Lipson, H. & Bonassar, L. J. Direct freeform fabrication of seeded hydrogels in arbitrary geometries. Tissue Eng. 12, 1325–1335 (2006).
16. Fedorovich, N. E. et al. Evaluation of photocrosslinked Lutrol hydrogel for tissue printing applications. Biomacromolecules 10, 1689–96 (2009).
17. Pescosolido, L. et al. Hyaluronic acid and dextran-based semi-IPN hydrogels as biomaterials for bioprinting. Biomacromolecules 12, 1831–1838 (2011).
18. Censi, R. et al. A Printable Photopolymerizable Thermosensitive p(HPMAm-lactate)-PEG Hydrogel for Tissue Engineering. Adv. Funct. Mater. 21, 1833–1842 (2011).
19. Dang, J. M. & Leong, K. W. Natural polymers for gene delivery and tissue engineering. Adv. Drug Deliv. Rev. 58, 487–99 (2006).
20. Nichol, J. W. et al. Cell-laden microengineered gelatin methacrylate hydrogels. Biomaterials 31, 5536–44 (2010).
21. Van Den Bulcke, A. I. et al. Structural and Rheological Properties of Methacrylamide Modified Gelatin Hydrogels. Biomacromolecules 1, 31–38 (2000).
22. Almarza, A. J. & Athanasiou, K. A. Design characteristics for the tissue engineering of cartilaginous tissues. Ann. Biomed. Eng. 32, 2–17 (2004).
23. Prakash, D. & Learmonth, D. Natural progression of osteo-chondral defect in the femoral condyle. Knee 9, 7–10 (2002).
24. Klein, T. J. et al. Strategies for Zonal Cartilage Repair using Hydrogels. Macromol. Biosci. 9, 1049–1058 (2009).
25. Levett, P. A. et al. A biomimetic extracellular matrix for cartilage tissue engineering centered on photocurable gelatin, hyaluronic acid and chondroitin sulfate. Acta Biomater. 10, 214–223 (2014).
26. Yue, K. et al. Synthesis, properties, and biomedical applications of gelatin methacryloyl (GelMA) hydrogels. Biomaterials 73, 254–271 (2015).
27. Gao, G. et al. Improved properties of bone and cartilage tissue from 3D inkjet-bioprinted human mesenchymal stem cells by simultaneous deposition and photocrosslinking in PEG-GelMA. Biotechnol. Lett. 37, 2349–2355 (2015).
28. Melchels, F. P. W., Dhert, W. J. A., Hutmacher, D. W. & Malda, J. Development and characterisation of a new bioink for additive tissue manufacturing. J. Mater. Chem. B 2, 2282–2289 (2014).
29. Oliveira, J. T. et al. Injectable gellan gum hydrogels with autologous cells for the treatment of rabbit articular cartilage defects. J. Orthop. Res. 28, 1193–9 (2010).
30. Rosenberg, L. Chemical basis for the histological use of safranin O in the study of articular cartilage. J. Bone Joint Surg. Am. 53, 69–82 (1971).
31. Farndale, R. W., Sayers, C. A. & Barrett, A. J. A Direct Spectrophotometric Microassay for Sulfated Glycosaminoglycans in Cartilage Cultures. Connect. Tissue Res. 9, 247–248 (1982).
32. Schuurman, W. et al. Bioprinting of hybrid tissue constructs with tailorable mechanical properties. Biofabrication 3, 021001 (2011).
33. Xu, T. et al. Hybrid printing of mechanically and biologically improved constructs for cartilage tissue engineering applications. Biofabrication 5, 015001 (2013).
34. Zhao, Y., Li, Y., Mao, S., Sun, W. & Yao, R. The influence of printing parameters on cell survival rate and printability in microextrusion-based 3D cell printing technology. Biofabrication 7, 045002 (2015).

35. Hoch, E., Hirth, T., Tovar, G. E. M. & Borchers, K. Chemical tailoring of gelatin to adjust its chemical and physical properties for functional bioprinting. J. Mater. Chem. B 1, 5675 (2013).
36. Ozbolat, I. T. & Hospodiuk, M. Current advances and future perspectives in extrusion-based bioprinting. Biomaterials 76, 321–343 (2016).
37. Kesti, M. et al. Bioprinting Complex Cartilaginous Structures with Clinically Compliant Biomaterials. Adv. Funct. Mater. 25, 7406–7417 (2015).
38. Highley, C. B., Rodell, C. B. & Burdick, J. A. Direct 3D Printing of Shear-Thinning Hydrogels into Self-Healing Hydrogels. Adv. Mater. 27, 5075–5079 (2015).
39. Fam, H., Kontopoulou, M. & Bryant, J. T. Effect of concentration and molecular weight on the rheology of hyaluronic acid/bovine calf serum solutions. Biorheology 46, 31–43 (2009).
40. Levett, P. A., Hutmacher, D. W., Malda, J. & Klein, T. J. Hyaluronic acid enhances the mechanical properties of tissue-engineered cartilage constructs. PLoS One 9, e113216 (2014).
41. Chen, A. C., Bae, W. C., Schinagl, R. M. & Sah, R. L. Depth- and strain-dependent mechanical and electromechanical properties of full-thickness bovine articular cartilage in confined compression. J. Biomech. 34, 1–12 (2001).
42. Athanasiou, K. A., Agarwal, A. & Dzida, F. J. Comparative study of the intrinsic mechanical properties of the human acetabular and femoral head cartilage. J. Orthop. Res. 12, 340–349 (1994).
43. Jurvelin, J. S., Buschmann, M. D. & Hunziker, E. B. Optical and mechanical determination of poisson's ratio of adult bovine humeral articular cartilage. J. Biomech. 30, 235–241 (1997).
44. Mauck, R. L., Wang, C. B., Oswald, E. S., Ateshian, G. A. & Hung, C. T. The role of cell seeding density and nutrient supply for articular cartilage tissue engineering with deformational loading. Osteoarthr. Cartil. 11, 879–890 (2003).
45. Reza, A. T. & Nicoll, S. B. Characterization of novel photocrosslinked carboxymethylcellulose hydrogels for encapsulation of nucleus pulposus cells. Acta Biomater. 6, 179–186 (2010).
46. Williams, G. M., Klein, T. J. & Sah, R. L. Cell density alters matrix accumulation in two distinct fractions and the mechanical integrity of alginate–chondrocyte constructs. Acta Biomater. 1, 625–633 (2005).
47. Ng, K. W. et al. A layered agarose approach to fabricate depth-dependent inhomogeneity in chondrocyte-seeded constructs. J. Orthop. Res. 23, 134–141 (2005).
48. Reza, A. T. & Nicoll, S. B. Characterization of novel photocrosslinked carboxymethylcellulose hydrogels for encapsulation of nucleus pulposus cells. Acta Biomater. 6, 179–186 (2010).
49. Schuurman, W. et al. Three-dimensional assembly of tissue-engineered cartilage constructs results in cartilaginous tissue formation without retainment of zonal characteristics. J. Tissue Eng. Regen. Med. n/a–n/a (2013). doi:10.1002/term.1726
50. Shim, J.-H., Kim, J. Y., Park, M., Park, J. & Cho, D.-W. Development of a hybrid scaffold with synthetic biomaterials and hydrogel using solid freeform fabrication technology. Biofabrication 3, 034102 (2011).
51. Visser, J. et al. Reinforcement of hydrogels using three-dimensionally printed microfibres. Nat. Commun. 6, 6933 (2015).
52. Discher, D. E., Janmey, P. & Wang, Y.-L. Tissue cells feel and respond to the stiffness of their substrate. Science 310, 1139–1143 (2005).
53. Huang, G. et al. Engineering three-dimensional cell mechanical microenvironment with hydrogels. Biofabrication 4, 042001 (2012).
54. Gong, Y. et al. An improved injectable polysaccharide hydrogel: modified gellan gum for long-term cartilage regeneration in vitro. J. Mater. Chem. 19, 1968 (2009).
55. Oliveira, J. T. et al. Gellan gum: A new biomaterial for cartilage tissue engineering applications. J. Biomed. Mater. Res. - Part A 93, 852–863 (2010).
56. Zhang, J., Mujeeb, A., Du, Y., Lin, J. & Ge, Z. Probing cell-matrix interactions in RGD-decorated macroporous poly (ethylene glycol) hydrogels for 3D chondrocyte culture. Biomed. Mater. 10, 035016 (2015).
57. Chen, J.-P. & Su, C.-H. Surface modification of electrospun PLLA nanofibers by plasma treatment and cationized gelatin immobilization for cartilage tissue engineering. Acta Biomater. 7, 234–43 (2011).
58. Lee, H. et al. Chondrocyte 3D-culture in RGD-modified crosslinked hydrogel with temperature-controllable modulus. Macromol. Res. 20, 106–111 (2012).
59. Trappmann, B. et al. Extracellular-matrix tethering regulates stem-cell fate. Nat. Mater. 11, 742–742 (2012).
60. Trappmann, B. & Chen, C. S. How cells sense extracellular matrix stiffness: A material's perspective. Current Opinion in Biotechnology 24, 948–953 (2013).
61. Schuh, E. et al. The influence of matrix elasticity on chondrocyte behavior in 3D. J. Tissue Eng. Regen. Med. 6, e31–e42 (2012).
62. Schuh, E. et al. Chondrocyte redifferentiation in 3D: the effect of adhesion site density and substrate elasticity. J. Biomed. Mater. Res. A 100, 38–47 (2012).
63. Kock, L. M., Geraedts, J., Ito, K. & van Donkelaar, C. C. Low Agarose Concentration and TGF-β3 Distribute Extracellular Matrix in Tissue-Engineered Cartilage. Tissue Eng. Part A 19, 1621–1631 (2013).

3

Chapter 4

Synthetic thermo-sensitive hydrogel for cartilage bioprinting and its biofunctionalization with polysaccharides

Anna Abbadessa*
Vivian H. M. Mouser*
Maarten M. Blokzijl
Debby Gawlitta
Wouter J. A. Dhert
Wim E. Hennink
Jos Malda
Tina Vermonden

* both authors contributed equally

This Chapter is also included in the PhD thesis of A. Abbadessa

Abstract

Hydrogels based on triblock copolymers of polyethylene glycol and partially methacrylated poly(*N*-(2-hydroxypropyl) methacrylamide mono/dilactate) are an attractive class of biomaterials due to their biodegradability, cytocompatibility, and tunable thermo-responsive and mechanical properties. By fine-tuning these properties, the hydrogels can be 3D bioprinted, to generate *e.g.* constructs for cartilage repair. This study investigated whether hydrogels based on the above mentioned polymer with a 10% degree of methacrylation ($M_{10}P_{10}$), support cartilage formation by chondrocytes, and whether the incorporation of methacrylated chondroitin sulfate (CSMA) or methacrylated hyaluronic acid (HAMA) can improve the mechanical properties, long-term stability, and printability.

Chondrocyte-laden $M_{10}P_{10}$ hydrogels were cultured for 42 days to evaluate chondrogenesis. $M_{10}P_{10}$ hydrogels with or without polysaccharides were evaluated for their mechanical properties (before and after UV photo-cross-linking), degradation kinetics, and printability.

Extensive cartilage matrix production occurred in $M_{10}P_{10}$ hydrogels, highlighting their potential for cartilage repair strategies. The incorporation of polysaccharides increased the storage modulus of polymer mixtures and decreased the degradation kinetics in cross-linked hydrogels. Addition of HAMA to $M_{10}P_{10}$ hydrogels improved printability and resulted in 3D constructs with excellent cell viability. Hence, this novel combination of $M_{10}P_{10}$ with HAMA forms an interesting class of hydrogels for cartilage bioprinting.

1. Introduction

Articular cartilage is the tissue that covers the extremities of the bones inside the joints. The tissue functions as a damper due to its high osmotic pressure and reduces surface friction due to its smooth surface structure. Articular cartilage contains proteoglycans, collagen type II, water, and cells, the chondrocytes. Since the tissue lacks vasculature and innervation, and contains only few chondrocytes, it has a limited regenerative capacity[1,2]. The implantation of cell-laden hydrogel scaffolds is regarded as a promising approach to treat cartilage defects. Hydrogels, networks of hydrophilic polymers, have high water content, which supports cell survival and allow homogeneous encapsulation of cells as well as biological and chemical cues. Therefore, cell-laden hydrogel implants can promote new tissue formation while initially providing structural support. For the generation of successful cell-laden constructs, it is essential to have control over the mechanical properties and degradation kinetics of the construct, as it should progressively be replaced by newly-formed tissue after implantation[3]. The mechanical properties and degradation kinetics of hydrogels can be easily tailored over a broad range and in a highly reproducible manner by a proper design of the building blocks[4–6]. In addition, thermo-responsive functionalities can be introduced in the building blocks, providing the opportunity to generate injectable and three-dimensional (3D) printable hydrogels[7].

Copolymers based on a polyethylene glycol (PEG) mid-block flanked by two poly(*N*-(2-hydroxypropyl) methacrylamide mono/dilactate) (polyHPMA-lac) outer blocks have recently been investigated for pharmaceutical and biomedical applications[8–12]. Methacrylated polyHPMA-lac-PEG triblock copolymers display lower critical solution temperature (LCST) behavior in aqueous solutions, meaning that these polymers are soluble at low temperatures and form physical gels, by self-assembly due to dehydration of polymer chains, at temperatures above a critical temperature, called the cloud point (CP)[13]. The thermo-sensitive behavior of methacrylated polyHPMA-lac-PEG triblock copolymers is highly tunable, *e.g.* to physiologically relevant temperatures, by adapting the content of the lactate groups present in the outer blocks as well as the number of methacrylate groups[9,13,14]. In addition, the methacrylate groups allow UV light-mediated photo-cross-linking, which prevents rapid disassembly of the polymer networks[13]. Chemically cross-linked hydrogels with tailored degradation rates and mechanical properties can be obtained by varying the number of methacrylate units per polymer chain, the molecular weight of the PEG mid-block, as well as that of the thermo-sensitive flanking blocks and the polymer concentration in the hydrogel[8,9,11,13]. The thermo-sensitive behavior of methacrylated polyHPMA-lac-PEG triblock copolymers allows easy handling of the polymer solution at low temperatures, when it behaves as a viscous liquid, to incorporate cells. Previous studies have shown high viability of encapsulated articular chondrocytes in methacrylated polyHPMA-lac-PEG triblock copolymer-based hydrogels[10]. However, long-term culture and actual cartilage matrix formation in these hydrogels has not been investigated so far.

Cell-laden hydrogels can accurately be shaped with 3D biofabrication techniques to mimic the architecture of native tissues *e.g.* the zonal organization of articular cartilage[15], and to generate patient specific construct shapes. 3D bioprinting is a form of biofabrication

based on computer-aided layer-by-layer material deposition[16–19]. As such, bioprinting also allows the incorporation of pores or perfusable channels in the 3D structure, for easy diffusion of nutrients, oxygen and metabolites during (*in vitro*) construct maturation[7]. Hydrogels composed of methacrylated polyHPMA-lac-PEG triblock copolymers have already been shown to be printable due to their thermo-sensitive behavior[10]. However, this required a relatively high polymer concentration and a high degree of methacrylation (DM)[10]. In general, dense polymer networks due to *e.g.* high polymer concentrations and high DM, have adverse effects on the matrix production of embedded cells[20,21] and are therefore unfavourable for the fabrication of tissue repair constructs. In order to tackle this well-known dilemma in bioprinting[7], hybrid materials can be designed, for example by incorporating polysaccharides, which increase the viscosity of the polymer solution and can potentially improve the printability without hampering the matrix production of embedded cells[22–26]. In this study, the polysaccharides chondroitin sulfate (CS) and hyaluronic acid (HA) were methacrylated to allow UV photo-cross-linking[27,28] and blended with low DM (10%) polyHPMA-lac-PEG triblock copolymers, as both are natural polysaccharides abundantly present in native cartilage. In addition, they have demonstrated anabolic effects on extracellular matrix synthesis by chondrocytes and stem cells[24,29–34]. Therefore, these polysaccharides are attractive candidates to optimize methacrylated polyHPMA-lac-PEG triblock copolymer-based hydrogels for cartilage bioprinting. It is hypothesized that the incorporation of methacrylated HA (HAMA) or methacrylated CS (CSMA) in methacrylated polyHPMA-lac-PEG triblock hydrogels will affect the mechanical properties, decrease the degradation rate and improve the 3D printability in comparison to hydrogels made of methacrylated polyHPMA-lac-PEG triblock only. The aim of this study was to characterize methacrylated polyHPMA-lac-PEG triblock copolymer-based hydrogels in terms of chondrogenesis, mechanical behavior, degradation kinetics and printability. It was also investigated whether the incorporation of HAMA or CSMA in this synthetic hydrogel can further improve the mechanical properties, affect the degradation rate, and enhance the printability.

2. Materials and methods

2.1. Materials
All chemicals were obtained from Sigma-Aldrich (Zwijndrecht, the Netherlands) and all solvents from Biosolve (Valkenswaard, the Netherlands) unless indicated otherwise. Chemicals and solvents were used as received. PEG 10 kDa was supplied by Merck (Darmstadt, Germany). HA sodium salt (1560 kDa) was supplied by Lifecore Biomedical (Chaska, MN, USA). CS A sodium salt from bovine trachea (Sigma-Aldrich, Zwijndrecht, the Netherlands) was analyzed with Viscotek Gel Permeation Chromatography (GPC) and showed a bimodal molecular weight distribution (number average molecular weight, M_n 26.9 kDa, 94% mass content and 353.8 kDa, 6% mass content; details are given in Figure S1). L-lactide was purchased from Corbion Purac (Amsterdam, the Netherlands) and Irgacure 2959 was a kind gift from BASF (Ludwigshafen, Germany). *N*-(2-hydroxypropyl) methacrylamide (HPMA), HPMA mono- and dilactate and PEG_{10000}-4,4'-

azobis(cyanopentanoate) macroinitiator were synthesized as previously reported[35–37]. Phosphate buffered saline (PBS), penicillin/streptomycin (pen/strep; 10,000 units/ml penicillin and 10 mg/ml streptomycin) and picogreen DNA assay were supplied by Invitrogen (Carlsbad, California, USA). Three different types of Dulbecco's Modified Eagle Medium (DMEM) were used: DMEM 31885 from Gibco (referred to as DMEM), high glucose DMEM D6429 from Sigma-Aldrich (referred to as high glucose DMEM) and DMEM/F-12+GlutaMax-1 31331 from Invitrogen (referred to as DMEM/F-12). Fetal bovine serum (FBS) was obtained from Gibco (Invitrogen corporation) and type II collagenase was purchased from Worthington Biochemical Corp (Lakewood, NJ, USA). ITS+ premix (human recombinant insulin, human transferrin, selenous acid, bovine serum albumin, linoleic acid) was obtained from BD Biosciences (Breda, the Netherlands), recombinant human TGF-β1 from Peprotech (London, UK), pronase (11459643001) from Roche Life Sciences (Indiana, USA), hyaluronidase (H2126) from Sigma-Aldrich and Tissucol Duo S (fibrin and thrombin) from Baxter (Utrecht, the Netherlands). Antibody against collagen type I (1:100; EPR7785, ab138492) was obtained from Abcam (Cambridge, UK). Antibodies against collagen types II and VI (1:100; II-6B3II and 1:5, 5C6, respectively) were obtained from the Developmental Studies Hybridoma Bank (Iowa City, IA, USA). Secondary horse radish-peroxidase conjugated antibodies for collagen type I (EnVision+, K4010), collagen type II (1:100, IgG HRP, P0447), and collagen type VI (EnVision+, K4007) were ordered from DAKO (Heverlee, the Netherlands). Calcein-AM (to stain living cells) and ethidium homodimer-1 (to stain nuclei of dead cells) were obtained from Life Technologies (L3224, Bleiswijk, the Netherlands). Finally, Dye-Trak 'F' microspheres (Fluorescent Orange) were ordered from Triton Technology Inc. (San Diego, CA, USA).

2.2. Synthesis of methacrylated poly(N-(2-hydroxypropyl) methacrylamide mono/dilactate)-PEG triblock

The synthesis of a methacrylated thermo-sensitive triblock copolymer, consisting of a hydrophilic PEG-based mid-block flanked by two partially methacrylated pHPMA-lac outer blocks was carried out as previously described by Vermonden et al.[13,14]. Briefly, a free radical polymerization in acetonitrile was carried out at 70°C for 40 hours under a N_2 atmosphere, using PEG_{10000}-4,4'-azobis(cyanopentanoate) as macroinitiator and HPMA mono- and dilactate (molar ratio mono/dilactate = 75:25) as monomers, with a mass ratio monomers/macroinitiator of 4:1. After precipitation in cold diethyl ether, the polymer was collected and further modified via partial esterification of the hydroxyl groups present on the lactate units with methacrylate groups. This reaction was carried out in dry tetrahydrofuran as solvent and methacrylic anhydride (MA, molar feed of 13.3% of the free hydroxyl groups of the polymer) was used as methacrylating agent in presence of triethylamine and 4-dimethylaminopyridine. The methacrylated polyHPMA-lac-PEG triblock copolymer is further referred to as $M_{10}P_{10}$ (M_{10} refers to a DM of 10% and P_{10} refers to a PEG block with a molecular weight (MW) of 10 kDa) and its precursor as M_0P_{10}. A low DM of 10% was chosen to achieve a low network density in the cross-linked hydrogel, which is likely beneficial for cell behavior[20].

4

2.3. Methacrylation of polysaccharides

Methacrylation of CS was carried out using a transesterification reaction, as described by Abbadessa *et al.*[38]. Briefly, CS A sodium salt was converted into tetrabuthylammonium (TBA) salt (CS-TBA) by using a Dowex® 50WX8 hydrogen form resin, previously saturated with TBA fluoride. Subsequently, 2.7 g (3.08 mmol of disaccharide units) of CS-TBA was dissolved in 100 ml of dry dimethyl sulfoxide (DMSO) under a N_2 atmosphere at 50°C. Next, 4-dimethylaminopyridine (0.495 g) and glycidyl methacrylate (GMA, 195 µl) were added and the reaction mixture was stirred at 50°C for 48 hours. After the reaction, the mixture was diluted with water and the pH was lowered to 5.5 using a 0.2 M solution of HCl in water. The polymer solution was further dialyzed against a 150 mM NaCl solution in water for 3 days and against water for 4 days. The polymer was finally collected, as Na^+ salt, after freeze-drying and it is further referred to as CSMA.

HA was methacrylated using a slightly modified method from the one reported by Hachet *et al*[28]. Briefly, 0.5 g (1.25 mmol of disaccharide units) of HA was dissolved in 80 ml of ultrapure water at 4°C overnight. Subsequently, *N*,*N*-dimethylformamide (DMF) was added to obtain a mixture with 1:1 water/DMF volume ratio. Next, 926 µl (6.25 mmol) of MA was added drop-wise at 4°C to the HA solution while the pH was kept between 8 and 9 by adding 0.5 M NaOH. The pH was monitored for 4 hours and adjusted to 8-9. After overnight stirring at 4°C, the polymer was precipitated by addition of NaCl (final concentration in the mixture 0.5 M) and cold ethanol (final ethanol/water ratio of 2.3:1), and further purified by means of dialysis (MWCO 10,000-14,000 Da). Purified HAMA was collected after freeze-drying.

The DM of HAMA was investigated using a method based on the detection of methacrylic acid, which is released after basic hydrolysis of the ester bonds present in the methacrylated polysaccharide[39]. The formed methacrylic acid was detected with a High Performance Liquid Chromatography (HPLC) Waters 2695 separating module equipped with a Waters 2487 dual λ absorbance detector (λ = 210 nm, Waters Corporation, Milford, MA, USA) and with a C18 column (Sunfire). HAMA (15 mg) was dissolved in 10 ml of 0.02 M NaOH at 37°C for 2 hours. Subsequently, 2 ml of 2 M acetic acid was added. After filtration using a 0.2 µm filter, the samples were injected in the HPLC system and eluted at 1 ml/minute using a mixture of acetonitrile/water (15:85, pH = 2) as mobile phase. Calibration was performed using solutions of methacrylic acid of different concentrations in the same eluent.

2.4. Experimental design and hydrogel groups

To investigate if $M_{10}P_{10}$ hydrogels support chondrogenesis of chondrocytes, UV cross-linked constructs from an equine chondrocyte (passage 1, n = 3 donors) laden $M_{10}P_{10}$ (18% w/w) polymer mixture were prepared. Constructs were cultured for 42 days and evaluated for evidence of chondrogenesis at days 0 (harvested directly after cell encapsulation), 28 and 42, via quantitative measurements and histology. This gel formulation is further referred to as cell-laden hydrogel M.

To investigate whether the incorporation of HAMA or CSMA in $M_{10}P_{10}$ can improve the mechanical properties, affect the degradation rate, and enhance the printability, cell-

free polymer mixtures based on $M_{10}P_{10}$ (18% w/w), $M_{10}P_{10}$ (14% w/w) blended with CSMA (4% w/w), or $M_{10}P_{10}$ (14% w/w) blended with HAMA (0.9% w/w) were prepared and are further referred to as mixtures M, MCS and MHA, respectively (Table 1). These mixtures were analyzed for their thermo-sensitive properties using rheological measurements. Cell-free UV cross-linked M, MCS and MHA hydrogels were further characterized for their Young's modulus and their degradation/swelling behavior in PBS (pH 7.4) enriched with 0.02% of NaN_3 at 37°C. Finally, 3D constructs were printed with polymer mixture MHA laden with fluorescent microspheres to assess homogeneous encapsulation, using a 3D bioprinter (regenHU, Villaz-St-Pierre, Switzerland). Additionally, constructs with primary chondrocytes were printed using mixtures M, MCS and MHA to assess viability 1 and 7 days after printing. All measurements were performed in triplicate.

Table 1. Compositions of the three hydrogel groups.

hydrogel	polymer concentration (w/w%)		
	$M_{10}P_{10}$	CSMA	HAMA
M	18%	-	-
MCS	14%	4%	-
MHA	14%	-	0.9%

2.5. Chondrocyte isolation and culture

Primary chondrocytes were isolated from full-thickness cartilage of the stifle joints of fresh equine cadavers (n = 3; 3-10 years old horses), with consent of the owners. Macroscopically healthy cartilage was removed from the joint under aseptic conditions and the cartilage was digested overnight at 37°C in DMEM supplemented with collagenase II (1.5 µg/ml), hyaluronidase (1 mg/ml), FBS (10%) and pen/strep (1%). After digestion, the cell suspension was filtered through a 40 µm cell strainer. Chondrocytes were washed with PBS and stored in liquid N_2 until further use.

In order to prepare cell-laden constructs, the chondrocytes were expanded in monolayer culture for 14 days (seeding density of $5*10^3$ cells/cm^2) in chondrocyte expansion medium consisting of DMEM, FBS (10%) and pen/strep (1%). The chondrocytes were harvested and mixed with the polymer mixture at passage 1 when they reached 80-90% confluence. Cell-laden constructs were cultured in chondrogenic differentiation medium consisting of high glucose DMEM supplemented with ITS+ premix (1%), dexamethasone (0.1 µM), L-ascorbic acid-2-phosphate (0.2 mM), recombinant human TGF-β1 (10 ng/ml) and pen/strep (1%) to stimulate chondrogensis and redifferentation of the chondrocytes[40,41].

2.6. Fabrication of cell-laden chemically cross-linked $M_{10}P_{10}$-based hydrogels

$M_{10}P_{10}$ was dissolved in PBS at 4°C and Irgacure was added (concentration: 0.05% w/w). The resulting mixture ($M_{10}P_{10}$ concentration: 20.5% w/w) was stirred overnight in the

dark at 4°C. The expanded chondrocytes were mixed on ice with the polymer mixture to obtain a concentration of 15-20*10^6 chondrocytes/ml (concentration varied per donor). Correcting for the average weight of the added cells, the final concentrations of Irgacure and M$_{10}$P$_{10}$ in the cell-laden polymer mixture were 0.044% w/w and 18% w/w, respectively. The cell-laden suspension was injected into a Teflon mold, which was covered with a glass slide to generate cylindrical samples (sample size: 6 mm in diameter, 2 mm in height). The filled molds were placed at 37°C for 5 minutes to allow physical gelation of the hydrogel. Subsequently, chemical cross-linking was induced with a UV lamp (CL-1000L Model, UVP, Cambridge, UK, Intensity: 7.2 mW/cm^2, irradiation time: 15 minutes). Next, the samples were cultured at 37°C and 5% CO$_2$ for 42 days in chondrogenic differentiation medium. The medium was refreshed twice a week. Fibrin gels were prepared as a positive control for cell behavior. Chondrocytes were mixed with fibrinogen (Tissucol Duo S, diluted 1:15 in PBS) to get a cell density of 30-40*10^6 cells/ml. Next, 30 µl of thrombin (Tissucol Duo S, diluted 1:50 in PBS, 500 IU) was pipetted into the cylindrical molds and 30 µl of cell-laden fibrinogen suspension was mixed into the thrombin solution to generate a final cell concentration of 15-20*10^6 chondrocytes/ml (same as for cell-laden M hydrogels). Samples were incubated for 15 minutes at room temperature and placed in culture with chondrogenic differentiation medium as described above.

2.7. Histology and Immunohistochemistry

At days 0 (harvested directly after cell encapsulation), 28 and 42, three samples of each hydrogel group (M and fibrin) were harvested. Part of each sample was fixed overnight in formalin (37%) and dehydrated through a graded ethanol series. After clearing in xylene, the samples were embedded in paraffin and sectioned at a thickness of 5 µm. Sections were stained with safranin-O to visualize proteoglycans, fast green to visualize collagens, and hematoxylin to stain cell nuclei, as previously described[42].

Collagen types I, II and VI were visualized with immunohistochemistry. First, the sections were deparaffinized and hydrated. Next, antigen retrieval was performed with pronase (1 mg/ml in PBS) and hyaluronidase (10 mg/ml in PBS) for 30 minutes at 37°C, followed by a blocking step of 10 minutes with H$_2$O$_2$ (0.3% in PBS) at room temperature. The primary antibody was incubated overnight at 4°C. Mouse IgG was used at matched concentrations for negative control staining. After incubation, the matching secondary antibody was added and incubated for 30 minutes for collagen type I and 60 minutes for collagen types II and VI, at room temperature. Finally, all stainings were visualized with 3,3'-diaminobenzidine peroxidase substrate solution for 3-10 minutes and counterstained with Mayer's hematoxylin. All stained sections were evaluated and photographed using a light microscope (Olympus BX51 microscope, Olympus DP70 camera, Hamburg, Germany).

2.8. Biochemical assays

The remaining part of each harvested cell-laden hydrogel was weighed, freeze dried, and weighed again to determine the sample dry weight and water content. Next, the dried hydrogels were digested overnight at 56°C in 200 µL papain digestion buffer (0.2 M NaH$_2$PO$_4$

+ 0.01 M EDTA · 2 H$_2$O in milliQ, pH = 6.0) supplemented with 250 µL/ml papain solution (16-40 units/mg protein) and 0.01 M cysteine. To determine the glycosaminoglycan (GAG) content, as a measure for proteoglycan, a dimethylmethylene blue (DMMB)[43] assay was used with known concentrations of chondroitin sulfate C as a reference. The amount of GAG was normalized to the dry weight and DNA content of the samples, as measured by the Quant-iT PicoGreen dsDNA kit and read on a spectrofluorometer (Biorad, Hercules, California, USA), all according to the manufacturer's protocols.

2.9. Fabrication of chemically cross-linked hydrogels modified with polysaccharides

Defined amounts of M$_{10}$P$_{10}$ and CSMA or HAMA (Table 1) were dissolved in PBS at 4°C and Irgacure was added as the last component (final concentration: 0.044% w/w). The polymer mixture containing CSMA was stirred overnight while the mixture containing HAMA was stirred for 48 hours at 4°C to allow complete dissolution. Subsequently, the polymer mixtures were injected into Teflon molds (sample size: 6 mm in diameter, 2 mm in height), incubated for 5 minutes at 37°C and UV irradiated as described for the cell-laden cross-linked M hydrogels (section 'Fabrication of cell-laden chemically cross-linked M$_{10}$P$_{10}$-based hydrogels'). Two different hydrogel compositions, MCS and MHA were prepared, in which M$_{10}$P$_{10}$ was partially replaced by either CSMA or HAMA, respectively. Finally, hydrogels containing only M$_{10}$P$_{10}$ in the maximum total polymer concentration used for hybrid gels were prepared as a control group (18% w/w, hydrogels M). The total polymer concentration in MHA hydrogels was slightly lower compared to the other two hydrogels, since it was not possible to dissolve more than 0.9% w/w of this polysaccharide due to its high MW.

2.10. Mechanical analysis

Thermo-responsive properties of the polymer mixtures (M, MCS and MHA) before chemical cross-linking were studied using an AR G-2 rheometer (TA-Instruments, Etten-Leur, The Netherlands), equipped with a cone-plate measuring geometry (cone diameter: 20 mm, angle: 1°). All polymer mixtures were tested under oscillation temperature sweeps from 4 to 50°C employing a frequency of 1 Hz and a strain of 1%, which was found to be within the linear viscoelastic range of all formulations (Figure S2). Values of storage and loss moduli (G' and G", respectively) were recorded for each sweep and the resulting rheograms were reported showing the lines interconnecting all data points for each run.

To investigate the stiffness of hydrogel constructs after UV cross-linking, all polymer mixtures (M, MCS and MHA) were molded as described in section 'Fabrication of chemically cross-linked hydrogels modified with polysaccharides' and allowed to swell for 3 hours in PBS at room temperature. Next, hydrogels were examined under unconfined compression test using a Dynamic Mechanical Analyzer, DMA (2980 DMA, TA Instruments, Etten-Leur, The Netherlands). The hydrogels were subjected to a preload force of 0.001 N and subsequently compressed with a force ramp rate of 0.25 N/minute and an upper force limit of 1 N[13]. The Young's Modulus was calculated as the slope of the initial linear segment of the stress/strain curve[22].

4

2.11. In vitro swelling-degradation study

For all polymer mixtures (M, MCS and MHA) cross-linked samples (6 mm of diameter, 2 mm of height, 56.5 µl of volume) prepared as described in section 'Fabrication of chemically cross-linked hydrogels modified with polysaccharides' were placed in glass vials (diameter: 1.75 cm) with 1 ml of PBS (pH 7.4), supplemented with 0.02% of NaN$_3$. The vials were incubated at 37°C and the solutions were refreshed twice per week. At multiple time points, the hydrogels were weighed and the swelling ratio (SR) was calculated as follows:

SR = $m_{day\,x}$/$m_{day\,0}$ \hfill equation 1

in which $m_{day\,x}$ represents the hydrogel mass after x days of incubation and $m_{day\,0}$ the hydrogel mass before the hydrogel was placed in PBS.

2.12. Printing of hydrogels

A 3DDiscovery bioprinter (regenHU, Villaz-St-Pierre, Switzerland) equipped with a Bluepoint 4 UV lamp (point light source, wavelength range: 300-600 nm, UV-A intensity at 5 cm = 103 mW/cm^2, Hönle UV Technology AG, Gräfelfing, Germany) was used for the 3D printing of hydrogels. Filaments were generated with a micro valve (CF300H) print head, for optimal control over volume deposition rates, using optimized printer settings (Table S1). To generate porous constructs, alternating layers of vertical and horizontal filaments were deposited in the x,y-plane. Cross-linking was performed in a layer-by-layer fashion, exposing each deposited layer for 3 seconds to UV light from a distance of 5 cm. After printing, the constructs were irradiated for an additional 9 seconds.

2.13. Printing of hydrogels loaded with fluorescent microspheres and cells

To evaluate the feasibility of homogeneous cell encapsulation, polymer mixture MHA was supplemented with fluorescently labeled microspheres (Fluorescent Orange Dye-Trak 'F' microspheres, Triton Technology, diameter 15 µm similar as a single cell, concentration in the polymer mixture 0.8 million/ml) and constructs were 3D printed using optimized print settings (Table S1). To visualize the distribution of the microspheres in the constructs, an Olympus BX51 microscope was used.

To evaluate cell viability after printing, primary chondrocytes (harvested and expanded as described in section 'Chondrocyte isolation and culture') were encapsulated in mixtures M, MCS and MHA. The cell-laden mixtures were heated to 37°C and three constructs were subsequently printed using the aforementioned print method. As a positive control, cast hydrogels were prepared for each mixture using the same method as for the equine chondrocyte laden hydrogels (section 'Fabrication of cell-laden chemically cross-linked $M_{10}P_{10}$-based hydrogels'). Each printed construct was cut into four pieces, which were cultured in separate wells with chondrocyte expansion medium. Viability was checked on two pieces at day 1 and for the other pieces after 7 days of culture. To check cell viability, the hydrogels were stained for 20 minutes with calcein-AM (4 µM in PBS) and ethidium homodimer-1 (2 µM in PBS) at 37 °C. After washing three times in PBS, the

red and green fluorescent signals were visualized using an Olympus BX51 microscope and three images of each hydrogel quarter were analyzed.

2.14. Statistics

Statistical analyses were performed using SPSS software (version 20, IBM Corporation, USA). Differences in Young's modulus between the hydrogel groups (M, MHA, MCS) and differences in chondrocyte viability after printing at each time point, were determined with a One-Way ANOVA test. For GAG values normalized to the DNA content, both hydrogels (M and fib) at all time-points (6 groups in total) were compared with each other using a Randomized Block Design ANOVA to correct for donor variability. The GAG, DNA, and water contents normalized to the dry weight at the different time points were compared to each other within each hydrogel formulation by a Randomized Block Design ANOVA. A significance level of 0.05 and a Tukey's Post-hoc analysis were used for all tests.

3. Results and discussion

3.1. Synthesis and characterization of thermo-sensitive polymers and methacrylated polysaccharides

M_0P_{10} and $M_{10}P_{10}$ (Figure 1) were obtained in a high yield (80% and 96%, respectively). Their chemical structures, confirmed by ^{1}H-NMR, were in accordance to previously reported data[13,14]. The M_n and DM of $M_{10}P_{10}$ determined by ^{1}H-NMR were 42.4 kDa and 10.7%, respectively, whereas the M_n according to GPC was 34.6 kDa with a PDI value of 2.0. The cloud points of M_0P_{10} and $M_{10}P_{10}$ were 35°C and 20°C, respectively. Table 2 summarizes the polymer characteristics for M_0P_{10} and $M_{10}P_{10}$.

The methods employed for the methacrylation of CS and HA resulted in high yields of CSMA and HAMA (>84% for both polysaccharides). The methacrylated polysaccharides (chemical structures shown in Figure 1) were analyzed by ^{1}H-NMR. The presence of the signals at 6.2 and 5.8 ppm, representative of the two vinyl protons present in the methacrylate groups, and the signal at 2.0 ppm, typical of the protons belonging to its methyl group, confirmed the partial functionalization of the hydroxyl groups with methacrylate groups.

The methacrylation of CS was performed in DMSO using GMA as methacrylating agent, and a molar feed of GMA and CS-TBA repeating units of 0.48:1 resulted in a DM of 15.2% (Table 2), calculated according to ^{1}H-NMR. Moreover, the absence in the ^{1}H-NMR spectrum of the signals at 5.5 and 5.2 ppm representative of a possible glyceryl spacer between the methacrylate group and the disaccharide unit, excluded the presence of products originating from ring opening reaction[44]. Thus, the reaction mechanism follows a transesterification mechanism, which is in line with our previous findings[38].

For the synthesis of HAMA, we selected the method reported by Hachet *et al.*[28]. This reaction was performed in a mixture of water and DMF using a large excess of MA (molar ratio of 5:1 between MA and repeating units of HA). This high feed ratio is generally used for methacrylation reactions in aqueous environment because it is necessary to compensate for the amount of MA lost as methacrylic acid due to hydrolysis[45,46]. A
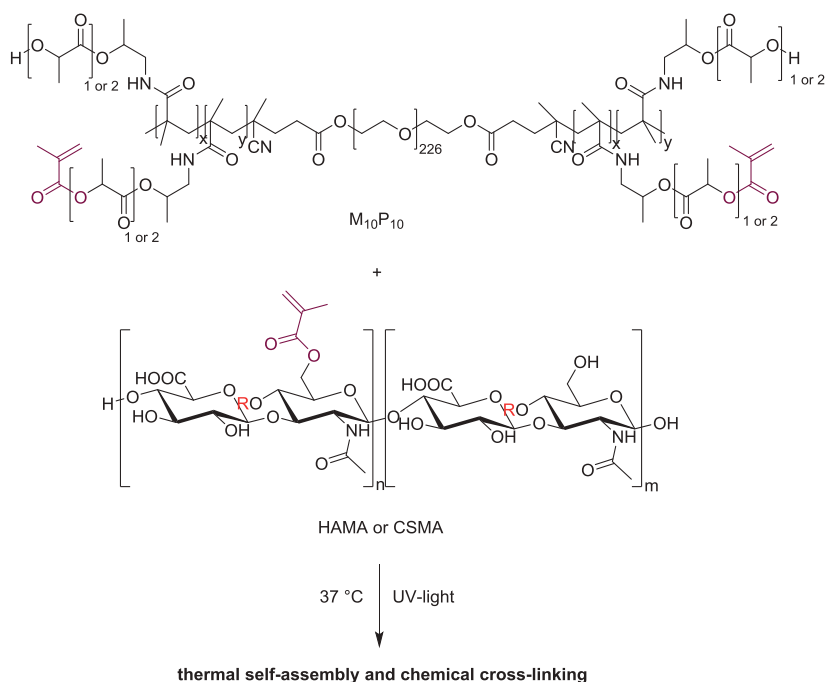
4

Figure 1. Chemical structure of M$_{10}$P$_{10}$ (top) and methacrylated HA (bottom, R = H in equatorial position) or CS (bottom, R = SO$_3$H in axial position). M$_{10}$P$_{10}$ confers thermo-sensitive properties to the gel, whereas the presence of methacrylate groups in both polymers allows UV-mediated chemical cross-linking.

lower polymer concentration, 3.1 versus 12.0 mg/ml was used compared to previously reported reactions, which were performed using a lower MW HA[28,47]. The use of relatively low concentration was necessary to facilitate pH monitoring and general handling of the reaction mixture, considering the high viscosity of high MW HA solutions. This low HA concentration likely explains our lower methacrylate incorporation (5%) compared with previous reports (≥ 14%)[28,47]. Because of the poor resolution of the ^{1}H-NMR spectra for high MW HAMA, an HPLC-based method was employed to accurately determine the DM, which was found to be 23.4% (Table 2).

3.2. Matrix production of embedded chondrocytes

Hydrogels composed of methacrylated polyHPMA-lac-PEG triblock copolymers have been shown to support the short-term survival of chondrocytes, however, the effect on the matrix production was not yet reported[10]. In this study, equine chondrocytes were encapsulated into an 18% M$_{10}$P$_{10}$-based hydrogel (hydrogel M) and cultured up to 42 days in chondrogenic differentiation medium. The matrix production in this hydrogel was compared to that of chondrocytes embedded in fibrin gel (positive control), which is the golden standard for clinical delivery of cells for cartilage repair procedures and is known to support chondrogenesis due to its bioactive peptide sequences[48,49]. Hydrogel M supported cartilage-like tissue formation of the encapsulated chondrocyte and Safranin-O

Table 2. Characteristics of thermo-sensitive polymers and polysaccharides.

Polymer	DM (%)	M_n (kDa)	PDI	CP (°C)
M_0P_{10}	0^a	43.9^a 36.2^b	1.9^b	35^c
$M_{10}P_{10}$	10.7^a	42.4^a 34.6^b	2.0^b	20^c
CS	0^a	$26.9 (94\%)^d$ $353.8 (6\%)^d$	1.4^d 1.3^d	n.a.
CSMA	15.2^a	n.d.	n.d.	n.a.
HA	0^a	1560^e	n.d.	n.a.
HAMA	23.4^f	n.d.	n.d.	n.a.

[a] Determined by ^{1}H-NMR
[b] Determined by GPC
[c] Determined by UV-VIS spectrophotometry
[d] Determined by Viscotek
[e] Average MW determined by Multi-Angle Light Scattering Size Exclusion Chromatography (MALS-SEC) as reported from the supplier
[f] Determined by HPLC
n.d.: not determined
n.a.: not applicable

4
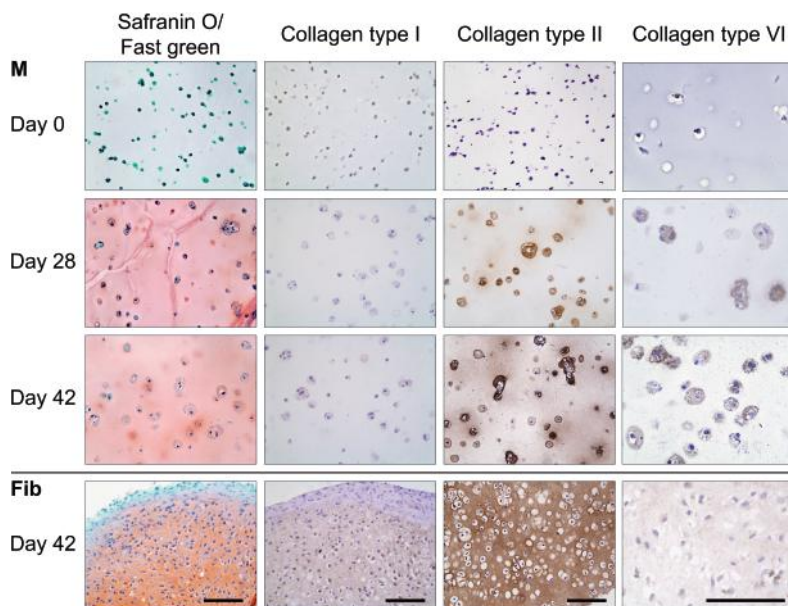
Figure 2. Histology and immunohistochemistry of chondrocytes differentiated in $M_{10}P_{10}$-based hydrogels (M) with fibrin (fib) as a positive control. From left to right: safranin-O staining, collagen types I, II and VI staining. Scale bars represents 100 µm and is the same for all images of the same staining (column).

staining revealed a homogeneous deposition of proteoglycans after 28 and 42 days of culture (Figure 2). In addition, immunolocalization of collagen type II revealed that its deposition was limited to distinct areas around the cells at day 28. However, after 42 days a more homogeneous distribution was observed. Both stainings were more intense in the fibrin gels at day 28 and 42 compared to hydrogel M samples at these time points (Figure 2). An explanation for this effect is the compaction of the fibrin gels during the first days of culture[50–52]. Because of this, the relative cell density and amount of matrix per gel volume increased as can be observed in the high DNA/dwt and GAG/dwt values for fibrin samples (Figure 3e, f). The sample dry weight was ten times higher for hydrogels M compared to fibrin gels and this difference remained over time (data not shown). Water volume normalized to the dry weight of M hydrogels increased at day 28 and 42 compared to day 0 (Figure 3d, 250% and 330% respectively). Although hydrogel compaction after implantation in a defect may localize the cells at the bottom of the defect, it will on the other hand result in an incomplete defect-fill. Moreover, contracting materials may be difficult to combine in hybrid scaffolds, *e.g.* hydrogel constructs reinforced with polymeric fibers, aimed to increase construct stiffness[7,22,53]. In these hydrid constructs, shrinking is

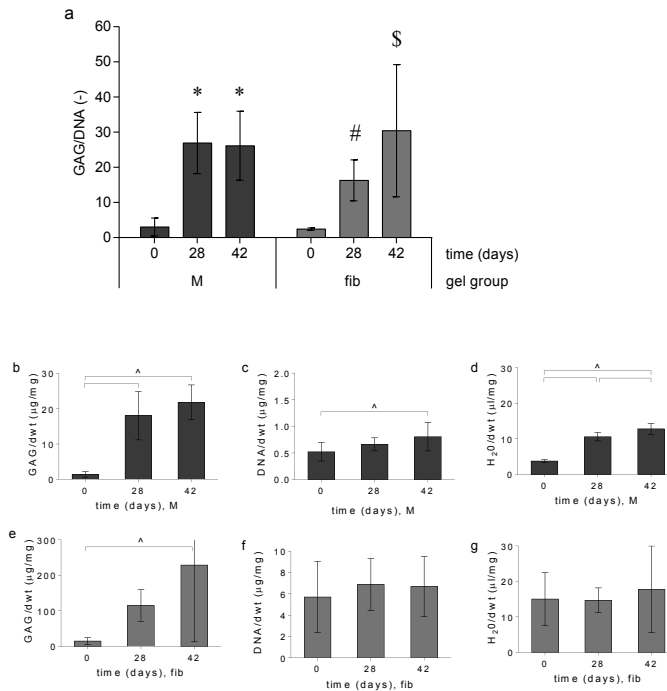**Figure 3. Quantitative GAG, DNA, and water measurements for equine chondrocytes encapsulated in $M_{10}P_{10}$-based hydrogels (M) and fibrin (fib) gels.** *a) GAG content normalized to DNA for both hydrogels over time. * denotes significant differences compared to day 0; # indicates that the group is significantly higher than the day 0 controls but lower compared to fibrin day 42. $ indicates that the group is significantly higher than the day 0 controls and day 28 fibrin samples but equal to the M hydrogels at days 28 and 42. b, c, d) GAG, DNA and water content normalized to the dry weight (dwt) for M hydrogels over time, respectively. e, f, g) GAG, DNA, and water content normalized to the dry weight (dwt) for fibrin gels over time. ^ significant difference between groups, respectively.*

a major drawback since it may cause stress at the interface and lead to loss of construct integrity.

A collagen type VI staining was performed to visualize chondron formation. Chondrons are chondrocytes with their pericellular matrix, consisting of proteoglycans, collagen types II and VI[54], and are known to be more active in matrix deposition than chondrocytes[55]. In hydrogels M, collagen type VI positive areas were found around the cells after 28 and 42 days of culture, indicating that chondrocytes formed chondron-like structures during culture. In fibrin samples a slight overall positive collagen type VI staining was found. Further, only limited positive staining for collagen type I was observed in all hydrogel samples, suggesting limited dedifferentiation of the embedded chondrocytes.

Quantitative measurements were performed for GAG, DNA and water content. However, a large variation in cell performance of the three different equine donors (age 3-10 years old) was observed (Figure 3), which is in line with previous reported studies[56]. GAG content normalized to DNA content (GAG/DNA) was similar in M hydrogels at days 28 and 42 (27±9 µg/µg and 26±10 µg/µg, respectively, Figure 3a). At day 28, GAG/DNA was statistically higher compared to the fibrin control gels (16±6 µg/µg, Figure 3a) at this time point. After 42 days of culture both hydrogel formulations performed equally. The GAG content normalized to the dry weight of both the M and fibrin hydrogels increased with time (Figure 3b and 3e). However, DNA levels normalized to the dry weight only showed a significant increase for the M hydrogels over time (0.52±0.18 µg/mg at day 0 and 0.81±0.30 µg/mg at day 42, Figure 3c), indicating cell proliferation. Finally, higher GAG/dry weight and DNA/dry weight values were found for fibrin gels compared to hydrogels with formulation M, which can be explained by the compaction and relatively fast degradation of the fibrin gels. In addition, M hydrogels seemed to swell during cultures as the H_2O/dry weight increased during culture.

Thus, chondrocytes in hydrogels with formulation M produced similar levels of cartilage-like matrix compared to chondrocytes in fibrin gels. In addition, no compaction occurred for M hydrogels. Encouraged by these results, hydrogels with formulation M were further evaluated and CSMA and HAMA were incorporated to optimize the mechanical properties, degradation kinetics, and printability.

3.3. Thermo-gelation of polymer mixtures before chemical cross-linking

Figure 4 shows storage and loss moduli, G' and G", as a function of temperature for all polymer mixtures. Mixtures based only on $M_{10}P_{10}$, exhibited an increase of G' when increasing the temperature, up to 29±2 Pa at 50°C, while G" displayed higher values over the whole temperature range (Figure 4a). $M_{10}P_{10}$ is a thermo-sensitive polymer capable to self-assemble and to form hydrophobic domains above defined temperatures, leading to a physical gel within a certain range of concentrations[13]. The absence of a gelation temperature (T_{gel}), here defined as the temperature at which G' crosses G", as well as the low value of G' reached upon rising the temperature for polymer mixture M, is due to the relatively low concentration and high CP (20°C) of the thermo-sensitive polymer used in this study.
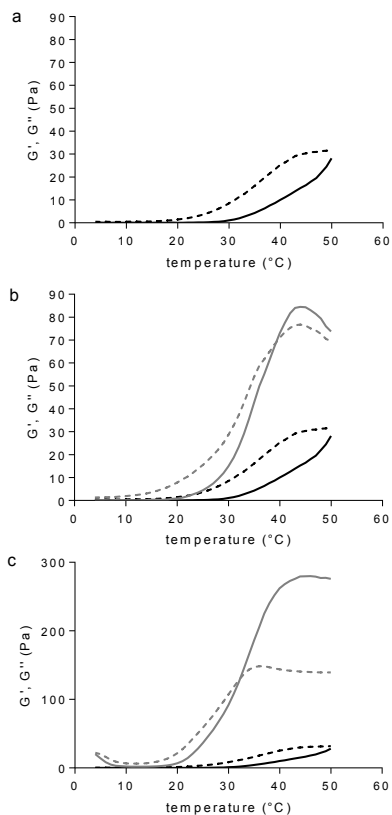
Figure 4. Rheograms of polymer mixtures. *G' (solid line) and G" (dotted line) moduli as a function of temperature, recorded during a temperature sweep experiment from 4 to 50 °C. a) hydrogels based on 18% (w/w) $M_{10}P_{10}$ (M hydrogels). b) hydrogels based on 14% (w/w) $M_{10}P_{10}$ and 4% (w/w) CSMA (MCS hydrogels, grey lines) compared with M hydrogels (black lines). c) hydrogels based on 14% (w/w) $M_{10}P_{10}$ and 0.9% (w/w) HAMA (MHA hydrogels, grey lines) compared with M hydrogels (black lines).*

Figures 4b and 4c show that a continuous increase in G' as a function of temperature was observed for aqueous systems of MCS and MHA. The values of the storage modulus at 37 and 50°C were 56±6 and 84±24 Pa, respectively, for MCS hydrogels, and 216±14 and 263±12 Pa, respectively, for MHA hydrogels. For both MCS and MHA mixtures a T_{gel} was found (39°C for MCS hydrogels and 32°C for MHA hydrogels). In line with previous findings, it can be observed that the partial replacement of $M_{10}P_{10}$ with CSMA or HAMA resulted in the formation of physical gels with much higher G' values above 20°C than polymer mixtures only composed of $M_{10}P_{10}$[38]. The beneficial role of the added polysaccharide on the mechanical properties of the hydrogel is more remarkable for MHA hydrogels, where an even lower total polymer concentration (Table 1) led to the formation of the stiffest hydrogel (G' = 216±14 at 37°C). The rheological behavior of the polysaccharide-enriched formulations clearly shows that the elastic properties of hydrogels based on $M_{10}P_{10}$ can be improved by the addition of polysaccharides, without increasing the total polymer concentration.

3.4. Mechanical properties and in vitro swelling-degradation behavior of chemically cross-linked hydrogels

The injection of polymer mixtures in a Teflon mold at 4°C, followed by a temperature increase to 37°C and UV irradiation for 15 min, resulted in the formation of cylindrically shaped constructs. Figure 5 shows the Young's moduli for the different hydrogel constructs after 3 hours of swelling in PBS. The Young's modulus values were 13.7±1.1, 16.0±1.4 and 16.0±1.9 kPa, for M, MCS and MHA hydrogels, respectively. No significant differences between the three hydrogel formulations were found. Hence, no differences in cell response due to different mechanical stimuli can be expected in the three hydrogels. The influence of polysaccharide molecular weight on the final stiffness can be illustrated by comparing MCS and MHA hydrogels. Hydrogels with comparable Young's moduli were obtained, despite the much lower concentration of the higher MW polysaccharide (0.9% *vs.* 4%) and the lower number of methacrylate groups in MHA hydrogels, calculated considering the slight difference in DM of the two polysaccharides (Figure 5). In line, the positive influence of HA with higher MW has been reported previously for hybrid hydrogel systems based on acrylated HA and thiol-modified 4-arm PEG or thiol-derivatives of HA and PEG-vinylsulfones, cross-linked via Michael addition-type reaction[57,58]. As can be expected for hydrogel materials, the stiffness of these hydrogel constructs is significantly lower than that of native cartilage (400-800 kPa[59–61]).
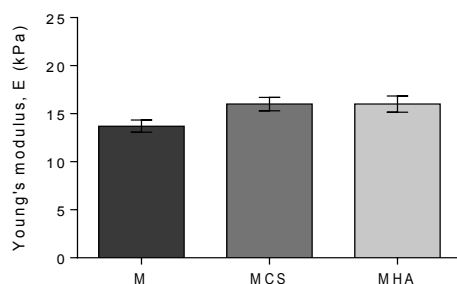

Figure 5. Dynamic mechanical analysis on chemically cross-linked hydrogels. *Young's moduli for hydrogels based on $M_{10}P_{10}$ (M), hydrogels based on $M_{10}P_{10}$ and CSMA (MCS) and hydrogels based on $M_{10}P_{10}$ and HAMA (MHA), measured under unconfined compression (n = 3).*

Figure 6 shows that M hydrogels initially swelled for 38 days during which the SR reached a maximum of 2.3±0.1. Complete degradation occurred in 56 days of incubation at 37°C. This degradation profile is in line with previously reported studies[8,13]. The degradability of hydrogels based on chemically cross-linked polyHPMA-lac-PEG triblock copolymers at pH 7.4 and 37°C is due to the hydrolysis of several ester bonds[9]. The first soluble degradation products are lactic acid units obtained by the hydrolysis of OH-terminated lactate side chains. Consequently, the remaining gel matrix exhibits an increased hydrophilic character with a higher water-uptake capacity, leading to the typical swelling phase. Mass loss is seen when the elimination of the water-soluble degradation products from the matrix exceeds the water uptake. This swelling-degradation behavior

might also explain the absence of GAG increase in the chondrocyte laden M hydrogels between 28 and 42 days of culture. The swelling process and the presence of a partially degraded and thus less dense hydrogel matrix between day 28 and 42 may have contributed to the leaching of newly formed GAGs out of the gel[62].

In contrast to M hydrogels, the hydrogels containing polysaccharides degraded much slower (Figure 6). More specifically, MCS hydrogels swelled for 91 days with a maximum SR of 2.1±0.2 and underwent complete disintegration in 100 days, whereas the degradation profile of MHA hydrogels showed a maximum in the SR of 2.3±0.1 at day 53, followed by partial mass loss during the subsequent 32 days and reached a plateau in SR of 1.4 for the subsequent 61 days of monitoring. Thus, the presence of the two polysaccharides, increased the stability of the hydrogels under the tested conditions. In fact, the loss of polysaccharides from these hydrogels can only occur after the polysaccharide molecules diffuse out of the hydrogel matrix and are dissolved in the surrounding buffer. This phenomenon can take place only after complete hydrolysis of the ester bonds of the polymerized methacrylate groups, which connect a polysaccharide chain to another polysaccharide or $M_{10}P_{10}$ chain. However, it has been reported that polymerized methacrylate groups directly attached to polysaccharide chains are very stable at pH 7.4 and 37°C[63,64]. Therefore, it was not surprising that no complete degradation of MHA hydrogels was observed under the applied conditions. Taking this in mind, the full mass loss observed for MCS hydrogels after 100 days can be ascribed to disintegration of the macroscopic hydrogel in smaller fragments, which is confirmed by the observation that the PBS buffer was slightly turbid during the last days of the study.
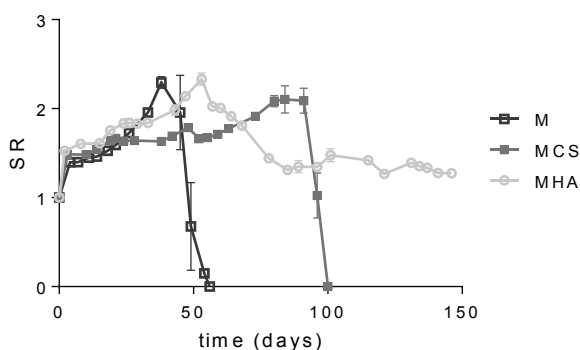

Figure 6. Swelling and degradation profiles for hydrogels based on $M_{10}P_{10}$ (M), hydrogels based on $M_{10}P_{10}$ and CSMA (MCS), and hydrogels based on $M_{10}P_{10}$ and HAMA (MHA) in PBS buffer at 37 °C. Error bars represent the standard deviation of experiments performed in triplicate. SR represents the swelling ratio and was calculated according to equation 1.

In general, the highest stability of the hydrogels is observed when $M_{10}P_{10}$ is partially replaced by HA (MHA hydrogels) at the tested concentrations. Nevertheless, it should be taken into consideration that the degradation profile of the polysaccharide-enriched hydrogels would likely be different if tested *in vivo*, because of the role played by enzymatic degradation via *e.g.* hyaluronidase[65].

3.5. Three-dimensional printing of hydrogels.

Shape-stable, 3D printed hydrogel constructs with highly regular internal porosity were obtained, when printing MHA hydrogels, above the T_{gel} (Figure 7a-c). Polymer mixtures M and MSC could not be printed with high shape-fidelity at cell friendly temperature, as polymer non methacrylated M did not form a stable physical gel below 40°C and the MCS polymer mixture had a too low viscosity at 37°C, forming only a weak physical gel at cell friendly temperatures.
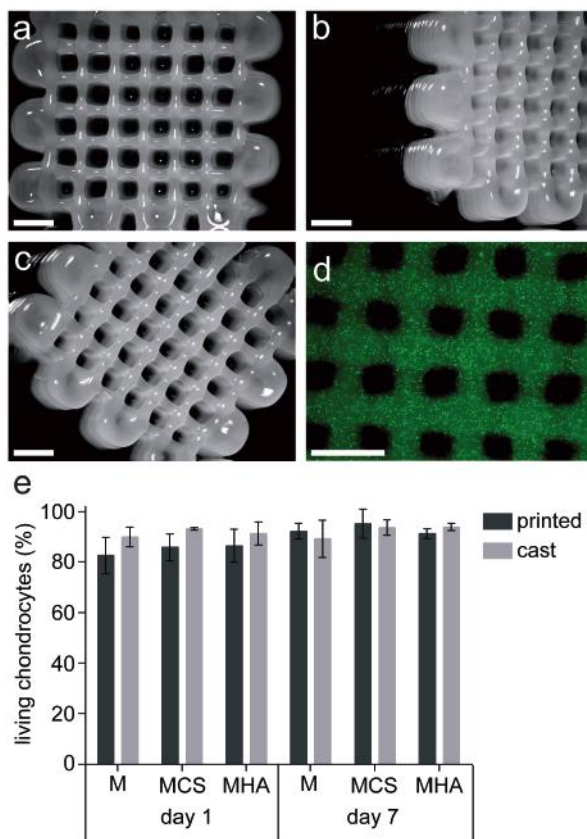

4

Figure 7. 3D printed porous constructs based on MHA. a) top view. b) top-side view. c) top-corner view. d) top view showing a homogeneous distribution of encapsulated green fluorescent beads. e) percentage of living chondrocytes in printed and cast (control) constructs for each hydrogel formulation after 1 and 7 days of culture. No statistical differences were observed between hydrogel formulations. Scale bar represents 2 mm.

In line with our previous findings, polymer mixtures exhibiting physical hydrogel formation and a relatively high G' (216±14 Pa) at 37°C allowed adequate stability of the extruded filaments on the deposition plate (pre-heated at 40°C), and thus 3D printing with high shape-fidelity (MHA hydrogels)[38]. On the contrary, the rheological properties of MCS polymer mixture were found insufficient for successful 3D printing.

Fluorescent microbeads with similar sizes as cells (diameter = 15 μm), were homogeneously dispersed in the MHA polymer mixture before printing. This homogeneous distribution was maintained during the printing process (Figure 7d). To investigate the influence of printing on cell viability, primary chondrocytes were dispersed in the three

polymer mixtures (M, MCS and MHA) and 3D constructs were printed. The cell viability was found to be between 85% and 95%, at both 1 and 7 days after printing, similar to those of the cast hydrogel controls (Figure 7e) indicating good biocompatibility for all three hydrogel formulations and no adverse effects due to the printing procedure.

In a previous study, a hydrogel based on cross-linkable pHPMA-lac-PEG triblock copolymers was used to print porous 3D structures. However, this required a relatively high polymer concentration (25% w/w) and DM (30%)[10]. The addition of HAMA has led to a hydrogel platform that could be printed at a considerable lower concentration (14% $M_{10}P_{10}$ + 0.9% HAMA) and DM of the thermo-sensitive polymer (10%), which is likely beneficial for the cartilage-like matrix deposition of incorporated cells[20,21]. In addition, the presence of HAMA itself is likely to improve the cartilage-like tissue production and remodeling by embedded chondrocytes[23,24,29–34,66]. In fact, the differentiation potential of chondrocytes in hydrogels with formulation MHA (and MCS) was confirmed by collagen type II detection after 42 days of culture (Figure S3). Nevertheless, the exact concentration of HAMA still needs further attention for this aspect, as studies have reported a dose-dependent effect in which high HA(MA) concentrations exhibit a less stimulating effect or even a reduction in cartilage-like tissue formation of chondrocytes compared to a lower HA(MA) concentration[24,67–71]. Taken together, the partial replacement of pHPMA-lac-PEG triblock copolymer with a low amount of HAMA, in combination with a layer-by-layer UV irradiation strategy during the printing process, is a promising approach for cell-friendly additive manufacturing of these hydrogels.

4. Conclusions

In this study, UV cross-linked hydrogels based on thermo-sensitive methacrylated pHPMA-lac-PEG triblock copolymer, laden with equine chondrocytes showed potential for significant cartilage-like tissue formation *in vitro*. Additionally, mechanical analysis and swelling/degradation studies proved that the partial replacement of methacrylated pHPMA-lac-PEG triblock copolymer with CSMA or HAMA can lead to the design of hydrogels with an improved thermo-sensitive profile, a similar stiffness after UV cross-linking, and a slower degradation rate compared to hydrogels consisting of only pHPMA-lac-PEG triblock copolymers. Moreover, hydrogels containing HAMA (MHA hydrogels) were used to 3D bioprint porous structures without adversely affecting cell viability. Taken together, MHA hydrogels are attractive systems for the design of 3D cell-laden constructs for cartilage regeneration.

5. Acknowledgements

Supporting information

S1. GPC characterization of chondroitin sulfate (CS)

S1.1. Methods

For the detection of the absolute molecular weight of CS, a Viscotek GPC solvent/sample delivery module (GPCmax) coupled with a Triple Detector Array (TDA 302) from Malvern (Malvern, UK), including Refractive Index (RI) and Light Scattering (LS) detectors as well as viscometer, was used. Samples of 5 mg/ml in PBS were injected in PL Aquagel Mixed Column under a flow of 1 ml/min, using PBS as eluent. A solution of Pullulan-P77K from Malvern (dn/dc = 0.147; M_w = 76,681 Da; M_n = 72,167 Da) in 0.3 M sodium acetate buffer (pH 6.5) was used as a standard. Data were processed using Omnisec software 4.7.

S1.2. Results

Figure S1 shows the RI and Right Angle LS chromatograms obtained for CS: the presence of two partially overlapping peaks indicates the co-existence of two MW distributions. Using the area under the RI peaks, it was found that 6% in weight is composed of polymer chains with a M_n of 353.8 kDa and a M_w of 457.5 kDa (PDI = 1.3) and the remaining fraction of 94% showed a M_n of 26.9 kDa and a M_w of 36.3 kDa (PDI = 1.4). It needs to be noticed that the remarkable difference in intensity between the two peaks visible in the RI detection graph is less evident in the LS chromatogram. This is due to the fact that high MW chains give much higher LS signal compared with low MW chains under the same conditions. The dn/dc found for CS was 0.1136.
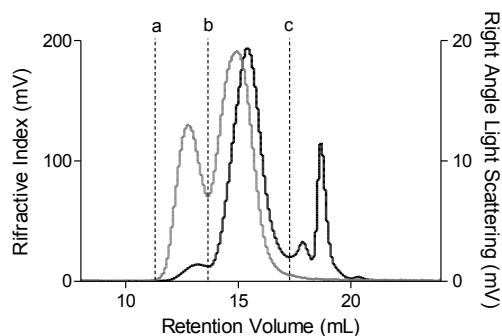

Figure S1. GPC-RI (black line, left Y axis, range = 0-200 mV) and -LS (grey line, right Y axis, range = 0-20 mV) chromatogram enlargement (X axis range = 8-24 ml) for CS. The peaks included between lines a and b are attributed to the higher molecular weight chains, whereas those included between lines b and c are representative of the smaller molecular weight chains.

S2. Identification of the linear viscoelastic range (LVR) for physical gels

S2.1. Methods.
For the identification of the Linear Viscoelastic Range (LVR), each gel (n = 3) was studied at 37°C in oscillation amplitude sweep mode (strain sweep from 0.01 to 100%, frequency = 1Hz), using an AR G-2 rheometer (TA-Instruments, Etten-Leur, The Netherlands), equipped with a cone-plate measuring geometry (cone diameter: 20 mm, angle: 1°).

S2.2. Results
For all thermal gels a LVR from 0.01 to 5-10% was found, after which G' decreased by increasing the strain (Figure S2). Only MHA gels showed a value of G' higher than G" at 37°C and this is in line with the results found during the temperature sweep runs.
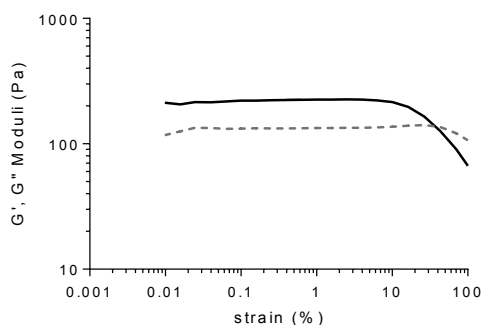
Figure S2. G' (full black line) and G" (dotted grey line) as function of strain, recorded during a strain sweep experiment for MHA hydrogels (strain ramp from 0.01 to 100%).

S3. Differentiation potential of chondrocytes in MCS and MHA hydrogels

S3.1. Methods
Equine chondrocytes (n = 3, 15-20*10^6, passage 1) were encapsulated in MCS and MHA polymer solutions. Cell-laden hydrogels were cast, UV cross-linked, and cultured as described for hydrogels M. To evaluate if chondrocytes had the potential to differentiate and deposit matrix, immunohistochemistry for collagen type II was performed (manuscript, section 'Histology & Immunohistochemistry').

S3.2. Results
In MCS and more dominantly in MHA hydrogels, positive areas for collagen type II were observed after 42 days of culture (Figure S3). During this long term culture, cells also maintained their typical round morphology. These aspects indicate that MCS and especially MHA hydrogels have the potential to be used for the fabrication of constructs for cartilage repair.
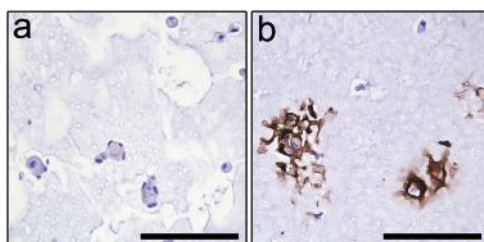
Figure S3. Immunohistochemistry for collagen type II (brown) of chondrocytes differentiated in MCS (a) and MHA (b) hydrogels for 42 days. *Scale bars represent 100 µm.*

Table S1. Input parameters for creating 3D printed constructs.

Parameter	Value
Construct	
• Dimensions (LxWxH) [mm]	12x12x2 or 10.4x10.4x2 mm
• Line spacing [mm]	1.5 or 1.3
• Layer height [mm]	0.1
Microvalve CF300H	
• Inner diameter [mm]	0.3
• Stroke [mm]	0.06
• Temperature [°C]	37
• Needle inner diameter [mm]	0.3
• Valve opening time [µs]	1000
• Dosing distance [mm]	0.05
Hönle Bluepoint 4	
• Distance to sample [mm]	50
• Intensity at 50 mm [mW/cm^2]	103
• Illumination time (each deposited layer) [s]	3
• Post-curing time [s]	9
• λ_{em} [nm]	350 – 450
RegenHU 3DDiscovery	
• Baseplate temperature [°C]	40
• Gel cartridge temperature [°C]	37
• Speed XY [mm/s]	35
• Pressure [bar]	1.5

4

References

1. Almarza, A. J. & Athanasiou, K. A. Design characteristics for the tissue engineering of cartilaginous tissues. *Ann. Biomed. Eng.* **32,** 2–17 (2004).
2. Prakash, D. & Learmonth, D. Natural progression of osteo-chondral defect in the femoral condyle. *Knee* **9,** 7–10 (2002).
3. Hutmacher, D. W. Scaffold design and fabrication technologies for engineering tissues--state of the art and future perspectives. *J. Biomater. Sci. Polym. Ed.* **12,** 107–124 (2001).
4. Vermonden, T., Censi, R. & Hennink, W. E. Hydrogels for Protein Delivery. *Chem. Rev.* **112,** 2853–2888 (2012).
5. Appel, E. A., del Barrio, J., Loh, X. J. & Scherman, O. A. Supramolecular polymeric hydrogels. *Chem. Soc. Rev.* **41,** 6195–6214 (2012).
6. Annabi, N. *et al.* 25th Anniversary Article: Rational Design and Applications of Hydrogels in Regenerative Medicine. *Adv. Mater.* **26,** 85–124 (2014).
7. Malda, J. *et al.* 25th anniversary article: Engineering hydrogels for biofabrication. *Adv. Mater.* **25,** 5011–28 (2013).
8. Censi, R. *et al.* Photopolymerized thermosensitive hydrogels for tailorable diffusion-controlled protein delivery. *J. Control. Release* **140,** 230–236 (2009).
9. Censi, R. *et al.* Photopolymerized thermosensitive poly(HPMAlactate)-PEG-based hydrogels: Effect of network design on mechanical properties, degradation, and release behavior. *Biomacromolecules* **11,** 2143–2151 (2010).
10. Censi, R. *et al.* A Printable Photopolymerizable Thermosensitive p(HPMAm-lactate)-PEG Hydrogel for Tissue Engineering. *Adv. Funct. Mater.* **21,** 1833–1842 (2011).
11. Vermonden, T. *et al.* Macromolecular diffusion in self-assembling biodegradable thermosensitive hydrogels. *Macromolecules* **43,** 782–789 (2010).
12. Censi, R. *et al.* The tissue response to photopolymerized PEG-p(HPMAm-lactate)-based hydrogels. *J. Biomed. Mater. Res. A* **97,** 219–29 (2011).
13. Vermonden, T. *et al.* Photopolymerized thermosensitive hydrogels: Synthesis, degradation, and cytocompatibility. *Biomacromolecules* **9,** 919–926 (2008).
14. Vermonden, T., Besseling, N. A. M., van Steenbergen, M. J. & Hennink, W. E. Rheological Studies of Thermosensitive Triblock Copolymer Hydrogels. *Langmuir* **22,** 10180–10184 (2006).
15. Klein, T. J. *et al.* Strategies for Zonal Cartilage Repair using Hydrogels. *Macromol. Biosci.* **9,** 1049–1058 (2009).
16. Visser, J. *et al.* Biofabrication of multi-material anatomically shaped tissue constructs. *Biofabrication* **5,** 35007 (2013).
17. Melchels, F. P. W. *et al.* Additive manufacturing of tissues and organs. *Prog. Polym. Sci.* **37,** 1079–1104 (2012).
18. Levato, R. *et al.* Biofabrication of tissue constructs by 3D bioprinting of cell-laden microcarriers. *Biofabrication* **6,** 35020 (2014).
19. Groll, J. *et al.* Biofabrication: reappraising the definition of an evolving field. *Biofabrication* **8,** 13001 (2016).
20. Seliktar, D. Designing cell-compatible hydrogels for biomedical applications. *Science* **336,** 1124–8 (2012).
21. Bryant, S. J. & Anseth, K. S. Hydrogel properties influence ECM production by chondrocytes photoencapsulated in poly(ethylene glycol) hydrogels. *J. Biomed. Mater. Res.* **59,** 63–72 (2002).
22. Schuurman, W. *et al.* Gelatin-methacrylamide hydrogels as potential biomaterials for fabrication of tissue-engineered cartilage constructs. *Macromol. Biosci.* **13,** 551–561 (2013).
23. Levett, P. A., Hutmacher, D. W., Malda, J. & Klein, T. J. Hyaluronic acid enhances the mechanical properties of tissue-engineered cartilage constructs. *PLoS One* **9,** e113216 (2014).
24. Levett, P. A. *et al.* A biomimetic extracellular matrix for cartilage tissue engineering centered on photocurable gelatin, hyaluronic acid and chondroitin sulfate. *Acta Biomater.* **10,** 214–223 (2014).
25. Choi, B., Kim, S., Lin, B., Wu, B. M. & Lee, M. Cartilaginous Extracellular Matrix-Modified Chitosan Hydrogels for Cartilage Tissue Engineering. *ACS Appl. Mater. Interfaces* **6,** 20110–20121 (2014).
26. Shim, J.-H. *et al.* Three-dimensional bioprinting of multilayered constructs containing human mesenchymal stromal cells for osteochondral tissue regeneration in the rabbit knee joint. *Biofabrication* **8,** 14102 (2016).
27. Oudshoorn, M. H. M., Rissmann, R., Bouwstra, J. A. & Hennink, W. E. Synthesis of methacrylated hyaluronic acid with tailored degree of substitution. *Polymer.* **48,** 1915–1920 (2007).
28. Hachet, E., Van Den Berghe, H., Bayma, E., Block, M. R. & Auzély-Velty, R. Design of biomimetic cell-interactive substrates using hyaluronic acid hydrogels with tunable mechanical properties. *Biomacromolecules* **13,** 1818–27 (2012).
29. Lesley, J. Hyaluronan Binding by Cell Surface CD44. *J. Biol. Chem.* **275,** 26967–26975 (2000).
30. Chung, C., Erickson, I. E., Mauck, R. L. & Burdick, J. A. Differential Behavior of Auricular and Articular Chondrocytes in Hyaluronic Acid Hydrogels. *Tissue Eng. Part A* **14,** 1121–1131 (2008).
31. Park, S.-H., Park, S. R., Chung, S. Il, Pai, K. S. & Min, B.-H. Tissue-engineered cartilage using fibrin/hyaluronan composite gel and its in vivo implantation. *Artif. Organs* **29,** 838–45 (2005).
32. Dinescu, S. *et al.* Biocompatibility Assessment of Novel Collagen-Sericin Scaffolds Improved with Hyaluronic Acid and Chondroitin Sulfate for Cartilage Regeneration. *Biomed Res. Int.* **2013,** 1–11 (2013).
33. Park, H., Choi, B., Hu, J. & Lee, M. Injectable chitosan hyaluronic acid hydrogels for cartilage tissue

engineering. *Acta Biomater.* **9,** 4779–4786 (2013).

34. Roberts, J. J., Nicodemus, G. D., Ciunta, S. & Bryant, S. J. Incorporation of biomimetic matrix molecules in PEG hydrogels enhances matrix deposition and reduces load-induced loss of chondrocyte-secreted matrix. *J biomed Mater Res A* **97,** 281–291 (2011).

35. Oupický, D., Konák, C. & Ulbrich, K. DNA complexes with block and graft copolymers of N-(2-hydroxypropyl)methacrylamide and 2-(trimethylammonio)ethyl methacrylate. *J. Biomater. Sci. Polym. Ed.* **10,** 573–590 (1999).

36. Neradovic, D. *et al.* Degradation Mechanism and Kinetics of Thermosensitive Polyacrylamides Containing Lactic Acid Side Chains. *Macromolecules* **36,** 7491–7498 (2003).

37. Neradovic, D., van Nostrum, C. F. & Hennink, W. E. Thermoresponsive Polymeric Micelles with Controlled Instability Based on Hydrolytically Sensitive N -Isopropylacrylamide Copolymers. *Macromolecules* **34,** 7589–7591 (2001).

38. Abbadessa, A. *et al.* A thermo-responsive and photo-polymerizable chondroitin sulfate-based hydrogel for 3D printing applications. *Carbohydr. Polym.* **149,** 163–174 (2016).

39. Stenekes, R. J. . & Hennink, W. . Polymerization kinetics of dextran-bound methacrylate in an aqueous two phase system. *Polymer.* **41,** 5563–5569 (2000).

40. Benya, P. Dedifferentiated chondrocytes reexpress the differentiated collagen phenotype when cultured in agarose gels. *Cell* **30,** 215–224 (1982).

41. Guo, J., Jourdian, G. W. & Maccallum, D. K. Culture and Growth Characteristics of Chondrocytes Encapsulated in Alginate Beads. *Connect. Tissue Res.* **19,** 277–297 (1989).

42. Wall, A. & Board, T. in *Classic Papers in Orthopaedics* **53,** 433–435 (Springer London, 2014).

43. Farndale, R. W., Sayers, C. A. & Barrett, A. J. A Direct Spectrophotometric Microassay for Sulfated Glycosaminoglycans in Cartilage Cultures. *Connect. Tissue Res.* **9,** 247–248 (1982).

44. Li, Q., Wang, D. & Elisseeff, J. H. Heterogeneous-phase reaction of glycidyl methacrylate and chondroitin sulfate: mechanism of ring-opening–transesterification competition. *Macromolecules* **36,** 2556–2562 (2003).

45. Burdick, J. A., Chung, C., Jia, X., Randolph, M. A. & Langer, R. Controlled degradation and mechanical behavior of photopolymerized hyaluronic acid networks. *Biomacromolecules* **6,** 386–391 (2005).

46. Smeds, K. A. & Grinstaff, M. W. Photocrosslinkable polysaccharides for in situ hydrogel formation. *J. Biomed. Mater. Res.* **54,** 115–121 (2001).

47. Messager, L. *et al.* Photochemical crosslinking of hyaluronic acid confined in nanoemulsions: towards nanogels with a controlled structure. *J. Mater. Chem. B* **1,** 3369 (2013).

48. Mastbergen, S. C., Saris, D. B. & Lafeber, F. P. Functional articular cartilage repair: here, near, or is the best approach not yet clear? *Nat Rev Rheumatol* **9,** 277–290 (2013).

49. Brittberg, M. Cell Carriers as the Next Generation of Cell Therapy for Cartilage Repair: A Review of the Matrix-Induced Autologous Chondrocyte Implantation Procedure. *Am. J. Sports Med.* **38,** 1259–1271 (2010).

50. Cummings, C. L., Gawlitta, D., Nerem, R. M. & Stegemann, J. P. Properties of engineered vascular constructs made from collagen, fibrin, and collagen-fibrin mixtures. *Biomaterials* **25,** 3699–3706 (2004).

51. Ahmed, T. A. E., Dare, E. V & Hincke, M. Fibrin: A Versatile Scaffold for Tissue Engineering Applications. *Tissue Eng. Part B Rev.* **14,** 199–215 (2008).

52. Eyrich, D. *et al.* Long-term stable fibrin gels for cartilage engineering. *Biomaterials* **28,** 55–65 (2007).

53. Visser, J. *et al.* Reinforcement of hydrogels using three-dimensionally printed microfibres. *Nat. Commun.* **6,** 6933 (2015).

54. Poole, C. A., Ayad, S. & Schofield, J. R. Chondrons from articular cartilage: I. Immunolocalization of type VI collagen in the pericellular capsule of isolated canine tibial chondrons. *J. Cell Sci.* **90 (Pt 4),** 635–643 (1988).

55. Zhang, Z. Chondrons and the Pericellular Matrix of Chondrocytes. *Tissue Eng. Part B Rev.* **21,** 267–277 (2015).

56. Visser, J. *et al.* Crosslinkable hydrogels derived from cartilage, meniscus, and tendon tissue. *Tissue Eng. Part A* **21,** 1195–206 (2015).

57. Kim, J. *et al.* Characterization of low-molecular-weight hyaluronic acid-based hydrogel and differential stem cell responses in the hydrogel microenvironments. *J. Biomed. Mater. Res. - Part A* **88,** 967–975 (2009).

58. Jeong, C. G. *et al.* Screening of hyaluronic acid-poly(ethylene glycol) composite hydrogels to support intervertebral disc cell biosynthesis using artificial neural network analysis. *Acta Biomater.* **10,** 3421–3430 (2014).

59. Chen, A. C., Bae, W. C., Schinagl, R. M. & Sah, R. L. Depth- and strain-dependent mechanical and electromechanical properties of full-thickness bovine articular cartilage in confined compression. *J. Biomech.* **34,** 1–12 (2001).

60. Athanasiou, K. A., Agarwal, A. & Dzida, F. J. Comparative study of the intrinsic mechanical properties of the human acetabular and femoral head cartilage. *J. Orthop. Res.* **12,** 340–349 (1994).

61. Jurvelin, J. S., Buschmann, M. D. & Hunziker, E. B. Optical and mechanical determination of poisson's ratio of adult bovine humeral articular cartilage. *J. Biomech.* **30,** 235–241 (1997).

62. Bolis, S., Handley, C. J. & Cornper, W. D. Passive loss of proteoglycan from articular cartilage explants. *Biochim. Biophys. Acta - Gen. Subj.* **993,** 157–167 (1989).

63. van Dijk-Wolthuis, W. N. E., Hoogeboom, J. A. M., van Steenbergen, M. J., Tsang, S. K. Y. & Hennink, W. E. Degradation and Release Behavior of Dextran-Based Hydrogels. *Macromolecules* **30,** 4639–4645

4

(1997).

64. van de Wetering, P. *et al.* A Mechanistic Study of the Hydrolytic Stability of Poly(2-(dimethylamino) ethyl methacrylate). *Macromolecules* **31,** 8063–8068 (1998).

65. Kurisawa, M., Chung, J. E., Yang, Y. Y., Gao, S. J. & Uyama, H. Injectable biodegradable hydrogels composed of hyaluronic acid–tyramine conjugates for drug delivery and tissue engineering. *Chem. Commun.* 4312 (2005).

66. Hwang, N. S. *et al.* Response of zonal chondrocytes to extracellular matrix-hydrogels. *FEBS Lett.* **581,** 4172–4178 (2007).

67. Akmal, M. *et al.* The effects of hyaluronic acid on articular chondrocytes. *J. Bone Jt. Surg. - Br. Vol.* **87–B,** 1143–1149 (2005).

68. Allemann, F. *et al.* Effects of hyaluronan on engineered articular cartilage extracellular matrix gene expression in 3-dimensional collagen scaffolds. *J. Biomed. Mater. Res.* (2001). doi:10.1002/1097-4636(200104)55:1<13::AID-JBM20>3.0.CO;2-G

69. Callahan, L. A. S. *et al.* ECM production of primary human and bovine chondrocytes in hybrid PEG hydrogels containing type I collagen and hyaluronic acid. *Biomacromolecules* **13,** 1625–31 (2012).

70. Kawasaki, K., Ochi, M., Uchio, Y., Adachi, N. & Matsusaki, M. Hyaluronic acid enhances proliferation and chondroitin sulfate synthesis in cultured chondrocytes embedded in collagen gels. *J. Cell. Physiol.* **179,** 142–148 (1999).

71. Villanueva, I., Gladem, S. K., Kessler, J. & Bryant, S. J. Dynamic loading stimulates chondrocyte biosynthesis when encapsulated in charged hydrogels prepared from poly(ethylene glycol) and chondroitin sulfate. *Matrix Biol.* **29,** 51–62 (2010).

4

Chapter 5

Development of a thermosensitive HAMA-containing bio-ink for the fabrication of composite cartilage repair constructs

Vivian H. M. Mouser*
Anna Abbadessa*
Riccardo Ievato
Wim E. Hennink
Tina Vermonden
Debby Gawlitta
Jos Malda

* both authors contributed equally

This Chapter is also included in the PhD thesis of A. Abbadessa

Abstract

Fine-tuning of bio-ink composition and material processing parameters is crucial for the development of biomechanically relevant cartilage constructs. This study aims to design and develop cartilage constructs with tunable internal architectures and relevant mechanical properties. More specifically, the potential of methacrylated hyaluronic acid (HAMA) added to thermosensitive hydrogels composed of methacrylated poly[*N*-(2-hydroxypropyl)methacrylamide mono/dilactate] (pHPMA-lac)/polyethylene glycol (PEG) triblock copolymers, to optimize cartilage-like tissue formation by embedded chondrocytes, and enhance printability was explored. Additionally, co-printing with polycaprolactone (PCL) was performed for mechanical reinforcement. Chondrocyte-laden hydrogels composed of pHPMA-lac-PEG and different concentrations of HAMA (0-1% w/w) were cultured for 28 days *in vitro* and subsequently evaluated for the presence of cartilage-like matrix. Young's moduli were determined for hydrogels with the different HAMA concentrations. Additionally, hydrogel/PCL constructs with different internal architectures were co-printed and analyzed for their mechanical properties. The results of this study demonstrated a dose-dependent effect of HAMA concentration on cartilage matrix synthesis by chondrocytes. Glycosaminoglycan (GAG) and collagen type II content increased with intermediate HAMA concentrations (0.25-0.5%) compared to HAMA-free controls, while a relatively high HAMA concentration (1%) resulted in increased fibrocartilage formation. Young's moduli of generated hydrogel constructs ranged from 14 to 31 kPa and increased with increasing HAMA concentration. The pHPMA-lac-PEG hydrogels with 0.5% HAMA were found to be optimal for cartilage-like tissue formation. Therefore, this hydrogel system was co-printed with PCL to generate porous or solid constructs with different mesh sizes. Young's moduli of these composite constructs were in the range of native cartilage (3.5-4.6 MPa). Interestingly, the co-printing procedure influenced the mechanical properties of the final constructs. These findings are relevant for future bio-ink development, as they demonstrate the importance of selecting proper HAMA concentrations, as well as appropriate print settings and construct designs for optimal cartilage matrix deposition and final mechanical properties of constructs, respectively.

1. Introduction

Three dimensional (3D) bioprinting is a promising technique for the fabrication of regenerative constructs. It allows accurate positioning of cells and biomaterials in a layered fashion and can thus be used for the fabrication of organized tissue-like structures[1], *e.g.* articular cartilage constructs in which a depth-dependent matrix composition and mechanical resistance are addressed[2–4]. Overall, cartilage tissue consists of glycosaminoglycans (GAGs), collagen type II, and water, and contains only a limited number of cells. The low cell number in combination with the lack of vasculature and nerves, leads to the limited regenerative capacity of this tissue[5]. As a consequence, most untreated cartilage defects eventually result in arthritic changes of the whole joint[6]. Therefore, regenerative treatments based on bioprinting to reproduce the cartilaginous organized architecture, are currently under investigation[7–9].

The most commonly used biomaterials for the 3D bioprinting of cartilage constructs are hydrogels, as they allow homogeneous encapsulation of cells and biological cues, and support survival of relevant cell types, *i.e.* mesenchymal stem cells and chondrocytes. Although hydrogels are potentially suitable for this purpose, optimizing them for bioprinting is challenging. In order to print with high shape-fidelity, the hydrogel needs to possess certain rheological properties, *e.g.* high yield stress and viscosity, while for cell encapsulation and optimal tissue production by embedded cells, low yield stresses and viscosities are favorable[10,11]. Hydrogels based on UV-curable copolymers of a polyethylene glycol (PEG) midblock flanked by two partially methacrylated poly[*N*-(2-hydroxypropyl)methacrylamide mono/dilactate] (pHPMA-lac) outer blocks are attractive systems for tissue-engineering applications because their characteristics, *e.g. in vitro* degradation rate and mechanical properties can be accurately tuned via adjustments of the building block's architecture and polymer concentration[12–15]. Recently, we have demonstrated that pHPMA-lac-PEG hydrogels with relatively low concentration and degree of methacrylation supported cartilage matrix deposition by embedded chondrocytes[16]. In addition, the partial replacement of pHPMA-lac-PEG triblock copolymers with methacrylated polysaccharides, *i.e.* hyaluronic acid (HAMA)[16] and chondroitin sulfate[17] further prolonged the *in vitro* degradation profile and enhanced the mechanical properties of the hydrogel blends. Importantly, the addition of HAMA to pHPMA-lac-PEG hydrogels allowed bioprinting with sufficient shape-fidelity of hydrogels even when a relatively low total polymer concentration was used[16]. Hyaluronic acid (HA) and chondroitin sulfate are polysaccharides present in articular cartilage tissue and have been reported to influence multiple biological processes, e.g. cell proliferation, migration, attachment, and differentiation[18–20]. Especially HA forms an interesting component for cartilage tissue-engineering as multiple studies have demonstrated an anabolic effect of both HA and HAMA on chondrocytes in various culture systems in vitro and in vivo[21–28]. However, several studies also indicated a critical role of the HA or HAMA concentration on chondrogenesis, as too low or too high HA or HAMA concentrations can be ineffective or even inhibitory[25–28]. Therefore, it is important to identify the currently unknown optimal concentration of HAMA in pHPMA-lac-PEG triblocks/HAMA hydrogels for cartilage regeneration.

5

An additional aspect that has to be taken into account for cartilage repair constructs, is the requirement to withstand the high compressive and shear forces present in the articulating joints. However, the maximum stiffness that any hydrogel can reach, without hampering matrix production of embedded cells, is limited[29]. Multiple reinforcement strategies, such as the inclusion of fibers[30,31] or microparticles[32], consisting of different materials, *e.g.* polycaprolactone (PCL)[33–35], poloxamer-based hydrogels[36], and ceramics[37] have been explored. Especially PCL is a promising reinforcement material as it is biocompatible, cost-effective, and it has a relatively slow degradation rate (ranging from months to years)[38]. The co-printing of a (cell-laden) hydrogel with a PCL fiber reinforcement offers a construct design in which the hydrogel provides the necessary milieu for cells to thrive, and the thermoplastic framework provides the required mechanical properties, to overall mimic the biomechanical profile of native cartilage. The mechanical performance of co-printed hydrogel/PCL constructs is dominated by that of the PCL framework[30]. Therefore, by modifying the PCL molecular weight and the geometry of the PCL skeleton, the compressive modulus and tensile strength can be tailored to that of the target tissue[39]. The strand size, strand distance, and to a lesser extent strand orientation, have been identified as the most important geometrical parameters to influence the mechanical features of the printed construct[33,39,40]. Hence, co-printing of pHPMA-lac-PEG triblocks/HAMA hydrogel with PCL might be an attractive approach for the fabrication of cartilage repair constructs. Hence, the aim of this study was to generate bioprinted constructs for cartilage regeneration with optimized bioactivity, and a tunable mechanical performance. As such, the optimal concentration of HAMA in pHPMA-lac-PEG triblocks/HAMA hydrogels for cartilage-like tissue formation of embedded chondrocytes was evaluated, and co-printing with PCL, using multiple construct architectures, was explored to match the mechanical properties of native cartilage.

2. Materials and methods

2.1. Materials

All chemicals were obtained from Sigma-Aldrich (Zwijndrecht, the Netherlands) and all solvents from Biosolve (Valkenswaard, the Netherlands) unless indicated otherwise. Chemicals and solvents were used as received. HA sodium salt (120 kDa) was supplied by Lifecore Biomedical (Chaska, MN, USA) and PEG (10 kDa) by Merck (Darmstadt, Germany). GMP grade homopolymer of ε-caprolactone (PCL, Parasorb PC 12, 185001) and L-lactide were obtained from Corbion (Gorinchem, The Netherlands), and Irgacure 2959 was a kind gift of BASF (Ludwigshafen, Germany). *N*-(2-hydroxypropyl) methacrylamide mono- and dilactate, and $PEG_{10 kDa}$-4,4'-azobis(cyanopentanoate) macroinitiator were synthesized as previously reported[41,42]. Phosphate buffered saline (PBS), penicillin/streptomycin (pen/strep; 10,000 units/ml penicillin and 10 mg/ml streptomycin) and picogreen DNA assay were supplied by Invitrogen (Carlsbad, California, USA). Fetal bovine serum (FBS) was purchased from Gibco (Invitrogen corporation) and type II collagenase was obtained from Worthington Biochemical Corp (Lakewood, NJ, USA).Two types of Dulbecco's Modified Eagle Medium (DMEM) were used: DMEM 31885 from Gibco (referred to as DMEM)

and high glucose DMEM D6429 from Sigma-Aldrich (referred to as high glucose DMEM). Recombinant human TGF-β1 was obtained from Peprotech (London, UK), hyaluronidase (H2126) from Sigma-Aldrich, pronase (11459643001) from Roche Life Sciences (Indiana, USA), and ITS+ premix (human recombinant insulin, human transferrin, selenous acid, bovine serum albumin, linoleic acid) from BD Biosciences (Breda, the Netherlands). Antibody against collagen type I (1:100; EPR7785, ab138492) was obtained from Abcam (Cambridge, UK). Antibodies against collagen types II and VI (1:100; II-6B3II and 1:5, 5C6, respectively) were obtained from the Developmental Studies Hybridoma Bank (Iowa City, IA, USA). Antibody against proteoglycan IV (1:50; H00010216-M01) was obtained from Novus (Abingdon, United Kindom). Secondary horse radish-peroxidase conjugated antibodies for collagen type I (EnVision+, K4010), collagen type II (1:100, IgG HRP, P0447), collagen type VI and proteoglycan IV (EnVision+, K4007) were ordered from DAKO (Heverlee, the Netherlands). Calcein-AM (to stain living cells) and ethidium homodimer-1 (to stain nuclei of dead cells) were obtained from Life Technologies (L3224, Bleiswijk, the Netherlands).

2.2. Synthesis and characterization of polymers

A triblock copolymer composed of two poly[N-(2-hydroxypropyl) methacrylamide mono/dilactate] outer blocks (~15 kDa) flanking a PEG (10 kDa) midblock, was synthesized and characterized as previously described, and 10% of the hydroxyl groups from the pendent lactate side-unites was methacrylated (chemical structure reported in Scheme S1)[12]. The methacrylated pHPMA-lac-PEG triblock copolymer is hereafter termed $M_{10}P_{10}$ [M_{10} refers to a degree of methacrylation (DM) of 10%, and P_{10} refers to a PEG block with a molecular weight (MW) of 10 kDa]. Hyaluronic acid was methacrylated (DM = 10%, indicating the presence of 10 methacrylate groups per 100 disaccharide units) as previously described (chemical structure reported in Scheme S1)[43]. The characteristics of $M_{10}P_{10}$, *i.e.* number average molecular weight (M_n), polydispersity index (PDI), CP and DM, as well as those of HAMA, *i.e.* MW and DM were in line with our previous findings[12,16,17].

2.3. Experimental design

First, a screening of five different hydrogel formulations (Table 1) was performed to find the optimal concentration of HAMA for cartilage tissue-engineering with chondrocyte-laden $M_{10}P_{10}$/HAMA hydrogels. Equine chondrocytes were encapsulated in the different hydrogel formulations and constructs were cast for *in vitro* culture. At days 1 and 28, the hydrogels were harvested and evaluated for cartilage-like tissue formation. In addition, Young's moduli were evaluated for cell-free cast hydrogel constructs of different compositions (Table 1).

Second, 3D printed constructs were fabricated with the best performing formulation of the first screening, *i.e.* $MHA_{0.5}$. Additionally, multiple constructs with different architectures were fabricated by co-printing $MHA_{0.5}$ and PCL, and the Young's moduli were determined.

5

Table 1. Overview of the concentrations of $M_{10}P_{10}$ and HAMA in PBS for the five evaluated hydrogel formulations with their abbreviations.

Abbreviation	Polymer concentration (% w/w)	
	$M_{10}P_{10}$	HAMA
M	20	-
$MHA_{0.1}$	19.9	0.1
$MHA_{0.25}$	19.75	0.25
$MHA_{0.5}$	19.5	0.5
MHA_1	19	1

2.4. Chondrocyte isolation and fabrication of chondrocyte-laden cast hydrogels

Primary chondrocytes were harvested from macroscopically healthy full-thickness cartilage of equine metacarpophalangeal joints (n = 3; 3-10 years old), obtained from the local slaughterhouse. Cartilage was removed from the joints and digested overnight at 37°C in DMEM supplemented with collagenase II (1.5 µg/ml), hyaluronidase (1 mg/ml), FBS (10%), and pen/strep (1%). After digestion, the cell suspension was filtered through a 40 µm cell strainer and the chondrocytes were stored in liquid nitrogen until further use.

Before use, chondrocytes (passage 0) were expanded in monolayer culture for ~14 days (seeding density of $5 * 10^3$ cells/cm²) in chondrocyte expansion medium consisting of DMEM, FBS (10%) and pen/strep (1%). The chondrocytes were harvested when they reached 80-90% confluence. Stock solutions of 30% $M_{10}P_{10}$ and 3% HAMA were prepared by dissolving the right amount of both polymers in PBS with Irgacure (0.05%) at 4°C overnight. Next, the stock solutions were mixed at different ratios and diluted if necessary to obtain the five different formulations (Table 1). Chondrocytes were mixed with the $M_{10}P_{10}$/HAMA mixtures on ice, to obtain a final concentration of 15-20 * 10^6 chondrocytes/ml (n = 3, concentration slightly varied per donor). Constructs were cast by injecting the cell-laden polymer mixtures into cylindrical Teflon molds (sample size: 6 mm in diameter, 2 mm in height). The molds were incubated for 15 minutes at 37°C to allow physical hydrogel formation. Subsequently, chemical cross-linking was induced by irradiation with UV light (UV-Handleuchte lamp A. Hartenstein, Germany, wavelength: 365 nm, intensity at 3 cm: 1.2 mW/cm², irradiation time: 5 minutes). Cross-linked constructs were removed from the molds and were cultured for 28 days at 37°C and 5% CO_2 in chondrogenic differentiation medium consisting of high glucose DMEM supplemented with ITS+ premix (1%), dexamethasone (0.1 µM), L-ascorbic acid-2-phosphate (0.2 mM), recombinant human TGF-β1 (10 ng/ml), and pen/strep (1%) to stimulate chondrogenesis and redifferentiation of the chondrocytes[44,45]. As a positive control, fibrin samples containing chondrocytes from the same donors were prepared and cultured as previously described[16].

2.5. Histology, immunohistochemistry, and biochemical assays

To evaluate cartilage-like tissue formation, hydrogels were harvested at days 1 and 28. Part of each sample was fixed overnight in formalin (37%) and dehydrated through a graded ethanol series. After a clearing step in xylene, the samples were embedded in paraffin. Sections with a thickness of 5 µm were generated and stained with safranin-O to visualize proteoglycans, fast green to visualize collagens, and hematoxylin to stain cell nuclei, as previously described[46]. Collagen types I, II, and VI were visualized on sections with immunohistochemistry as previously described[16]. For proteoglycan IV immunohistochemistry, the same protocol was used as previously described for collagen type VI, but with only a pronase antigen retrieval. All sections were visualized with a light microscope (Olympus BX51 microscope, Olympus DP70 camera, Hamburg, Germany). The remaining parts of the different harvested cell-laden hydrogels were weighed, freeze dried, and weighed again to determine the water content. Next, the samples were digested overnight at 60°C in digestion buffer (0.2 M NaH_2PO_4 + 0.01 M EDTA · 2 H_2O in milliQ, pH = 6.0) supplemented with papain (31 units/mg protein, final concentration of 0.24 mg protein/ml) and cysteine (0.01 M). After digestion, the glycosaminoglycan (GAG) content was determined as a measure for proteoglycan, with a dimethylmethylene blue (DMMB) assay[47], using chondroitin sulfate C as standard. The amount of DNA as a measure of proliferation was measured with the Quant-iT PicoGreen dsDNA kit and read on a spectrofluorometer (Biorad, Hercules, California, USA), according to the manufacturer's protocols. The GAG content measured at day 28 was corrected for the initial readout at day 0, due to the presence of HAMA (Figure S1). This corrected GAG content was normalized to the DNA content for comparison between groups. In addition, the average change in water content normalized to the samples wet weight (wwt) was determined for each hydrogel formulation. The DNA content was normalized to the dry weight (dwt) of the samples.

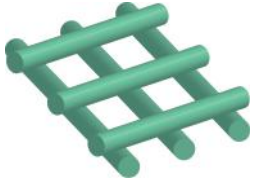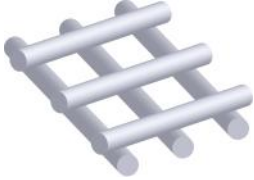### 2.6. Evaluation of mechanical properties of hydrogel constructs
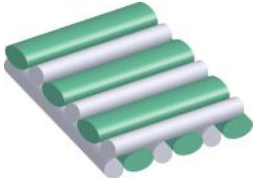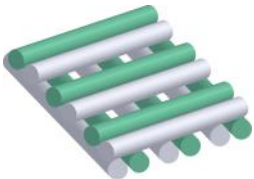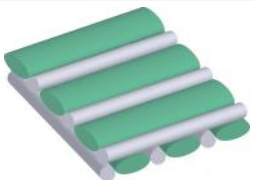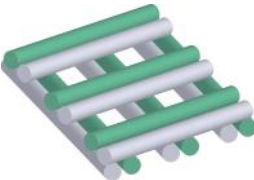
Cell free, cylindrical hydrogels cast as described in section 2.4. were analyzed using a Dynamic Mechanical Analyzer, DMA (DMA Q800, TA Instruments, Etten-Leur, The Netherlands) in an uniaxial unconfined compression test, after the equilibrium state of swelling (≥ 5h) was reached in PBS. A preload force of 0.001 N and a ramp force of 0.1 N/min with an upper force limit of 1 N were applied, and the elastic modulus (E, Young's modulus) was calculated as the slope of the initial linear segment of the stress/strain curves (n = 3).

2.7. Fabrication and characterization of printed constructs with and without reinforcement

Constructs of different designs and with or without PCL reinforcement were printed with formulation M or $MHA_{0.5}$ (Table 2) using a 3DDiscovery bioprinter (regenHU, Villaz-St-Pierre, Switzerland) equipped with a Bluepoint 4 UV lamp (point light source, wavelength range: 300-600 nm, UV-A intensity at 5 cm = 103 mW/cm², Hönle UV Technology AG, Gräfelfing, Germany). Pneumatically driven robotic dispensers were used for the

5

extrusion of the hydrogel and PCL filaments. The hydrogel precursor mixture was loaded into a syringe connected to a micro valve (CF300H) nozzle, while PCL pellets were loaded into a stainless steel cartridge furnished with a phosphor bronze thin-wall conical nozzle (inner diameter = 0.56 mm; Integrated Dispensing Solutions, Agoura Hills, CA). Each layer of the PCL/hydrogel hybrid constructs was generated by printing parallel filaments of PCL (strand distance = 1.5 or 2.0 mm), followed by deposition of hydrogel filaments between adjacent PCL strands. Subsequent layers were printed with a filament orientation perpendicular to that of the underlying layer. To achieve a solid or a porous hydrogel filling of the PCL framework, the hydrogel was deposited in the center of adjacent PCL filaments or at a distance of ¼ of the strand distance, respectively. Additionally, the amount of the extruded hydrogel was adjusted by varying the valve opening time (v.o.t.) and pressure (detailed print settings reported in Table 3). Different temperatures of the deposition plate were used to obtain desired flow-behavior of the hydrogel after extrusion. For all designs (Table 2), square sheets (15 x 15 mm) were printed with a height of 2.4 mm, and after each hydrogel layer was printed, chemical cross-linking was induced by 3 seconds of irradiation with the Bluepoint UV lamp from a distance of 5 cm. After printing, constructs were irradiated for an additional time period to reach a total irradiation time of 69 seconds. After crosslinking, cylindrical samples were punched out of the printed sheets with a 6 mm biopsy punch, and visually inspected and photographed using an Olympus ZS61 microscope (Tokyo, Japan) coupled with an Olympus digital camera (Tokyo, Japan). As controls, hydrogel-free PCL constructs and PCL constructs infused with hydrogel by injection molding were generated. More specifically, two PCL sheets with different strand distances, *i.e.* 1.5 or 2.0 mm were printed as described above but without dispensing hydrogel between the PCL filaments. Subsequently, six cylindrical samples were punched out from each sheet, and three constructs per sheet were inserted in a Teflon-based injection mold, infused with the hydrogel, incubated at 37 °C for 5 minutes, and cross-linked for 69 seconds using the Bluepoint UV lamp from a distance of 5 cm. The remaining three constructs per sheet were used as hydrogel-free controls. Finally, the mechanical stiffness of the different printed constructs was evaluated using a DMA with an unconfined compression set up. Samples were preloaded with a force of 0.1 N and further compressed up to 18 N using a force ramp rate of 1.8 N/min. Young's moduli were calculated using stress strain curves.

Table 2. Construct designs for printing with hydrogel MHA$_{0.5}$ (green) with and without PCL (white) reinforcement.

Abbreviation	Materials	Layer design	Description*
pMH	MHA$_{0.5}$		Porous s.d.=1.5 mm
pPCL_1	PCL		Porous s.d.=1.5 mm
pPCL_2	PCL		Porous s.d.=2.0 mm
pMH/PCL_1	MHA$_{0.5}$ + PCL		Solid s.d.=1.5 mm
pMH/PCL_2	MHA$_{0.5}$ + PCL		Porous s.d.=1.5 mm
pMH/PCL_3	MHA$_{0.5}$ + PCL		Solid s.d.=2.0 mm
pMH/PCL_4	MHA$_{0.5}$ + PCL		Porous s.d.=2.0 mm

*s.d. = strand distance

5

Table 3. Optimized settings applied for the 3D printing of hydrogel, PCL and hydrogels/PCL constructs.

pMH	Hydrogel print settings	PCL print settings
Pressure	0.1 MPa	-
Temperature		
Cartridge	37°C	
Deposition plate	40°C	
XY plane speed	40 mm/s	
Microvalve CF300H		
Dosing distance	0.1 mm	
Valve opening time	300 µs	
PCL	**Hydrogel print settings**	**PCL print settings**
Pressure	-	0.3 MPa
Temperature		
Cartridge		80°C
Deposition plate		35°C
XY plane speed		1 mm/s
pMH/PCL	**Hydrogel print settings**	**PCL print settings**
Pressure	0.1^a or 0.13^b MPa	0.3 MPa
Temperature		
Cartridge	37°C	80°C
Deposition plate	35^c or 40°C^d	35^c or 40°C^d
XY plane speed	40 mm/s	1 mm/s
Microvalve CF300H		
Dosing distance	0.1 mm	
Valve opening time	300^e, 500^f or 1300^g µs	
Cellularized pMH/PCL	**Hydrogel print settings**	**PCL print settings**
Pressure	0.2 MPa	0.3 MPa
Temperature		
Cartridge	37°C	80°C
Deposition plate	35°C	35°C
XY plane speed	40 mm/s	1 mm/s
Microvalve CF300H		
Dosing distance	0.1 mm	
Valve opening time	650 µs	

[a] Applied to pMH_1, pMH_2 and pMH_4
[b] Applied to pMH_3
[c] Applied to pMH_1 and pMH_3
[d] Applied to pMH_2 and pMH_4
[e] Applied to pMH_2 and pMH_4
[f] Applied to pMH_1
[g] Applied to pMH_3

2.8. Statistics

Statistical analysis was performed with SPSS software (version 21, IMB Corp.). For quantitative measurements of matrix production within one cell donor, a one-way analysis of variance (ANOVA) was performed, while a randomized block design ANOVA was performed for the average matrix production, to correct for donor variations. Differences in Young's moduli and viability were determined with a one-way ANOVA. Differences in Young's moduli between constructs fabricated with a different strand distance within each co-print condition were determined with an independent t-test. A significance level of 0.05 was used. When the ANOVA highlighted significant differences, a Bonferroni post hoc test was performed except for the GAG/DNA data in the cast hydrogels which were compared with a Dunnett post hoc test to explore whether the presence of HAMA had an effect compared to HAMA free hydrogels.

3. Results and discussion

3.1. Effect of HAMA concentration on chondrogenesis by embedded chondrocytes

The evaluated hydrogel formulations supported cartilage matrix production of embedded chondrocytes with a hydrogel composition-dependent extent (Figure 1). During culture, rounded cell clusters rich in newly formed matrix were observed in samples with average HAMA concentrations (MHA$_{0.25}$, MHA$_{0.5}$, Table 1) and to a lesser extent in the hydrogels without HAMA or with the lowest HAMA concentration (M and MHA$_{0.1}$). The largest cell clusters surrounded by newly formed matrix were observed in samples with the highest HAMA concentration (MHA$_1$), however these clusters were observed sporadically and had irregular shapes compared to the rounded clusters in the other formulations. Additionally, the cells and cell nuclei within these irregular shaped clusters had a stretched appearance (samples MHA$_1$). Contrarily, cells and cell nuclei in the hydrogels with lower HAMA concentrations or without HAMA contained a rounded shape after 28 days of culture. The tissue matrix around the circular cell clusters reacted strongly with the collagen type II antibody, as well as with safranin-O, indicating the presence of cartilage-like tissue (Figure 1). As safranin-O also stains HAMA, a pink color was observed in all HAMA-containing hydrogels also at day 0. However, the intensity of the staining was higher near the cells for samples at day 28. More collagen type II positive and intense red (safranin-O) areas were observed in hydrogels with intermediate HAMA concentrations (MHA$_{0.25}$, MHA$_{0.5}$) compared to hydrogels without HAMA or with the lowest HAMA concentrations (M and MHA$_{0.1}$). Hydrogels with formulation MHA$_1$ contained hardly any safranin-O positive areas at day 28, but did reveal intense collagen type II positive areas. However, the collagen type II staining was restricted to the sporadic cell clusters. On the other hand, in hydrogels with intermediate HAMA concentrations (MHA$_{0.25}$, MHA$_{0.5}$) some collagen type II positive areas were also observed in the inter-territorial regions. The presence of collagen type I, a marker for fibrocartilage, increased with increasing HAMA concentration (Figure 1). Additionally, the presence of collagen type VI, a marker of chondron formation, decreased in the areas directly around the chondrocyte membranes in hydrogels with increasing HAMA concentrations, although the matrix clusters in MHA$_1$

stained overall positive for collagen type VI. Finally, proteoglycan IV, a zonal marker found predominantly in the cartilage surface, was mainly expressed at the hydrogel border of constructs without HAMA or with a low HAMA concentration (0.1%). Overall, all samples showed some proteoglycan IV positive areas.
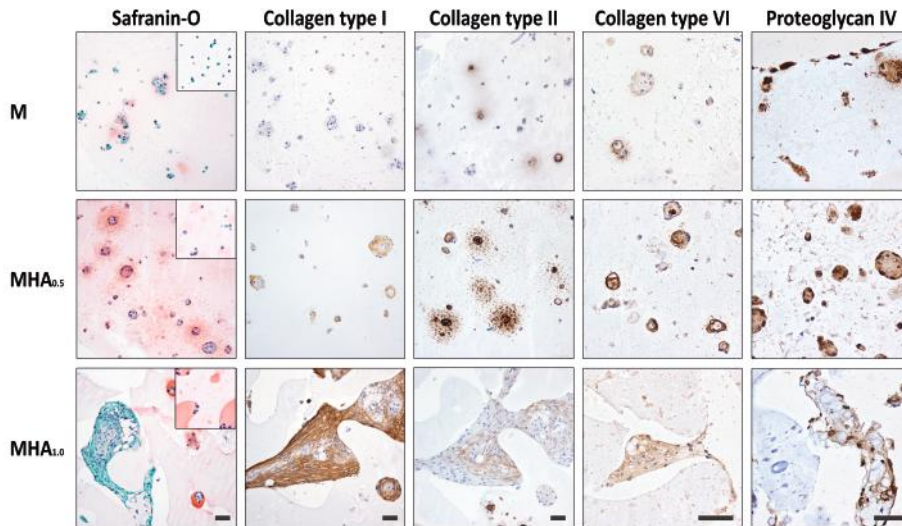

Figure 1. Overview of the histology and immunohistochemistry of chondrocytes cultured in $M_{10}P_{10}$/HAMA hydrogels with different HAMA concentrations for 28 days. Scale bar represent 50 µm and it is the same for all images of the same staining. Square insert in the safranin-O images are from day 1 samples.

Quantitative measurements for GAG content normalized to the DNA content of donor 1 and 2 (Figure 2a and b) matched the visualization of GAGs with the safranin-O staining in Figure 1. Contrary, no clear differences between hydrogels with different HAMA concentrations were observed in samples cultured with chondrocytes from donor 3 (Figure 2c). This illustrates that the influence of HAMA on matrix synthesis by the chondrocytes is varying between chondrocyte donors[48,49]. On average, significantly more GAG/DNA was measured in hydrogels with intermediate HAMA concentrations ($MHA_{0.25}$, $MHA_{0.5}$), compared to the hydrogels without HAMA (M) (Figure 2d). Hydrogels with the lowest ($MHA_{0.1}$) and highest (MHA_1) HAMA concentrations did not show significant differences in GAG/DNA compared to hydrogels without HAMA (M). Samples with 1% HAMA, cultured with chondrocytes of donor 2, did contain significantly less GAG/DNA compared to the HAMA free hydrogels (Figure 2b). Moreover, GAG/DNA levels measured in samples with intermediate HAMA concentrations (0.25-0.5%) were similar to the fibrin controls for donors 1 and 2, while the GAG/DNA levels were higher in the fibrin samples for donor 3 (Figure S2).
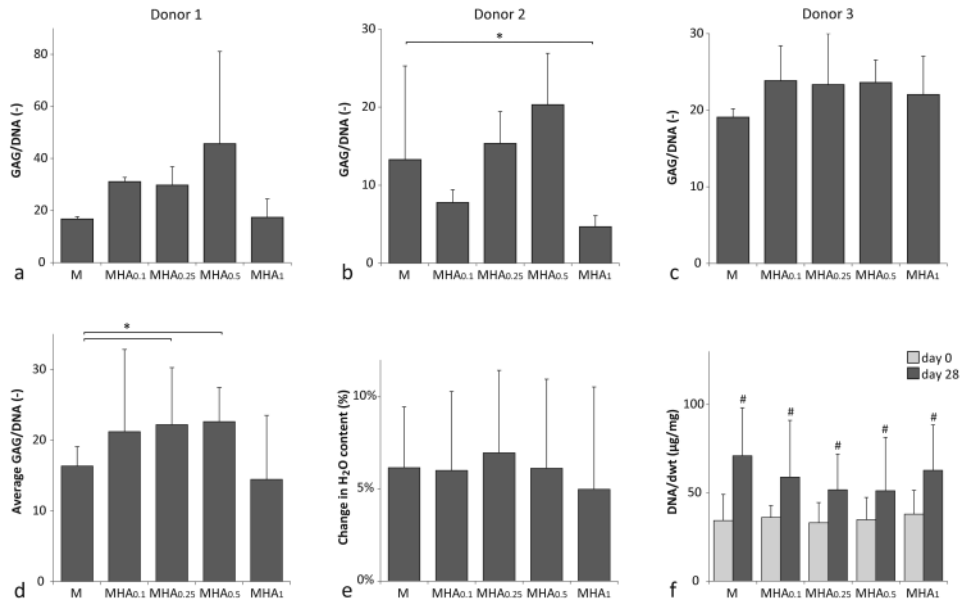
Figure 2. Biochemical analysis of multiple chondrocyte-laden hydrogel formulations. *a-d) GAG content normalized to the DNA content at day 28 for (a) donor 1, (b) donor 2, (c) donor 3, and (d) the average of all donors. e) Difference in water content between day 28 and day 0. f) DNA content normalized to the dwt. * indicates a significant difference between the groups. # indicates a significant difference compared to groups without a # but similar to groups with a #.*

These observations demonstrate a dose-dependent effect of HAMA on the cartilage matrix production by chondrocytes in pHPMA-lac-PEG/HAMA hydrogels. More specifically, hydrogels with intermediate HAMA concentrations (0.25 and 0.5%) showed increased cartilage-like matrix production by the embedded cells compared to HAMA-free hydrogels, while a higher HAMA concentration (1%) stimulated a shift from hyaline cartilage to fibrocartilage formation. Chondrocytes are known to interact with HA via their membrane receptors *e.g.* CD44, intercellular adhesion molecule-1 (ICAM-1), and receptor for hyaluronan mediated motility (RHAMM)[26,50–53]. This interaction is believed to be responsible for the anabolic effect that HA can have on the matrix production by chondrocytes, as disruption of this HA-chondrocyte binding is associated with matrix degradation in native cartilage[54]. The dose-dependent response of chondrocytes to HA may be attributed to a negative feedback system, in which limited receptor binding with HA, especially via CD44, stimulates matrix production by chondrocytes, while more receptor interactions inhibit chondrocyte redifferentiation[26,43,44,55]. The hypothesis of receptor binding, would also explain why the optimal HA and HAMA concentration for cartilage matrix stimulation appears to increase with increasing cell numbers. In the present study, we demonstrate an optimum with 0.25-0.5% HAMA in pHPMA-lac-PEG triblock copolymers based hydrogels with $20 * 10^6$ chondrocytes/ml. Kawasaki *et al.* (1999)[28] reported an optimum with 0.001-0.01% of HA in collagen-based hydrogels with

2 * 10^6 chondrocytes/ml, Akmal et al. (2005)[26] found an optimum with 0.01-0.1% HA in alginate beads with 5 * 10^6 chondrocytes/ml, whereas Levett et al. (2014)[27] found an optimum with 0.5% HAMA in collagen type I based hydrogels with 10 * 10^6 chondrocytes/ml. Nevertheless, in contrast to our findings, Levett et al. (2014)[27] and Akmal et al (2005)[26] reported a decrease in collagen type I gene expression and protein level, respectively, by chondrocytes in hydrogels with increasing HA or HAMA concentrations. Both studies were conducted with hydrogels based on natural polymers with known cell attachment sites that influence cell behavior, which could explain the different findings[43]. Intuitively, the optimal HA or HAMA concentration for matrix production is likely also dependent on the hydrogel system in which the cells are cultured. The polymer network influences cell migration, which can affect the establishment of a receptor-HA interaction[56]. Additionally, other materials properties, such as construct stiffness and cross-linking densities, have also been demonstrated to influence cell behavior and could, therefore, also influence the response of chondrocytes to the presence of HAMA[57,58].

The water content normalized to the samples wet weight increased for all hydrogel formulations during culture with approximately 5-7% (Figure 2e). However, no significant differences in swelling were observed between the various formulations, regardless the HAMA content. This finding is in line with previous studies that also reported a negligible change in swelling of samples with 0-1% HAMA[21,27].

The DNA content normalized to the samples' dry weight significantly increased for all hydrogel formulations during the culture period (Figure 2c). All hydrogel formulations reached a similar DNA/dwt content at day 28 (~50-70 µg/mg), implying that all hydrogels supported proliferation to a similar extent. Although HA is capable to influence proliferation of multiple cell types, this was not observed in the current study for chondrocytes, in line with Levett et al. (2014)[27]. Contrarily, Kawasaki et al. (1999)[28], Akmal et al. (2005)[26], and Park et al. (2013)[23], reported an increase in DNA content due to the presence of HA. However, the initial cell densities used in those studies were lower compared to the cell density used by Levett et al. (2014)[27] and by us in the current study which may explain the observed difference[59]. Additionally, Akmal et al. (2005)[26] only observed an increase in proliferation in hydrogels with the lowest HA concentrations, suggesting that this effect can also be dose-dependent and thus not present in the higher HA concentrations used by Levett et al. (2014)[27] and in this study.

3.2. Effect of HAMA concentration on hydrogel mechanical properties
All studied hydrogel formulations were shape-stable after swelling in PBS (≥ 5h). Young's moduli ranged from 14.0±0.6 to 30.8±0.9 kPa (Figure 3).

Figure 3 shows that the Young's modulus of $M_{10}P_{10}$/HAMA hydrogels increased with increasing HAMA concentration. The Young's moduli of all evaluated hydrogel formulations were statistically different from each other, except for MHA0.1 and MHA0.25 that had similar moduli. Clearly, the presence of HAMA led to stiffer hydrogels compared to hydrogel M, despite an equal total polymer concentration, i.e. 20% w/w and a comparable total number of methacrylate groups. These findings are in line with our previous observations[15] and can find an explanation in the microstructure of these
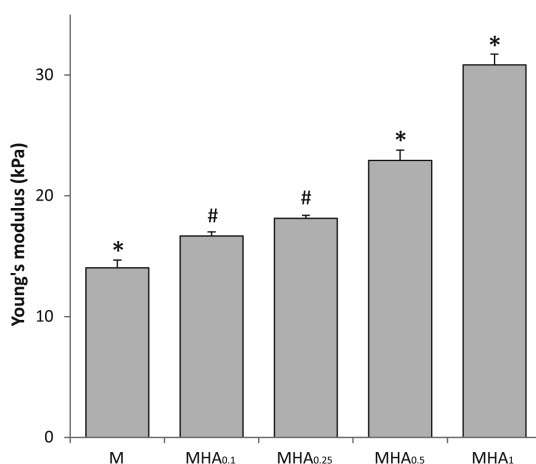
Figure 3. Young's moduli obtained from stress/strain curves which were generated with unconfined compression, where * indicates a significant difference (p < 0.05) from all other groups and # indicates a significant difference to all groups except to each other.

hydrogels. $M_{10}P_{10}$/HAMA hydrogels are known to exhibit phase separation[60], as also observed in the safranin-O histology at day 0 (Figure 1) for HAMA-containing hydrogels. We have recently demonstrated that micro-phase separation in these hydrogels leads to the formation of highly hydrated, HAMA-rich domains and partially dehydrated more hydrophobic regions, where the majority of $M_{10}P_{10}$ is located[60]. The extent of this phase separation is highly dependent on the HAMA concentration. In that study, we have also found that when using low HAMA concentrations (< 1% w/w), the relative increase in $M_{10}P_{10}$ concentration in the hydrophobic domains due to their partial dehydration (driven by the presence of HAMA), resulted in stiffer physical hydrogels. In a similar way, this phenomenon could explain the effect of HAMA concentration on the Young's moduli of chemically cross-linked hydrogels found in the present study. The effect of HAMA on construct stiffness may also be partially attributed to the much higher MW of HAMA (120 kDa) compared to that of $M_{10}P_{10}$ (40 kDa). In fact, the relatively longer HAMA molecules are likely able to generate more chain entanglements that provide higher stiffness to the entire polymer network. The general increase of hydrogel stiffness with increasing HAMA concentration, likely responsible for a tighter network in hydrogels with higher HAMA content, can also explain the observed cell clusters with irregular shapes and confined matrix deposition in the histological analysis of MHA_1 hydrogels. In fact, it has been reported that dense polymer networks can hamper the diffusion of newly formed matrix[11,29,61]. In addition, the differences in construct stiffness may also contribute to the difference in matrix production by the embedded chondrocytes[57,58].

3.3. Fabrication of hydrogel/PCL co-printed constructs

Among all evaluated hydrogel formulations, hydrogels containing 0.5% HAMA ($MHA_{0.5}$)

induced the highest cartilage-like tissue formation, and displayed a medium/high Young's modulus, which is beneficial for the hydrogel filament stability during printing and handling. Hence, the printing experiments were performed with this formulation. Additionally, the incorporation of 0.5% HAMA introduced yield stress behavior to $MHA_{0.5}$ (yield stress = 28.7±0.2 Pa), which is reported to improve shape-fidelity of 3D bioprinted constructs[11,16,62,63], whereas in accordance with our previously reported findings[17], no yield stress was found for the HAMA-free formulation M (control, Figure S3). In fact, 3D printing of shape-stable $MHA_{0.5}$ constructs without supporting structures or reinforcement was successfully achieved (Figure 4a). Printing of PCL under optimized conditions and using a strand distance of 1.5 or 2.0 mm, resulted in the generation of stiff thermoplastic meshes with interconnected pores (Figure 4f). For the co-printing of PCL and $MHA_{0.5}$, constructs with four different designs, having a PCL framework with variable strand distance and a final architecture with or without pores, were printed (Figure b-e and g-j). To obtain porosity in pMH/PCL constructs, a hydrogel dispensing pressure of 0.1 MPa and a valve opening time (v.o.t.) of 300 μs were used. To obtain solid co-printed constructs, higher v.o.t. (500 or 1300 μs when using a strand distance of 1.5 and 2.0 mm, respectively) and a slightly higher pressure (0.13 MPa, when using a strand distance of 2.0 mm) were used to increase the amount of extruded hydrogel. The temperature of the deposition plate was set at 35°C while printing solid constructs. In contrast, a higher temperature, *i.e.* 40°C was found to be beneficial for the stability of the hydrogel filaments, required to maintain a constant shape and size of the pores in the porous co-printed constructs (pMH/PCL_2 and pMH/PCL_4).

Figure 4k shows that PCL meshes without hydrogel and with a strand distance of 1.5 and 2.0 mm possessed Young's moduli of 7.3±0.4 and 5.1±0.7 MPa, respectively. The Young's moduli of pMH/PCL co-printed constructs ranged from 3.5 and 4.6 MPa, with slightly higher values for constructs with lower strand distance (*i.e.* 1.5 mm), and no statistical difference between porous and non-porous constructs. Porosity is considered beneficial for cartilage tissue-engineering as it facilitates the nutrients/waste products exchange between the cell-laden hydrogel matrix and the surrounding fluids[64,65]. Moreover, pore size and organization have been shown to affect *in vivo* tissue maturation of tissue-engineered constructs[66,67]. Additionally, in an *in vivo* orthotopic scenario, cell-free co-printed porous scaffolds combined with marrow-stimulation techniques *e.g.* microfracture, may facilitate penetration of stem cells from the bone marrow into the implanted hydrogels[68].

Importantly, all the PCL-based constructs had Young's moduli of approximately three orders of magnitude higher than non-reinforced hydrogel constructs (Figure 3), reaching a stiffness comparable to that of native cartilage (0.4-0.8 MPa)[69–71]. This result confirmed the suitability of PCL as reinforcing material for cartilage tissue-engineering, in line with previously reported findings[72,73]. Interestingly, co-printed PCL/hydrogel constructs had lower Young's moduli compared to the hydrogel-free PCL meshes. This finding was reproducible and the decrease was significant for constructs with a strand distance of 1.5 mm. In contrast, printed PCL meshes infused with hydrogel $MHA_{0.5}$ had similar Young's moduli as the hydrogel-free PCL meshes (7.9±0.3 and 6.4±0.9 MPa for constructs
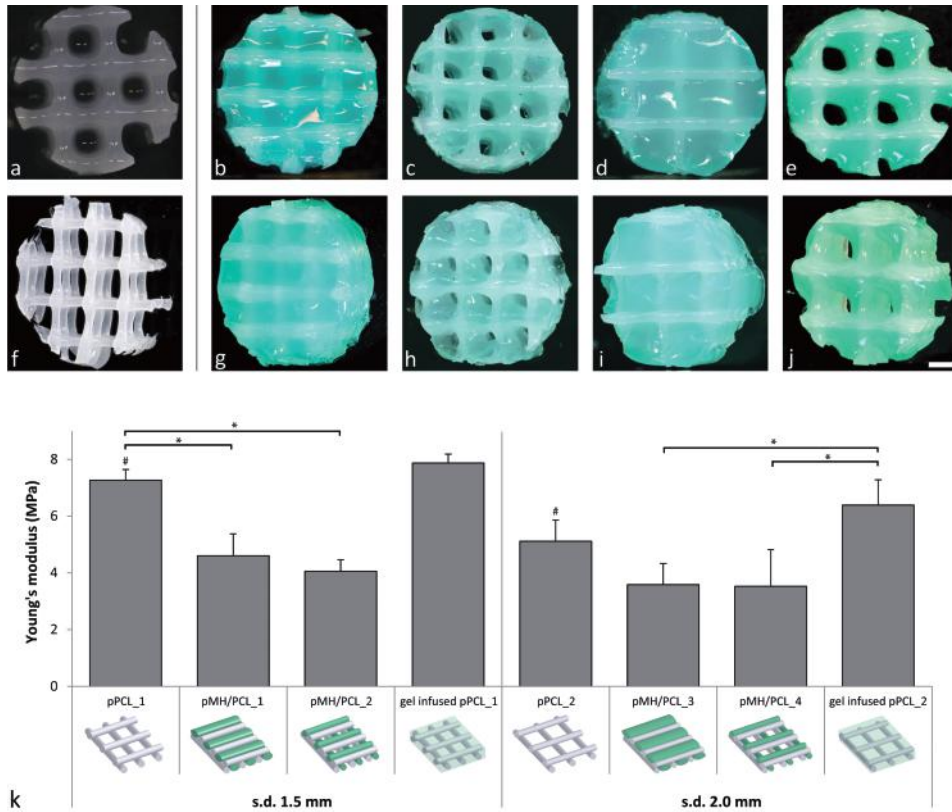
Figure 4. Evaluation of co-printed constructs. *a) Top view of a 3D shape stable printed hydrogel construct with formulation MHA$_{0.5}$. b and g) Top and top-side view of pMH/PCL_1 (MHA$_{0.5}$/PCL, non- porous, strand distance: 1.5 mm). c and h) Top and top-side view of pMH/PCL_2 (MHA$_{0.5}$/PCL, porous, strand distance: 1.5 mm). d and i) Top and top-side view of pMH/PCL_3 (MHA$_{0.5}$/PCL, non-porous, strand distance: 2.0 mm). e and j) Top and top-side view of pMH/PCL_4 (MHA$_{0.5}$/PCL, porous, strand distance: 2.0 mm). f) Top-side view of a PCL reinforcement structure. k) Young's moduli of the different printed constructs. Significant differences (p < 0.05) between conditions with the same strand distance are indicated with *, while # indicates a significant difference between strand distance within the same print conditions. For visualization purposes, MHA$_{0.5}$ hydrogel was stained green in the reinforced constructs. Scale bar represent 1 mm and it is the same for all images, s.d. = strand distance.*

with strand distance of 1.5 and 2.0 mm, respectively), indicating that the difference in construct stiffness is a result of the co-printing process. Likely, the layer-by-layer hydrogel deposition partially interfered with the adhesion of newly printed PCL filaments with underlining PCL strands. Nevertheless, co-printed constructs were macroscopically stable and the PCL skeleton appeared intact and coherent to the desired design, after selective removal of the hydrogel for visualization purposes (data not shown). However, this observation highlights the critical role of the chosen print settings and construct design on the mechanical properties of the final construct.

4. Conclusions

In this study, hydrogel-based cartilage repair constructs with optimized bioactivity and mechanical properties were successfully fabricated, via the addition of HAMA to a thermosensitive pHPMA-lac-PEG hydrogel and via co-printing with PCL. Results of the HAMA concentrations screening demonstrate a dose-dependent effect of HAMA on the cartilage matrix production by embedded chondrocytes. More specifically, intermediate HAMA concentrations (0.25-0.5%) increased cartilage-like matrix production compared to HAMA-free hydrogels, while higher (1%) concentrations resulted in undesirable fibrocartilage formation. These results may impact the choice of HAMA content in bio-ink development. In addition, the presence of HAMA was found to increase the construct stiffness with increasing concentration. These findings allowed the identification of an optimal hydrogel composition of 19.5% pHPMA-lac-PEG with 0.5% HAMA. This formulation supported increased cartilage matrix production compared to HAMA-free hydrogels, contained limited fibrocartilage formation, and displayed a medium/high Young's modulus, and yielding behavior, beneficial for the 3D printing of these hydrogels. Hydrogel/PCL co-printing enabled the generation of complex 3D constructs with mechanical stiffness in the range of native cartilage. However, the co-printing procedure influenced the final construct properties, highlighting the crucial role of the print settings in determining the final construct properties. In conclusion, we developed advanced composite cartilage repair constructs, with a chondrogenic hydrogel component and a mechanically adequate PCL reinforcement. Whilst this further mimics biomechanical properties of native articular cartilage, this is an interesting approach for further optimization.

5. Acknowledgments

Supporting information

a

b

Scheme S1. Chemical structures of methacrylated pHPMA-lac-PEG triblock copolymer (a) and HAMA (b).
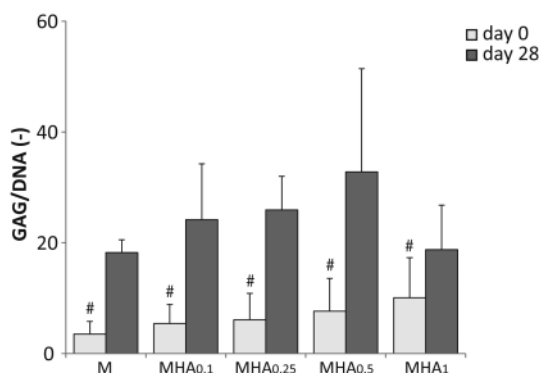
Figure S2. GAG/DNA content at day 0 and 28 for the five different hydrogel formulations. # indicates a significant difference compared to groups without a # but similar as groups with a #.

a   b
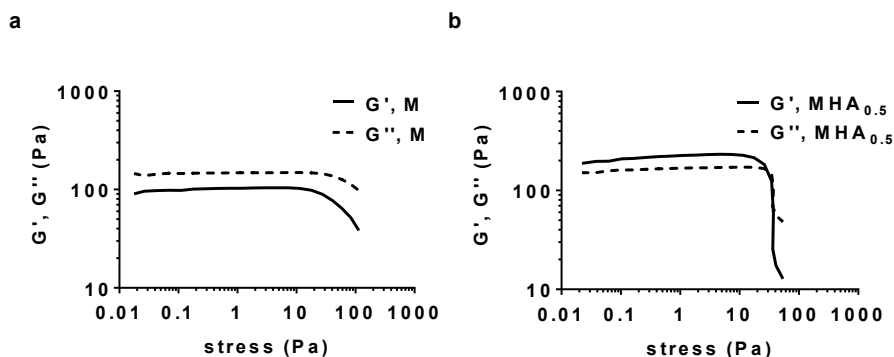
Figure S3. G' and G'' as function of oscillatory stress for formulations M (a) and MHA$_{0.5}$ (b) before UV-cross-linking, recorded at 37°C using a frequency of 1 Hz. Yield stress is defined as the stress at which G' crosses G''.

5

References

1. Murphy, S. V & Atala, A. 3D bioprinting of tissues and organs. Nat. Biotechnol. 32, 773–785 (2014).
2. Buckley, M. R., Gleghorn, J. P., Bonassar, L. J. & Cohen, I. Mapping the depth dependence of shear properties in articular cartilage. J. Biomech. 41, 2430–2437 (2008).
3. Silverberg, J. L. et al. Structure-Function Relations and Rigidity Percolation in the Shear Properties of Articular Cartilage. Biophys. J. 107, 1721–1730 (2014).
4. Schuurman, W. et al. Zonal Chondrocyte Subpopulations Reacquire Zone-Specific Characteristics During In Vitro Redifferentiation. Am. J. Sports Med. 37, 97S–104S (2009).
5. Almarza, A. J. & Athanasiou, K. A. Design characteristics for the tissue engineering of cartilaginous tissues. Ann. Biomed. Eng. 32, 2–17 (2004).
6. Prakash, D. & Learmonth, D. Natural progression of osteo-chondral defect in the femoral condyle. Knee 9, 7–10 (2002).
7. Mouser, V. H. M. et al. Three-Dimensional Bioprinting and Its Potential in the Field of Articular Cartilage Regeneration. Cartilage (2016). doi:10.1177/1947603516665445
8. Klein, T. J., Malda, J., Sah, R. L. & Hutmacher, D. W. Tissue Engineering of Articular Cartilage with Biomimetic Zones. Tissue Eng. Part B Rev. 15, 143–157 (2009).
9. Liao, J. et al. Recent Developments in Scaffold-Guided Cartilage Tissue Regeneration. J. Biomed. Nanotechnol. 10, 3085–3104 (2014).
10. Malda, J. et al. 25th Anniversary Article: Engineering Hydrogels for Biofabrication. Adv. Mater. 25, 5011–5028 (2013).
11. Mouser, V. H. M. et al. Yield stress determines bioprintability of hydrogels based on gelatin-methacryloyl and gellan gum for cartilage bioprinting. Biofabrication 8, 035003 (2016).
12. Vermonden, T. et al. Photopolymerized thermosensitive hydrogels: Synthesis, degradation, and cytocompatibility. Biomacromolecules 9, 919–926 (2008).
13. Censi, R. et al. Photopolymerized thermosensitive hydrogels for tailorable diffusion-controlled protein delivery. J. Control. Release 140, 230–236 (2009).
14. Censi, R. et al. Photopolymerized thermosensitive poly(HPMAlactate)-PEG-based hydrogels: Effect of network design on mechanical properties, degradation, and release behavior. Biomacromolecules 11, 2143–2151 (2010).
15. Censi, R. et al. A Printable Photopolymerizable Thermosensitive p(HPMAm-lactate)-PEG Hydrogel for Tissue Engineering. Adv. Funct. Mater. 21, 1833–1842 (2011).
16. Abbadessa, A. et al. A Synthetic Thermosensitive Hydrogel for Cartilage Bioprinting and Its Biofunctionalization with Polysaccharides. Biomacromolecules 17, 2137–2147 (2016).
17. Abbadessa, A. et al. A thermo-responsive and photo-polymerizable chondroitin sulfate-based hydrogel for 3D printing applications. Carbohydr. Polym. 149, 163–174 (2016).
18. Ponta, H., Sherman, L. & Herrlich, P. A. CD44: From adhesion molecules to signalling regulators. Nat. Rev. Mol. Cell Biol. 4, 33–45 (2003).
19. Lesley, J. Hyaluronan Binding by Cell Surface CD44. J. Biol. Chem. 275, 26967–26975 (2000).
20. Liao, J., Qu, Y., Chu, B., Zhang, X. & Qian, Z. Biodegradable CSMA/PECA/Graphene Porous Hybrid Scaffold for Cartilage Tissue Engineering. Sci. Rep. 5, 9879 (2015).
21. Levett, P. A. et al. A biomimetic extracellular matrix for cartilage tissue engineering centered on photocurable gelatin, hyaluronic acid and chondroitin sulfate. Acta Biomater. 10, 214–223 (2014).
22. Chung, C., Erickson, I. E., Mauck, R. L. & Burdick, J. A. Differential Behavior of Auricular and Articular Chondrocytes in Hyaluronic Acid Hydrogels. Tissue Eng. Part A 14, 1121–1131 (2008).
23. Park, H., Choi, B., Hu, J. & Lee, M. Injectable chitosan hyaluronic acid hydrogels for cartilage tissue engineering. Acta Biomater. 9, 4779–4786 (2013).
24. Liao, E., Yaszemski, M., Krebsbach, P. & Hollister, S. Tissue-Engineered Cartilage Constructs Using Composite Hyaluronic Acid/Collagen I Hydrogels and Designed Poly(Propylene Fumarate) Scaffolds. Tissue Eng. 13, 537–550 (2007).
25. Allemann, F. et al. Effects of hyaluronan on engineered articular cartilage extracellular matrix gene expression in 3-dimensional collagen scaffolds. J. Biomed. Mater. Res. 55, 13–19 (2001).
26. Akmal, M. et al. The effects of hyaluronic acid on articular chondrocytes. J. Bone Jt. Surg. - Br. Vol. 87-B, 1143–1149 (2005).
27. Levett, P. A., Hutmacher, D. W., Malda, J. & Klein, T. J. Hyaluronic acid enhances the mechanical properties of tissue-engineered cartilage constructs. PLoS One 9, e113216 (2014).
28. Kawasaki, K., Ochi, M., Uchio, Y., Adachi, N. & Matsusaki, M. Hyaluronic acid enhances proliferation and chondroitin sulfate synthesis in cultured chondrocytes embedded in collagen gels. J. Cell. Physiol. 179, 142–148 (1999).
29. Bryant, S. J. & Anseth, K. S. Hydrogel properties influence ECM production by chondrocytes photoencapsulated in poly(ethylene glycol) hydrogels. J. Biomed. Mater. Res. 59, 63–72 (2002).
30. Schuurman, W. et al. Bioprinting of hybrid tissue constructs with tailorable mechanical properties. Biofabrication 3, 021001 (2011).
31. Jang, J., Lee, J., Seol, Y.-J., Jeong, Y. H. & Cho, D.-W. Improving mechanical properties of alginate hydrogel by reinforcement with ethanol treated polycaprolactone nanofibers. Compos. Part B Eng. 45, 1216–1221 (2013).
32. Iviglia, G. et al. Novel bioceramic-reinforced hydrogel for alveolar bone regeneration. Acta Biomater. 44, 97–109 (2016).
33. Lee, J.-S. et al. 3D printing of composite tissue with complex shape applied to ear regeneration. Biofabrication 6, 024103 (2014).

34.   Kundu, J., Shim, J.-H. H., Jang, J., Kim, S.-W. W. & Cho, D.-W. W. An additive manufacturing-based PCL-alginate-chondrocyte bioprinted scaffold for cartilage tissue engineering. J. Tissue Eng. Regen. Med. 9, 1286–1297 (2015).
35.   Visser, J. et al. Biofabrication of multi-material anatomically shaped tissue constructs. Biofabrication 5, 035007 (2013).
36.   Melchels, F. P. W. et al. Hydrogel-based reinforcement of 3D bioprinted constructs. Biofabrication 8, 035004 (2016).
37.   Martin, J. J., Fiore, B. E. & Erb, R. M. Designing bioinspired composite reinforcement architectures via 3D magnetic printing. Nat. Commun. 6, 8641 (2015).
38.   Woodruff, M. A. & Hutmacher, D. W. The return of a forgotten polymer—Polycaprolactone in the 21st century. Prog. Polym. Sci. 35, 1217–1256 (2010).
39.   Olubamiji, A. D. et al. Modulating mechanical behaviour of 3D-printed cartilage-mimetic PCL scaffolds: influence of molecular weight and pore geometry. Biofabrication 8, 025020 (2016).
40.   Woodfield, T. B. F. et al. Design of porous scaffolds for cartilage tissue engineering using a three-dimensional fiber-deposition technique. Biomaterials 25, 4149–4161 (2004).
41.   Neradovic, D. et al. Degradation Mechanism and Kinetics of Thermosensitive Polyacrylamides Containing Lactic Acid Side Chains. Macromolecules 36, 7491–7498 (2003).
42.   Neradovic, D., van Nostrum, C. F. & Hennink, W. E. Thermoresponsive Polymeric Micelles with Controlled Instability Based on Hydrolytically Sensitive N -Isopropylacrylamide Copolymers. Macromolecules 34, 7589–7591 (2001).
43.   Hachet, E., Van Den Berghe, H., Bayma, E., Block, M. R. & Auzély-Velty, R. Design of biomimetic cell-interactive substrates using hyaluronic acid hydrogels with tunable mechanical properties. Biomacromolecules 13, 1818–27 (2012).
44.   Benya, P. Dedifferentiated chondrocytes reexpress the differentiated collagen phenotype when cultured in agarose gels. Cell 30, 215–224 (1982).
45.   Guo, J., Jourdian, G. W. & Maccallum, D. K. Culture and Growth Characteristics of Chondrocytes Encapsulated in Alginate Beads. Connect. Tissue Res. 19, 277–297 (1989).
46.   Wall, A. & Board, T. in Classic Papers in Orthopaedics 53, 433–435 (Springer London, 2014).
47.   Farndale, R. W., Sayers, C. A. & Barrett, A. J. A Direct Spectrophotometric Microassay for Sulfated Glycosaminoglycans in Cartilage Cultures. Connect. Tissue Res. 9, 247–248 (1982).
48.   Gawlitta, D., van Rijen, M. H. P., Schrijver, E. J. M., Alblas, J. & Dhert, W. J. A. Hypoxia Impedes Hypertrophic Chondrogenesis of Human Multipotent Stromal Cells. Tissue Eng. Part A 18, 1957–1966 (2012).
49.   Zwickl, H., Niculescu-Morzsa, E. & Nehrer, S. Investigation of Collagen Transplants Seeded with Human Autologous Chondrocytes at the Time of Transplantation. Cartilage 1, 194–199 (2010).
50.   Yasuda, T. Nuclear factor-κB activation by type II collagen peptide in articular chondrocytes: its inhibition by hyaluronan via the receptors. Mod. Rheumatol. 23, 1116–1123 (2012).
51.   Viola, M. et al. Biology and biotechnology of hyaluronan. Glycoconj. J. 32, 93–103 (2015).
52.   Dowthwaite, G. P., Edwards, J. C. W. & Pitsillides, a. a. An Essential Role for the Interaction Between Hyaluronan and Hyaluronan Binding Proteins During Joint Development. J. Histochem. Cytochem. 46, 641–651 (1998).
53.   Onodera, Y., Teramura, T., Takehara, T. & Fukuda, K. Hyaluronic acid regulates a key redox control factor Nrf2 via phosphorylation of Akt in bovine articular chondrocytes. FEBS Open Bio 5, 476–484 (2015).
54.   Ariyoshi, W., Takahashi, N., Hida, D., Knudson, C. B. & Knudson, W. Mechanisms involved in enhancement of the expression and function of aggrecanases by hyaluronan oligosaccharides. Arthritis Rheum. 64, 187–197 (2012).
55.   Schuh, E. et al. Chondrocyte redifferentiation in 3D: the effect of adhesion site density and substrate elasticity. J. Biomed. Mater. Res. A 100, 38–47 (2012).
56.   Vu, L. T., Jain, G., Veres, B. D. & Rajagopalan, P. Cell Migration on Planar and Three-Dimensional Matrices: A Hydrogel-Based Perspective. Tissue Eng. Part B Rev. 21, 67–74 (2015).
57.   Discher, D. E. Tissue Cells Feel and Respond to the Stiffness of Their Substrate. Science (80-.). 310, 1139–1143 (2005).
58.   Huang, G. et al. Engineering three-dimensional cell mechanical microenvironment with hydrogels. Biofabrication 4, 042001 (2012).
59.   Heng, B. C. et al. Effect of cell-seeding density on the proliferation and gene expression profile of human umbilical vein endothelial cells within ex vivo culture. Cytotherapy 13, 606–617 (2011).
60.   Abbadessa, A., Landín, M., Blenke, E. O., Hennink, W. E. & Vermonden, T. Two-component thermosensitive hydrogels: phase separation affecting rheological behavior. Submitt. Publ.
61.   Kock, L. M., Geraedts, J., Ito, K. & van Donkelaar, C. C. Low Agarose Concentration and TGF-β3 Distribute Extracellular Matrix in Tissue-Engineered Cartilage. Tissue Eng. Part A 19, 1621–1631 (2013).
62.   Jungst, T., Smolan, W., Schacht, K., Scheibel, T. & Groll, J. Strategies and Molecular Design Criteria for 3D Printable Hydrogels. Chem. Rev. 116, 1496–1539 (2016).
63.   Melchels, F. P. W., Dhert, W. J. A., Hutmacher, D. W. & Malda, J. Development and characterisation of a new bioink for additive tissue manufacturing. J. Mater. Chem. B 2, 2282–2289 (2014).
64.   Hollister, S. J. Porous scaffold design for tissue engineering. Nat. Mater. 5, 590–590 (2006).
65.   Hutmacher, D. W. Scaffolds in tissue engineering bone and cartilage. Biomaterials 21, 2529–2543 (2000).

5

66.   Malda, J. et al. The effect of PEGT/PBT scaffold architecture on oxygen gradients in tissue engineered cartilaginous constructs. Biomaterials 25, 5773–5780 (2004).
67.   Malda, J. et al. The effect of PEGT/PBT scaffold architecture on the composition of tissue engineered cartilage. Biomaterials 26, 63–72 (2005).
68.   Steadman, J. R., Rodkey, W. G. & Rodrigo, J. J. Microfracture: surgical technique and rehabilitation to treat chondral defects. Clin Orthop Relat Res S362–9 (2001). doi:10.1097/00003086-200110001-00033
69.   Chen, A. C., Bae, W. C., Schinagl, R. M. & Sah, R. L. Depth- and strain-dependent mechanical and electromechanical properties of full-thickness bovine articular cartilage in confined compression. J. Biomech. 34, 1–12 (2001).
70.   Athanasiou, K. A., Agarwal, A. & Dzida, F. J. Comparative study of the intrinsic mechanical properties of the human acetabular and femoral head cartilage. J. Orthop. Res. 12, 340–349 (1994).
71.   Jurvelin, J. S., Buschmann, M. D. & Hunziker, E. B. Optical and mechanical determination of poisson's ratio of adult bovine humeral articular cartilage. J. Biomech. 30, 235–241 (1997).
72.   Visser, J. et al. Reinforcement of hydrogels using three-dimensionally printed microfibres. Nat. Commun. 6, 6933 (2015).
73.   Boere, K. W. M. et al. Biofabrication of reinforced 3D-scaffolds using two-component hydrogels. J. Mater. Chem. B 3, 9067–9078 (2015).

5

Chapter 6

Bio-ink development for three-dimensional bioprinting of organized cartilage constructs using different cell types

Vivian H. M. Mouser
Riccardo Levato
Anneloes Mensinga
Wouter J. A. Dhert
Debby Gawlitta
Jos Malda
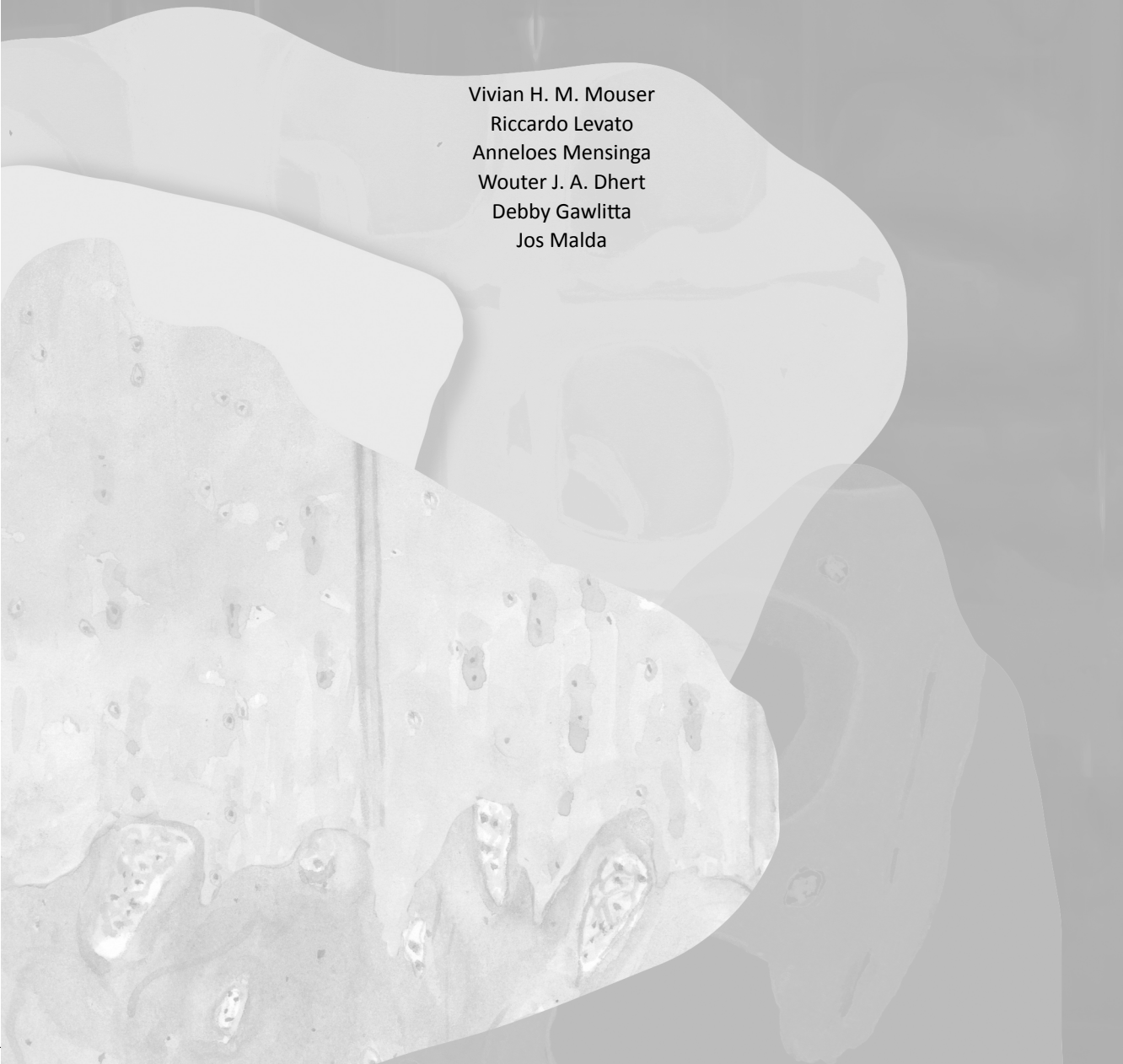
Abstract

Bioprinting is a promising tool to fabricate organized cartilage. This study aimed to investigate the printability of gelatin-methacryloyl/gellan gum (gelMA/gellan) hydrogels with(out) methacrylated hyaluronic acid (HAMA), and to explore (zone-specific) chondrogenesis of chondrocytes, articular cartilage progenitor cells (ACPCs) and multipotent mesenchymal stromal cells (MSCs) embedded in these bio-inks.

Incorporating HAMA in gelMA/gellan increased filament stability, as measured using a filament collapse assay, but did not influence (zone-specific) chondrogenesis of any of the cell types. Highest chondrogenic potential was observed for MSCs, followed by ACPCs, which displayed relatively high proteoglycan IV mRNA levels. Two-zone constructs were printed with gelMA/gellan/HAMA containing ACPCs in the superficial region and MSCs in the middle/deep region. Chondrogenic differentiation was confirmed, however printing influence cellular differentiation.

ACPC- and MSC-laden gelMA/gellan/HAMA hydrogels are of interest for the fabrication of cartilage constructs. Nevertheless, this study underscores the need for careful evaluation of the effects of printing on cellular differentiation.

1. Introduction

Articular cartilage damage often results in osteoarthritic changes of the joint if no interventions are taken[1,2]. Articular cartilage is the tissue covering the bone extremities and consists of predominantly water, proteoglycans, and collagen type II[2,3]. The tissue contains depth-dependent characteristics and can be divided in three zones: the superficial zone (10-20%), the middle or intermediate zone (40-60%), and the deep zone (30-40%). Matrix composition, collagen orientation, and mechanical properties differ within these different locations, as well as chondrocyte density and their matrix synthesis[4,5]. In the superficial layer, chondrocytes synthetize relatively more proteoglycan IV (PRG4, or lubricin)[6,7], clusterin[8], and collagen type I[7] compared to chondrocytes in the other zones. Additionally, proteins such as cartilage oligomeric protein (COMP)[9] and collagen type X[7] are predominantly synthesized by cells in the middle and deep zones. Current clinical therapies *e.g.* microfracture or (matrix-induced) autologous chondrocyte implantation, result in the formation of homogeneous (fibro)cartilage, which provides pain relief for the patient but often fails mechanically on the long term[10,11]. The implantation of tissue-engineered hydrogel constructs is a promising future approach to repair cartilage defects. Additionally, the incorporation of depth-dependent organization similar to that of native cartilage, is believed to improve construct integration in the defect site compared to traditional cartilage repair strategies, and might therefore improve clinical outcomes[12,13].

Bioprinting techniques may be a unique tool to implement spatial variations in a tissue-engineered construct, as they enable precise control over the positioning of biomaterials and cells[14]. However, the search for suitable biomaterials, the bio-inks, remains challenging. Hydrogels have been identified as the most promising materials for bioprinting as their high water content provides easy incorporation and sustenance of cells and other biological components *e.g.* growth factors or proteins. However, multiple material properties identified as beneficial for the printing process, such as high polymer concentrations, cross-linking densities, yield stresses, and viscosities, interfere with matrix synthesis of embedded cells[15,16]. A strategy to overcome this challenge, involves the fine-tuning of a bio-ink with additives to generate polymer blends with both the required material properties for accurate printing and biological properties to support matrix production and chondrogenesis of embedded cells.

A promising cartilage bio-ink consists of the collagen-based gelatin-methacryloyl (gelMA). GelMA contains methacryloyl groups to allow UV cross-linking and was demonstrated to support cartilage-like matrix production of embedded chondrocytes and multipotent mesenchymal stromal cells (MSCs)[17–19]. However, printing of gelMA is challenging as the filament stability, during printing, has to rely on the thermo-sensitive behavior of gelMA, which is a relatively slow process[20,21]. The printability of gelMA can be improved by the incorporation of the polysaccharide gellan gum[21]. Gellan gum increases the viscosity of the gelMA/gellan blend and initiates ionic interactions. These ionic interactions induce pseudo-plastic behavior and increase the yield stress, which increases the filament stability during printing, resulting in constructs with high shape-fidelity[16,21]. In addition, we recently demonstrated that the presence of relatively low gellan gum concentrations did not hamper the cartilage matrix production by embedded

chondrocytes, making gellan gum an interesting additive to gelMA bio-inks for cartilage bioprinting[16]. Also, hyaluronic acid (HA), an element of native cartilage, has been demonstrated to improve the printability of hydrogels by increasing the viscosity of the polymer blend[22–24]. In addition, HA can be methacrylated (HAMA) to allow UV cross-linking with gelMA and its presence in low concentrations was demonstrated to improve cartilage tissue formation by embedded chondrocytes[17]. Therefore, the incorporation of HAMA in gelMA/gellan hydrogels may further improve the bio-ink properties.

Multiple cell types can potentially be incorporated in bioprinted cartilage constructs. Most research groups focus on the incorporation of chondrocytes, as these cells are already in the correct lineage for cartilage formation[14]. However, obtaining autologous chondrocytes can result in donor site morbidity and chondrocyte expansion in monolayer culture stimulates chondrocyte dedifferentiation towards a fibroblastic phenotype[25]. An alternative cell source is the sub-population of articular cartilage progenitor cells (ACPCs, or chondroprogenitor cells), which are located in cartilage tissue, mainly in the superficial zone[26,27]. ACPCs allow expansion in monolayer culture without losing their chondrogenic phenotype[26]. Another alternative are MSCs, derived from *e.g.* bone marrow, adipose tissues, or muscle[28], and thus limiting donor site morbidity. MSCs may also be expanded in monolayer culture and can be manipulated to differentiate into chondrocyte-like cells with specific growth factors, such as the members of the transforming growth factor beta (TGF-β) superfamily[29]. Therefore, chondrocytes, ACPCs, and MSCs form interesting cell types for cartilage tissue-engineering purposes.

The aim of this study was to generate constructs for cartilage repair that mimic depth-dependent characteristics of the native cartilage. This requires the identification and optimization of specific bio-ink/cell type combinations for each zone. Therefore, this study explored the suitability of two hydrogel systems, gelMA/gellan and gelMA/gellan/HAMA, for 3D printing. Additionally, chondrocytes, ACPCs, and MSCs were embedded in both bio-inks and the production of (zone-specific) cartilage matrix was evaluated. Finally, this study explored the feasibility of obtaining a two-zone construct with zone-specific matrix production in each layer, via the bioprinting of the two optimal bio-ink/cell combinations for superficial zone cartilage and middle/deep zone cartilage.

2. Materials and methods

2.1. Experimental design

Filament collapse, as a measure for the printability, was evaluated for two gelMA-based bio-inks, gelMA/gellan (GG) and gelMA/gellan/HAMA (GGH) (Table 1), with plain gelMA (G) as a control. Next, constructs were cast using both bio-ink formulations laden with either chondrocytes, ACPCs, or MSCs. The cell-laden constructs were cross-linked and cultured for 1 and 28 days to evaluate (zone-specific) cartilage matrix production and chondrogenic gene expression levels.

Based on the results of the first experiments, two-zone constructs were printed using an optimized hydrogel formulation/cell type combination for the superficial and

Table 1. Overview of the polymer concentrations within the evaluated bio-ink compositions. All polymers were dissolved in MiliQ with 10% PBS v/v, 0.1% Irgacure, and 4.86% D-(+)-mannose.

Name	% gelMA (w/v)	% gellan gum (w/v)	% HAMA (w/v)
G	10.5	-	-
GG	10	0.5	-
GGH	9.5	0.5	0.5

the middle/deep region. Two-zone constructs were cultured for 1, 28, and 42 days, and samples were analyzed for (zone-specific) cartilage matrix production and chondrogenic gene expression levels.

2.2. Preparation of polymer solutions

GelMA and HAMA were synthesized from gelatine (type A from porcine skin, 175 g Bloom; Sigma Aldrich, Zwijndrecht, the Netherlands) and hyaluronic acid (120 kDa, degree of methacrylation = 10%, indicating the presence of 10 methacrylate groups for each 100 disaccharide units, Lifecore Biomedical, Chaska, USA) respectively, as previously described[21,30].

GelMA, gellan gum, and HAMA stock solutions were prepared as previously discribed[16]. In short, gelMA and gellan gum were dissolved at 70°C and HAMA at 4°C in Mili-Q with 10% PBS v/v, 0.1% Irgacure 2959 (gift from BASF, Ludwigshafen, Germany), and 4.86% D-(+)-mannose (Sigma Aldrich, to generate an isotonic solution). Stock solutions were stored overnight at 4°C, after which they were mixed in the correct ratio at 80°C to obtain the desired formulations (Table 1).

2.3. Screening of filament stability

The different polymer solutions were pipetted into 3 ml syringe barrels (Nordson EFD, Bedfordshire, England), which were loaded into a 3DDiscovery bioprinter (regenHU, Villaz-St-Pierre, Switzerland). For each formulation, five filaments were printed onto substrates with aligned pillars with 1, 2, 4, 8, and 16 mm intervals, as previously described[31], using a 23 gauge metal needle (Precision Tip PN, Nordson EFD) and optimized print settings for each formulation (Table S1). Filament deposition was recorded with a USB microscope (Bresser, Rhede, Germany) at a magnification of 20x. The average overhang the filaments reached without collapsing was determined for each formulation as a measure for filament stability.

2.4. Isolation, characterization, and expansion of cells

Chondrocytes and ACPCs were isolated, characterized and expanded as previously described[16,32,33]. In short, both cell types were isolated from macroscopically healthy full-thickness cartilage of equine metacarpophalangeal joints (N=3 for each cell type; 3-10 years old). The multipotency of the ACPCs was evaluated *in vitro* with a three-way

6

differentiation assay, and the expression of the characteristic cell membrane markers was determined using reverse transcription-polymerase chain reaction (RT-PCR). Both chondrocytes and ACPCs were stored in liquid nitrogen and expanded in monolayer culture upon construct preparation (chondrocytes passage 1, ACPCs passage 4).

MSCs were isolated from bone marrow aspirate of the sternum of healthy living equine donors (N=3), with approval of the local animal ethical committee. The bone marrow was diluted in PBS, filtered through a 100 µm cell strainer, and pipetted onto a Ficoll-Paque (1.077 g/cm^3). After centrifugation, the white mononuclear cell layer was isolated. Subsequently, the cells were washed and cultured in monolayer (seeding density of 0.25*10^6 cells/cm^2) with high glucose Dulbecco's modified Eagle's medium (DMEM, D6429, Sigma Aldrich) supplemented with 10% fetal bovine serum (FBS; Gibco), 1% penicillin/streptomycin (final concentration of 100 units/ml penicillin and 100 µg/ml streptomycin), and 1 ng/ml recombinant human fibroblast growth factor-basic (bFGF, E.coli produced, R&D systems, Abingdon, UK). The multilineage potential of the MSCs was determined with an *in vitro* three-way differentiation assay as previously described[34,35].

2.5. Construct preparation for the screening of zone-specific cartilage-like tissue formation

Polymer solutions with formulations GG and GGH were cooled to 45°C and mixed with the different cell pellets, chondrocytes (passage 1, 20*10^6 cells/ml), ACPCs (passage 4, 20*10^6 cells/ml), and MSCs (passage 4, 20*10^6 cells/ml). Cell-laden polymer solutions were pipetted into custom-made cylindrical Teflon molds (diameter 6 mm, height 2 mm) to be cross-linked with UV light (UV-Handleuchte lamp A., Hartenstein, Germany, wavelength: 365 nm, intensity at 3 cm: 1.2 mW/cm^2, irradiation time: 5 minutes). After cross-linking, hydrogel constructs were cultured for 28 days at 37°C and 5% CO_2 in chondrogenic differentiation medium consisting of high glucose DMEM (D6429, Sigma Aldrich) supplemented with 1% ITS + premix (BD Biosciences, Breda, The Netherlands), 0.1 µM dexamethasone (Sigma Aldrich), 0.2 mM L-ascorbic acid-2-phosphate (Sigma Aldrich), 10 ng/ml recombinant human TGF-β1 (Peprotech) and 1% penicillin/streptomycin (final concentration: 100 units/ml penicillin and 100 µg/ml streptomycin) to stimulate chondrogenesis of the embedded cells[36,37]. Culture medium was refreshed twice a week and 0.1 µM monensin (Sigma Aldrich) was added to the culture medium of samples used for quantitative and histological evaluation, the night before sample harvest, to trap proteoglycan IV intracellularly [38].

2.6. Evaluation of (zone-specific) cartilage matrix production

Three samples of each hydrogel/cell combination were harvested at days 1 and 28. Half of each sample was weighed (wet weight), freeze dried, and weighed again (dry weight) to determine the water content. Next, samples were digested and GAG and DNA contents were measured with a dimethylmethylene blue (DMMB) assay and a Quant-iT PicoGreen dsDNA kit, respectively, as previously described[16]. Since the DMMB assay also detects the introduced HAMA, the GAG content measured at day 28 was corrected for the initial readout at day 1 for the samples of the bio-ink screening.

The other half of each sample was fixed overnight in 4% formalin, followed by dehydration through a graded ethanol series, and clearing in xylene. Sequentially, samples were embedded in paraffin and tissue sections with a thickness of 5 μm were cut. Tissue sections were stained with safranin-O and fast green to visualize proteoglycans (red) and collagens (green), respectively[39]. Collagen types I, II, and VI, and proteoglycan IV were visualized with immunohistochemistry as previously described[40]. All sections were evaluated and photographed with a light microscope (Olympus BX51 microscope, Olympus DP70 camera, Hamburg, Germany).

2.7. Gene expression of embedded cells

At days 1 and 28, three samples of each condition were harvested in RLT-buffer (Qiagen, Germany). Samples were crushed manually and then minced with a QIAshredder column (Qiagen, Germany). Subsequently, mRNA was isolated, and amplification and cDNA synthesis were performed, all as previously described[33]. Quantitative RT-PCR (qPCR) was used to analyze the mRNA expression levels of aggrecan (ACAN), collagen type II (COL2A1), collagen type I (COL1A1), proteoglycan IV (PRG4), collagen type X (COL10A1), and the housekeeping gene HPRT1 for normalization, using the primers as reported by Levato *et al.* (2016)[33].

2.8. Three-dimensional bioprinting of two-zone constructs

Two-zone constructs were bioprinted with an optimized bio-ink for each region. Based on the results of the previous experiments hydrogel formulation GGH with ACPCs was selected for the superficial region and formulation GGH with MSCs was selected for the middle/deep region. Cell-laden polymer solutions were prepared as described in section 2.5 (N=1). Sequentially, the bio-inks were loaded into a 3DDiscovery bioprinter (regenHU) and printed on top of each other in square constructs (15 x 15 x 3 mm , 1 mm superficial region and 2 mm middle/deep region) with optimized print settings (Table S1). To reduce the shear stresses on the embedded cells a 22 gauge conical needle (Precision Tip PN, Nordson EFD) was used, with a decreased print pressure compared to the settings used for the filament screening (Table S1). After printing, the printed sheets were covered with a glass slide and cross-linked for 96 seconds with a Bluepoint 4 UV lamp (point light source, wavelength range: 300-600 nm, UV-A intensity at 5 cm = 103 mW/cm^2, Hönle UV Technology AG, Gräfelfing, Germany). The printed sheets were cut into 9 samples of (5 x 5 x 3 mm) which were cultured in chondrogenic differentiation medium as described in section 2.5. As controls, constructs consisting solely out of GGH with ACPCs or MSCs were printed and cross-linked. Additionally, both bio-inks were cast in cylindrical Teflon molds and constructs were cross-linked with the Bluepoint 4 UV lamp using the same protocol as for the printed constructs, as extra controls. Samples were harvested at days 1, 28, and 42 of culture to evaluate (zone-specific) cartilage-like tissue formation as described in section 2.6. For the evaluation of the gene expression of embedded cells, the upper part of the superficial region and bottom part of the middle/deep region were removed from the two-zone constructs to be analyzed separately. The other constructs were evaluated in whole, all according to the protocol described in section 2.7.

6

2.9. Statistics

For the screening of (zone-specific) chondrogenesis in the bio-inks, differences between cell types within a hydrogel formulation and time points were determined with a randomized block design ANOVA to correct for donor variability. Differences between the hydrogel formulations GG and GGH within a cell type were determined with an independent t-test. Comparison of the gene expression levels or GAG and DNA contents of the printed constructs (layered or single layer) were determined with a one-way ANOVA per time point. Furthermore, differences between printed and cast constructs were determined with an independent t-test. Normality and homogeneity were assumed and a significance level of $p < 0.025$ was used for all statistical tests (Bonferroni correction of the p value to correct for the double tests). When the ANOVA tests indicated a significant difference, a Bonferroni post-hoc test was performed.

3. Results

3.1. Screening of filament stability

All filaments printed with formulation G were able to bridge a gap of 2 mm before breaking, while only 3 out of 5 filaments could bridge a 4 mm gap (Figure 1). The addition of 0.5% gellan to the gelMA hydrogel (formulation GG) increased the bridging distance; 100% of the filaments were able to bridge a gap of 4 mm wide without breaking and one filament could also bridge a gap of 8 mm wide. The bridging distance was further increased by the addition of HAMA (formulation GGH). Printing with this formulation allowed the bridging of gaps of 8 mm wide for all filaments and one filament was able to bridge a gap of 16 mm.
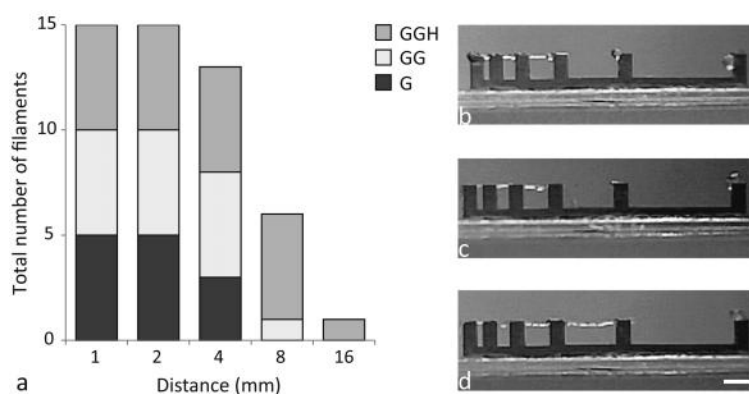
Figure 1. Evaluation of filament collapse in gap bridging as a measure of filament stability. *a) Overview of the total number of filaments that could bridge each distance. Each shade of grey represents the proportion of filaments for each separate hydrogel formulation. Three-dimensional printing with formulation GGH formed the most stable filaments as these could bridge the largest gaps without collapsing (8 mm, all evaluated filaments; 16 mm, one filament). b-c) Examples of the filament appearance of formulations G (b), GG (c), and GGH (d). Scale represents 4 mm for all pictures.*

3.2. Screening of (zone-specific) chondrogenesis in GG and GGH hydrogels

GAG content normalized to the DNA content was significantly lower in chondrocyte-laden hydrogels compared to ACPC, and MSC-laden constructs at day 28 (Figure 2a). Moreover, no differences in GAG content were observed between the hydrogel formulations (GG and GGH) for each cell type. The DNA content normalized to the dry weight and the water content normalized to the wet weight were similar for all cell types and hydrogel formulations (Figure 2b and 2c). Additionally, no changes in DNA per dry weight and water per wet weight contents were observed between days 1 and 28 of culture.
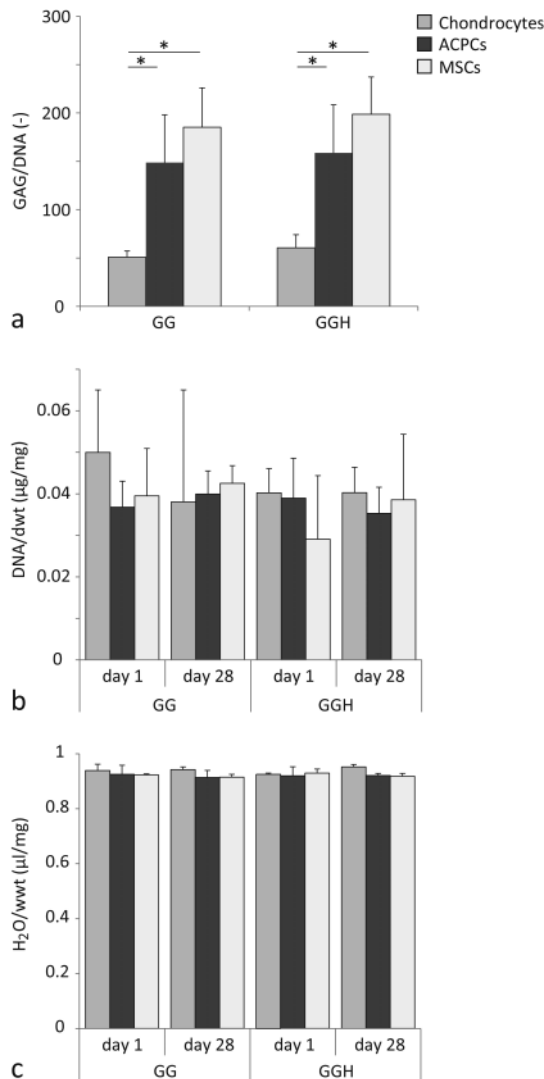
Figure 2. Quantitative evaluation of cartilage-like tissue formation. *GAG/DNA was highest in samples with MSCs and ACPCs (a). No differences in DNA/dry weight (dwt, b) or water/wet weight (H_2O/wwt, c) were measured between cell types or hydrogel formulations. * Indicates a significant difference (p < 0.025).*

6

Hydrogels with embedded chondrocytes had a limited overall safranin-O and collagen type II staining (Figure 3a and 3b). In contrast, MSC-laden hydrogels and to a lesser extent ACPC-laden hydrogels, revealed intense staining for GAGs (safranin-O) and collagen type II. In addition, in these hydrogels large cell clusters formed and most intense staining was observed around these clusters. All hydrogel samples stained positive for collagen type I, both at day 1 and day 28 (Figure 3c). However, the staining intensity was higher at day 28 compared to their day 1 control for all conditions. No differences in staining intensity for safranin-O, collagen type I, or collagen type II were observed between hydrogel formulations GG and GGH with the same cell type.
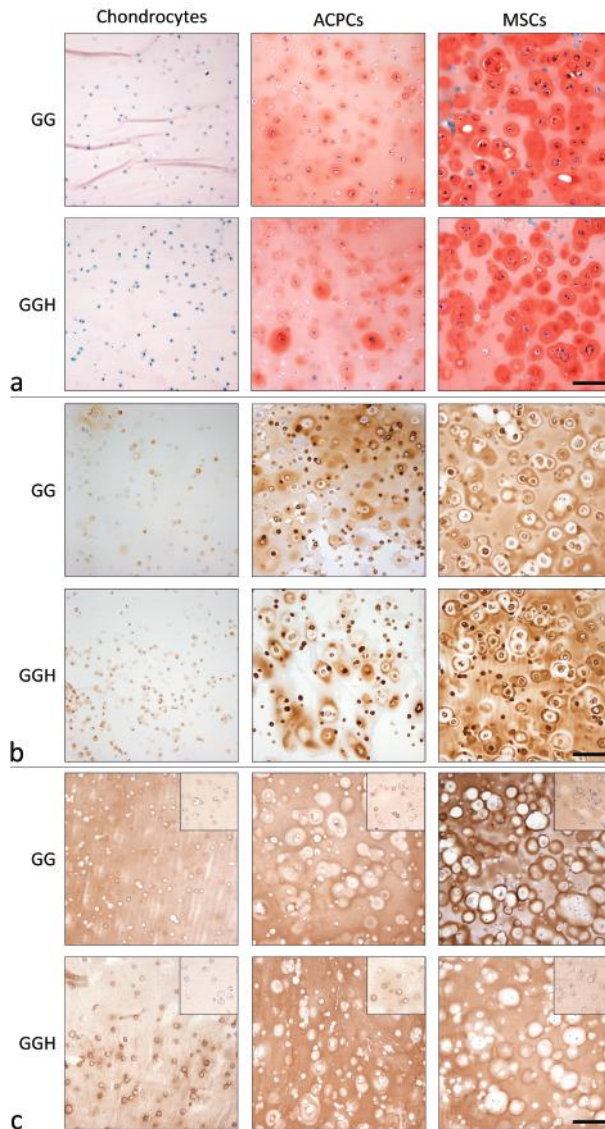
Figure 3. Histological assessment of cartilage-like tissue formation at day 28 in hydrogel constructs with the different cell types and formulation. *Safranin-O/fast green staining (a). Collagen type II staining (b). Collagen type I staining with the day 1 morphology in the inserts (c). Scale bar represents 100 μm for all images.*

6

For all cell types aggrecan and collagen type II mRNA expression relative to HPRT was upregulated at day 28 compared to day 1 (Figure 4a). No significant differences were observed for aggrecan gene expression levels between the different cell types in formulation GG at day 28. However, in formulation GGH, chondrocytes had significantly lower aggrecan mRNA levels compared to ACPCs and MSCs at day 28. In addition, MSCs had highest mRNA expression levels of collagen type II, while chondrocytes had the lowest at the end of the culture period (Figure 4b). Furthermore, collagen type I mRNA expression was highest for MSCs at day 1, but no differences were measured between the different cell types at day 28 for hydrogel GGH (Figure 4c). Moreover, ACPCs embedded

6
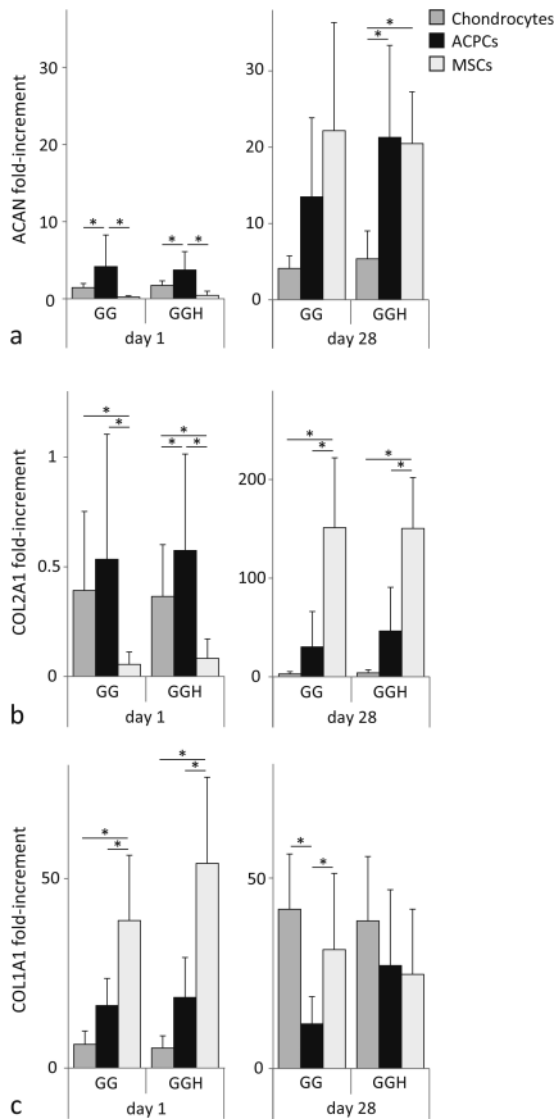
Figure 4. mRNA expression of chondrogenic genes relative to the housekeeping gene (HPRT), for chondrocytes, ACPCs, and MSCs, within the two hydrogel formulations (GG and GGH). Aggrecan (ACAN) expression increased for all cell types during culture (a). Collagen type II (COL2A1) gene expression increased for all cell types, but highest mRNA levels were measured in MSC-laden constructs at day 28, please note the double axis. (b). Collagen type I (COL1A1) expression was highest for MSCs at day 1, but at day 28 similar levels were measured for all cell types in formulation GGH while a lower expression was observed for ACPCs in formulation GG (c). No significant differences were observed between formulation GG and GGH for any of the cell types.

125

in formulation GG had significantly lower mRNA levels for collagen type I compared to chondrocytes and MSCs in this formulation. No differences in gene expression levels were observed between the hydrogel formulations, GG and GGH, for each of the cell types.

All cell types synthesised proteoglycan IV at day 28 of culture, as determined with immunohistochemistry (Figure 5a). No differences were observed between formulations GG and GGH for each cell type (Figure S1). Moreover, proteoglycan IV mRNA was detected for all cell types at both day 0 and day 28 (Figure 5b). Significnatly higher mRNA expression levels were observed for chondrocytes and ACPCs embedded GGH compared to MSCs in this formulation. In formulation GG, ACPCs contained significantly higher proteoglycan IV mRNA levels compared to both chondrocytes and MSCs in this formulation. Futhermore, collagen type X mRNA expression was similar for all cell types at day 1 and 28, except for chondrocytes embedded in formulation GG at day 28, which had significantly lower collagen type X mRNA levels compared to ACPCs and MSCs.
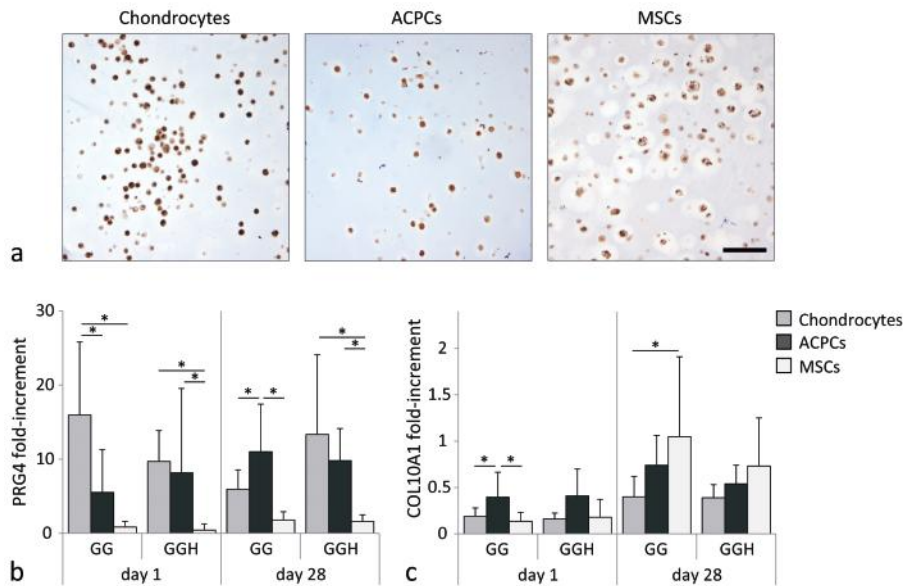
Figure 5. Evaluation of zone-specific cartilage production. *All cell types produced proteoglycan IV (PRG4) during culture (a). Highest relative mRNA expression of proteoglycan IV was measured in chondrocytes and ACPCs at day 28. Relative mRNA expression of collagen type X (COL10A1) was similar for all cell types after 28 days of culture (b). Scale bar represents 100 µm for all images.*

3.3. Printed two-zone constructs

Constructs with two regions were successfully 3D printed with ACPC-laden GGH for the top region (representing the superficial zone cartilage) and MSC-laden GGH for the bottom region (representing the middle/deep zone cartilage), as well as constructs consisting of only one of the two material/cell combinations (superficial or middle/deep). GAG content

normalized to the DNA content increased during culture for both the two-zone constructs and the single-zone constructs (Figure 6a). In addition, the DNA content normalized to the sample dry weight remained stable during culture for all constructs (Figure 6b). After 42 days of culture, the two regions of the two-zone constructs could be distinguished on histological sections. In both regions cell clusters had formed which stained positive for GAGs (safranin-O, Figure 6c). The extracellular matrix surrounding the cell clusters also stained positive for GAGs. Immunohistochemical stainings of collagen types I and II stained distinctive areas, which were present in both regions (Figure 6d and 6e). Collagen type II was most intense in and around the cell clusters, while the collagen type I staining was weakest at these locations. Moreover, both the ACPCs in the superficial region and the MSCs in the middle/deep region stained positive for proteoglycan IV (Figure 6f).
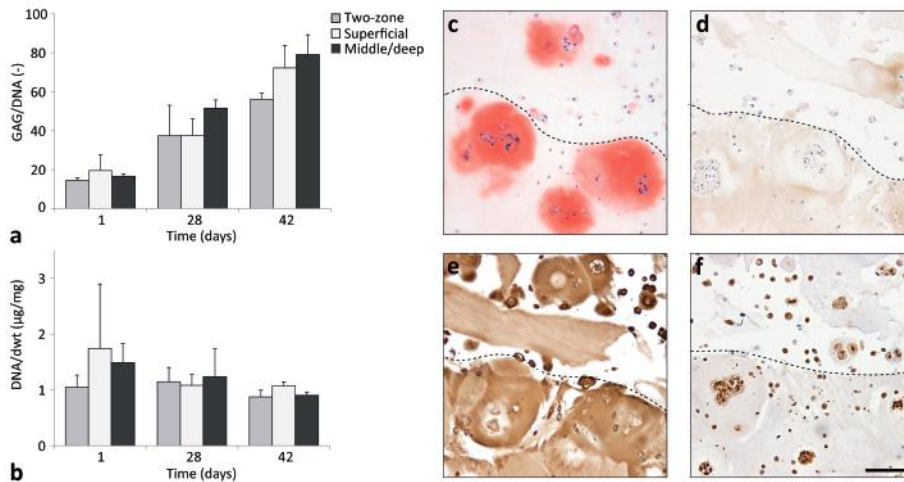
Figure 6. Cartilage production within the printed two-zone constructs. *GAG normalized to the DNA content (a) and DNA normalized to the dry weight (dwt, b) for printed two-zone constructs (two-zone), printed superficial zone only constructs (Superficial), and printed middle/deep zone constructs (Middle/deep). Histological assessment of two-zone constructs, safranin-O (c), collagen type I (d), collagen type II (e), and proteoglycan IV (f). The dotted lines indicate the transition between the superficial zone (top) and middle/deep zone (bottom). Scale bar represents 100 µm for all images.*

The mRNA expression of chondrogenic markers was upregulated for all printed constructs during culture. Both aggrecan and collagen type II gene expression were upregulated at day 28 compared to day 1, while no differences were observed between day 28 and 42 of culture (Figure 7a and 7b). A significantly higher collagen type II gene expression level was measured for the ACPCs in the superficial region of the two-zone constructs, compared to the ACPCs in the single-zone construct and compared to MSCs in the single-zone hydrogels. Furthermore, mRNA expression of collagen type I was similar in both regions of the two-zone constructs, and in the single-zone controls at all time-

points (Figure 7c). In addition, the mRNA expression of proteoglycan IV increased for all conditions between day 1 and 28, while no difference was observed between days 28 and 42 (Figure 7d). Moreover, no differences in proteoglycan IV gene expression were measured between the ACPCs in the superficial region or the MSCs in the middle/deep region of the two-zone constructs, nor in the single-zone constructs. Furthermore, mRNA expression for collagen type X was similar for all printed constructs at all time-points (Figure 7e).
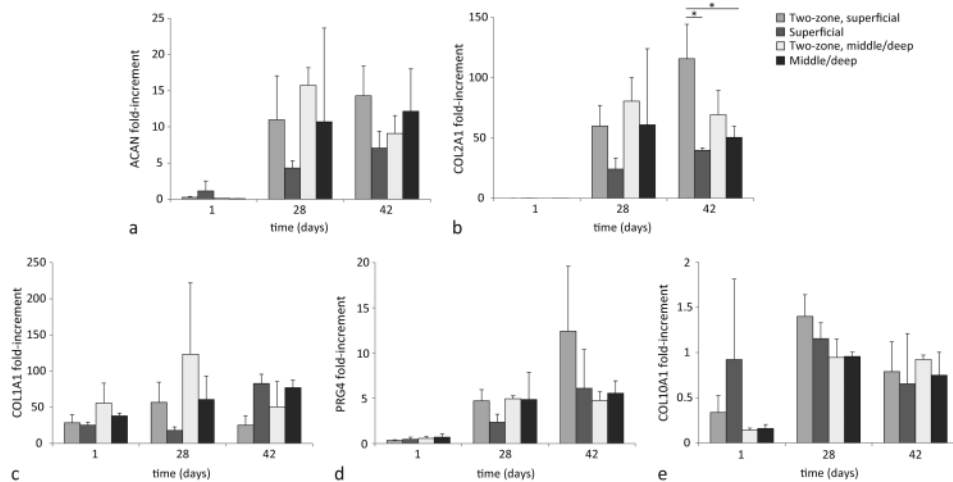
Figure 7. Gene expression for the superficial and middle/deep regions of the two-zone constructs (two-zone, superficial and two-zone, middle/deep, respectively), and the single-zone constructs (superficial or middle/deep). Expression levels of mRNA for aggrecan (ACAN, a), collagen type II (COL12A1, b), collagen type I (COL1A1, c), proteoglycan IV (PRG4, d), and collagen type X (COL10A1, e).

Along with the printed single-zone constructs, also cast controls were cultured. Histological assessment of the cast controls revealed more intense safranin-O staining compared to the printed single-zone hydrogels at day 42 (Figure 8a). Furthermore, all printed constructs contained several single cells without an intensely stained matrix surrounding them, while these single cells were only observed sporadically in the cast controls. Additionally, the histological appearance of the printed single-zone constructs was similar to the matching region in the printed two-zone constructs. The GAG content normalized to the DNA content, and the mRNA expression levels for aggrecan and collagen type II revealed a similar trend as observed in the histological sections; lower values in printed hydrogels compared to the cast hydrogels (Figure 8b, 8c, and 8d). Furthermore, collagen type I staining was more intense and relative mRNA expression was significantly higher for the printed constructs compared to the cast controls with the same cell type (Figure 8a and 8e).
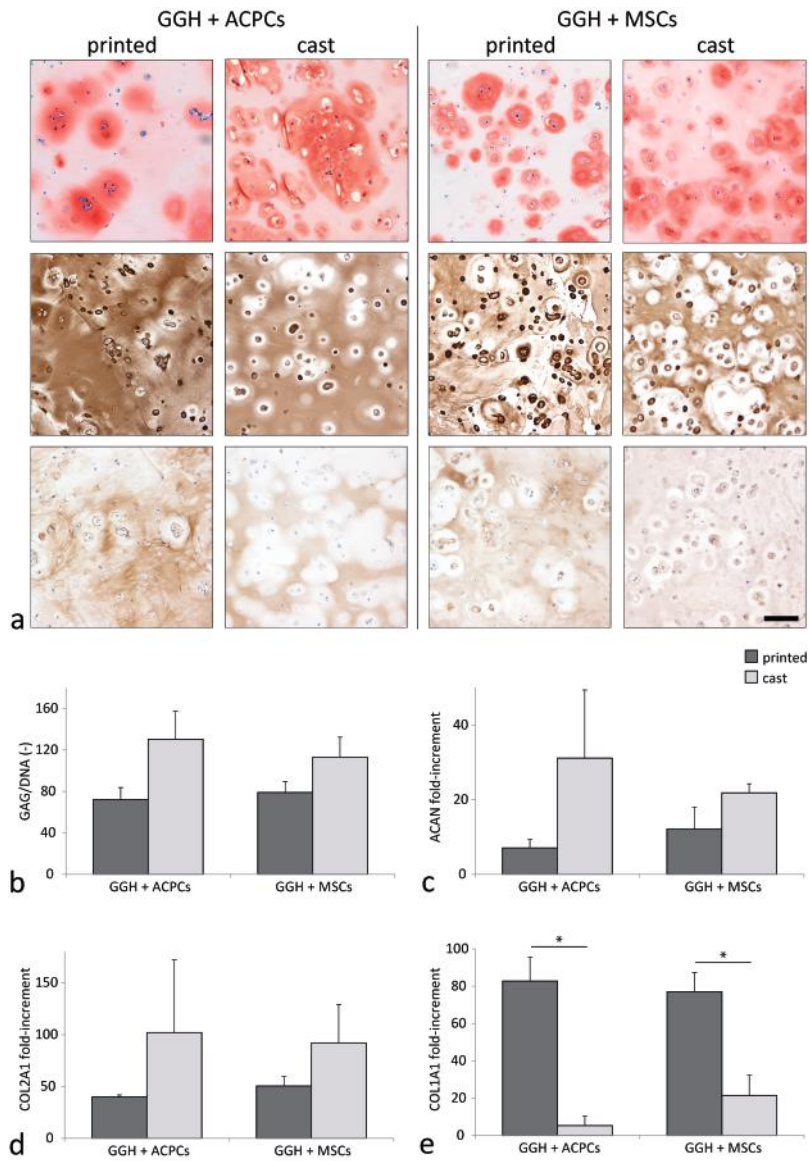
Figure 8. Chondrogenic potential of ACPCs and MSCs in printed and cast hydrogels at day 42 of culture. *a) Histological assessment of GAGs (safranin-O, top), collagen type II (middle), and collagen type I (bottom) matrix production. b) GAG content normalized to the DNA content for printed and cast hydrogels with ACPCs or MSCs. c-d) Relative gene expression of aggrecan (ACAN, c), collagen type I (COL1A1, d), and collagen type II (COL12A1, e) for or printed and cast hydrogels with ACPCs or MSCs.*

4. Discussion

The results of this study demonstrate improved printability of gelMA/gellan hydrogels with the incorporation of HAMA (formulation GGH). Moreover, ACPCs, MSCs, and to a lesser extent chondrocytes produced cartilage-like tissue in cast GGH hydrogels. More specifically, MSCs expressed the highest levels of collagen type II mRNA, while ACPCs exhibited higher proteoglycan IV mRNA expression levels compared to the MSCs. Therefore, two-zone constructs were printed with GGH bio-ink with ACPCs in the top region and MSCs in the middle/deep region. Although both the ACPCs and MSCs produced GAGs and collagen type II in their designated zone, bioprinting of both cell types resulted in changes in the quality of the produced neo-cartilage, compared to cast cell-laden hydrogel controls. Both the ACPCs and MSC-laden constructs stained less intense for GAGs after printing, while an increase in collagen type I staining intensity was observed, although collagen type II remained prominent. Similar trends were detected for mRNA expression levels and GAG content. These results strongly suggest that the printing procedure influenced the chondrogenesis of the embedded cells. Comparable observations were made by Müller *et al.* (2016)[41], who demonstrated that high shear stresses due to relatively small nozzle diameters affected cell spreading and delayed matrix synthesis, but not viability. They reported compromised chondrocyte behavior when exposing the cells to shear forces above ~160 Pa. Furthermore, finite element simulations estimated that shear forces within that range could occur when printing cells with the needle used in the current study, already at a pressure of 6 kPa, using an alginate-based hydrogel. However, due to the relatively high yield stress of gelMA/gellan/HAMA hydrogels, we used a significantly higher pressure (80 kPa) for successful filament deposition. Therefore, the embedded ACPCs and MSCs were likely exposed to relatively high shear forces (> 160 Pa) during printing, which could explain the differences in matrix deposition observed between printed and cast constructs. These findings underscore that printing techniques can influence more biological functions of cells than just viability. Importantly, viability is often the only biological response evaluated to confirm the successful printing of cells[42–44]. The current results clearly demonstrates that more extensive biological evaluations after printing, as well as the inclusion of cast control samples, are essential for future evaluation of bio-inks. Such more extensive assessments will provide valuable insight on the boundary conditions for effective bioprinting[41].

Although the detailed mechanism behind the longer-term influence of printing on cells is currently unclear, it is known that shear forces can deform cells, which causes cell adaptation and realignment of the cytoskeleton[42,45]. Such adaptations start already after several seconds of mechanical stress, and might therefore play a role in the altered cell behavior observed after printing. Moreover, cell deformations were demonstrated to steer MSC differentiation fate[46,47]. For example, stretching of MSCs stimulates differentiation towards the myogenic lineage[46] and shear forces via fluid flow can drive MSC differentiation into the osteogenic lineage[47]. Thus, gaining deeper understanding of these processes might provide printing protocols to steer cell fate in the future.

In the current study, also the possibility to improve the printability of a gelMA/gellan bio-ink with the incorporation of HAMA was explored. Indeed, the addition of HAMA

further improved the filament stability. On average, filaments printed with bio-ink GG started to collapse when bridging a gap of 8 mm while filaments printed with bio-ink GGH bridged this distance without collapsing. This observation is in line with previous findings that demonstrated enhanced printability, via an increase in viscosity and yield stress, by the incorporation of HAMA in gelMA or PEG-based hydrogels[22,24].

The incorporation of HAMA in a hydrogel has also been demonstrated to improve cartilage-like tissue formation by embedded chondrocytes (Chapter 5). However, no significant differences in matrix production or gene expression by chondrocytes, ACPCs, or MSCs were observed due to the presence of HAMA in the current study (formulation GG compared to GGH). The effect of HAMA on chondrogenesis is expected to be the result of cell receptor binding with HAMA (*i.e.* CD44 and hyaluronan mediated motility receptor)[48–51]. Chondrocytes, ACPCs, and MSCs all have membrane receptors capable of binding with HAMA and thus may be influenced by the presence of HAMA[50,52]. However, the effect of HAMA on chondrocytes embedded in PEG-based hydrogels was demonstrated to be dose-dependent (Chapter 5), possibly via negative feedback of receptor binding with HAMA[30,36,50,53]. Likely, the optimal concentration of 0.5% HAMA, which was found for chondrocyte-laden gelMA and PEG-based hydrogels in previous studies, will depend on the hydrogel platform and cell type[17]. Although, the presence of HAMA could not increase cartilage-like tissue formation or gene expression, it did improve filament stability. Therefore gelMA/gellan/HAMA hydrogels were used for the fabrication of two-zone constructs.

Significantly more cartilage matrix was produced by the ACPCs and MSCs compared to the chondrocytes. The GAG content measured in the chondrocyte-laden GG(H) hydrogels in the current study is in line with previously reported values for chondrocytes embedded in similar hydrogels[16,33]. This implies that the ACPCs and MSCs are more effective for *in vitro* cartilage tissue-engineering using GG(H) hydrogels. Furthermore, both ACPCs and MSCs can be expanded in monolayer culture to obtain sufficient numbers of cells. For these reasons, ACPCs and MSCs may represent promising cell sources for cartilage tissue-engineering purposes. However, isolation of autologous ACPCs from a patient is associated with donor site morbidity[54]. Therefore, careful consideration of the harvest location is required or the use of allogeneic ACPCs should be explored[55]. In contrast to ACPCs, autologous MSCs can be obtained from easier accessible tissues compared to articular cartilage. However, a downside of MSCs for cartilage repair is their tendency to progress into hypertrophic chondrogenesis or endochondral bone formation after *in vivo* implantation[56]. Strategies to overcome this, may be the incorporation of growth factors, *e.g.* TGF-β, into the hydrogel to steer chondrogenic differentiation[29,57], or direct co-culture of MSCs with *e.g.* chondrocytes[58]. However, further research on such methods is required for clinical translation of tissue-engineered cartilage constructs containing MSCs.

Based on the results from the cast hydrogel cultures, ACPCs were found most suitable for the fabrication of superficial zone cartilage, while MSCs have potential for the fabrication of middle and deep zone cartilage. The mRNA expression levels of proteoglycan IV were significantly higher in ACPCs compared to the MSCs in formulation GGH. As ACPCs are mainly found in the native superficial cartilage[27], it is likely that they

6

retain their ability for producing superficial zone matrix components. Indeed, previous studies have also reported higher proteoglycan IV gene expression levels in ACPCs compared to MSCs[33,59]. Furthermore, MSC-laden hydrogels stained more intensely for GAGs (safranin-O) and collagen type II compared to the chondrocyte or ACPC-laden hydrogels. Additionally, similar trends in gene expression levels were observed between these cell types at day 28. Therefore, MSCs may be beneficial for relatively fast production of hyaline-like cartilage within GGH constructs. Thus, MSCs in a GGH bio-ink, form a promising combination for the fabrication of the middle and deep cartilage regions of zonal constructs.

Two-zone constructs were successfully printed with different cell types in each zone. However, limited differences between the two regions were observed during culture (day 28 and 42), despite of the differences observed in monocultures. MSCs produced slightly more GAGs compared to the ACPCs in the top layer, as observed with the safranin-O staining. However, GAG content and aggrecan mRNA expression was similar for both layers at all time-points. Furthermore, proteoglycan IV mRNA expression levels increased during the first 28 days of culture for both ACPCs and MSCs, reaching similar levels at days 28 and 42. This is in contrast to the proteoglycan IV mRNA expression levels measured for the cast hydrogels used for the evaluation of (zone-specific) cartilage-matrix production, where proteoglycan IV mRNA expression levels of MSCs did not increase during culture (mRNA expression relative to HPRT in the cast MSC-laden hydrogels of the first experiment: 0.6±0.9, in printed two-zone constructs: 5.0±0.3, and in printed single-zone constructs: 4.9±3.0, at day 28). This observation may indicate that the printing of MSCs stimulates gene expression of proteoglycan IV. Other studies demonstrated an increase in proteoglycan IV production by chondrocytes due to shear forces[6,60]. However, a similar effect would then be expected for the ACPCs, which was not the case (mRNA expression relative to HPRT in the cast ACPC-laden hydrogels of the first experiment: 9.8±4.0, in printed two-zone constructs: 4.7±1.2, and in printed single-zone constructs: 2.4±0.9, at day 28). Possibly, ACPCs and MSCs react differently to the printing procedure, highlighting the importance of gaining deeper understanding of this process.

Although two-zone cartilage constructs were printed, limited zonal differences were observed after culture. Additional strategies to stimulate zone-specific matrix production by the embedded cells may improve zonal tissue formation within hydrogel constructs. For example, the incorporation of biological cues *e.g.* chondroitin sulfate, matrix metalloproteinase-sensitive peptides, growth factors, differences in cell densities[12,61–63], all have been demonstrated to steer cells into producing zone-specific cartilage-like tissue. Furthermore, imposing mechanical loading (compression and shear) onto cell-laden hydrogel constructs was shown to increase cartilage-like matrix production[64,65], proteoglycan IV production at the hydrogel surface[6,60], and may induce the alignment of collagen fibers[66,67].

6

5. Conclusion

GelMA/gellan/HAMA (GGH) hydrogel is a promising bio-ink that allows the printing of stable cell-laden hydrogel filaments. Cast GGH constructs supported chondrogenic differentiation of embedded ACPCs, MSCs, and to a lesser extent chondrocytes. However, cell differentiation was influenced by the printing procedure. The results of this study highlight the importance of including cast controls when evaluating bioprinted cartilage constructs. Additionally, further evaluation of the influence of the printing procedure on advanced biological functions of embedded cells is required to provide more detailed boundary conditions for successful bioprinting.

6. Acknowledgements

Supporting Information

6

Figure S1. Proteoglycan IV staining of chondrocytes, ACPCs, and MSCs in hydrogels with formulation GG and GGH. No differences were observed between the different hydrogel formulations. Scale bar represents 100 µm for all images.

Table S1. Print-settings used for the evaluation of filament collapse (G, GG, and GGH) and the bioprinting of zonal constructs (cell-laden GGH).

Formulation	Needle (gauge)	Pressure (MPa)	Temperature cartridge (°C)	Feed rate (mm s^{-1})
G	23 (straight)	0.13	25	10
GG	23 (straight)	0.19	28	28
GGH	23 (straight)	0.22	28	20
Cell-laden GGH	22 (conical)	0.08	28	20

6

References

1. Prakash, D. & Learmonth, D. Natural progression of osteo-chondral defect in the femoral condyle. *Knee* **9,** 7–10 (2002).
2. Browne, J. E. & Branch, T. P. Surgical alternatives for treatment of articular cartilage lesions. *J. Am. Acad. Orthop. Surg.* **8,** 180–189 (2000).
3. Almarza, A. J. & Athanasiou, K. A. Design characteristics for the tissue engineering of cartilaginous tissues. *Ann. Biomed. Eng.* **32,** 2–17 (2004).
4. Buckley, M. R., Gleghorn, J. P., Bonassar, L. J. & Cohen, I. Mapping the depth dependence of shear properties in articular cartilage. *J. Biomech.* **41,** 2430–2437 (2008).
5. Schuurman, W. *et al.* Cartilage regeneration using zonal chondrocyte subpopulations: a promising approach or an overcomplicated strategy? *J. Tissue Eng. Regen. Med.* **9,** 669–678 (2015).
6. Li, Z., Yao, S., Alini, M. & Grad, S. Different response of articular chondrocyte subpopulations to surface motion. *Osteoarthr. Cartil.* **15,** 1034–1041 (2007).
7. Hayes, A. J., Hall, A., Brown, L., Tubo, R. & Caterson, B. Macromolecular Organization and In Vitro Growth Characteristics of Scaffold-free Neocartilage Grafts. *J. Histochem. Cytochem.* **55,** 853–866 (2007).
8. Malda, J. *et al.* Localization of the potential zonal marker clusterin in native cartilage and in tissue-engineered constructs. *Tissue Eng. Part A* **16,** 897–904 (2010).
9. DiCesare, P. E., Mörgelin, M., Carlson, C. S., Pasumarti, S. & Paulsson, M. Cartilage oligomeric matrix protein: Isolation and characterization from human articular cartilage. *J. Orthop. Res.* **13,** 422–428 (1995).
10. Brittberg, M. Cell Carriers as the Next Generation of Cell Therapy for Cartilage Repair: A Review of the Matrix-Induced Autologous Chondrocyte Implantation Procedure. *Am. J. Sports Med.* **38,** 1259–1271 (2010).
11. Dewan, A. K., Gibson, M. A., Elisseeff, J. H. & Trice, M. E. Evolution of autologous chondrocyte repair and comparison to other cartilage repair techniques. *Biomed Res. Int.* **2014,** (2014).
12. Klein, T. J., Malda, J., Sah, R. L. & Hutmacher, D. W. Tissue Engineering of Articular Cartilage with Biomimetic Zones. *Tissue Eng. Part B Rev.* **15,** 143–157 (2009).
13. Hollander, A. P., Dickinson, S. C. & Kafienah, W. Stem Cells and Cartilage Development: Complexities of a Simple Tissue. *Stem Cells* **28,** 1992–1996 (2010).
14. Mouser, V. H. M. *et al.* Three-Dimensional Bioprinting and Its Potential in the Field of Articular Cartilage Regeneration. *Cartilage* (2016). doi:10.1177/1947603516665445
15. Malda, J. *et al.* 25th Anniversary Article: Engineering Hydrogels for Biofabrication. *Adv. Mater.* **25,** 5011–5028 (2013).
16. Mouser, V. H. M. *et al.* Yield stress determines bioprintability of hydrogels based on gelatin-methacryloyl and gellan gum for cartilage bioprinting. *Biofabrication* **8,** 035003 (2016).
17. Levett, P. A. *et al.* A biomimetic extracellular matrix for cartilage tissue engineering centered on photocurable gelatin, hyaluronic acid and chondroitin sulfate. *Acta Biomater.* **10,** 214–223 (2014).
18. Yue, K. *et al.* Synthesis, properties, and biomedical applications of gelatin methacryloyl (GelMA) hydrogels. *Biomaterials* **73,** 254–271 (2015).
19. Gao, G. *et al.* Improved properties of bone and cartilage tissue from 3D inkjet-bioprinted human mesenchymal stem cells by simultaneous deposition and photocrosslinking in PEG-GelMA. *Biotechnol. Lett.* **37,** 2349–2355 (2015).
20. Billiet, T., Gevaert, E., De Schryver, T., Cornelissen, M. & Dubruel, P. The 3D printing of gelatin methacrylamide cell-laden tissue-engineered constructs with high cell viability. *Biomaterials* **35,** 49–62 (2014).
21. Melchels, F. P. W., Dhert, W. J. A., Hutmacher, D. W. & Malda, J. Development and characterisation of a new bioink for additive tissue manufacturing. *J. Mater. Chem. B* **2,** 2282–2289 (2014).
22. Schuurman, W. *et al.* Gelatin-methacrylamide hydrogels as potential biomaterials for fabrication of tissue-engineered cartilage constructs. *Macromol. Biosci.* **13,** 551–561 (2013).
23. Levett, P. A., Hutmacher, D. W., Malda, J. & Klein, T. J. Hyaluronic acid enhances the mechanical properties of tissue-engineered cartilage constructs. *PLoS One* **9,** e113216 (2014).
24. Abbadessa, A. *Thermosensitive hydrogels for 3D bioprinting of cartilage constructs.* (2017).
25. Ma, B. *et al.* Gene expression profiling of dedifferentiated human articular chondrocytes in monolayer culture. *Osteoarthr. Cartil.* **21,** 599–603 (2013).
26. Jiang, Y. & Tuan, R. S. Origin and function of cartilage stem/progenitor cells in osteoarthritis. *Nat. Rev. Rheumatol.* **11,** 206–12 (2015).
27. Dowthwaite, G. P. The surface of articular cartilage contains a progenitor cell population. *J. Cell Sci.* **117,** 889–897 (2004).
28. Dominici, M. *et al.* Minimal criteria for defining multipotent mesenchymal stromal cells. The International Society for Cellular Therapy position statement. *Cytotherapy* **8,** 315–317 (2006).
29. Spiller, K. L., Maher, S. a & Lowman, A. M. Hydrogels for the Repair of Articular Cartilage Defects. *Tissue Eng. Part B Rev.* **17,** 281–299 (2011).
30. Hachet, E., Van Den Berghe, H., Bayma, E., Block, M. R. & Auzély-Velty, R. Design of biomimetic cell-interactive substrates using hyaluronic acid hydrogels with tunable mechanical properties. *Biomacromolecules* **13,** 1818–27 (2012).
31. Blokzijl, M. M. *et al.* Structural deformation of bioink filaments. in (Biofabrication conference, 2016).
32. Williams, R. *et al.* Identification and Clonal Characterisation of a Progenitor Cell Sub-Population in Normal Human Articular Cartilage. *PLoS One* **5,** e13246 (2010).

6

33. Levato, R. *et al.* Opportunities for zonal cartilage regeneration: progenitor cell-laden hydrogels and bioprinting. in (TERMIS - EU Chapter Conference, 2016).
34. Pittenger, M. F. Multilineage Potential of Adult Human Mesenchymal Stem Cells. *Science (80-.).* **284,** 143–147 (1999).
35. Benders, K. E. M. *et al.* Multipotent Stromal Cells Outperform Chondrocytes on Cartilage-Derived Matrix Scaffolds. *Cartilage* **5,** 221–230 (2014).
36. Benya, P. Dedifferentiated chondrocytes reexpress the differentiated collagen phenotype when cultured in agarose gels. *Cell* **30,** 215–224 (1982).
37. Guo, J., Jourdian, G. W. & Maccallum, D. K. Culture and Growth Characteristics of Chondrocytes Encapsulated in Alginate Beads. *Connect. Tissue Res.* **19,** 277–297 (1989).
38. Schumacher, B. L., Hughes, C. E., Kuettner, K. E., Caterson, B. & Aydelotte, M. B. Immunodetection and partial cDNA sequence of the proteoglycan, superficial zone protein, synthesized by cells lining synovial joints. *J. Orthop. Res.* **17,** 110–120 (1999).
39. Wall, A. & Board, T. in *Classic Papers in Orthopaedics* **53,** 433–435 (Springer London, 2014).
40. Abbadessa, A. *et al.* A Synthetic Thermosensitive Hydrogel for Cartilage Bioprinting and Its Biofunctionalization with Polysaccharides. *Biomacromolecules* **17,** 2137–2147 (2016).
41. Müller, M., Öztürk, E., Arlov, Ø., Gatenholm, P. & Zenobi-Wong, M. Alginate Sulfate–Nanocellulose Bioinks for Cartilage Bioprinting Applications. *Ann. Biomed. Eng.* 1–14 (2016). doi:10.1007/s10439-016-1704-5
42. Ersumo, N., Witherel, C. E. & Spiller, K. L. Differences in time-dependent mechanical properties between extruded and molded hydrogels. *Biofabrication* **8,** 035012 (2016).
43. Nair, K. *et al.* Characterization of cell viability during bioprinting processes. *Biotechnol. J.* **4,** 1168–1177 (2009).
44. Chang, R., Nam, J. & Sun, W. Effects of Dispensing Pressure and Nozzle Diameter on Cell Survival from Solid Freeform Fabrication–Based Direct Cell Writing. *Tissue Eng. Part A* **14,** 41–48 (2008).
45. Matthews, B. D. Cellular adaptation to mechanical stress: role of integrins, Rho, cytoskeletal tension and mechanosensitive ion channels. *J. Cell Sci.* **119,** 508–518 (2006).
46. Yang, Y., Beqaj, S., Kemp, P., Ariel, I. & Schuger, L. Stretch-induced alternative splicing of serum response factor promotes bronchial myogenesis and is defective in lung hypoplasia. *J. Clin. Invest.* **106,** 1321–1330 (2000).
47. Sonam, S., Sathe, S. R., Yim, E. K. F., Sheetz, M. P. & Lim, C. T. Cell contractility arising from topography and shear flow determines human mesenchymal stem cell fate. *Sci. Rep.* **6,** 20415 (2016).
48. Yasuda, T. Nuclear factor-κB activation by type II collagen peptide in articular chondrocytes: its inhibition by hyaluronan via the receptors. *Mod. Rheumatol.* **23,** 1116–1123 (2012).
49. Viola, M. *et al.* Biology and biotechnology of hyaluronan. *Glycoconj. J.* **32,** 93–103 (2015).
50. Akmal, M. *et al.* The effects of hyaluronic acid on articular chondrocytes. *J. Bone Jt. Surg. - Br. Vol.* **87-B,** 1143–1149 (2005).
51. Ariyoshi, W., Takahashi, N., Hida, D., Knudson, C. B. & Knudson, W. Mechanisms involved in enhancement of the expression and function of aggrecanases by hyaluronan oligosaccharides. *Arthritis Rheum.* **64,** 187–197 (2012).
52. Bian, L., Guvendiren, M., Mauck, R. L. & Burdick, J. a. Hydrogels that mimic developmentally relevant matrix and N-cadherin interactions enhance MSC chondrogenesis. *Proc. Natl. Acad. Sci.* **110,** 10117–10122 (2013).
53. Schuh, E. *et al.* Chondrocyte redifferentiation in 3D: the effect of adhesion site density and substrate elasticity. *J. Biomed. Mater. Res. A* **100,** 38–47 (2012).
54. McCarthy, H. S., Richardson, J. B., Parker, J. C. E. & Roberts, S. Evaluating Joint Morbidity after Chondral Harvest for Autologous Chondrocyte Implantation (ACI): A Study of ACI-Treated Ankles and Hips with a Knee Chondral Harvest. *Cartilage* **7,** 7–15 (2016).
55. Matricali, G. A., Dereymaeker, G. P. E. & Luvten, F. P. Donor site morbidity after articular cartilage repair procedures: A review. *Acta Orthopaedica Belgica* **76,** 669–674 (2010).
56. Visser, J. *et al.* Endochondral bone formation in gelatin methacrylamide hydrogel with embedded cartilage-derived matrix particles. *Biomaterials* **37,** 174–182 (2015).
57. Jung, H. H., Park, K. & Han, D. K. Preparation of TGF-β1-conjugated biodegradable pluronic F127 hydrogel and its application with adipose-derived stem cells. *J. Control. Release* **147,** 84–91 (2010).
58. Windt, T. S. De *et al.* Direct Cell – Cell Contact with Chondrocytes Is a Key Mechanism in Multipotent Mesenchymal. *Tissue Eng. Part A* **21,** 2536–2547 (2015).
59. Seol, D. *et al.* Chondrogenic progenitor cells respond to cartilage injury. *Arthritis Rheum.* **64,** 3626–3637 (2012).
60. Grad, S. *et al.* Surface Motion Upregulates Superficial Zone Protein and Hyaluronan Production in Chondrocyte-Seeded Three-Dimensional Scaffolds. *Tissue Eng.* **11,** 249–256 (2005).
61. Karimi, T., Barati, D., Karaman, O., Moeinzadeh, S. & Jabbari, E. A developmentally inspired combined mechanical and biochemical signaling approach on zonal lineage commitment of mesenchymal stem cells in articular cartilage regeneration. *Integr. Biol.* **7,** 112–127 (2015).
62. Tatman, P. D. *et al.* Multiscale Biofabrication of Articular Cartilage: Bioinspired and Biomimetic Approaches. *Tissue Eng. Part B Rev.* **21,** 543–559 (2015).
63. Trappmann, B. *et al.* Extracellular-matrix tethering regulates stem-cell fate. *Nat. Mater.* **11,** 742–742 (2012).
64. Wong, M. & Carter, D. R. Articular cartilage functional histomorphology and mechanobiology: A research perspective. *Bone* **33,** 1–13 (2003).

6

65.   Klein, T. J. *et al.* Strategies for Zonal Cartilage Repair using Hydrogels. *Macromol. Biosci.* **9,** 1049–1058 (2009).

66.   Kock, L. M., Ito, K. & van Donkelaar, C. C. Sliding Indentation Enhances Collagen Content and Depth-Dependent Matrix Distribution in Tissue-Engineered Cartilage Constructs. *Tissue Eng. Part A* **19,** 1949–1959 (2013).

67.   Khoshgoftar, M., van Donkelaar, C. C. & Ito, K. Mechanical stimulation to stimulate formation of a physiological collagen architecture in tissue-engineered cartilage: a numerical study. *Comput. Methods Biomech. Biomed. Engin.* **14,** 135–144 (2011).

6

Chapter 7

The spatial distribution of chondrocytes in a hydrogel construct dictates cartilage defect repair

Vivian H. M. Mouser
Noël M. M. Dautzenberg
Riccardo Levato
Mattie H. P. van Rijen
Wouter J. A. Dhert
Jos Malda
Debby Gawlitta
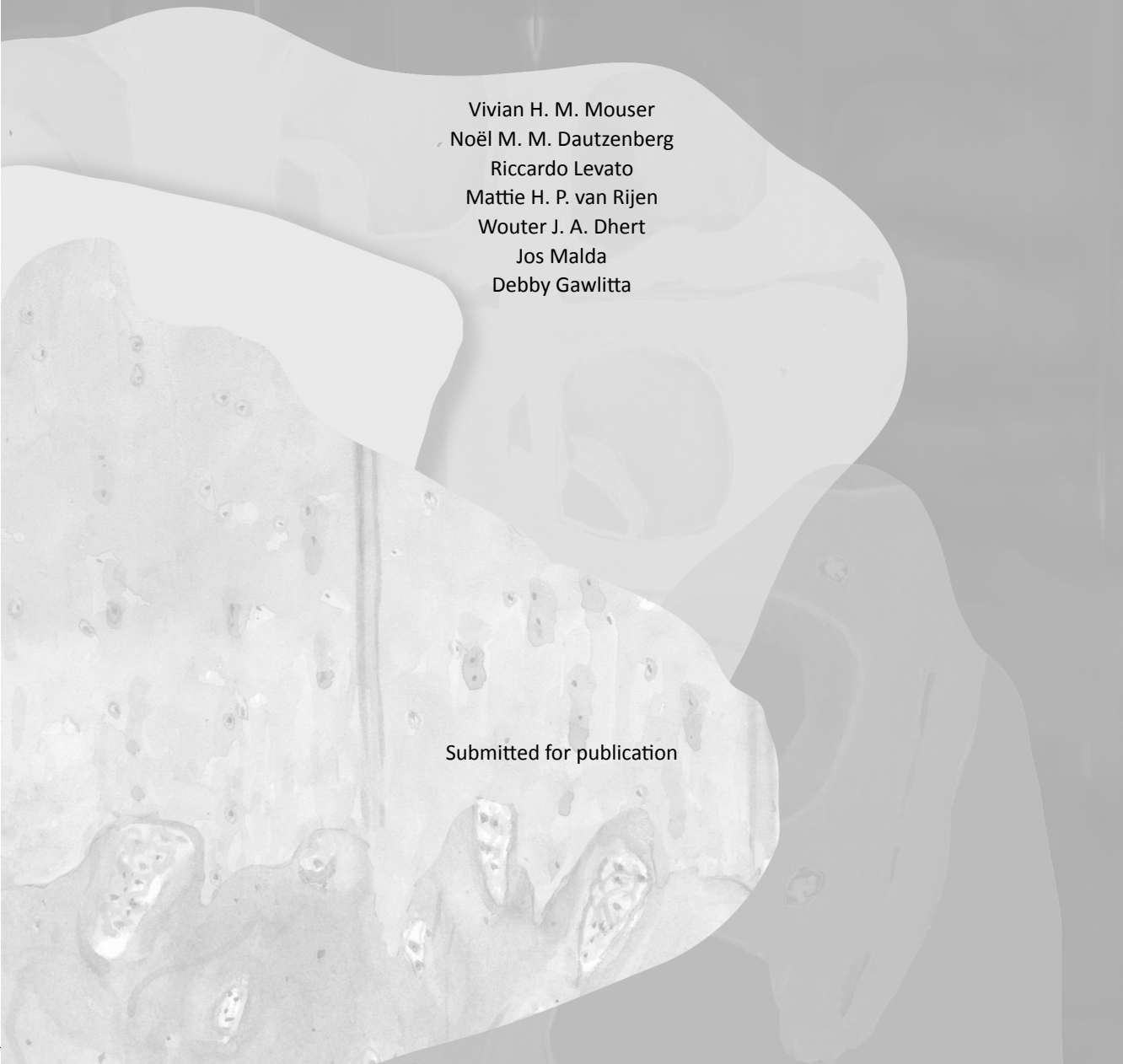
Abstract

Implantation of chondrocyte-laden hydrogels is a promising cartilage repair strategy. Chondrocytes can be spatially positioned in hydrogels and thus in the defect, while current clinical cell-therapies are based on the introduction of chondrocytes in the defect depth. The aim of this study was to evaluate the effect of the spatial chondrocyte distribution on the reparative process in an *ex vivo* osteochondral plug model. Further, the role of delivered and endogenous cells in the repair process was investigated.

Full thickness cartilage defects were created in equine osteochondral plugs. Defects were filled with (A) chondrocytes at the bottom of the defect, covered with a cell-free hydrogel, (B) chondrocytes homogeneously encapsulated in a hydrogel, (C, D) combinations of A and B with different cell densities. Plugs were cultured up to 57 days, after which the cartilage and repair tissues were characterized and compared to baseline samples. Moreover, plugs cultured for 21 days were used to assess the origin of the cells in the repair tissue.

Best outcomes were obtained with conditions C and D, which resulted in well-integrated cartilage-like tissue that completely filled the defect, regardless of the initial cell density. Chondrocytes seeded at the defect bottom contributed to integration of the construct in the defect, while encapsulated chondrocytes provided complete defect filling within 57 days. Moreover, repair tissue originated from the delivered cells.

These findings confirm the potential of cell implantation for cartilage repair, and highlight the critical role of the spatial chondrocyte distribution in the repair process.

1. Introduction

The implantation of tissue-engineered constructs is a promising approach for the treatment of articular cartilage defects. Articular cartilage consists of predominantly water, aggrecan, collagen type II, and chondrocytes[1,2]. As adult articular cartilage lacks vascularization and innervation, and contains relatively low total cell numbers, the tissue has a limited regenerative capacity. Thus, untreated cartilage injuries generally lead to osteoarthritic joint changes [2,3].

The most commonly used strategies to repair chondral defects are based on marrow stimulation techniques (microfracture), or on active cell delivery (autologous chondrocyte implantation, ACI)[2,4,5]. Third-generation ACI-based strategies involve chondrocyte seeding into a biomaterial or scaffold such as collagen type I/III membranes, that are fixated in the defect with *e.g.* fibrin glue[6,7]. This matrix-induced ACI (MACI) technique was demonstrated to stimulate the formation of hyaline-like repair tissue[8,9]. However, full restoration of the defect site or reconstruction of the complex depth-dependent architecture of native cartilage is not achieved, indicating the need for further development.

Novel strategies for cell delivery and cartilage tissue-engineering employ cell-laden hydrogels, which can be cast or three-dimensionally (3D) bioprinted with depth-dependent architectures and/or patient-specific geometries[10]. Subsequently, the constructs can be pre-cultured *in vitro* to stimulate chondrocyte differentiation before implantation. A promising hydrogel for the biofabrication of such implants is gelatin methacryloyl (gelMA) with gellan gum, which was demonstrated to support chondrogenesis of embedded chondrocytes[11]. Additionally, gelMA/gellan is compatible with 3D printing techniques to facilitate accurate positioning of the (cell-laden) biomaterial[11,12].

For clinical translation of new cartilage repair technologies, evaluation of the approaches in animal models is indispensable. In view of the replacement of animal studies, an *ex vivo* osteochondral (OC) plug model was developed[13–15]. This model entails OC plugs obtained from cadaveric joints, which can be cultured in a recently developed culture platform[16]. A cartilage defect of the desired depth can be generated in the cartilage tissue of the OC plug. Accordingly, cartilage repair mechanisms can be studied in this model when mimicking treatment strategies[13].

It is important to understand the repair mechanisms underlying new cartilage therapies, to optimize the therapy for clinical use. Current clinical therapies are based on the introduction of a dense cell layer in the defect depth. Although the initial situation is different with MACI, as the chondrocytes are pre-seeded in the collagen membrane, it was observed that the seeded chondrocytes migrate from the patch into the fibrin glue in the defect depth, during the first days after implantation[17]. Therefore, it has been suggested that cartilage repair in MACI also originates from a dense chondrocyte layer in the defect depth [18,19]. Contrarily, new hydrogel-based repair strategies allow homogeneous chondrocyte encapsulation and delivery into the defect, representing an alternative chondrocyte delivery approach compared to traditional techniques. In order to optimize hydrogel-based therapies for clinical use, it is crucial to better understand the associated repair mechanisms[20] and to optimize the spatial chondrocyte distribution for cartilage repair. Therefore, the first aim of this study was to investigate the effect of

7

spatial variations in chondrocyte distribution within a hydrogel construct, on cartilage repair. The second aim was to assess the contribution of endogenous and delivered cells in the formation of repair tissue. The repair mechanisms were investigated in an *ex vivo* OC plug model with full-thickness cartilage defects.

2. Materials and methods

2.1. Experimental design

Equine OC plugs were isolated and full-thickness cartilage defects were created. Defects were filled with gelMA/gellan using four different spatial chondrocyte distributions ($20*10^6$/ml of the defect volume; Figure 1). Condition A consisted of chondrocytes seeded at the bottom of the defect that were covered with an empty hydrogel. In condition B, the chondrocytes were homogeneously encapsulated in the hydrogel. Conditions C and D were a combination of conditions A and B, in which chondrocytes were both seeded at the defect bottom and homogeneously encapsulated in the hydrogel. To investigate the influence of cell density on tissue formation the cell concentration was double for condition D. Condition E consisted of a cell-free hydrogel in the defect model, while a molded, chondrocyte-laden hydrogel construct (HC) cultured in medium was included as additional control. Plugs from all conditions were harvested at days 0 or 1 (baseline), 29, and 57 to evaluate the native cartilage and cartilage tissue formation in the defect area. In a separate experiment plugs filled with condition D were collected at day 21 to compare DNA profiles of the newly formed tissue to those of the OC plug and chondrocyte donors.
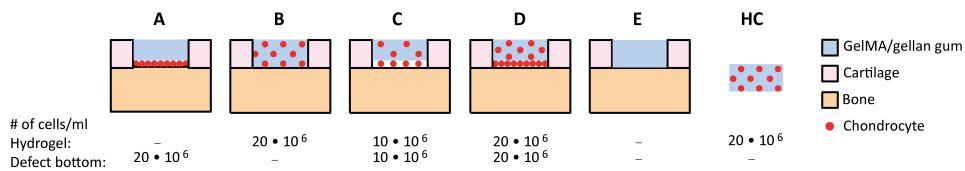
Figure 1. A schematic cross-sectional overview of the different defect filling conditions in the ex vivo OC plug model. *Chondrocytes were seeded at the bottom of the defect (A, $20*10^6$ cells/ml), homogeneously in the hydrogel (B, $20*10^6$ cell/ml), both at the bottom of the defect and in the hydrogel (C, $10*10^6$ cell/ml + $10*10^6$ cell/ml respectively; D, $20*10^6$ cell/ml + $20*10^6$ cell/ml respectively). An empty hydrogel was used as control (E). To evaluate the influence of the ex vivo OC plug model on the tissue production of the delivered chondrocytes also a cell-laden hydrogel control (HC, $20*10^6$ cell/ml) was cultured.*

2.2. Chondrocytes

Primary chondrocytes were harvested from full-thickness cartilage of metacarpophalangeal joints of a fresh equine cadaver obtained from the local slaughterhouse (N=1, 5 years old), as previously discribed[21], and cryopreserved in liquid nitrogen until used. Before use, chondrocytes were expanded in monolayer culture for 14 days ($5*10^3$ cells/cm^2) in expansion medium (Table 1) to passage 1.

7

Table 1. Overview of the medium compositions used for the different cultures.

Name	Composition
Expansion medium	- Dulbecco's Modified Eagle Medium (31885, Gibco) - Fetal bovine serum (10% v/v, Gibco) - Pen/strep (100 units/ml penicillin and 100 µg/ml streptomycin, Gibco)
Incubation medium	- α-Minimum Essential Medium (22561, Gibco) - Fetal bovine serum (10% v/v, Gibco) - Pen/strep (200 units/ml penicillin and 200 µg/ml streptomycin, Gibco) - Gentamicin sulphate (50 µg/ml, Lonza BioWhittaker)
Bone medium	- α-Minimum Essential Medium (22561, Gibco) - Fetal bovine serum (10% v/v, Gibco) - Pen/strep (100 units/ml penicillin and 100 µg/ml streptomycin, Gibco) - L-ascorbic acid-2-phosphate (0.2 mM, Sigma Aldrich) - Dexamethasone (10 nM, Sigma Aldrich) - β-glycerophosphate (10 mM, Sigma Aldrich) - Gentamicin sulphate (50 µg/ml)*
Chondrogenic differentiation medium	- High glucose Dulbecco's Modified Eagle Medium (D6429, Sigma Aldrich) - Pen/strep (100 units/ml penicillin and 100 µg/ml streptomycin, Gibco) - L-ascorbic acid-2-phosphate (0.2 mM, Sigma Aldrich) - Dexamethasone (0.1 µM, Sigma Aldrich) - ITS + premix (1%, BD biosciences) - Recombinant human transforming growth factor-β1 (TGF-β1, 10 ng/ml, Peprotech) - Gentamicin sulphate (50 µg/ml)*

* only supplemented during the first 7 days of culture

2.3. Osteochondral plugs

OC plugs (diameter 8.5 mm, bone height 3 mm, cartilage thickness ~1 mm) were drilled and cut under sterile conditions from the condyles of equine metacarpophalangeal joints (N=1, 3 years old for evaluation of tissue repair; N=1, 5 years old for DNA profiling). Next, full-thickness cartilage defects were created with a diameter of 4 mm. Prepared plugs were incubated overnight in incubation medium (Table 1).

The following day, the plugs were inserted into a culture platform, which provided separate medium compartments for the cartilage and bone tissue (LifeTec Group B.V., Eindhoven, The Netherlands)[16]. The required number of chondrocytes defined for

7

conditions A, C, and D, (Figure 1) was seeded by pipetting 10 µl cell-suspension into the defect. Plugs were incubated in the culture platform for 2 hours at 37°C in a humidified environment to allow chondrocytes to attach to the defect bottom. During this time, the bone compartment was supplemented with bone medium (Table 1). Next, incubation medium (Table 1) was pipetted onto the cartilage, until completely covered.

To fill the defects, gelMA was synthesized from porcine gelatin and 10% gelMA + 0.5% gellan gum solution was freshly prepared, both as previously described[11,12]. GelMA/gellan was dispensed into the defect without chondrocytes (groups A, E) or with embedded chondrocytes (groups B, C, D). Subsequently, filled defects were covered with silicon-coated microscopy cover glasses (Sigmacote, Sigma-Aldrich, Zwijndrecht, The Netherlands) and cross-linked with UV light (UV-Handleuchte lamp A., Hartenstein, Germany, wavelength: 365 nm, intensity: 1.2 mW/cm^2). Finally, cover glasses were removed and the OC plugs were cultured with bone medium in the bone compartment and chondrogenic differentiation medium in the cartilage compartment (Table 1). Hydrogel control (HC) samples were prepared by casting chondrocyte-laden gelMA/gellan in Teflon cylindrical molds (diameter: 4 mm, height: 2 mm). HCs were UV cross-linked and cultured in chondrogenic differentiation medium. Samples were obtained at days 0 and 1 (n=4) for the baseline detection of the native cartilage and defect filling, respectively. The remaining samples were harvested at days 29 (n=3; n=2 for condition E), 21 (n=4, condition D), and 57 (n=4; n=3 for condition E). Medium samples were taken from the cartilage compartment upon each medium change (twice a week).

2.4. Quantitative biochemical analysis

At days 0 or 1, 29 and 57, the cartilage of the OC plugs was cut in half and the tissue inside the defect area was separated from the surrounding cartilage. Tissue samples were processed and digested as previously described[21]. The amount of sulfated glycosaminoglycans (GAGs), both in the digested tissue and the medium, was determined with a dimethylmethylene blue (DMMB, pH=3.0) assay[22]. DNA quantification was performed with a Quant-iT-PicoGreen-dsDNA-kit according to manufacturer's instructions (Molecular Probes, Invitrogen, Carlsbad, USA).

2.5. Histology and immunohistochemistry

After harvesting half of the cartilage and repair tissue, the remaining tissue was fixed overnight in formalin (10%) and decalcified for 21 days in ethylenediaminetetraacetic acid solution (EDTA, 12.5%, VWR chemicals, Amsterdam, The Netherlands) at 37°C. The OC plugs were embedded in paraffin and tissue sections (5 µm) were cut for the visualization of matrix components[21]. A safranin-O/fast green staining was performed to visualize collagens (green/blue) and GAGs (red)[23]. To visualize the orientation of the collagen fibers, other sections were stained with picrosirius red (1 µg/mL, 60 minutes) with Weigert's hematoxylin as counterstain. Collagen types I, II, and VI were visualized with immunohistochemistry as previously described[21]. The stained sections were scanned with a NanoZoomer-XR Digital slide scanner (C12000-02, Hamamatsu, Almere, The Netherlands) while the picrosirius stained sections were evaluated with a

light microscope and a polarizing filter (BX51 with a DP70 camera, Olympus, Hamburg, Germany).

2.6. Origin of repair tissue
At day 21, the newly formed tissue overgrowing the native cartilage was isolated. Samples, including the cartilage and chondrocyte samples taken at day 0, were washed in ice cold PBS and digested overnight in digestion buffer (100 mM NaCl, 10 mM TrisCl pH 8, 25 mM EDTA pH 8, 0.5% sodium dodecyl sulfate, 0.1 mg/ml proteinase K from tritirachium album, 50˚C). DNA was extracted with phenol/chloroform/isoamyl alcohol and purified via precipitation with ammonium acetate (7.5M, ½x sample volume) and ethanol (100%, 2x sample volume). Purified DNA was rinsed with ethanol (70%), air dried, and resuspended in Tris-EDTA buffer (TE buffer, 10 mM Tris, 1mM EDTA, pH 8). Sequentially, DNA profiles were generated and compared by Van Haeringen Laboratorium B.V. (Wageningen, The Netherlands).

2.7. Statistical analyses
Statistical analysis was performed with SPSS software (version 21, IMB Corp.). A one-way ANOVA was used to determine differences between conditions (and the baseline values when analyzing the tissue surrounding the defect) at day 29 or day 57. Normality and homogeneity were assumed and a significance level of $p < 0.05$ was used. When significant differences were detected, a Bonferroni post-hoc test was performed. In all graphs, the error bars depict the standard error of the mean (SEM).

3. Results

3.1. Evaluation of the osteochondral plugs
The overall morphology of the bone and native cartilage, surrounding the defect area of the plugs, was similar after 57 days of culture to the morphology of day 1 samples, as observed in the safranin-O staining (Figure 2). In the native cartilage, the intensity of the safranin-O staining decreased during the culture period for all plugs. Nevertheless, the native cartilage stained positive for collagen type II and negative for collagen type I at day 57, with similar intensity to what was observed at day 0. The orientation of the collagen fibers remained unchanged during culture and the cells kept their pericellular matrix intact as visualized with picrosirius red and collagen type VI stainings. However, the collagen type VI staining intensity within the extracellular matrix decreased during culture.

Unexpectedly, the formation of an additional tissue layer was observed on top of the superficial cartilage of the plugs, which had defects filled with cells, regardless of the delivery method (Figure 2). Generally, this newly formed tissue stained positive for collagen type I, and to a lesser extent for collagen type II, while only sporadic safranin-O positive areas were observed. It contained a relatively high cell density and cells had a stretched morphology. Collagen type VI was found in the extracellular matrix of the newly formed tissue, but only sparsely in the pericellular matrix of the present cells.

7
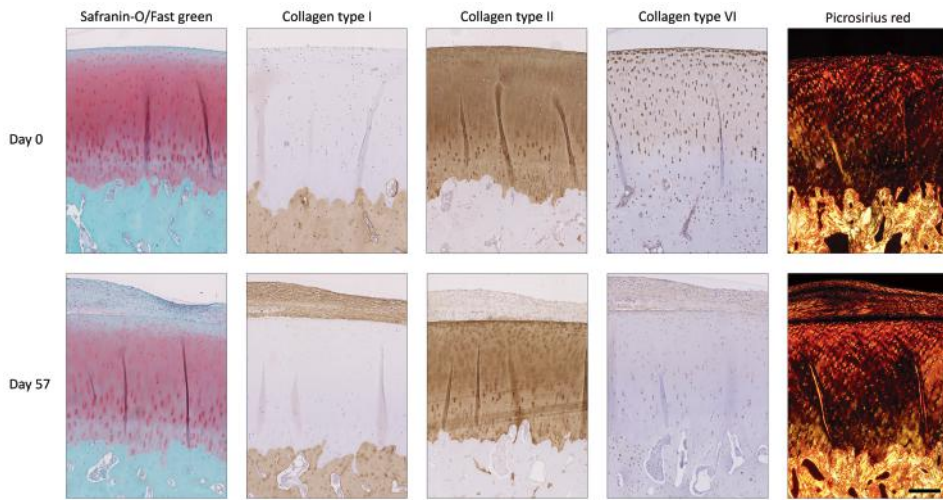
Figure 2. Change in native cartilage and bone morphology of the OC plugs during the culture period. *Images of day 57 are from the tissue surrounding the cartilage defect which was filled with condition A and are representative for all conditions with received chondrocytes in the defect. GAG content of the cartilage stained less intense after 57 days of culture. Additionally, new tissue grew over the defect area and covered the cartilage surface during culture. Scale bar represents 400 µm and is valid for all images.*

Additionally, picrosirius red staining revealed a collagen fiber orientation parallel to the cartilage surface in this tissue layer.

Quantitative measurements of the native cartilage surrounding the defects showed minor changes compared to baseline values (day 0). DNA content normalized to the sample dry weight (dwt) increased at day 29 compared to the baseline for conditions A, C, and D, and at day 57 for conditions A and D (Figure 3a). The water content normalized to the wet weight (wwt) was significantly increased at both time points compared to the baseline, except for condition E (Figure 3b). GAG per dwt decreased for condition C at day 29 compared to the baseline (Figure 3c), while no significant differences were observed at day 57 between groups or with the baseline. Additionally, a constant GAG release was measured in the medium for all conditions (Figure 3d). On average 19.1±5.2 µg/day of GAG leached into the medium.

3.2. Cartilage regeneration in the defect
Multiple differences in repair tissue were observed between the tested conditions (Figure 4a). In plugs of condition A, a dense tissue layer was visible at days 29 and 57 at the defect bottom and at the cartilage-hydrogel interface. This tissue layer contained relatively high cell numbers and stained positive for collagen type II and safranin-O and negative for collagen type I. Additionally, the tissue layer filled irregularities at the sides and near the tidemark (Figure 4a,b). The cell-free hydrogel used in condition A, was still present at the end of culture and cell infiltration was absent. However, the hydrogel stained positive for GAGs (safranin-O) and collagen type II with a gradient in intensity. The highest staining
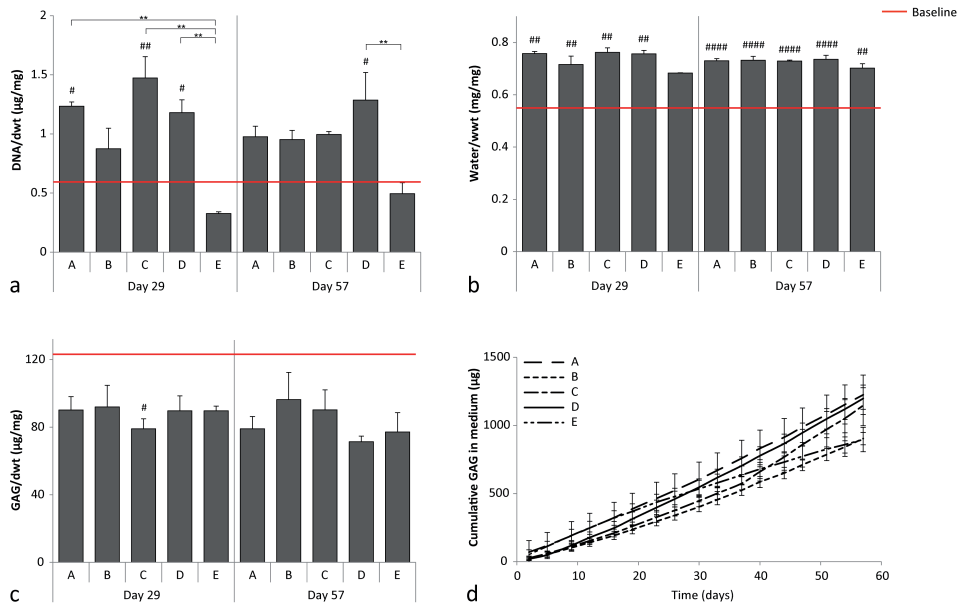
*Figure 3. Quantitative measurements of the DNA, GAGs, and water content of the native cartilage surrounding the defect. a) DNA normalized to the dry weight (dwt). b) Water content normalized to the wet weight (wwt), c) GAG normalized to the dwt. d) Cumulative GAGs measured in the medium. Baseline (red) indicates the average value measured at day 0. # represents a significant difference compared to the baseline (#, p<0.05; ##, p<0.01; ####, p<0.0001), and ** indicates a significant difference between the connected conditions (p<0.01).*

intensity was observed at the defect bottom and sides and it faded towards the hydrogel surface.

In contrast to condition A, more intense staining for cartilaginous matrix components was detected throughout the defect area in condition B (Figure 4). After 29 and 57 days of culture, homogeneously distributed cells and cell clusters were observed in the hydrogel. The hydrogel stained positive for GAGs (safranin-O) and collagen type II and negative for collagen type I. The pericellular matrix of cells within cell clusters stained positive for collagen type VI (Figure S1).

Defects filled with conditions C and D revealed a dense tissue layer at the bottom of the defect and at the cartilage-hydrogel interfaces, comparable to observations in condition A (Figures 4, S1). Additionally, cells and cell clusters were visible in the hydrogel with a homogeneous distribution, similar to the observations for condition B. Both the tissue layer and hydrogel stained strongly with safranin-O and the collagen type II antibody. In addition, the pericellular matrix of the cell clusters in the hydrogel and that of cells in the underlying dense tissue layer were respectively positive and negative for collagen type VI (Figure S2). In few samples of conditions B, C, and D, inhomogeneous remodeling was observed (Figure S3).

After 57 days of culture the defect area filled with condition E looked comparable to day 0 controls (Figure S4). However, in one of the five samples a thin cell layer formed at the bottom of the defect, below the hydrogel (Figure S4).

7
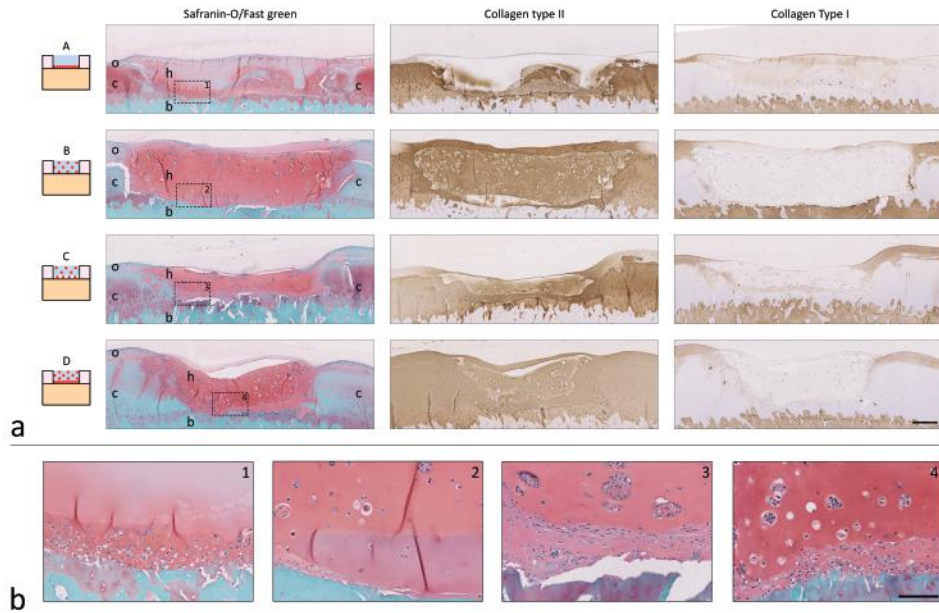
Figure 4. Histological analysis at day 57 of the cartilage defects filled with conditions A-D. *a) Cross-sectional overview of each condition. Scale bar represents 400 µm and is the same for all histological images. In the safranin-O images c = native cartilage, b = bone, h = hydrogel, and o = tissue outgrowth. b) Magnification of the area indicated with the dotted square and number in the Safranin-O pictures of the cross-sectional overview (a). From left to right condition A-D. Scale bar represents 100 µm and is the same for all magnified images.*
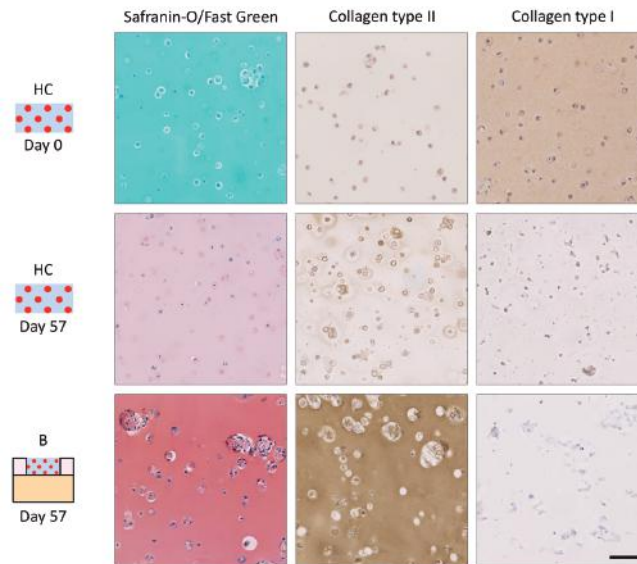
Figure 5. Overview of matrix production in hydrogel controls (HCs) and the hydrogel constructs in condition B. *Scale bar represents 200 µm for all images.*

HCs reacted strongly with the collage type I antibody at day 0, but staining intensity decreased during culture (Figure 5). At days 29 and 57, HCs stained positive with safranin-O and collagen type II, with highest staining intensities at day 57. Tissue formation in HCs differed from the tissue formation in the hydrogel constructs in condition B. Both safranin-O and collagen type II stainings were more intense in the constructs of condition B and contained larger cell clusters compared to HCs.

The amount of GAG/wwt was significantly higher in the newly formed tissue in conditions B and D compared to condition A at day 29 (Figure 6a). At day 57, only the tissue in condition B contained significantly more GAG/wwt compared to A. No significant differences in GAG/wwt were observed between conditions C and D. At both time points, the GAG/wwt was significantly lower for the cell-free condition E compared to the conditions that had cells homogeneously encapsulated in the hydrogels (B-D).

No differences in DNA/wwt were measured between conditions at day 29 (Figure 6b). However, at day 57 significantly less DNA/wwt was present in the defect area of plugs with condition E compared to the conditions which had chondrocytes encapsulated within the hydrogel (B, C, and D). Additionally, condition A had significantly less DNA/wwt compared to the tissue of condition B and the HCs had lower DNA/wwt values compared to conditions B and D.
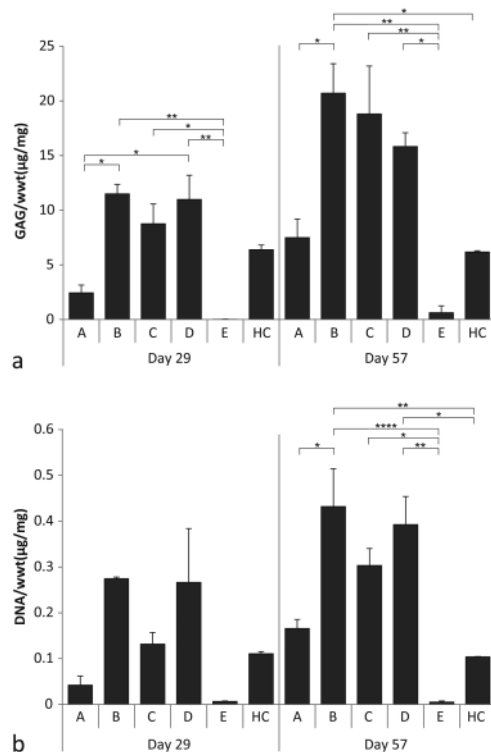
Figure 6. Quantitative measurements of the defect filling. *a) GAG normalized to the wet weight (wwt). No GAGs were detected in the defect filling at day 1. b) DNA normalized to the wwt. At day 1, 0.27±0.06 µg/mg DNA/wwt was detected for defects filled with conditions A, B, C, and HC, while 0.54±0.12 µg/mg DNA/wwt was detected in plugs filled with condition D, and no DNA was detected for plugs filled with condition E. * indicates a significant difference (*, p<0.05; **, p<0.01; ****, p<0.0001) between the connected conditions.*

7

3.3. Origin of repair tissue

DNA profiles of the cells isolated from the repair tissue were identical to the DNA profiles of the chondrocyte donor (S5). DNA of the plug donor was not detected in the repair tissue.

4. Discussion

This study confirms the potential of chondrocyte-laden hydrogels for cartilage repair and demonstrates the crucial role of the initial spatial chondrocyte distribution in a hydrogel on tissue repair. More specifically, homogeneous chondrocyte encapsulation in gelMA/gellan hydrogels is beneficial for fast defect filling with new cartilage-like tissue, while seeding the chondrocytes at the defect bottom improves local construct integration. When chondrocytes were positioned at the bottom of the defect, enclosed by a cell-free hydrogel (condition A), a dense cartilage-like tissue layer, rich in GAGs and collagen type II, formed on the calcified layer. Nevertheless, after 57 days of culture, the defect was not completely filled with tissue. When encapsulating the same amount of chondrocytes homogeneously in the hydrogel (condition B), differentiating clusters rich in GAGs and collagen type II formed, and after 57 days of culture neo-tissue was distributed throughout the entire defect. Although condition A resulted in less cartilage-like tissue, the tissue that had formed filled all irregularities of the bottom of the defect, while the newly formed tissue in condition B revealed an abrupt transition. When filling the defect with a combination of both methods (conditions C and D) the best results were obtained; both a dense tissue layer developed at the defect bottom and differentiating cell clusters formed in the hydrogel, regardless of the initial cell density.

Significantly more DNA/wwt and GAG/wwt was measured in the repair tissue of condition B compared to A. To ensure proper chondrocyte engraftment at the defect bottom, OC plugs with seeded chondrocytes were incubated for a total of three hours, exceeding the attachment-time recommended by Chen *et al.*[24]. Additionally, no cells were detected in the incubation medium when it was refreshed in the present study, confirming effective cell delivery. The lower DNA/wwt values in condition A are, therefore, expected to be the result of less proliferation compared to conditions B-D. Due to the relatively high cell density at the defect bottom in condition A, the chondrocytes have limited space to proliferate. Additionally, absence of cell-cell contact is known to stimulate chondrocyte proliferation, which also explains the formation of cell clusters in the hydrogels with homogeneous cell encapsulation[25]. Moreover, in pellet cultures where chondrocyte densities are relatively high, limited chondron formation is observed[26], while chondrons are more active in cartilage-like matrix production compared to chondrocytes without their pericellular matrix[27]. Indeed, the pericellular matrix of the cells encapsulated in the hydrogel stained positive for collagen type VI while this was not the case for the cells in the dense tissue layer, highlighting the potential of hydrogels with encapsulated chondrocytes for cartilage repair.

Increasing the total number of delivered chondrocytes did not result in increased tissue formation or DNA levels (condition C compared to D). This observation is in line with other studies that demonstrated that difference in DNA levels and tissue formation,

7

due to different initial cell densities, disappear during long-term culture[28,29]. However, different studies reported beneficial effects with increased cell densities, using a higher range of cell densities compared to the current study[24,30,31]. Possibly, the effect of different cell densities is influenced by the cell density range and the scaffold/hydrogel in which the chondrocytes are grown.

The findings of this study may impact cell-based cartilage repair strategies currently used in the clinic, as the majority of these do not provide homogeneous spatial distributed chondrocytes[20]. ACI involves cell seeding in the defect depth and scaffold-based approaches *e.g.* NOVOCART 3D®, Bioseed®, or MACI, are often associated with limited penetration of seeded chondrocytes into the scaffold[20]. Although scaffold-based approaches show promising results, incomplete and moderate defect filling was reported in patients treated with NOVOCART 3D®[32] or Bioseed®[33] and MACI[8], respectively. Chondrocyte penetration into a scaffold can be improved by pre-culturing the cell-laden scaffolds in perfusion bioreactors[34]. Contrarily, hydrogels are ideal candidates for the generation of constructs with homogeneously encapsulated chondrocytes without requiring bioreactors.

Tissue outgrowth was observed for all conditions which received chondrocytes in the defect, in the current study. This might be prevented by incorporating a thin dense polymer layer at the hydrogel surface facing the joint-space, as demonstrated to be effective for MACI[6,20] and NOVOCART 3D®[20] scaffolds. Three-dimensional printing techniques may facilitate the development of cell-laden hydrogel constructs with such a 'sealed' surface, as well as more complex chondrocyte delivery approaches *e.g.* depth-dependent differences, to further resemble the zonal architecture of native cartilage[10].

To obtain repair tissue in the defect, cell delivery was required. No tissue was formed in plugs filled with cell-free hydrogels (condition E) and repair tissue was solely formed by the delivered cells as determined by genetic profiling, confirming the potential of cell implantation for cartilage repair. However, chondrocytes from the native cartilage can migrate into the defect area, as demonstrated with cell-free collagen type I hydrogels [35]. However, these hydrogels likely contained different polymer and cross-linking densities favoring migration, and were glued in the defectfixated with chemo-attractive fibrin glue[36], which could explain the different observation compared to our study[36].

The current study focused on equine OC plugs, as the horse is a widely used pre-clinical model for cartilage repair strategies[37]. Similar changes in the cartilage during culture were observed for the equine plugs as previously reported for other species[13,16,24,38]. The native cartilage swelled and GAGs leached into the medium, possibly due to the damaged collagen network at the outline of the plugs and the defect edges[13,16,24,38]. However, in the current study both the water and GAG content were stable between 29 and 57 days, even though GAGs leached continuously into the medium, indicating that GAGs were produced and that a new stable situation was obtained. Although a new stable situation was obtained, the OC plug model forms a simplification of the native environment, therefore, validation of our findings in animal models is required.

Culturing cell-laden hydrogels in the OC plug influenced matrix deposition by the delivered chondrocytes. Significantly higher DNA/wwt and GAG/wwt contents were

7

observed in the cartilage defects of plugs filled with condition B, compared to the HCs, which contained the same chondrocyte density. Additionally, the hydrogel in condition B stained more intensely for GAGs and collagen type II and contained larger cell clusters compared to the HCs. GAG and DNA levels of the HC samples are in line with previous findings [11]. The hydrogel in condition B was thinner compared to HC constructs (~1 mm and 2 mm, respectively), which might result in differences in the availability of nutrients. However, HCs were cultured floating in medium and the diffusion distance to reach the core of the samples was much smaller than the maximal distance for sufficient diffusion of nutrients[39]. Therefore, the increase in proliferation and matrix production in the hydrogel of condition B is expected to be the result of culturing the cell-laden hydrogels within cartilage defects, suggesting that the cells within the OC plug secrete factors that influence the delivered chondrocytes[40]. Indeed, it has been demonstrated before that chondrocytes release factors when cartilage damage occurs *e.g.* fibroblast growth factor, TGF-β, and bone morphogenetic proteins, which stimulate chondrocyte proliferation, matrix synthesis, and remodeling[40–43].

Although complete defect filling could be reached in two months with the delivery of cell-laden gelMA/gellan (conditions B, C, and D), none of the cell-based strategies resulted in the restoration of the depth-dependent organization of articular cartilage. To accomplish this, other strategies should be implemented such as the incorporation of zonally harvested chondrocytes or zonal distribution of tissue-inductive cues[44,45]. Another important next step is the incorporation of mechanical stimulation, which can increase matrix production of delivered chondrocytes and is believed to contribute to the organization of collagen fibers[46–49].

5. Conclusions

The morphology and quantity of repair tissue in a full-thickness cartilage defect, filled with chondrocyte-laden gelMA/gellan hydrogel, is dominated by the initial spatial chondrocyte distribution. Seeding cells at the defect bottom and encapsulating them in the hydrogel, resulted in a well-integrated repair tissue that completely filled the defect after two months. Repair tissue was formed by the delivered chondrocytes, confirming the potential of cell delivery for cartilage repair. Additionally, the OC plug model stimulated cartilage-like tissue formation by the delivered cells, illustrating its potential for the evaluation of new cartilage repair therapies. Overall, these findings demonstrate the important role of spatial chondrocyte distribution in hydrogel constructs on cartilage tissue formation. Hence, this study may impact future cell delivery approaches for cartilage repair.

6. Acknowledgements

Supplementary information

S1. Comparison between tissue formation in the defect at days 29 and 57
No clear differences were observed between days 29 and 57 for each condition. The dense tissue layer observed at the defect bottom in conditions A, C, and D did not thicken over time and cells clusters observed in conditions B, C, and D kept a similar size (Figure S1).
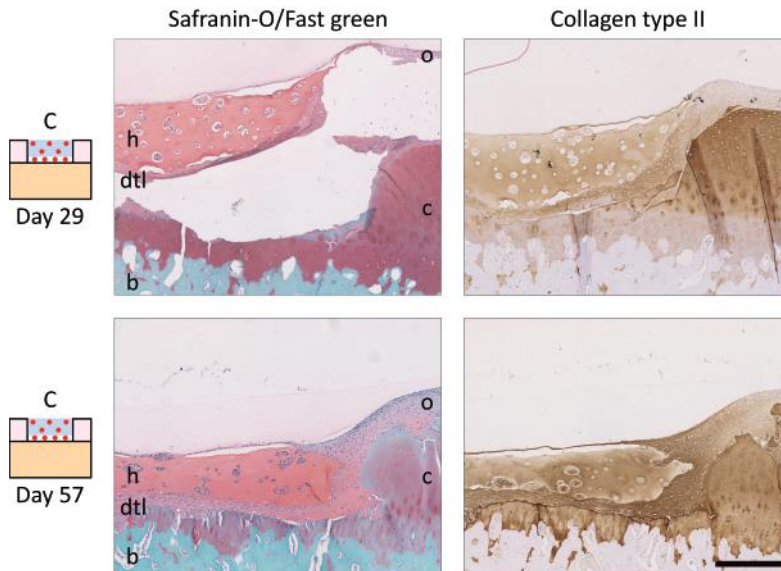
Figure S1. Cross-sectional overview of the defect sites of condition C at days 29 and 57. In the safranin-O images, c = native cartilage, b = bone, h = hydrogel, o = tissue outgrowth, and dtl = dense tissue layer.

S2. Collagen type VI staining of the hydrogels of conditions B and C
The pericellular matrix of the cells in the hydrogel stained positive for collagen type VI, while the pericellular matrix of the chondrocytes in the dense tissue layer was negative for collagen type VI (Figure S2).

7
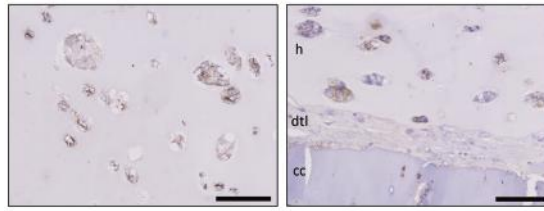
Figure S2. Collagen type VI staining of the hydrogel in a defect of condition B (left) and of a defect cross-section of condition C (right), at day 57. Scale bars represent 100 µm and h = hydrogel, dtl = dense tissue layer, and cc = calcified cartilage.

S3. Inhomogeneous remodeling in conditions B, C, and D

Inhomogeneous tissue remodeling was observed in a few samples of conditions B, C, or D (Figure S3). These samples showed a sharp transition in the cell-laden hydrogel from an area with relatively large cell clusters and intense safranin-O and collagen type II staining to an area with smaller cell clusters and less intense safranin-O and collagen type II staining. In addition, collagen type I staining was more intense in the areas containing the lower collagen type II and safranin-O staining compared to the other area.

The inhomogeneous remodeling, resulting in areas with relatively high or low cartilage-like tissue formation, is likely related to inhomogeneous degradation of gelMA/ gellan hydrogels. This hypothesis is supported by the collagen type I staining. As gelMA is generated from denatured collagens, mainly type I, it stains positive for collagen type I at the beginning of culture. However, after the culture period, the collagen type I positive signal of the hydrogel diminished (Figure 5, main text), indicating degradation of the hydrogel. Contrarily, the tissue areas containing relatively low cartilage-like tissue were still homogeneously positive for collagen type I at day 57. A possible explanation for this observation could be limitations in diffusion of degradation or remodeling factors secreted by the cells of the OC plug or of the TGF-β supplemented in the medium.

7
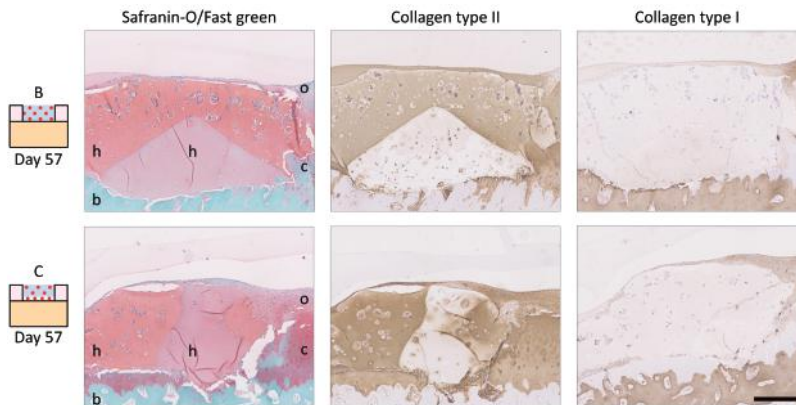
Figure S3. Examples of inhomogeneous matrix formation in the xy-plane of defects in conditions B (top) and C (bottom) at day 57. Scale bar represents 400 µm, and c = native cartilage, b = bone, h = hydrogel, and o = tissue outgrowth.

S4. Evaluation of the defect area of condition E

Cartilage-like tissue was absent in the defect area of plugs filled with condition E (Figure S4). In 4 out of 5 samples no cells were observed in the defect area. Nevertheless, in one OC plug with condition E, cells were present at the defect bottom underneath the hydrogel. This cell layer stained positive for safranin-O and collagen type II, however, staining intensity was much lower compared to the repair tissue in the cell-laden conditions.
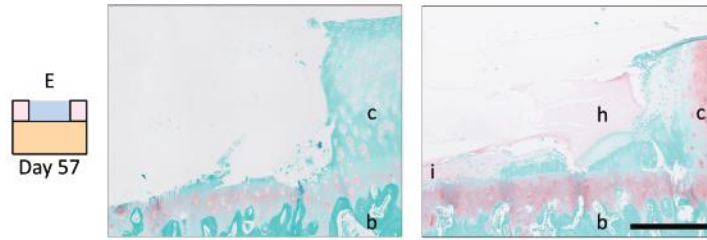
Figure S4. Cross-sectional overview of the side of the defect area of plugs filled with condition E. *No signs of tissue remodeling or repair were visible in most of the samples (left, hydrogel absent) while in one sample, cells were visible at the bottom of the defect after 57 days of culture (right). Scale bar represents 400 µm, and c = native cartilage, b = bone, I = cell infiltration, and h = hydrogel.*

S5. Genetic profiling

The DNA profiles of the tissue growing out of the defect area were identical to the DNA profile of the chondrocyte donor, while no DNA of the OC plug donor was present in the outgrowth tissue (Table S1).

7

Table S1. DNA profiles, generated by Van Haeringen Laboratorium B.V., of the OC plug donor, chondrocyte donor, and the repair tissue growing out of the defect area.

DNA marker	ISAG code*		
	OC plug donor	Chondrocyte donor	Samples
AHT4	H / J	O / -	O / -
AHT5	N / -	J / K	J / K
HMS1	M / -	I / M	I / M
HMS2	M / -	K / R	K / R
HMS6	L / O	M / P	M / P
HMS7	L / O	L /N	L /N
HTG4	L / -	K / M	K / M
HTG6	J / -	G / -	G / -
HTG7	M / N	M / O	M / O
VHL20	I / -	I / N	I / N
ASB2	- / -	K / N	K / N
HMS3	I / M	P / -	P / -
HTG10	M / O	I / O	I / O
ASB17	N / R	M / O	M / O
ASB23	I / K	K / -	K / -
LEX3	N / -	P / -	P / -
CA425	M / N	J / -	J / -

*ISAG = International Society of Animal Genetics

References

1. Almarza, A. J. & Athanasiou, K. A. Design characteristics for the tissue engineering of cartilaginous tissues. *Ann. Biomed. Eng.* **32,** 2–17 (2004).
2. Browne, J. E. & Branch, T. P. Surgical alternatives for treatment of articular cartilage lesions. *J. Am. Acad. Orthop. Surg.* **8,** 180–189 (2000).
3. Prakash, D. & Learmonth, D. Natural progression of osteo-chondral defect in the femoral condyle. *Knee* **9,** 7–10 (2002).
4. Judet, T., Marmorat, J.-L. & Mullins, M. M. Effective Treatment of Fracture-Dislocations of the Olecranon Requires a Stable Trochlear Notch. *Clin. Orthop. Relat. Res.* **&NA;,** 276–277 (2005).
5. Mandelbaum, B. *et al.* Treatment outcomes of autologous chondrocyte implantation for full-thickness articular cartilage defects of the trochlea. *Am. J. Sports Med.* **35,** 915–921 (2007).
6. Brittberg, M. Cell Carriers as the Next Generation of Cell Therapy for Cartilage Repair: A Review of the Matrix-Induced Autologous Chondrocyte Implantation Procedure. *Am. J. Sports Med.* **38,** 1259–1271 (2010).
7. Marlovits, S., Zeller, P., Singer, P., Resinger, C. & Vécsei, V. Cartilage repair: Generations of autologous chondrocyte transplantation. *Eur. J. Radiol.* **57,** 24–31 (2006).
8. Meyerkort, D. *et al.* Matrix-induced autologous chondrocyte implantation (MACI) for chondral defects in the patellofemoral joint. *Knee Surgery, Sport. Traumatol. Arthrosc.* **22,** 2522–2530 (2014).
9. Ebert, J. R., Fallon, M., Wood, D. J. & Janes, G. C. A Prospective Clinical and Radiological Evaluation at 5 Years After Arthroscopic Matrix-Induced Autologous Chondrocyte Implantation. *Am. J. Sports Med.* (2016). doi:10.1177/0363546516663493
10. Mouser, V. H. M. *et al.* Three-Dimensional Bioprinting and Its Potential in the Field of Articular Cartilage Regeneration. *Cartilage* (2016). doi:10.1177/1947603516665445
11. Mouser, V. H. M. *et al.* Yield stress determines bioprintability of hydrogels based on gelatin-methacryloyl and gellan gum for cartilage bioprinting. *Biofabrication* **8,** 035003 (2016).
12. Melchels, F. P. W., Dhert, W. J. A., Hutmacher, D. W. & Malda, J. Development and characterisation of a new bioink for additive tissue manufacturing. *J. Mater. Chem. B* **2,** 2282–2289 (2014).
13. De Vries-van Melle, M. L. *et al.* An osteochondral culture model to study mechanisms involved in articular cartilage repair. *Tissue Eng. Part C Methods* **18,** 45–53 (2012).
14. De Vries-van Melle, M. L. *et al.* Chondrogenic differentiation of human bone marrow-derived mesenchymal stem cells in a simulated osteochondral environment is hydrogel dependent. *Eur. Cell. Mater.* **27,** 112–23; discussion 123 (2014).
15. De Vries-van Melle, M. L. *et al.* Chondrogenesis of Mesenchymal Stem Cells in an Osteochondral Environment Is Mediated by the Subchondral Bone. *Tissue Eng. Part A* **20,** 23–33 (2014).
16. Schwab, A. Ex vivo culture platform for assessment of cartilage repair treatment strategies. *ALTEX* (2016). doi:10.14573/altex.1607111
17. Jones, C. W. *et al.* Matrix-induced autologous chondrocyte implantation in sheep: objective assessments including confocal arthroscopy. *J. Orthop. Res.* **26,** 292–303 (2008).
18. Nixon, A. J. *et al.* A chondrocyte infiltrated collagen type I/III membrane (MACI® implant) improves cartilage healing in the equine patellofemoral joint model. *Osteoarthr. Cartil.* **23,** 648–660 (2015).
19. Brittberg, M., Tallheden, T., Sjögren-Jansson, B., Lindahl, A. & Peterson, L. Autologous chondrocytes used for articular cartilage repair: an update. *Clin. Orthop. Relat. Res.* S337–48 (2001).
20. Huang, B. J., Hu, J. C. & Athanasiou, K. a. Cell-based tissue engineering strategies used in the clinical repair of articular cartilage. *Biomaterials* **98,** 1–22 (2016).
21. Abbadessa, A. *et al.* A Synthetic Thermosensitive Hydrogel for Cartilage Bioprinting and Its Biofunctionalization with Polysaccharides. *Biomacromolecules* **17,** 2137–2147 (2016).
22. Farndale, R. W., Sayers, C. A. & Barrett, A. J. A Direct Spectrophotometric Microassay for Sulfated Glycosaminoglycans in Cartilage Cultures. *Connect. Tissue Res.* **9,** 247–248 (1982).
23. Wall, A. & Board, T. in *Classic Papers in Orthopaedics* **53,** 433–435 (Springer London, 2014).
24. Chen, A. C., Nagrampa, J. P., Schinagl, R. M., Lottman, L. M. & Sah, R. L. Chondrocyte transplantation to articular cartilage explantsin vitro. *J. Orthop. Res.* **15,** 791–802 (1997).
25. Abbott, J. & Holtzer, H. The loss of phenotypic traits by differentiated cells. 3. The reversible behavior of chondrocytes in primary cultures. *J. Cell Biol.* **28,** 473–487 (1966).
26. Stewart, M. C., Saunders, K. M., Burton-Wurster, N. & Macleod, J. N. Phenotypic stability of articular chondrocytes in vitro: the effects of culture models, bone morphogenetic protein 2, and serum supplementation. *J. Bone Miner. Res.* **15,** 166–74 (2000).
27. Zhang, Z. Chondrons and the Pericellular Matrix of Chondrocytes. *Tissue Eng. Part B Rev.* **21,** 267–277 (2015).
28. Kon, E. *et al.* Orderly osteochondral regeneration in a sheep model using a novel nano-composite multilayered biomaterial. *J. Orthop. Res.* **28,** 116–124 (2010).
29. Hansen, O. M., Foldager, C. B., Christensen, B. B., Everland, H. & Lind, M. Increased chondrocyte seeding density has no positive effect on cartilage repair in an MPEG-PLGA scaffold. *Knee Surgery, Sport. Traumatol. Arthrosc.* **21,** 485–493 (2013).
30. Puelacher, W. C. *et al.* Tissue-engineered growth of cartilage: the effect of varying the concentration of chondrocytes seeded onto synthetic polymer matrices. *Int. J. Oral Maxillofac. Surg.* **23,** 49–53 (1994).
31. Talukdar, S., Nguyen, Q. T., Chen, A. C., Sah, R. L. & Kundu, S. C. Effect of initial cell seeding density on 3D-engineered silk fibroin scaffolds for articular cartilage tissue engineering. *Biomaterials* **32,** 8927–8937 (2011).

7

32.   Niethammer, T. R. *et al.* Incomplete defect filling after third generation autologous chondrocyte implantation. *Arch. Med. Sci.* **4,** 785–192 (2016).

33.   Kreuz, P. C. *et al.* Repair of Focal Cartilage Defects With Scaffold-Assisted Autologous Chondrocyte Grafts: Clinical and Biomechanical Results 48 Months After Transplantation. *Am. J. Sports Med.* **39,** 1697–1705 (2011).

34.   Pei, M. *et al.* Bioreactors mediate the effectiveness of tissue engineering scaffolds. *FASEB J.* **16,** 1691–1694 (2002).

35.   Gavenis, K. *et al.* A cell-free collagen type I device for the treatment of focal cartilage defects. *Artif. Organs* **34,** 79–83 (2010).

36.   Kirilak, Y. *et al.* Fibrin sealant promotes migration and proliferation of human articular chondrocytes: Possible involvement of thrombin and protease-activated receptors. *Int. J. Mol. Med.* **17,** 551–558 (2006).

37.   Malda, J. *et al.* Comparative study of depth-dependent characteristics of equine and human osteochondral tissue from the medial and lateral femoral condyles. *Osteoarthr. Cartil.* **20,** 1147–1151 (2012).

38.   Elson, K. M. *et al.* Non-Destructive Monitoring of Viability in an Ex Vivo Organ Culture Model of Osteochondral Tissue. **29,** 356–369 (2015).

39.   Griffith, C. K. *et al.* Diffusion limits of an in vitro thick prevascularized tissue. *Tissue Eng.* **11,** 257–266 (2005).

40.   Sherwood, J. C., Bertrand, J., Eldridge, S. E. & Dell'Accio, F. Cellular and molecular mechanisms of cartilage damage and repair. *Drug Discov. Today* **19,** 1172–1177 (2014).

41.   Vincent, T., Hermansson, M., Bolton, M., Wait, R. & Saklatvala, J. Basic FGF mediates an immediate response of articular cartilage to mechanical injury. *Proc. Natl. Acad. Sci. U. S. A.* **99,** 8259–64 (2002).

42.   Ellsworth, J. L. *et al.* Fibroblast growth factor-18 is a trophic factor for mature chondrocytes and their progenitors. *Osteoarthr. Cartil.* **10,** 308–320 (2002).

43.   Dell'Accio, F., De Bari, C., Eltawil, N. M., Vanhummelen, P. & Pitzalis, C. Identification of the molecular response of articular cartilage to injury, by microarray screening: Wnt-16 expression and signaling after injury and in osteoarthritis. *Arthritis Rheum.* **58,** 1410–1421 (2008).

44.   Fujie, H. *et al.* Zone-specific integrated cartilage repair using a scaffold-free tissue engineered construct derived from allogenic synovial mesenchymal stem cells: Biomechanical and histological assessments. *J. Biomech.* **48,** 4101–4108 (2015).

45.   Schuurman, W. *et al.* Cartilage regeneration using zonal chondrocyte subpopulations: a promising approach or an overcomplicated strategy? *J. Tissue Eng. Regen. Med.* **9,** 669–678 (2015).

46.   Benninghoff, A. Form und Bau der Gelenkknorpel in ihren Beziehungen zur Funktion. *Z. Anat. Entwicklungsgesch.* **76,** 43–63 (1925).

47.   Mauck, R. L., Seyhan, S. L., Ateshian, G. A. & Hung, C. T. Influence of Seeding Density and Dynamic Deformational Loading on the Developing Structure/Function Relationships of Chondrocyte-Seeded Agarose Hydrogels. *Ann. Biomed. Eng.* **30,** 1046–1056 (2002).

48.   Kock, L. M., Ito, K. & van Donkelaar, C. C. Sliding Indentation Enhances Collagen Content and Depth-Dependent Matrix Distribution in Tissue-Engineered Cartilage Constructs. *Tissue Eng. Part A* **19,** 1949–1959 (2013).

49.   Bian, L. *et al.* Dynamic Mechanical Loading Enhances Functional Properties of Tissue-Engineered Cartilage Using Mature Canine Chondrocytes. *Tissue Eng. Part A* **16,** 1781–1790 (2010).

7

Chapter 8

General discussion

The work presented in this thesis demonstrates the potential and challenges of two hydrogel platforms, gelatin-methacryloyl (gelMA) and polyethylene glycol midblock, flanked by two poly[N-(2-hydroxypropyl) methacrylamide mono/dilactate] (polyHPMA-lac-PEG) hydrogels, for the application as bio-inks in the three-dimensional (3D) printing of organized cartilage implants. Properties for bioprinting were improved for gelMA-based bio-inks by the incorporation of gellan gum and/or methacrylated hyaluronic acid (HAMA), while the incorporation of HAMA and to a lesser extent methacrylated chondroitin sulfate (CSMA) led to improvements for the polyHPMA-lac-PEG-based system. Herein, the yield stress was identified as an important rheological property that dictates the printability and the possibility of cell encapsulation. To further mimic the depth-dependent properties of the native cartilage, layered constructs were fabricated using articular cartilage progenitor cells (ACPCs) in the superficial region and multipotent mesenchymal stromal cells (MSCs) for the middle and deep regions. Finally, the spatial cell distribution in hydrogel implants was optimized using an *ex vivo* osteochondral (OC) plug model.

8.1. Material properties governing 3D bioprinting

A proper bio-ink should allow the printing of shape-stable filaments with encapsulated cells. However, a clear understanding of the material properties required to accomplish this, is still missing in the relatively young field of bioprinting. Multiple properties that influence the printing process and filament stability have been identified; these include the viscosity, polymer concentration, and gelation time[1,2]. In Chapter 3, we identified the yield stress as a dominating material property affecting the shape-fidelity of extruded gelMA/gellan filaments. More specifically, increasing yield stress resulted in increasing shape-fidelity. In addition, an increasing yield stress and not viscosity was found to be the main cause for the decreasing cell miscibility, when using relatively high gelMA or gellan gum concentrations. These findings suggest the presence of a yield stress range, in which gelMA/gellan formulations are suitable for the application as a bio-ink (printing of shape-stable filaments with encapsulated cells). As yield stress is rarely acknowledged in literature as a key factor in determining bioprintability, it is recommended to also validate the significance of yield stress for other bioprintable hydrogel systems.

Although the yield stress dominated the bioprintability of gelMA/gellan hydrogels, the overall bio-ink behavior during printing is influenced by an interplay of different materials properties (viscosity, yield stress, gelation time), which are generally also interdependent[2–4]. Due to this interplay, the studying and mapping of the exact material properties required for bioprinting is challenging. Currently, the identification of new bio-inks is often established via trial and error, after which the material properties responsible for accurate printing are identified. Furthermore, experience has learned that the overall properties of the biomaterial are significantly affected by the incorporation of cells (unpublished results), which is seldom considered. Likely, the additional volume of the cells decreases the absolute polymer content per volume of hydrogel-cell mixture. Moreover, the encapsulated cells might interfere with the formation of reversible bounds *e.g.* ionic or hydrogen, and thus alter the physical gelation and yield stress of the polymer

8

blend. Taken together, gaining a deeper understanding of the general material properties governing the bioprinting process of cell-laden bio-inks, as well as the development of guidelines for the bio-ink requirements, may benefit the development and optimization of future bio-inks.

In addition, the establishment of a standardized protocol to quantify the quality of printed filaments and constructs, will help to index and compare the rapidly increasing amount of bio-inks. Currently, the printing quality is determined via subjective observations post-printing[5,6]. A quantification protocol could include observational scoring of the geometrical appearance of a construct, as also proven effective in other fields, for example the O'Driscoll score or ICRS score for cartilage repair[7,8]. So far, attempts for observational scoring have been made *e.g.* measuring the maximum overhang that a filament can reach before collapsing[3]; or comparing the filament thickness to the nozzle diameter[9,10], the construct pore shape to the theoretical pore shape[11], or the printed construct to the 3D computer design[12,13]. However, the quality of a printed construct is not only determined by the bio-ink itself. For example, the collection plate of the bioprinter determines the surface tension of a printed filament, and thus affects the filament shape. In addition, the accuracy of the printer itself *e.g.* temperature control or printhead movement, also influences the final result. These additional factors further complicate the development of a universal quantification protocol to assess the quality of printed filaments and constructs[14]. Ideally, the quantification protocol would consist of basic printing methods, executable with any bioprinter *e.g.* printing of single lines or simple 3D shapes without support materials. Moreover, a scoring protocol should include standardized conditions *e.g.* a fixed material for the collection plate to standardize the surface tension. When taking all aforementioned aspects into account, a universal quality control protocol may be established, as well as a universal comparison of print quality between different bio-inks.

8.2. Bio-ink improvement with the incorporation of gellan gum, HAMA, or CSMA

A common strategy to enhance and tailor bio-ink properties, is the incorporation of additives. Here, we aimed to improve the bio-ink properties of gelMA hydrogels with the incorporation of gellan gum and/or HAMA, and the properties of polyHPMA-lac-PEG hydrogels with the incorporation of HAMA or CSMA.

8.2.1. Gellan gum

In Chapter 3, the printability and mechanical properties of gelMA hydrogels were enhanced with the incorporation of the polysaccharide gellan gum. The incorporation of gellan gum improved the shape-fidelity of printed filaments, in line with previous studies[15–17]. The enhanced filament stability was also demonstrated in Chapter 6, where larger overhangs could be bridged with printed gelMA/gellan filaments compared to gelMA filaments with the same polymer concentration. The incorporation of gellan gum improves the printability of the polymer blend by increasing the yield stress, as discussed above. However, too high yield stresses hamper cell encapsulation.

Furthermore, the incorporation of relatively low gellan gum concentrations (~0.5%)

8

in gelMA hydrogels significantly increased the stiffness of UV cross-linked constructs, due to the high molecular weight of gellan gum. Although gellan gum can be modified to allow UV cross-linking[18], no such modifications were made to the gellan gum used in this research. The gellan gum polymer chains are hypothesized to be trapped in the cross-linked gelMA network, via the ionic interactions and via physical entanglement. This hypothesis was supported by a pilot study (unpublished data), where cell-free UV cross-linked gelMA/gellan hydrogels, with different concentrations and ratios, were stored in PBS for 28 days. During this period the construct stiffness remained unchanged compared to the day 1 controls, implying that the gellan gum polymer chains remained in the construct.

Although a relatively high stiffness of cross-linked hydrogels could be beneficial for the generation of stable cartilage implants, increasing the construct stiffness is often associated with a decrease of matrix production by embedded cells[19,20]. However, in Chapter 3, no such relation was observed, nor in Chapter 5 for polyHPMA-lac-PEG/HAMA hydrogels. Studying the influence of construct stiffness on cell behavior is challenging, as other material properties are interlinked with the stiffness[19,21]. Often an increase in stiffness is accomplished via an increase in polymer concentration[22] or cross-linking density[23]. These methods result in an increase in (relative) network density and often also in a decrease of hydrogel permeability[24,25]. Therefore, they may alter the migration and proliferation capability of embedded cells or the availability of nutrients and biochemical cues[22–27], and thus cloud the direct effects of the construct stiffness on cell behavior. In Chapter 3, an increase in construct stiffness via an increase in gelMA concentration from 10% to 20%, resulted in similar matrix production and proliferation rates of the embedded chondrocytes for both concentrations. This outcome may be the result of an increased availability of gelMA polymer chains, and thus cell attachment sites in the 20% gelMA constructs[28,29], or a change in permeability. Furthermore, the matrix produced in the 20% gelMA hydrogels was confined around the cell clusters, while newly formed matrix in the 10% gelMA constructs could diffuse through the hydrogel. Hence, with these gelMA concentrations an increase in initial stiffness and network density did not alter the matrix production by embedded cells, but did hamper the matrix distribution.

Moreover, constructs consisting of 3% gelMA with 1% gellan gum had a similar initial stiffness as constructs composed of 10% gelMA, but contained significantly less GAG and DNA after 42 days of culture, implying that relatively high gellan gum concentrations restrict the matrix production by embedded chondrocytes. This may be caused by a difference in network density or hydrogel permeability between both formulations. However, an alternative explanation could be a reduction in the availably of gelMA polymer, due to physical hindrance of the gellan gum polymer chains. The reduced availability of gelMA molecules might reduce the stimulatory effect that gelMA has on embedded cells[30–33], likely via its bioactive sequences such as arginine-glycine-aspartic acid (RGD) or matrix metalloproteinase (MMP)-sensitive degradation sites to support remodeling[28,34,35]. This hypothesis would also explain why the matrix deposition in 10% gelMA hydrogels decreased with an increasing gellan gum concentration. Moreover, gellan gum itself is not expected to inhibit matrix production by chondrocytes, as

8

previous studies reported sufficient chondrocyte survival and differentiation in hydrogels consisting of only gellan gum (1.25-1.8%)[18,36,37]. Nevertheless, the results in this thesis demonstrate that the incorporation of relatively high gellan gum concentrations hamper cartilage-like tissue formation by embedded chondrocytes. Therefore, the use of gellan gum for the enhancement of gelMA bio-inks is restricted.

Overall, gelMA-based bio-inks can be further optimized by the addition of gellan gum. Gellan gum increases the printability and construct stiffness. However, careful consideration of the gellan gum concentration is required, as relatively high gellan gum concentrations hamper both the cell encapsulation procedure (due to a too high yield stress, threshold between 2-10 Pa) and the cartilage-like tissue formation by embedded cells (gellan gum concentration ≥ 9% of the total polymer concentration for the evaluated formulations in Chapter 3).

8.2.2. Methacrylated hyaluronic acid

Hyaluronic acid (HA) is a large polysaccharide that forms the backbone of proteoglycans, which are abundantly present in native cartilage. HA can be modified with methacrylic groups to allow chemical cross-linking with UV light, similar to gelMA and polyHPMA-lac-PEG polymers. Moreover, the addition of HAMA to a hydrogel increases the overall viscosity and yield stress, and thus improves its printability[38–40]. As HAMA is soluble at both high and low temperatures, HAMA could be added to both gelMA and polyHPMA-lac-PEG hydrogels. In Chapter 4, the incorporation of HAMA in polyHPMA-lac-PEG hydrogels reduced the gelation temperature (from > 50°C to 32°C), and increased the stiffness and degradation time (from ~56 days to > 100 days) of UV cross-linked constructs. These features contributed to an improvement of filament deposition and stability. As a result, shape-stable constructs could be printed with polyHPMA-lac-PEG/HAMA hydrogels as demonstrated for multiple HAMA concentrations in Chapters 4 and 5. Additionally, the incorporation of HAMA also improved the printability of gelMA/gellan hydrogels as demonstrated in Chapter 6. Specifically, all evaluated gelMA/gellan/HAMA filaments were able to bridge a gap of 8 mm wide before collapsing, while only 20% of the gelMA/gellan filaments could bridge this distance, indicating an improvement in filament stability and thus printability.

Furthermore, the presence of HAMA has been demonstrated to stimulate anabolic processes of chondrocytes via the binding with multiple cell surface receptors *e.g.* CD44, intercellular adhesion molecule-1 (ICAM-1), and the receptor for hyaluronan mediated motility (RHAMM)[41–46]. In Chapter 5, a dose-dependent effect of HAMA on the matrix production by chondrocytes embedded in polyHPMA-lac-PEG/HAMA hydrogels was demonstrated: intermediate HAMA concentrations (0.25-0.5%) increased cartilage-like tissue formation by embedded chondrocytes, while higher HAMA concentrations (1%) stimulated fibrocartilage formation. This dose-dependent effect may be caused by a negative feedback loop via the receptor bindings[43,47–49], as discussed in detail in Chapter 5. The optimal HAMA concentration, for chondrogenesis and printability of chondrocyte-laden polyHPMA-lac-PEG/HAMA hydrogels (0.5%) was also added to gelMA/gellan hydrogels with embedded chondrocytes, ACPCs, or MSCs. However, the incorporation

8

of 0.5% HAMA in gelMA/gellan hydrogels did not improve the chondrogenesis of any of the evaluated cell types compared to plain gelMA/gellan gels. This may imply that cells in gelMA/gellan hydrogels are not affected by HAMA or that the optimal HAMA concentration differs for different hydrogel systems, possibly by differences in permeability, stiffness, or cell adhesion sites. The latter hypothesis would also explain why previously reported studies, using different hydrogels, demonstrate contradictory results concerning the influence of different HA or HAMA concentrations on embedded cells[43,50–56]. Moreover, the optimal HAMA concentration is likely also dependent on the cell type, as ACPCs and MSCs have different compositions of membrane receptors, which can bind with HAMA compared to chondrocytes. Therefore, further evaluation of the HAMA concentration is required in order to determine if HAMA is capable to enhance the chondrogenesis of embedded ACPCs and MSCs, and to find the optimal HAMA concentration in gelMA/gellan/HAMA hydrogels for each cell type.

To conclude, HAMA is an interesting additive to improve the printability of a cartilage bio-ink, and to increase the degradation time and construct stiffness of cross-linked hydrogels. However, the HAMA concentration simultaneously affects the chondrogenesis of embedded chondrocytes. Additionally, the optimal concentration for chondrogenesis is likely dependent on the hydrogel properties and cell type. Therefore, careful tailoring of the HAMA concentration in the construct makeup is essential when using HAMA as additive for the improvement of cartilage bio-ink properties.

8.2.3. Methacrylated chondroitin sulfate

The potential of CSMA for the enhancement of polyHPMA-lac-PEG hydrogels for cartilage bioprinting was evaluated in Chapter 4. The incorporation of a relatively high CSMA concentration (4%) increased the degradation time of UC cross-linked constructs (~56 days to ~100 days), and decreased the gelation temperature to 39°C. However, to print shape-stable constructs a baseplate temperature well above the gelation temperature is required. Therefore, bioprinting of stable filaments with polyHPMA-lac-PEG/CSMA was not possible at cell-friendly temperatures. Moreover, embedded chondrocytes produced limited cartilage-like tissue in polyHPMA-lac-PEG/CSMA hydrogels during 42 days of *in vitro* culture (unpublished data), similar to studies with other hydrogels and CSMA[53,54]. Nevertheless, one study did report an upregulation of chondrogenic genes due to the incorporation of CSMA[57]. Possibly, the effect of CSMA on embedded cells is dose-dependent, as was also observed for HAMA. However, as we observed that lower CSMA concentrations in polyHPMA-lac-PEG hydrogels resulted in less improvement of the rheological properties compared to the relatively high concentration of 4% (unpublished data), CSMA is not recommended for the optimization of polyHPMA-lac-PEG hydrogels for cartilage bioprinting.

8.3. Mechanical enhancement of hydrogel constructs

Articular cartilage tissue has a unique matrix composition and organization in order to withstand the relatively high compressive and shear forces present in the joint[58]. A successful construct for cartilage repair should provide (temporary) mechanical

8

support while new tissue is formed to replace the degrading construct[59]. Although the incorporation of gellan gum and HAMA significantly increased the construct stiffness of gelMA and polyHPMA-lac-PEG hydrogel constructs, respectively (Chapters 3, 4, and 5), the overall construct stiffness did not reach values representative of native cartilage: 0.4-0.8 MPa[60–62]. To further increase the construct stiffness, reinforcement with thermoplastic polymers is beneficial[63]. Indeed, in Chapter 5, reinforcement of the hydrogel constructs significantly increased the Young's moduli (from 22-24 kPa to 3,500-4,600 kPa), via the co-printing of PCL and polyHPMA-lac-PEG/HAMA hydrogel.

The overall stiffness of a PCL reinforced construct can be tuned by adjusting the molecular weight of the PCL, the geometry of the PCL mesh, or the thickness of the fibers[64]. Three-dimensional printing of PCL provides fibers with a thickness of ~100 μm. Thinner fibers can be accomplished via *e.g.* melt electrospinning writing (MEW), which provides organized filaments with a thickness of 820 nm to 45 μm[65–67]. Meshes of MEW fibers infused with hydrogel were demonstrated to possess stress-strain curves similar to those of native cartilage, highlighting the potential of incorporating thinner PCL fibers. Moreover, thinner fibers allow more detailed tailoring of the reinforcement which might further improve the mechanical behavior of printed constructs. For example, the incorporation of stabilizing diagonal filaments were demonstrated to improve the construct resistance to shear forces[68]. Bioprinters with incorporated ME(W) printheads are under development and will facilitate the production of constructs with more advanced PCL skeletons[69].

Although co-printing techniques of fibers and hydrogels have great potential for the fabrication of cartilage constructs, the observations in Chapter 5 implicate that the co-printing procedure alters the properties of the PCL frame. Lower Young's moduli were measured for co-printed hybrid constructs compared to a separately printed PCL mesh that was later infused with hydrogel. A possible explanation could be a reduced integration between the PCL filaments of different layers. This may be the result of the hydrogel filaments that tend to creep towards the PCL filaments and, therefore, might partially cover the PCL surface where the second PCL layer should adhere. Furthermore, limitations of the bioprinter might also contribute to the hindrance of PCL integration by the hydrogel filaments. For example, irregularities of the nozzles cause minor errors in the offset measurements and thus the distance between the filaments of both materials. Further, the temperature control at the baseplate of the printer allows ultimate control for the first printed layers of thermosensitive hydrogels, but the higher layers experience lower temperatures than the ideal temperature, which causes sagging of the hydrogel. Although current bioprinters are advanced machines with great potential, further development is necessary and will improve control over the final construct architecture, as well as the accuracy of advanced printing strategies such as the co-printing of multiple materials.

8.4. Cell source

In Chapter 6, the potential of full thickness chondrocytes, ACPCs, and MSCs for cartilage tissue-engineering was evaluated, using cell-laden gelMA/gellan and gelMA/gellan/

HAMA constructs cultured *in vitro*. The highest potential was found for ACPCs. This sub-population of chondrocytes is isolated from articular cartilage and can be expanded in monolayer culture without losing their phenotype[70,71]. Because of this, sufficient numbers of cells can be obtained from a cartilage biopsy of the patient. Moreover, ACPCs produced the highest levels of GAGs, and collagen type II, and contained highest mRNA expression levels for aggrecan and proteoglycan IV when cultured in gelMA/gellan(/HAMA) hydrogels. A downside of using ACPCs for tissue-engineering purposes is the risk for donor site morbidity when obtaining the cells from a patient[72]. Careful consideration of the harvesting location is therefore required. Already, research is focusing on the optimization of the biopsy procedure and the harvest location to reduce the risk for donor site morbidity[73]. In addition, it may be possible to isolate ACPCs from the damaged rim of the cartilage defect, excluding the risk for donor site morbidity.

MSCs embedded in gelMA/gellan(/HAMA) hydrogels produced similar levels of GAG and collagen type II compared to the ACPCs, and demonstrated even higher mRNA expression levels for collagen type II, illustrating their potential for the fabrication of cartilage implants. Moreover, MSCs can be isolated from multiple tissues including bone marrow, adipose tissues, and muscles[74], and also allow expansion in monolayer culture. Furthermore, some clinical trials with MSCs for cartilage repair have already been performed[75]. Thus, protocols for the isolation and handling of MSCs for clinical use, in accordance to Good Manufacturing Practices (GMP), are already available, as well as facilities that can execute these protocols. However, a major challenge of MSCs for cartilage tissue-engineering is their tendency to progress into undesired hypertrophic chondrocytes or even differentiate towards the osteogenic lineage once implanted *in vivo*[75,76]. Precise control of MSC fate is required for clinical application. During *in vitro* cultures, the presence of transforming growth factor-β (TGF-β) stimulates the MSCs to differentiate into an chondrocyte-like phenotype[77]. TGF-β can be incorporated in hydrogel systems[78,79], which might be a tool to prevent undesired differentiation of the MSCs *in vivo*. However, until MSC fate after *in vivo* implantation can be guaranteed, the use of MSCs in hydrogel cartilage implants remains suboptimal[75].

Finally, full thickness chondrocytes produced the least amount of cartilage-like matrix and had lowest mRNA expression levels of chondrogenic genes. In addition, obtaining sufficient numbers of chondrocytes is a challenge in clinical practice as chondrocytes lose their chondrogenic phenotype during monolayer culture for cell expansion[80]. Therefore, chondrocytes may not be the ideal cell type to use for the fabrication or cell-laden cartilage repair implants. However, chondrocyte implantation techniques are already used in the daily clinic and safety of re-implanting them for cartilage repair has been demonstrated[81]. Therefore, the use of chondrocytes in cell-laden cartilage implants might provide the fastest clinical translation.

To conclude, full thickness chondrocytes, ACPCs, and MSCs, all have potential and challenges for the use in cartilage implants. Currently, ACPCs are most beneficial for cartilage-like tissue formation within the hydrogel construct and for obtaining sufficient cell numbers. However, using ACPCs requires an additional intervention for the patient.

8

8.5. Spatial distribution of cells in a hydrogel construct and the OC plug model

Bioprinting of hydrogel constructs for cartilage repair facilitates accurate positioning of cells throughout the construct volume. Although control over the cell positioning within a construct sounds ideal, little is known about the influence of spatial cell distribution on cartilage repair. Therapies currently used in the clinic are mainly based on the delivery of a dense cell layer in the defect depth, either stem cells via marrow stimulation *e.g.* microfracture, or chondrocytes via autologous cartilage implantation (ACI) techniques[82,83,81]. Also, with the scaffold-based, third generation ACI techniques, the cell density is highest in the defect depth as chondrocyte penetration into the scaffold is limited[84]. Moreover, once scaffolds are fixed in the defect with fibrin glue, the cells tend to migrate towards the fibrin glue in the defect depth[85]. Because of this, cartilage repair is often suggested to be a 'bottom-up' process in which cartilage formation starts in the defect depth and newly formed tissue grows towards the joint-space. In Chapter 7, this 'bottom-up' approach was evaluated with gelMA/gellan constructs using the OC plug model. Results demonstrated complete defect filling with hyaline cartilage after 2 months of culture when chondrocytes were homogeneously encapsulated in the hydrogel, while this was not the case when chondrocytes were seeded at the defect bottom and covered with an empty hydrogel. However, seeding the chondrocytes at the defect bottom improved construct integration. Consequently, a combination of both methods was found to be the optimal method of cell delivery for cartilage repair with gelMA/gellan constructs. These results highlight the potential of chondrocyte-laden hydrogel constructs for cartilage repair. However, future *in vivo* validation of this established optimal chondrocyte distribution is required before these findings can be translated into clinical applications. In addition, optimal chondrocyte distribution will likely also depend on the hydrogel itself and the construct design. For example, hydrogel constructs with encapsulated biological cues, *e.g.* TGF-β, can actively attract cells from the surrounding tissue and might, therefore, support tissue formation from the defect depth towards the joint-space. Also, the hydrogel stiffness and cross-linking density is likely to influence cell migration, as cells can easier migrate through a weak hydrogel with a loose polymer network compared to a stiff hydrogel with a dense polymer network[86].

As demonstrated in Chapter 7 and previous studies[87–90], the OC plug model forms an auspicious tool for the evaluation of new cartilage repair strategies. Both the cartilage and bone tissue of the OC plugs remained viable and stable during culture, as the bone-cartilage interface remained intact[87–90]. However, some initial GAG loss of the cartilage tissue, likely caused by the damaged collagen network at the excision outline of the OC plugs, is currently still unavoidable[89–92]. Moreover, the results in Chapter 7 demonstrated an increase in proliferation and cartilage-like tissue formation in cell-laden hydrogels cultured within a cartilage defect in the OC plug, compared to constructs maintained under free floating conditions. These findings suggest that the cells within the OC plug influence the cartilage repair by the delivered chondrocytes, possibly via secreted stimulating factors[93]. Chondrocytes in native cartilage are known to be able to release factors that stimulate chondrocyte proliferation, matrix synthesis, and remodeling, when cartilage damage occurs *e.g.* fibroblast growth factor (FGF), TGF-β, and bone

morphogenetic proteins (BMPs), which may explain this observation[93–96]. The results of Chapter 7 illustrate the potential of the OC plug model for the evaluation of new cartilage repair strategies.

Moreover, the OC plug model may also be used for the evaluation of basic research questions about cartilage damage and regeneration. For example, cartilage damage or osteoarthritis may be artificially induced via cartilage grooves[97] or the incubation with enzymes *e.g.* collagenase[98,99]. Subsequently, cartilage remodeling may be studied in order to obtain deeper understanding of the repair capacity of the tissue itself.

Overall, the OC plug model is an interesting system to use for the optimization of new cartilage therapies. Validation of the OC plug model in animal models will determine the extent to which the OC plug model can replace animal models. However, complete replacement of animal models will not be feasible, as the OC plug model remains a simplification of the native environment. By further mimicking the native environment in the model *e.g.* by the addition of synovial fluid or the incorporation of mechanical loading (currently under development by LifeTec Group BV.), the possibilities of the OC plug model may be expanded.

8.6. Three-dimensional printing of cell-laden organized cartilage implants

The stratified architecture of native cartilage is essential for its ability to support physiological joint forces[100]. Likely, the organization adjust itself to the demands at the specific location in the cartilage, as slight differences in cartilage organization *e.g.* collagen fibers and total thickness are observed between joints and locations within a joint[101–103]. Moreover, in animal models *e.g.* lapine and equine, it was demonstrated that the zonal organization of collagen fibers, changes with age and with exercise at an early age[104,105], supporting the idea that the tissue remodels to the environmental demands, with most severe remodeling at the early age. Therefore, it is likely that an exact replication of native cartilage is not necessary for an cartilage implant. However, the incorporation of a certain level of stratified organization is hypothesized to improve the functioning of a cartilage implant compared to homogeneous implants[106,107]. The zonal characteristics may better support embedded cells, and stimulate them to further remodel and fine-tune the matrix to the most suitable organization of the specific joint and implantation site. Additionally, matching the depth-dependent mechanical properties of the implant may reduce strain discontinuities at the cartilage-implant interface, which might improve construct integration with the surrounding cartilage tissue and underlying bone.

Although the incorporation of the zonal differences in repair constructs is likely beneficial, current layering methods are not sufficiently advanced to recapitulate the complex structural organization of native cartilage to evaluate this hypothesis. Therefore, current knowledge is based on outcomes with less complex zonal approaches. For example the two-layer cell delivery approach discussed in Chapter 7, consisting of cells in the defect depth and homogeneously in a hydrogel construct, which did indeed improve cartilage repair in the OC plug model. The cells in the two layers provided each a different aspect of the total cartilage repair strategy. More specifically, the chondrocytes in the defect depth contributed to the integration of the construct in the defect, while the

8

chondrocytes in the hydrogel provided relatively fast defect filling with hyaline cartilage. These findings highlight the potential of cartilage repair with organized implants and thus encourage further development.

For the generation of complex zonal implants, embedded cells should be stimulated to produce zone-specific matrix components. To accomplish this, the most straightforward approach would be to use zonal chondrocytes, as these cells are already in the correct sub-lineage[108,109]. However, the isolation of zonal chondrocytes is challenging. There are no clear boundaries between the different zones *in vivo,* and zone-specific cell surface markers to allow cell sorting are lacking[110]. Alternative cell sources are the full thickness chondrocytes, ACPCs, and MSCs. Previous studies demonstrated the possibility of steering MSCs into the different zone-specific chondrocytes via the incorporation of HA, CS, and matrix metalloproteinase-sensitive peptides in PEG-based hydrogels[111,112]. Furthermore, differences in cell densities, growth factors, and mechanical properties may also steer MSC fate, as well as the fate of other cell types[106,113–116]. In Chapter 6, MSCs cultured in gelMA/gellan(/HAMA) hydrogels exhibited an upregulation of collagen type X while proteoglycan IV mRNA expression remained unchanged compared to the initial expression. Therefore, MSCs encapsulated in gelMA/gellan(/HAMA) might be suitable for the generation of middle and deep zone cartilage. Contrarily, ACPCs encapsulated in gelMA/gellan(/HAMA) hydrogels revealed an upregulation of proteoglycan IV mRNA levels, in line with previous studies[71,117]. Therefore, ACPCs in gelMA/gellan(/HAMA) hydrogels might be suitable for the generation of superficial zone cartilage. However, further evaluation of zone-specific matrix production at protein level is required, as well as, further research towards appropriate cues that direct zone-specific cartilage matrix production by MSCs and ACPCs.

Another zonal characteristic of native cartilage is the depth-dependent collagen organization. Mimicking this organization in tissue-engineered constructs remains a major challenge. In native cartilage, the arrangement of the collagen fibers is directed by mechanical loading[102,104,118–120]. Therefore, mechanical loading might provide a tool to recapitulate the collagen organization in *in vitro* cultured implants. Specifically, a combination of shear and compression forces are promising for the establishment of the physiological collagen orientation[121,122]. In addition, loading has been demonstrated to increase matrix synthesis by embedded chondrocytes[100,123–125] and shear forces were demonstrated to increase the proteoglycan IV secretion[126,127]. To apply loading regimes on cartilage implants *in vitro*, bioreactor systems are already being developed[121]. Thus, *in vitro* culture with mechanical loading has great potential for the maturation of spatially organized cartilage implants before implantation.

Although significant steps have been made to generate tissue-engineered cartilage with depth-dependent characteristics, so far replication of all elements of native cartilage in one construct has not been accomplished. A challenge researchers encounter is the close resemblance of cartilage from the different zones. Nevertheless, several zonal markers have been identified, however, most of the markers are not restricted to a single zone. For example, COMP and collagen type X are found in both the middle and deep zone which together represent 80-90% of the cartilage thickness[128–130]. In addition, CILP

8

can be found in all zones, although highest expression is observed in the middle zone[110,131]. Furthermore, collagen type I is predominantly expressed in the superficial layer[128]. However, levels of collagen type I found in cell-laden hydrogels cultured *in vitro* often exceed the desirable levels, making it a challenge to decrease collagen type I production for the use of any zone. An increased understanding of the differences between cartilage zones and obtaining more robust zonal markers would provide better direction for the development of spatially organized cartilage implants.

Finally, bioprinting techniques are ideal for the fabrication of spatially organized constructs. Nnumerous printing protocols have been developed that allow the printing of cell-laden hydrogels with excellent cell viability[11,15,17,132–135]. In general, cell viability is impaired when the shear stresses on the cells become too high during printing[133,136]. Although cell viability is commonly evaluated after printing, long-term cultures to analyze the differentiation potential and matrix production of the bioprinted cells are often not performed. Therefore, In Chapter 6, long-term differentiation of printed ACPCs and MSCs was evaluated after extrusion printing in gelMA/gellan/HAMA hydrogels. Results demonstrated decreased cartilage matrix production and an upregulation of collagen type I mRNA for the printed cells compared to cast controls, after 42 days of culture. Similar observations were made for polyHPMA-lac-PEG/HAMA hydrogels printed with a micro-valve printhead. Chondrocytes, printed under these conditions remained viable during 28 days of culture, however, matrix production was significantly impaired (unpublished data). Similar observation were reported by Muller *et al.* (2016)[137] who demonstrated that high shear stresses due to relatively small nozzle diameters affected cell spreading and delayed matrix synthesis. These recent findings highlight the importance of including cast controls when evaluating printed constructs, as well as the importance of evaluating the effect of the printing process and conditions on different biological functions. Further evaluation of this effect will provide printing boundaries for effective bioprinting[137]. In addition, these boundaries might be broadened with techniques to protect the cells during the printing process[138].

8.7. GelMA and polyHPMA-lac-PEG hydrogels for cartilage bioprinting

Both gelMA and polyHPMA-lac-PEG hydrogels have interesting features for the fabrication of spatially organized cartilage implants. The incorporation of both 0.5% gellan gum and 0.5% HAMA in 9.5% gelMA hydrogels or the incorporation of 0.5% HAMA in 19.5% polyHPMA-lac-PEG were found to be optimal for printing, mechanical properties, and chondrogenesis. Both bio-ink blends demonstrated favorable, yet different, properties. Synthesis of gelMA/gellan/HAMA hydrogels require limited chemical reactions. Moreover, gelMA/gellan/HAMA hydrogels are printable with high shape-fidelity, making them interesting for the 3D printing of large implants or large numbers of implants. However, as the gelation temperature of gelMA/gellan/HAMA lies close to 43°C, cell encapsulation has to be performed within several seconds during the cooling of the mixture. Current encapsulation methods allow, therefore, only for the encapsulation of small volumes at a time, making the production of large volumes of cell-laden hydrogel time-consuming. Thus, scale-up and optimization of the cell encapsulation procedure is necessary *e.g.*

8

development of more effective mixing methods compared to pipetting, in order to provide large enough quantities to allow clinical use.

In addition, for clinical translation medical grade gelMA is required. The fabrication of medical grade gelMA has two main challenges: the production of endotoxin-free gelMA, and the elimination of batch-to-batch variations[29]. Currently, protocols are improved to overcome these challenges and gelatin with low endotoxin levels is now commercially available[139]. Moreover, also methods to remove the remaining endotoxins are under development[140]. Additionally, for clinical translation of gelMA, the synthesis from gelatin to gelMA needs to be performed according to GMP protocols. Finally, the new gelMA needs to be re-evaluated *in vitro* before switching to *in vivo* evaluation, as the adjustments to the gelatin and methacrylation procedure might influence the overall material properties of the bio-ink.

PolyHPMA-lac-PEG/HAMA hydrogels are more complex and expensive to synthesize compared to gelMA. However, cell encapsulation is performed on ice instead of at the high temperatures required for cell encapsulation in gelMA/gellan/HAMA hydrogels. Therefore, no problematic time-constraints on the mixing procedure exist[141–143], allowing the mixing of large cell numbers with large volumes of hydrogel. In addition, polyHPMA-lac-PEG/HAMA hydrogels have limited batch-to-batch variations and endotoxin levels are low[39], which is beneficial for clinical translation. However, the 3D printing of polyHPMA-lac-PEG/HAMA hydrogels was feasible but with a lower resolution compared to gelMA/gellan/HAMA hydrogels, as the filament stability of polyHPMA-lac-PEG/HAMA hydrogels is limited. Therefore, polyHPMA-lac-PEG/HAMA hydrogels are more suitable for the co-printing with reinforcement structures, as demonstrated in Chapter 5, or for the generation of cast or injectable cartilage implants.

8.8. Perspectives

In this thesis, multiple tools are presented that contribute to the development of organized cartilage implants. Ideally, such an implant should be gradually replaced by new organized hyaline cartilage tissue. Meanwhile, it should provide mechanical stability in the joint and thus have sufficient mechanical properties, and integrate properly with the surrounding tissue(s) to prevent strain discontinuities at the cartilage-implant or bone-implant interfaces. Additionally, the construct fabrication process should be cost-effective and preferably require minimal handling. In this section future opportunities for the key elements of bioprinting organized cartilage implants are explored.

One of the challenges for the field of cartilage tissue-engineering is to have materials that provide chondrogenic support to the embedded cells. Both gelMA/gellan/HAMA and polyHPMA-lac-PEG/HAMA hydrogels are suitable for this purpose (Chapters 2-5). However, both hydrogels may also be of value for more broad applications. For example, gelMA-based hydrogels have been demonstrated to also support other cell types in their production of different matrix compositions *e.g.* MSCs for bone tissue[76], keratinocyte for epidermal tissue[144], or MSCs combined with endothelial colony-forming cells for vasculature-like structures[145]. Moreover, the reversed thermo-sensitivity of polyHPMA-lac-PEG/HAMA hydrogels allow this material to be used for injection purposes, in which

the material is liquid in the cooled syringe and forms a physical gel after injection due to body heat. Therefore, this hydrogel in particular might also be valuable as carrier for the delivery of growth factors or therapeutic agents[146].

Another challenge for the engineering of cartilage-like tissue is the selection of an appropriate cell type. As discussed in Chapter 6, with current knowledge the ACPCs are most promising cell population to be embedded in cartilage implants as they can be expanded *in vitro* to obtain sufficient cell numbers and produced relatively high amounts of cartilage-like tissue. However, harvesting of ACPCs requires an additional intervention in the patient. Therefore, alternative cell types might become more suitable in the future. For example, a switch to MSCs may be desirable, if strategies have been developed to control the differentiation of MSCs *in vivo*, as MSCs can be obtained from easier accessible tissues compared to articular cartilage. Further research may also allow the use of allogeneic cells. Issues like foreign-body responses can in the future possibly be solved with advanced cell coating techniques, which may hide cell recognition sides[147].

Moreover, the research in this thesis demonstrated the critical role of initial cell positioning on cartilage repair in the OC plug model (Chapter 7). A layered cell organization provided well integrated repair tissue with a hyaline cartilage character. This knowledge, once validated in *in vivo* models, may also impact cartilage repair strategies currently used in the clinic *e.g.* MACI. Current therapies often rely on the delivery of a dense cell layer in the defect depth. Combining this strategy with homogeneously distributed cells within the scaffold may improve clinical outcomes.

In terms of the construct design for optimal biological function, the ideal cartilage implant may require a dense porous layer near the joint-space, preventing tissue outgrowth as observed for gelMA/gellan hydrogels in the OC plug model (Chapter 7). The incorporation of such a barrier has already been demonstrated sufficient in implants used for matrix-induced autologous chondrocyte implantation (MACI)[84,148]. For the fabrication of such a layer, bioprinting techniques are ideal. The implant surface can be further improved with the incorporation of cells and stimuli for proteoglycan IV production to reducing the surface friction. Alternatively, advanced surface chemistry could be used to covalently bind a lubricant on the surface.

Another challenge for the fabrication of organized cartilage implants is to provide the construct with sufficient mechanical stability without compromising its biological performance. This can be accomplished via the co-printing of thermoplastic polymers, such as PCL, with cell-laden hydrogels (Chapter 5). The incorporation of a simple PCL raster significantly increases the mechanical behavior of the final construct, reaching Young's moduli comparable to native cartilage. Further development of bioprinters and the convergence of technologies, such as bioprinting with MEW, will allow the fabrication of more advanced reinforcement structures in the future. Such structures could include depth-dependent mechanical properties by, for example, changing the filament thickness or orientation[103] as is the case for the collagen fibers in native cartilage. Moreover, arching structures might be printed using fibers with a thickness in the order of nanometers, to further resemble the native collagen orientation. Currently, the most common reinforcement strategies involve PCL. However alternative reinforcement materials are

8

already emerging *e.g.* poloxamer[135]. Future research will provide even more alternatives, for example collagen-based reinforcement may be more beneficial for remodeling after *in vivo* implantation compared to PCL. Furthermore, increasing print resolution fosters the idea of printing of single collagen fibers, which would allow accurate replication the cartilage collagen organization.

Within a wider perspective, convergence of bioprinting technologies with microfluidics increases the application opportunities of bioprinting[149]. This combination of technologies would enable the fabrication of hydrogel filaments with tailored inhomogeneity. For example, elastic polymer coatings around single cells could be used to reduce the shear forces on cells during printing[150], which may solve the reduced differentiation observed for printed cells (Chapter 6). Moreover, cell coating with a low thermal conduction material might allow the bioprinting at temperatures above 37°C. The application of such 'protective coatings' are already being explored for inkjet printing, to reduce the impact forces of the collection plate on the cells, and thus increase cell viability[150].

Finally, the fabrication of cartilage implants with the zonal characteristics of native cartilage is faced by steep challenges. As discussed in section 8.6., it is likely that the incorporation of zonal differences in the implant will improve construct functioning. However, exact replication of the native cartilage may not be feasible nor required for successful regeneration. To steer zonal matrix production by cells and matrix organization, multiple factors have potential *e.g.* incorporation of biological components, growth factors, mechanical loading, and different cell types, but clear understanding of these factors or their optimal combination is currently lacking.

Similar challenges have been found in related fields *e.g.* bioprinting of liver or kidney tissue, where organization and cell fate at the different locations is crucial. Therefore, advancement in the bioprinting of organized constructs may benefit from collaboration with other tissue-engineering fields. To facilitate such a collaboration, it is necessary to have common procedures and protocols. However, for the fabrication of successful organized tissues, collaborations should go beyond the biomedical field and should encompass biologists, engineers, chemists, and doctors[151,152]. Thus, the main challenge for the upcoming years is to combine and translate the findings in all fields into the successful bioprinting of living tissues. A crucial first step would be to index bio-inks and their properties, such that knowledge on existing combinations of properties are readily available. Moreover, a systematic overview of current knowledge may provide clear directions for future research in bio-ink development.

To conclude, the role of bioprinting in tissue-engineering is rapidly advancing, as well as the development of new and improved bio-inks. It is a matter of time before the first bioprinted living implants will appear in the clinic. One may think of placing bioprinters in the operation theater but it would be more realistic to incorporate bioprinters in a GMP facility that prints the constructs, as well as provides pre-culture and pre-conditioning of the implant. Likely, bioprinting for clinical purposes will start with implants of relatively low complexity, such as a living bandage, which does not fully mimic the target tissue but provides support and cues for tissue repair. Once clinical translation of bioprinting

is reality, more complex implants, such as the organized cartilage implant will soon follow. Although cartilage tissue-engineering has proven to be more complicated than anticipated, both materials and techniques have advanced steadily during the resent years. Therefore, we may expect that 3D printing of organized cartilage implants will be clinically viable in the near future.

8

References

1. Malda, J. *et al.* 25th Anniversary Article: Engineering Hydrogels for Biofabrication. *Adv. Mater.* **25,** 5011–5028 (2013).
2. Jungst, T., Smolan, W., Schacht, K., Scheibel, T. & Groll, J. Strategies and Molecular Design Criteria for 3D Printable Hydrogels. *Chem. Rev.* **116,** 1496–1539 (2016).
3. Therriault, D., White, S. R. & Lewis, J. A. Rheological behavior of fugitive organic inks for direct-write assembly. *Appl. Rheol.* **17,** 1–8 (2007).
4. Smay, J. E., Cesarano, J. & Lewis, J. A. Colloidal Inks for Directed Assembly of 3-D Periodic Structures. *Langmuir* **18,** 5429–5437 (2002).
5. Stichler, S. *et al.* Thiol-ene Clickable Poly(glycidol) Hydrogels for Biofabrication. *Ann. Biomed. Eng.* 1–13 (2016). doi:10.1007/s10439-016-1633-3
6. Shim, J.-H. *et al.* Three-dimensional bioprinting of multilayered constructs containing human mesenchymal stromal cells for osteochondral tissue regeneration in the rabbit knee joint. *Biofabrication* **8,** 014102 (2016).
7. O'Driscoll, S. W. *et al.* Validation of a Simple Histological-Histochemical Cartilage Scoring System. *Tissue Eng.* **7,** 313–320 (2001).
8. Mainil-Varlet, P. *et al.* Histological assessment of cartilage repair: a report by the Histology Endpoint Committee of the International Cartilage Repair Society (ICRS). *J. Bone Joint Surg. Am.* (2003).
9. Kang, K. H., Hockaday, L. A. & Butcher, J. T. Quantitative optimization of solid freeform deposition of aqueous hydrogels. *Biofabrication* **5,** 035001 (2013).
10. Wüst, S., Godla, M. E., Müller, R. & Hofmann, S. Tunable hydrogel composite with two-step processing in combination with innovative hardware upgrade for cell-based three-dimensional bioprinting. *Acta Biomater.* **10,** 630–640 (2014).
11. Billiet, T., Gevaert, E., De Schryver, T., Cornelissen, M. & Dubruel, P. The 3D printing of gelatin methacrylamide cell-laden tissue-engineered constructs with high cell viability. *Biomaterials* **35,** 49–62 (2014).
12. Murphy, S. V, Skardal, A. & Atala, A. Evaluation of hydrogels for bio-printing applications. *J. Biomed. Mater. Res. - Part A* **101 A,** 272–284 (2013).
13. Kesti, M. *et al.* Bioprinting Complex Cartilaginous Structures with Clinically Compliant Biomaterials. *Adv. Funct. Mater.* **25,** 7406–7417 (2015).
14. Blokzijl, M. M. *et al.* Structural deformation of bioink filaments. in (Biofabrication conference, 2016).
15. Melchels, F. P. W., Dhert, W. J. A., Hutmacher, D. W. & Malda, J. Development and characterisation of a new bioink for additive tissue manufacturing. *J. Mater. Chem. B* **2,** 2282–2289 (2014).
16. Levato, R. *et al.* Biofabrication of tissue constructs by 3D bioprinting of cell-laden microcarriers. *Biofabrication* **6,** 035020 (2014).
17. Visser, J. *et al.* Biofabrication of multi-material anatomically shaped tissue constructs. *Biofabrication* **5,** 035007 (2013).
18. Stevens, L. R., Gilmore, K. J., Wallace, G. G. & in het Panhuis, M. Tissue engineering with gellan gum. *Biomater. Sci.* **4,** 1276–1290 (2016).
19. Huang, G. *et al.* Engineering three-dimensional cell mechanical microenvironment with hydrogels. *Biofabrication* **4,** 042001 (2012).
20. Discher, D. E. Tissue Cells Feel and Respond to the Stiffness of Their Substrate. *Science (80-.).* **310,** 1139–1143 (2005).
21. Erickson, I. E. *et al.* Macromer density influences mesenchymal stem cell chondrogenesis and maturation in photocrosslinked hyaluronic acid hydrogels. *Osteoarthr. Cartil.* **17,** 1639–1648 (2009).
22. Cha, C., Jeong, J. H., Shim, J. & Kong, H. Tuning the dependency between stiffness and permeability of a cell encapsulating hydrogel with hydrophilic pendant chains. *Acta Biomater.* **7,** 3719–3728 (2011).
23. Cha, C., Kim, S. Y., Cao, L. & Kong, H. Decoupled control of stiffness and permeability with a cell-encapsulating poly(ethylene glycol) dimethacrylate hydrogel. *Biomaterials* **31,** 4864–4871 (2010).
24. Klein, E. A. *et al.* Cell-Cycle Control by Physiological Matrix Elasticity and In Vivo Tissue Stiffening. *Curr. Biol.* **19,** 1511–1518 (2009).
25. Munoz-Pinto, D. J., Bulick, A. S. & Hahn, M. S. Uncoupled investigation of scaffold modulus and mesh size on smooth muscle cell behavior. *J. Biomed. Mater. Res. Part A* **90A,** 303–316 (2009).
26. Saha, K. *et al.* Substrate Modulus Directs Neural Stem Cell Behavior. *Biophys. J.* **95,** 4426–4438 (2008).
27. Dikovsky, D., Bianco-Peled, H. & Seliktar, D. Defining the Role of Matrix Compliance and Proteolysis in Three-Dimensional Cell Spreading and Remodeling. *Biophys. J.* **94,** 2914–2925 (2008).
28. Van den Steen, P. E. *et al.* Biochemistry and Molecular Biology of Gelatinase B or Matrix Metalloproteinase-9 (MMP-9). *Crit. Rev. Biochem. Mol. Biol.* **37,** 375–536 (2002).
29. Klotz, B. J., Gawlitta, D., Rosenberg, A. J. W. P., Malda, J. & Melchels, F. P. W. Gelatin-Methacryloyl Hydrogels: Towards Biofabrication-Based Tissue Repair. *Trends Biotechnol.* **34,** 394–407 (2016).
30. Nichol, J. W. *et al.* Cell-laden microengineered gelatin methacrylate hydrogels. *Biomaterials* **31,** 5536–44 (2010).
31. Zhang, J., Mujeeb, A., Du, Y., Lin, J. & Ge, Z. Probing cell-matrix interactions in RGD-decorated macroporous poly (ethylene glycol) hydrogels for 3D chondrocyte culture. *Biomed. Mater.* **10,** 035016 (2015).
32. Chen, J.-P. & Su, C.-H. Surface modification of electrospun PLLA nanofibers by plasma treatment and cationized gelatin immobilization for cartilage tissue engineering. *Acta Biomater.* **7,** 234–43 (2011).
33. Lee, H. *et al.* Chondrocyte 3D-culture in RGD-modified crosslinked hydrogel with temperature-controllable modulus. *Macromol. Res.* **20,** 106–111 (2012).

34. Nichol, J. W. *et al.* Cell-laden microengineered gelatin methacrylate hydrogels. *Biomaterials* **31,** 5536–5544 (2010).
35. Heino, J., Huhtala, M., Käpylä, J. & Johnson, M. S. Evolution of collagen-based adhesion systems. *Int. J. Biochem. Cell Biol.* **41,** 341–348 (2009).
36. Gong, Y. *et al.* An improved injectable polysaccharide hydrogel: modified gellan gum for long-term cartilage regeneration in vitro. *J. Mater. Chem.* **19,** 1968 (2009).
37. Oliveira, J. T. *et al.* Injectable gellan gum hydrogels with autologous cells for the treatment of rabbit articular cartilage defects. *J. Orthop. Res.* **28,** 1193–9 (2010).
38. Schuurman, W. *et al.* Gelatin-methacrylamide hydrogels as potential biomaterials for fabrication of tissue-engineered cartilage constructs. *Macromol. Biosci.* **13,** 551–561 (2013).
39. Abbadessa, A. *Thermosensitive hydrogels for 3D bioprinting of cartilage constructs.* (2017).
40. Duan, B., Kapetanovic, E., Hockaday, L. A. & Butcher, J. T. Three-dimensional printed trileaflet valve conduits using biological hydrogels and human valve interstitial cells. *Acta Biomater.* **10,** 1836–1846 (2014).
41. Yasuda, T. Nuclear factor-κB activation by type II collagen peptide in articular chondrocytes: its inhibition by hyaluronan via the receptors. *Mod. Rheumatol.* **23,** 1116–1123 (2012).
42. Viola, M. *et al.* Biology and biotechnology of hyaluronan. *Glycoconj. J.* **32,** 93–103 (2015).
43. Akmal, M. *et al.* The effects of hyaluronic acid on articular chondrocytes. *J. Bone Jt. Surg. - Br. Vol.* **87-B,** 1143–1149 (2005).
44. Dowthwaite, G. P., Edwards, J. C. W. & Pitsillides, A. A. An Essential Role for the Interaction Between Hyaluronan and Hyaluronan Binding Proteins During Joint Development. *J. Histochem. Cytochem.* **46,** 641–651 (1998).
45. Onodera, Y., Teramura, T., Takehara, T. & Fukuda, K. Hyaluronic acid regulates a key redox control factor Nrf2 via phosphorylation of Akt in bovine articular chondrocytes. *FEBS Open Bio* **5,** 476–484 (2015).
46. Ariyoshi, W., Takahashi, N., Hida, D., Knudson, C. B. & Knudson, W. Mechanisms involved in enhancement of the expression and function of aggrecanases by hyaluronan oligosaccharides. *Arthritis Rheum.* **64,** 187–197 (2012).
47. Schuh, E. *et al.* Chondrocyte redifferentiation in 3D: the effect of adhesion site density and substrate elasticity. *J. Biomed. Mater. Res. A* **100,** 38–47 (2012).
48. Benya, P. Dedifferentiated chondrocytes reexpress the differentiated collagen phenotype when cultured in agarose gels. *Cell* **30,** 215–224 (1982).
49. Hachet, E., Van Den Berghe, H., Bayma, E., Block, M. R. & Auzély-Velty, R. Design of biomimetic cell-interactive substrates using hyaluronic acid hydrogels with tunable mechanical properties. *Biomacromolecules* **13,** 1818–27 (2012).
50. Allemann, F. *et al.* Effects of hyaluronan on engineered articular cartilage extracellular matrix gene expression in 3-dimensional collagen scaffolds. *J. Biomed. Mater. Res.* **55,** 13–19 (2001).
51. Callahan, L. A. S. *et al.* ECM production of primary human and bovine chondrocytes in hybrid PEG hydrogels containing type I collagen and hyaluronic acid. *Biomacromolecules* **13,** 1625–31 (2012).
52. Kawasaki, K., Ochi, M., Uchio, Y., Adachi, N. & Matsusaki, M. Hyaluronic acid enhances proliferation and chondroitin sulfate synthesis in cultured chondrocytes embedded in collagen gels. *J. Cell. Physiol.* **179,** 142–148 (1999).
53. Villanueva, I., Gladem, S. K., Kessler, J. & Bryant, S. J. Dynamic loading stimulates chondrocyte biosynthesis when encapsulated in charged hydrogels prepared from poly(ethylene glycol) and chondroitin sulfate. *Matrix Biol.* **29,** 51–62 (2010).
54. Levett, P. A. *et al.* A biomimetic extracellular matrix for cartilage tissue engineering centered on photocurable gelatin, hyaluronic acid and chondroitin sulfate. *Acta Biomater.* **10,** 214–223 (2014).
55. Jaipaew, J., Wangkulangkul, P., Meesane, J., Raungrut, P. & Puttawibul, P. Mimicked cartilage scaffolds of silk fibroin/hyaluronic acid with stem cells for osteoarthritis surgery: Morphological, mechanical, and physical clues. *Mater. Sci. Eng. C* **64,** 173–182 (2016).
56. Yeh, H.-Y. *et al.* Neocartilage formation from mesenchymal stem cells grown in type II collagen–hyaluronan composite scaffolds. *Differentiation* **86,** 171–183 (2013).
57. Hwang, N. S. *et al.* Response of zonal chondrocytes to extracellular matrix-hydrogels. *FEBS Lett.* **581,** 4172–4178 (2007).
58. Cohen, N. P., Foster, R. J. & Mow, V. C. Composition and Dynamics of Articular Cartilage: Structure, Function, and Maintaining Healthy State. *J. Orthop. Sport. Phys. Ther.* **28,** 203–215 (1998).
59. Hutmacher, D. W. Scaffolds in tissue engineering bone and cartilage. *Biomaterials* **21,** 2529–2543 (2000).
60. Chen, A. C., Bae, W. C., Schinagl, R. M. & Sah, R. L. Depth- and strain-dependent mechanical and electromechanical properties of full-thickness bovine articular cartilage in confined compression. *J. Biomech.* **34,** 1–12 (2001).
61. Athanasiou, K. A., Agarwal, A. & Dzida, F. J. Comparative study of the intrinsic mechanical properties of the human acetabular and femoral head cartilage. *J. Orthop. Res.* **12,** 340–349 (1994).
62. Jurvelin, J. S., Buschmann, M. D. & Hunziker, E. B. Optical and mechanical determination of poisson's ratio of adult bovine humeral articular cartilage. *J. Biomech.* **30,** 235–241 (1997).
63. Schuurman, W. *et al.* Bioprinting of hybrid tissue constructs with tailorable mechanical properties. *Biofabrication* **3,** 021001 (2011).
64. Olubamiji, A. D. *et al.* Modulating mechanical behaviour of 3D-printed cartilage-mimetic PCL scaffolds: influence of molecular weight and pore geometry. *Biofabrication* **8,** 025020 (2016).

8

65. Visser, J. *et al.* Reinforcement of hydrogels using three-dimensionally printed microfibres. *Nat. Commun.* **6,** 6933 (2015).

66. Hochleitner, G. *et al.* Additive manufacturing of scaffolds with sub-micron filaments via melt electrospinning writing. *Biofabrication* **7,** 035002 (2015).

67. Brown, T. D., Dalton, P. D. & Hutmacher, D. W. Direct Writing By Way of Melt Electrospinning. *Adv. Mater.* **23,** 5651–5657 (2011).

68. De Ruijter, M., Melchels, F. P. ., Levato, R. & Malda, J. Hydrogel encapsulation and Micro-aggregation of co-culture MSC/AC for tissue regeneration. in (World Biomaterials Conference, 2016).

69. Xu, T. *et al.* Hybrid printing of mechanically and biologically improved constructs for cartilage tissue engineering applications. *Biofabrication* **5,** 015001 (2013).

70. Jiang, Y. & Tuan, R. S. Origin and function of cartilage stem/progenitor cells in osteoarthritis. *Nat. Rev. Rheumatol.* **11,** 206–12 (2015).

71. Dowthwaite, G. P. The surface of articular cartilage contains a progenitor cell population. *J. Cell Sci.* **117,** 889–897 (2004).

72. Matricali, G. A., Dereymaeker, G. P. E. & Luvten, F. P. Donor site morbidity after articular cartilage repair procedures: A review. *Acta Orthopaedica Belgica* **76,** 669–674 (2010).

73. McCarthy, H. S., Richardson, J. B., Parker, J. C. E. & Roberts, S. Evaluating Joint Morbidity after Chondral Harvest for Autologous Chondrocyte Implantation (ACI): A Study of ACI-Treated Ankles and Hips with a Knee Chondral Harvest. *Cartilage* **7,** 7–15 (2016).

74. Dominici, M. *et al.* Minimal criteria for defining multipotent mesenchymal stromal cells. The International Society for Cellular Therapy position statement. *Cytotherapy* **8,** 315–317 (2006).

75. Pelttari, K., Steck, E. & Richter, W. The use of mesenchymal stem cells for chondrogenesis. *Injury* **39,** 58–65 (2008).

76. Visser, J. *et al.* Endochondral bone formation in gelatin methacrylamide hydrogel with embedded cartilage-derived matrix particles. *Biomaterials* **37,** 174–182 (2015).

77. Johnstone, B., Hering, T. M., Caplan, A. I., Goldberg, V. M. & Yoo, J. U. In VitroChondrogenesis of Bone Marrow-Derived Mesenchymal Progenitor Cells. *Exp. Cell Res.* **238,** 265–272 (1998).

78. Spiller, K. L., Maher, S. A. & Lowman, A. M. Hydrogels for the Repair of Articular Cartilage Defects. *Tissue Eng. Part B Rev.* **17,** 281–299 (2011).

79. Jung, H. H., Park, K. & Han, D. K. Preparation of TGF-β1-conjugated biodegradable pluronic F127 hydrogel and its application with adipose-derived stem cells. *J. Control. Release* **147,** 84–91 (2010).

80. Ma, B. *et al.* Gene expression profiling of dedifferentiated human articular chondrocytes in monolayer culture. *Osteoarthr. Cartil.* **21,** 599–603 (2013).

81. Mandelbaum, B. *et al.* Treatment outcomes of autologous chondrocyte implantation for full-thickness articular cartilage defects of the trochlea. *Am. J. Sports Med.* **35,** 915–921 (2007).

82. Browne, J. E. & Branch, T. P. Surgical alternatives for treatment of articular cartilage lesions. *J. Am. Acad. Orthop. Surg.* **8,** 180–189 (2000).

83. Judet, T., Marmorat, J.-L. & Mullins, M. M. Effective Treatment of Fracture-Dislocations of the Olecranon Requires a Stable Trochlear Notch. *Clin. Orthop. Relat. Res.* **&NA;,** 276–277 (2005).

84. Huang, B. J., Hu, J. C. & Athanasiou, K. a. Cell-based tissue engineering strategies used in the clinical repair of articular cartilage. *Biomaterials* **98,** 1–22 (2016).

85. Kirilak, Y. *et al.* Fibrin sealant promotes migration and proliferation of human articular chondrocytes: Possible involvement of thrombin and protease-activated receptors. *Int. J. Mol. Med.* **17,** 551–558 (2006).

86. Vu, L. T., Jain, G., Veres, B. D. & Rajagopalan, P. Cell Migration on Planar and Three-Dimensional Matrices: A Hydrogel-Based Perspective. *Tissue Eng. Part B Rev.* **21,** 67–74 (2015).

87. De Vries-van Melle, M. L. *et al.* Chondrogenesis of Mesenchymal Stem Cells in an Osteochondral Environment Is Mediated by the Subchondral Bone. *Tissue Eng. Part A* **20,** 23–33 (2014).

88. De Vries-van Melle, M. L. *et al.* Chondrogenic differentiation of human bone marrow-derived mesenchymal stem cells in a simulated osteochondral environment is hydrogel dependent. *Eur. Cell. Mater.* **27,** 112–23; discussion 123 (2014).

89. De Vries-van Melle, M. L. *et al.* An osteochondral culture model to study mechanisms involved in articular cartilage repair. *Tissue Eng. Part C. Methods* **18,** 45–53 (2012).

90. Schwab, A. Ex vivo culture platform for assessment of cartilage repair treatment strategies. *ALTEX* (2016). doi:10.14573/altex.1607111

91. Chen, A. C., Nagrampa, J. P., Schinagl, R. M., Lottman, L. M. & Sah, R. L. Chondrocyte transplantation to articular cartilage explantsin vitro. *J. Orthop. Res.* **15,** 791–802 (1997).

92. Elson, K. M. *et al.* Non-Destructive Monitoring of Viability in an Ex Vivo Organ Culture Model of Osteochondral Tissue. **29,** 356–369 (2015).

93. Sherwood, J. C., Bertrand, J., Eldridge, S. E. & Dell'Accio, F. Cellular and molecular mechanisms of cartilage damage and repair. *Drug Discov. Today* **19,** 1172–1177 (2014).

94. Vincent, T., Hermansson, M., Bolton, M., Wait, R. & Saklatvala, J. Basic FGF mediates an immediate response of articular cartilage to mechanical injury. *Proc. Natl. Acad. Sci. U. S. A.* **99,** 8259–64 (2002).

95. Ellsworth, J. L. *et al.* Fibroblast growth factor-18 is a trophic factor for mature chondrocytes and their progenitors. *Osteoarthr. Cartil.* **10,** 308–320 (2002).

96. Dell'Accio, F., De Bari, C., Eltawil, N. M., Vanhummelen, P. & Pitzalis, C. Identification of the molecular response of articular cartilage to injury, by microarray screening: Wnt-16 expression and signaling after injury and in osteoarthritis. *Arthritis Rheum.* **58,** 1410–1421 (2008).

97. De Visser, H. M. *et al.* Groove model of tibia-femoral osteoarthritis in the rat. *J. Orthop. Res.* 1–10

(2016). doi:10.1002/jor.23299

98. Nirmal, P. S., Jagtap, S. D., Narkhede, A. N., Nagarkar, B. E. & Harsulkar, A. M. New herbal composition (OA-F2) protects cartilage degeneration in a rat model of collagenase induced osteoarthritis. *BMC Complement. Altern. Med.* **17,** 6 (2017).

99. McCoy, A. M. Animal Models of Osteoarthritis: Comparisons and Key Considerations. *Vet. Pathol.* **52,** 803–818 (2015).

100. Wong, M. & Carter, D. R. Articular cartilage functional histomorphology and mechanobiology: A research perspective. *Bone* **33,** 1–13 (2003).

101. Kaab, M. J., Ap Gwynn, I. & Notzli, H. P. Collagen fibre arrangement in the tibial plateau articular cartilage of man and other mammalian species. *J. Anat.* **193,** 23–34 (1998).

102. Benninghoff, A. Form und Bau der Gelenkknorpel in ihren Beziehungen zur Funktion. *Z. Anat. Entwicklungsgesch.* **76,** 43–63 (1925).

103. Responte, D. J., Natoli, R. M. & Athanasiou, K. A. Collagens of Articular Cartilage: Structure, Function, and Importance in Tissue Engineering. *Crit. Rev. Biomed. Eng.* **35,** 363–411 (2007).

104. Weeren, P. R. *et al.* Early exercise advances the maturation of glycosaminoglycans and collagen in the extracellular matrix of articular cartilage in the horse. *Equine Vet. J.* **40,** 128–135 (2008).

105. Bland, Y. & Ashhurst, D. Development and ageing of the articular cartilage of the rabbit knee joint: distribution of the fibrillar collagens. *Anat. Embryol. (Berl).* **194,** 607–619 (1996).

106. Klein, T. J., Malda, J., Sah, R. L. & Hutmacher, D. W. Tissue Engineering of Articular Cartilage with Biomimetic Zones. *Tissue Eng. Part B Rev.* **15,** 143–157 (2009).

107. Hollander, A. P., Dickinson, S. C. & Kafienah, W. Stem Cells and Cartilage Development: Complexities of a Simple Tissue. *Stem Cells* **28,** 1992–1996 (2010).

108. Schuurman, W. *et al.* Zonal Chondrocyte Subpopulations Reacquire Zone-Specific Characteristics During In Vitro Redifferentiation. *Am. J. Sports Med.* **37,** 97S–104S (2009).

109. Kim, T.K. *et al.* Experimental Model for Cartilage Tissue Engineering to Regenerate the Zonal Organization of Articular Cartilage. *Osteoarthr. Cartil.* **11,** 653–664 (2003).

110. Schuurman, W. *et al.* Cartilage regeneration using zonal chondrocyte subpopulations: a promising approach or an overcomplicated strategy? *J. Tissue Eng. Regen. Med.* **9,** 669–678 (2015).

111. Nguyen, L. H., Kudva, A. K., Saxena, N. S. & Roy, K. Engineering articular cartilage with spatially-varying matrix composition and mechanical properties from a single stem cell population using a multi-layered hydrogel. *Biomaterials* **32,** 6946–6952 (2011).

112. Nguyen, L. H., Kudva, A. K., Guckert, N. L., Linse, K. D. & Roy, K. Unique biomaterial compositions direct bone marrow stem cells into specific chondrocytic phenotypes corresponding to the various zones of articular cartilage. *Biomaterials* **32,** 1327–1338 (2011).

113. Karimi, T., Barati, D., Karaman, O., Moeinzadeh, S. & Jabbari, E. A developmentally inspired combined mechanical and biochemical signaling approach on zonal lineage commitment of mesenchymal stem cells in articular cartilage regeneration. *Integr. Biol.* **7,** 112–127 (2015).

114. Tatman, P. D. *et al.* Multiscale Biofabrication of Articular Cartilage: Bioinspired and Biomimetic Approaches. *Tissue Eng. Part B Rev.* **21,** 543–559 (2015).

115. Trappmann, B. *et al.* Extracellular-matrix tethering regulates stem-cell fate. *Nat. Mater.* **11,** 742–742 (2012).

116. Li, K. W. *et al.* in *Cartilage and Osteoarthritis* **100,** 325–352 (Humana Press, 2004).

117. Levato, R. *et al.* Opportunities for zonal cartilage regeneration: progenitor cell-laden hydrogels and bioprinting. in (TERMIS - EU Chapter Conference, 2016).

118. Mauck, R. L., Seyhan, S. L., Ateshian, G. A. & Hung, C. T. Influence of Seeding Density and Dynamic Deformational Loading on the Developing Structure/Function Relationships of Chondrocyte-Seeded Agarose Hydrogels. *Ann. Biomed. Eng.* **30,** 1046–1056 (2002).

119. Bian, L. *et al.* Dynamic Mechanical Loading Enhances Functional Properties of Tissue-Engineered Cartilage Using Mature Canine Chondrocytes. *Tissue Eng. Part A* **16,** 1781–1790 (2010).

120. Brama, P. A. J. *et al.* Effect of loading on the organization of the collagen fibril network in juvenile equine articular cartilage. *J. Orthop. Res.* **27,** 1226–1234 (2009).

121. Kock, L. M., Ito, K. & van Donkelaar, C. C. Sliding Indentation Enhances Collagen Content and Depth-Dependent Matrix Distribution in Tissue-Engineered Cartilage Constructs. *Tissue Eng. Part A* **19,** 1949–1959 (2013).

122. Khoshgoftar, M., van Donkelaar, C. C. & Ito, K. Mechanical stimulation to stimulate formation of a physiological collagen architecture in tissue-engineered cartilage: a numerical study. *Comput. Methods Biomech. Biomed. Engin.* **14,** 135–144 (2011).

123. Meinert, C. *et al.* Tailoring hydrogel surface properties to modulate cellular response to shear loading. *Acta Biomater.* (2016). doi:10.1016/j.actbio.2016.10.011

124. Klein, T. J. *et al.* Strategies for Zonal Cartilage Repair using Hydrogels. *Macromol. Biosci.* **9,** 1049–1058 (2009).

125. Mouser, V. H. M. *et al.* Three-Dimensional Bioprinting and Its Potential in the Field of Articular Cartilage Regeneration. *Cartilage* (2016). doi:10.1177/1947603516665445

126. Li, Z., Yao, S., Alini, M. & Grad, S. Different response of articular chondrocyte subpopulations to surface motion. *Osteoarthr. Cartil.* **15,** 1034–1041 (2007).

127. Grad, S. *et al.* Surface Motion Upregulates Superficial Zone Protein and Hyaluronan Production in Chondrocyte-Seeded Three-Dimensional Scaffolds. *Tissue Eng.* **11,** 249–256 (2005).

128. Hayes, A. J., Hall, A., Brown, L., Tubo, R. & Caterson, B. Macromolecular Organization and In Vitro Growth Characteristics of Scaffold-free Neocartilage Grafts. *J. Histochem. Cytochem.* **55,** 853–866

8

(2007).

129. DiCesare, P. E., Mörgelin, M., Carlson, C. S., Pasumarti, S. & Paulsson, M. Cartilage oligomeric matrix protein: Isolation and characterization from human articular cartilage. *J. Orthop. Res.* **13,** 422–428 (1995).

130. Murray, R. C., Smith, R. K., Henson, F. M. & Goodship, A. The distribution of cartilage oligomeric matrix protein (COMP) in equine carpal articular cartilage and its variation with exercise and cartilage deterioration. *Vet. J.* **162,** 121–128 (2001).

131. Lorenzo, P., Bayliss, M. T., Heinegårdt, D. & Heinegard, D. A Novel Cartilage Protein (CILP) Present in the Mid-zone of Human Articular Cartilage Increases with Age. *J. Biol. Chem.* **273,** 23463–23468 (1998).

132. Tasoglu, S. & Demirci, U. Bioprinting for stem cell research. *Trends Biotechnol.* **31,** 10–19 (2013).

133. Ouyang, L., Yao, R., Zhao, Y. & Sun, W. Effect of bioink properties on printability and cell viability for 3D bioplotting of embryonic stem cells. *Biofabrication* **8,** 035020 (2016).

134. Pescosolido, L. *et al.* Hyaluronic acid and dextran-based semi-IPN hydrogels as biomaterials for bioprinting. *Biomacromolecules* **12,** 1831–1838 (2011).

135. Melchels, F. P. W. *et al.* Hydrogel-based reinforcement of 3D bioprinted constructs. *Biofabrication* **8,** 035004 (2016).

136. Snyder, J. *et al.* Mesenchymal stem cell printing and process regulated cell properties. *Biofabrication* **7,** 044106 (2015).

137. Müller, M., Öztürk, E., Arlov, Ø., Gatenholm, P. & Zenobi-Wong, M. Alginate Sulfate–Nanocellulose Bioinks for Cartilage Bioprinting Applications. *Ann. Biomed. Eng.* 1–14 (2016). doi:10.1007/s10439-016-1704-5

138. Murphy, S. V & Atala, A. 3D bioprinting of tissues and organs. *Nat. Biotechnol.* **32,** 773–785 (2014).

139. Matsui, M. & Tabata, Y. Enhanced angiogenesis by multiple release of platelet-rich plasma contents and basic fibroblast growth factor from gelatin hydrogels. *Acta Biomater.* **8,** 1792–1801 (2012).

140. De Oliveira Magalhães, P. *et al.* Methods of endotoxin removal from biological preparations: A review. *Journal of Pharmacy and Pharmaceutical Sciences* **10,** 388–404 (2007).

141. Williams, R. J. Chondrocyte Survival and Material Properties of Hypothermically Stored Cartilage: An Evaluation of Tissue Used for Osteochondral Allograft Transplantation. *Am. J. Sports Med.* **32,** 132–139 (2004).

142. Brockbank, K. G. M., Rahn, E., Wright, G. J., Chen, Z. & Yao, H. Impact of Hypothermia upon Chondrocyte Viability and Cartilage Matrix Permeability after 1 Month of Refrigerated Storage. *Transfus. Med. Hemotherapy* **38,** 387–392 (2011).

143. Kim, W. *et al.* Functional Viability of Chondrocytes Stored at 4°C. *Tissue Eng.* **2,** 75–81 (1996).

144. Zhao, X. *et al.* Photocrosslinkable Gelatin Hydrogel for Epidermal Tissue Engineering. *Adv. Healthc. Mater.* **5,** 108–118 (2016).

145. Lin, R.-Z., Chen, Y.-C., Moreno-Luna, R., Khademhosseini, A. & Melero-Martin, J. M. Transdermal regulation of vascular network bioengineering using a photopolymerizable methacrylated gelatin hydrogel. *Biomaterials* **34,** 6785–6796 (2013).

146. Censi, R. *et al.* Photopolymerized thermosensitive hydrogels for tailorable diffusion-controlled protein delivery. *J. Control. Release* **140,** 230–236 (2009).

147. Granicka, L. H. Nanoencapsulation of Cells Within Multilayer Shells for Biomedical Applications. *J. Nanosci. Nanotechnol.* **14,** 705–716 (2014).

148. Brittberg, M. Cell Carriers as the Next Generation of Cell Therapy for Cartilage Repair: A Review of the Matrix-Induced Autologous Chondrocyte Implantation Procedure. *Am. J. Sports Med.* **38,** 1259–1271 (2010).

149. Kang, A., Park, J., Ju, J., Jeong, G. S. & Lee, S.-H. Cell encapsulation via microtechnologies. *Biomaterials* **35,** 2651–2663 (2014).

150. Hopp, B. Femtosecond laser printing of living cells using absorbing film-assisted laser-induced forward transfer. *Opt. Eng.* **51,** 014302 (2012).

151. Chang, J., Wong, S., Newcomb, R. & Hafliger, P. The Third Revolution in Medicine - the Convergence of Life Sciences with Physical Sciences, Mathematics, and Engineering [From the Guest Editors]. *IEEE Circuits Syst. Mag.* **12,** 4–7 (2012).

152. Sharp, P. A. & Langer, R. Promoting Convergence in Biomedical Science. *Science (80-.).* **333,** 527–527 (2011).

8

Addendum

List of abbreviations

^{1}H-NMR	^{1}H-nuclear magnetic resonance
3D	Three-dimensional
ACI	Autologous chondrocyte implantation;
ACPC	Articular cartilage progenitor cell
AMF	Additive manufacturing files
ANOVA	Analysis of variance
ASTM	American society for testing and materials
ATMP	Advanced therapy medicinal product
bFGF	Fibroblast growth factor-basic
BMP	Bone morphogenetic protein
BSI	British standards institute
CILP	Cartilage intermediate layer protein
COMP	Cartilage oligomeric protein
CP	Cloud point
CS	Chondroitin sulfate
CSMA	Methacrylated chondroitin sulfate
CS-TBA	Chondroitin sulfate tetrabuthylammonium salt
CT	Computed tomography
CZ	Calcified cartilage
DM	Degree of methacrylation
DMA	Dynamic mechanical analyzer
DMEM	Dulbecco's modified eagle medium
DMF	N,N-dimethylformamide
DMMB	Dimethylmethylene blue
DMSO	Dimethyl sulfoxide
dwt	Dry weight
DZ	Deep zone
EDTA	Ethylenediaminetetraacetic acid solution
FBS	Fetal bovine serum
FGF	Fibroblast growth factor
GAG	gycosamminoglycan
GelMA	Gelatin-methacryloyl
GMA	Glycidyl methacrylate
GMP	Good manufacturing practice
GPC	Gel permeation chromatography
HA	Hyaluronic acid
HAMA	Methacrylated hyaluronic acid
HA-pNIPAAM	Poly(N-isopropylacrylamide) grafted hyaluronan
HC	Hydrogel construct
HPLC	High performance liquid chromatography
HPMA	N-(2-hydroxypropyl) methacrylamide
ICAM-1	Intercellular adhesion molecule-1
ICRS	International cartilage repair society

&

iPSC	Induced pluripotent stem cell
ISO	International organization for standardization
LCST	Lower critical solution temperature
M_0P_{10}	Not methacrylated polyHPMA-lac-PEG triblock copolymer
$M_{10}P_{10}$	Partially methacrylated polyHPMA-lac-PEG triblock copolymer
MA	Methacrylic anhydride
MACI	Matrix induced autologous chondrocyte implantation
MEW	Melt electrospinning writing
MMP	Matrix metalloproteinase
Mn	Number average molecular weight
MRI	Magnetic resonance imaging
MSC	Multipotent mesenchymal stromal cell
MW	Molecular weight
MZ	Middle zone
OC	Osteochondral
p/s	Penicillin/streptomycin
pen/strep	Penicillin/streptomycin
PBS	Phosphate buffered saline
PCL	Polycaprolactone
PDI	Polydispersity index
PEG	Poly-ethylene glycol
PEGDMA	Poly(ethylene) glycol dimethacrylate
PEGT-PBT	Poly(ethylene glycol)-terephthalate-poly(butylene terephthalate)
pHMGCL/PCL	Poly(hydroxylmethylglycolide-co-ε-caprolactone)/poly(ε-caprolactone)
pHPMA-lac	Methacrylated poly[N-(2-hydroxypropyl)methacrylamide mono/dilactate]
polyHPMA-lac	Poly (N-(2-hydroxypropyl) methacrylamide mono/dilactate
polyHPMA-lac-PEG	Polyethylene glycol midblock flanked by two poly[N-(2-hydroxypropyl) methacrylamide mono/dilactate]
PRG4	Proteoglycan IV (or lubricin)
PVA	Polyvinyl alcohol
RGD	Arginine-glycine-aspartic acid
RHAMM	Hyaluronan mediated motility
RT-PCR	Reverse transcription-polymerase chain reaction
s.d.	Strand distance
SB	Subchondral bone
SEM	Standard error of the mean
SR	Swelling ratio
STL	Stereolithography

&

SZ	Superficial zone
TBA	Tetrabuthylammonium
T_{gel}	Gelation temperature
TGF	Transforming growth factor
TKA	Total knee arthroplasty;
v.o.t.	Valve opening time
wt	Wet weight
wwt	Wet weight

&

Addendum

Summary

A promising approach to treat cartilage defects is the implantation of cell-laden hydrogel implants. The functioning of such implants may be improved with the incorporation of depth-dependent characteristics (stratification), similar to those of native cartilage. For the fabrication of stratified cartilage implants, three-dimensional (3D) bioprinting techniques are promising, as they allow accurate deposition of (cell-laden) biomaterials, the so-called bio-inks, as well as biological cues and reinforcement structures. Several hydrogels have been suggested as bio-inks, including hydrogels based on gelatin-methacryloyl (gelMA) with gellan gum or triblock copolymers of polyethylene glycol (PEG) and partially methacrylated poly(N-(2-hydroxypropyl) methacrylamide mono/dilactate (polyHPMA-lac). However, for the bioprinting of successful cartilage regenerative constructs with a high resolution, the bio-ink properties are crucial. Therefore, the main aim of this thesis is **to investigate the application of gelMA and polyHPMA-lac-PEG based hydrogels, as bio-ink platforms for the 3D bioprinting of cell-laden organized cartilage implants**. Here, the optimal cartilage bio-ink properties are based on both the ability to print the material with a high shape-fidelity and the ability of the material to support chondrogenesis.

To accomplish this, the rheological properties governing the printability and cell encapsulation of gelMA/gellan hydrogels were investigated. Secondly, the possibility to improve the bio-ink properties of gelMA and polyHPMA-lac-PEG hydrogels, by the incorporation of additives or reinforcement was explored. More specifically, the bio-ink and construct properties after addition of gellan gum or methacrylated hyaluronic acid (HAMA) in gelMA hydrogels, and HAMA, methacrylated chondroitin sulfate (CSMA), or poly-ε-caprolactone (PCL) reinforcement in polyHPMA-lac-PEG hydrogels were investigated. Thirdly, zone-specific cartilage matrix production was explored for chondrocytes, articular cartilage progenitor cells (ACPCs), and multipotent mesenchymal stromal cells (MSCs) in gelMA/gellan(/HAMA) hydrogels. Finally, the optimal spatial positioning of chondrocytes in hydrogel constructs for cartilage repair was investigated using an *ex vivo* osteochondral plug model.

The feasibility of bioprinting and cell encapsulation with gelMA/gellan hydrogel was governed by the yield stress of the blend. In addition, the printability and construct stiffness after crosslinking was enhanced for gelMA hydrogels by the incorporation of gellan gum and/or HAMA. Furthermore, these characteristics were improved for polyHPMA-lac-PEG hydrogels with the incorporation of HAMA or to a lesser extent CSMA. Moreover, the co-printing of a hydrogel with PCL provided porous constructs with Young's moduli comparable to those of native cartilage. Nevertheless, the chondrogenic potential of embedded chondrocytes could only be improved with specific concentrations of HAMA added to the polyHPMA-lac-PEG hydrogels. Additionally, relatively high gellan gum or CSMA concentrations hampered cartilage-like matrix production by the embedded cells.

For the generation of spatially organized implants, ACPCs were found to be the most suitable cell type to produce a superficial zone-like cartilage matrix. Additionally, the highest amount of cartilage-like tissue was produced by the MSCs, which are therefore interesting for the fabrication of middle and deep zone cartilage. Overall, the zone-specific matrix production by embedded cells, was not influenced by the incorporation of HAMA in gelMA/gellan hydrogels. Finally, a homogeneous spatial cell distribution within

&

hydrogel constructs was beneficial for defect filling with hyaline-like cartilage tissue, while a dense cell layer at the bottom of the defect improved construct integration in full thickness cartilage defects in the OC plug model.

Altogether, the work in this thesis resulted in two optimized cartilage bio-inks: gelMA/gellan/HAMA and polyHPMA-lac-PEG/HAMA hydrogels. Moreover, strategies to fabricate mechanically stable and organized implants were explored *e.g.* PCL reinforcement, layered chondrocyte delivery, layered distribution of ACPCs and MSCs. Although several steps towards the bioprinting of organized cartilage implants have been made, some challenges still need to be overcome, such as finding the optimal combination of factors to stimulate zone-specific cartilage production by embedded cells. However, the results of this thesis encourage further development of organized cartilage implants using gelMA/gellan/HAMA and polyHPMA-lac-PEG/HAMA bio-inks.

&

Addendum

Dutch summary / Nederlandse samenvatting

Het implanteren van hydrogelconstructen met cellen vormt een veelbelovende strategie voor de behandeling van kraakbeendefecten. Het functioneren van deze implantanten kan mogelijk verbeterd worden door de gelaagde (zonale) organisatie van natuurlijk kraakbeen na te bootsen in het construct. Een kansrijke techniek om gelaagde kraakbeenimplantaten te fabriceren is driedimensionaal (3D) bioprinten. Deze techniek maakt het mogelijk om een biomateriaal (met cellen), ook wel bekend als de bio-inkt, nauwkeurig te positioneren. Door het simultaan printen van biologische stimulatoren en verstevigende structuren met de bio-inkt kunnen kraakbeenconstructen verder worden geoptimaliseerd. Verschillende hydrogels zijn voorgedragen als bio-inkt, bijvoorbeeld hydrogels gebaseerd op gelatine-methacryloyl (gelMA) met gellan gum of op het tri-blok polymeer van gemethacryleerd poly[N-(2-hydroxypropyl)methacrylamide mono-dilactaat]/polyethyleen glycol (pHPMAlac-PEG). De materiaaleigenschappen van een bio-inkt zijn cruciaal voor het succesvol printen van regeneratieve kraakbeen-constructen met een hoge resolutie. Daarom is het hoofddoel van dit proefschrift om **de eigenschappen van hydrogels gebaseerd op gelMA of polyHPMA-lac-PEG in kaart te brengen en te optimaliseren als bio-inkt platform voor het 3D bioprinten van gelaagde kraakbeenimplantaten met cellen.** Een bio-inkt is geschikt als hij printbaar is met een hoge resolutie en gelijktijdig de vorming van kraakbeenweefsel door ingesloten cellen ondersteunt.

Als eerste is onderzocht welke reologische eigenschappen van gelMA/gellan hydrogels van primair belang zijn voor de printbaarheid van de gel en welke eigenschappen de mengbaarheid van de gel met de cellen beïnvloeden. Daarnaast is onderzocht of met het gebruik van verschillende additieven of met vezelversterking, de eigenschappen van gelMA en polyHPMA-lac-PEG hydrogelconstructen verbeterd kunnen worden. Hiertoe zijn de eigenschappen van de volgende hydrogel combinaties onderzocht: gelMA met gellan gum of met gemethacryleerd hyaluronzuur (HAMA) en polyHPMA-lac-PEG met HAMA, met gemethacryleerd chondroïtinesulfaat (CSMA), en/of met poly-ε-caprolacton (PCL) vezels. Verder is gekeken naar kraakbeenvorming die specifiek is voor een bepaalde kraakbeenlaag door chondrocyten, gewrichtskraakbeenvoorlopercellen (ACPCs), of mesenchymale stamcellen (MSCs) in gelMA/gellan(/HAMA) hydrogels op te nemen. Tot slot is onderzocht wat de optimale ruimtelijke plaatsing van de chondrocyten in hydrogelconstructen is om tot kraakbeenregeneratie in een defect te komen. Om dit te onderzoeken is gebruik gemaakt van een *ex vivo* osteochondraal plugmodel.

Uit de resultaten bleek dat de kritische deformatieweerstand (yield stress) de dominante factor is die bepaalt of een gelMA/gellan hydrogel printbaar is en of er cellen in gemengd kunnen worden. Daarnaast zijn de printbaarheid en de stijfheid van de gecrosslinkte gelMA constructen verbeterd met de toevoeging van gellan gum en/of HAMA. De resultaten lieten soortgelijke verbeteringen zien voor polyHPMA-lac-PEG hydrogels met toevoeging van HAMA of CSMA, waarbij HAMA een sterker effect had dan CSMA. Het simultaan printen van hydrogel met PCL resulteerde in poreuze constructen met een vergelijkbare Young's modulus als voor natuurlijk kraakbeen. De kraakbeenvorming door inkapselde chondrocyten kon echter alleen verbeterd worden met de toevoeging van specifieke concentraties HAMA in polyHPMA-lac-PEG hydrogels. De toevoeging van

&

relatief hoge gellan gum of CSMA concentraties resulteerde daarentegen in een afname van de kraakbeenweefsel productie door de ingekapselde cellen.

Bij het fabriceren van gelaagde kraakbeenimplantaten waren de ACPCs het meest geschikt voor de productie van de superficiële kraakbeenmatrix. Het meeste kraakbeenachtige weefsel werd gevormd door de MSCs, waardoor dit celtype potentie biedt voor gebruik in de tussen- en diepe kraakbeenlaag van zonale constructen. Verder werd de zone-specifieke kraakbeenvorming van cellen die ingekapseld waren in gelMA/gellan hydrogel, niet beïnvloed door de aanwezigheid van HAMA. Tot slot was een homogene ruimtelijke verdeling van de cellen in de hydrogelconstructen het efficiëntst voor de vorming van gewrichtskraakbeenachtig weefsel in het plugmodel. Verder bevorderde het aanbrengen van een cellaag met een hoge cel-dichtheid op de bodem van het kraakbeendefect de integratie van het construct met het omliggende defectweefsel.

Samengevat resulteerde het onderzoek in dit proefschrift in twee geoptimaliseerde kraakbeenbio-inkten: de gelMA/gellan/HAMA en polyHPMA-lac-PEG/HAMA hydrogels. Verder zijn verschillende strategieën onderzocht om gelaagde, mechanisch stabiele implantaten te genereren bijvoorbeeld met PCL voor vezelversterking, een gelaagde positionering van chondrocyten, of met een gelaagde organisatie van ACPCs en MSCs. Hoewel verschillende stappen gezet zijn in de richting van het bioprinten van gelaagde kraakbeenimplantaten resteren er nog verschillende uitdagingen. Onder andere dient de optimale combinatie van factoren om laag-specifieke kraakbeenweefselvorming aan te sturen nog beter in kaart gebracht te worden. Over het geheel genomen moedigen de resultaten van dit proefschrift aan tot de verdere ontwikkeling van georganiseerde kraakbeenimplantaten met behulp van gelMA/gellan/HAMA en polyHPMA-lac-PEG/HAMA bio-inkten.

Addendum

HydroZONES

The work presented in this thesis is part of the HydroZONES consortium (Seventh Framework Programme FP7/2007-2013, www.hydrozones.eu). HydroZONES is a European consortium which aims to develop hierarchically structured hydrogel-based cartilage scaffolds (1) and to develop and validate predictive *in vitro* and *in silico* test systems for the evaluation of new cartilage regeneration therapies (2). To accomplish these goals, several hydrogel systems have been evaluated and optimized as bio-ink platform by various partners. These systems include thiol-ene clickable poly(glycidol) hydrogels[1], starPEG/heparin hydrogels[2], and the polyHPMA-lac-PEG-based hydrogels presented in this thesis (Chapters 3, 4, and 5). Additionally, these three materials have been evaluated *in vivo* with subcutaneous implantations in rodent models, to determine safety and biocompatibility. All three materials were found to be biocompatible, therefore further *in vivo* evaluation is ongoing. With these experiments, the optimal constructs found with the *in vitro* experiments are implanted at orthotropic locations in porcine and equine models to evaluation fixating methods and the regenerative capacity of the constructs. For example, based on the data presented in this thesis, 19.5/0.5% polyHPMA-lac-PEG/HAMA hydrogels with and without PCL reinforcement are used. Moreover, current *in vitro* research is focussing on the development and optimization of spatially organized constructs, in order to fabricate zonal cartilage implants.

In parallel to the *in vitro* and *in vivo* experiments, the *ex vivo* OC plug model was developed[3] and used to evaluate repair mechanisms, as also discussed in Chapter 7. Current development of the *ex vivo* model is focussed on the implementation of mechanical loading to further mimic the native situation. Finally, computational models are under development to better understand and predict the *in vitro* outcomes.

References

1. Stichler, S. et al. Thiol-ene Clickable Poly(glycidol) Hydrogels for Biofabrication. Ann. Biomed. Eng. 1–13 (2016). doi:10.1007/s10439-016-1633-3
2. Hesse, E. et al. Peptide-functionalized starPEG/heparin Hydrogels Direct Mitogenicity, Cell Morphology and Cartilage Matrix Distribution in vitro and in vivo. J. Tissue Eng. Regen. Med. (2017). doi:10.1002/term.2404
3. Schwab, A. Ex vivo culture platform for assessment of cartilage repair treatment strategies. ALTEX (2016). doi:10.14573/altex.1607111

Addendum

Papers not included in this thesis

Arkesteijn, I.T.M., Mouser, V.H.M., Mwale, F., van Dijk, B.G.M., Ito, K. A Well-Controlled Nucleus Pulposus Tissue Culture System with Injection Port for Evaluating Regenerative Therapies. Ann. Biomed. Eng. 44, 1798–1807 (2016)

Abbadessa, A., Blokzijl, M.M., Mouser, V.H.M., Marica, P., Malda, J., Hennink, W.E., Vermonden, T. A thermo-responsive and photo-polymerizable chondroitin sulfate-based hydrogel for 3D printing applications. Carbohydr. Polym. 149, 163–174 (2016)

&

Addendum

Acknowledgements / Dankwoord

Beste Jos, dankjewel dat je me de kans hebt gegeven dit leuke uitdagende project te doen. Je hebt me tijdens mijn PhD de ruimte gegeven om veel nieuwe ervaringen op te doen wat ik erg waardeer. Ik heb veel geleerd van alle samenwerkingen, reizen, congressen en onze discussies. Daarnaast heb je me altijd aangespoord om het onderste uit de kan te halen maar wel met oog op de tijdsplanning, waardoor het uiteindelijk allemaal binnen de tijd is gelukt. Hartelijk bedankt hiervoor!

Beste Wouter, je bent altijd erg enthousiast geweest over mijn onderzoek, ondanks dat je naar de andere kant van de Uithof bent verhuisd. Ik wil je graag bedanken voor je begeleiding en je waardevolle input bij het tot stand brengen van dit proefschrift.

Beste Debby, ik bewonder het enthousiasme waarmee jij in het onderzoek staat. Je hebt me veel geholpen met het bedenken van creatieve oplossingen en wanneer het onderzoek even allemaal tegen zat, kon ik altijd bij je terecht. Hiervoor ben ik je erg dankbaar! Daarnaast mag ik je kritische oog voor detail natuurlijk niet vergeten. Hopelijk kom je geen typfouten meer tegen in dit proefschrift.

Dear Riccardo, thank you for all your feedback and our fruitful collaborations. I enjoyed working with you in the lab and learned a lot from your devoted and precise approach.

Dear Anna, you were my partner in crime from the very start. We have had so many crazy days in the lab and formed a strong team. Thank you for the great collaboration, our many adventures together, and all your help with experiments, writing, and also moral support. I really appreciate our 'scientific marriage' as you always call it, and the friendship that grew from it.

Beste Maarten, mijn collega en buurman, ik wil je graag bedanken voor al je hulp met de bioprinter en je enthousiasme bij alle rare (en soms praktisch onmogelijke) print-uitdagingen. Ik heb veel plezier gehad tijdens alle reizen samen en waardeer jouw gaven om altijd dat rare/unieke tentje te vinden om heerlijk te eten voor weinig geld.
Maarten en Sasja, ik waardeer het enorm hoe ik altijd bij jullie welkom ben. Ik heb erg genoten van onze vele diners samen en hoop dat er nog veel zullen volgen ook al zijn we geen buren meer.

Dear Irina, you joined the HydroZONES team later than the rest but we soon became good friends. You were always in for a coffee when experiments were causing frustration and founded the 'dinner support club' for the times when just a coffee was not enough. Thank you for all the good times and many diners!

I would like to thank everyone from the HydroZONES consortium. It was a pleasure to work on such a big project and to have the opportunity to meet so many people and get to know so many cities and cultures. Special thanks to the founders of HydroZONEs; Prof. Groll, Prof. Prosper, and Prof. Malda.

Dear Emma, Froi, and Felipe, thank you for making me always feel so welcome in Pamplona! Emma, I really enjoyed our work together and the famous 'pinchios' (eaten while sitting in the middle of the road in the old town centre).

Dear Simone, Tomasz, Andrea, and Franziska, thank you for making me feel so welcome in Wurzburg. I really love the city and enjoyed our collaborations. Tomasz and Simone, I appreciate that you showed me around in the city and loved going to the different festivals. Especially the 'Hofgarten weinfest' was amazing, thank you for this!

Thank you Linda and Lars for the fruitful collaboration concerning the bioreactors and Linda thank you for helping me starting up my experiments when you were still a Post-doc in Utrecht.

Jelle, Jan-Jaap, Claartje, I really enjoyed fiddling with the Ultimakers at Protospace.

Also many thanks to Eliane, Yvonne, Friederike, Anne-Kathrin, Wiltrud, Helen, Laura, Colin, Sarah, Heike, Torsten, Thomas, Sarah, Jan, Oliver, Uwe, Felix, Jörg, Clayton, Roderick, Jurgen, Reka, and Stefanie for the fruitful collaborations.

Beste Mattie, gedurende mijn PhD ben je steeds meer betrokken geraakt met mijn projecten, vooral bij de eindsprint zou ik het niet gered hebben zonder jouw hulp, dankjewel! Je staat altijd open voor nieuwe uitdagingen en ik waardeer het enorm dat je zelfs in je weekenden bent komen helpen met het boren van osteochondrale pluggen.

Beste Anneloes, ook jij hebt me enorm geholpen tijdens de laatste loodjes van mijn experimenten. Dankjewel voor alle hulp met de PCR en het maken van de hydroZONES constructen. Ik vond het erg gezellig samen in de LAF-kast!

Ferry, bedankt dat je altijd je chocolade klaar had liggen voor wanneer het onderzoek even tegen zat.

Kim, Miguel, Iris, Inge, Pedro, Alex, Lotte, Ingrid, Imke, Anita, Paweena, Michiel, Maaike, Behdad, Parisa, Razmara, Saber, Alessia, Iris, Luuk, Chella, Koen, Mylene, Willemijn, Maurits, Anne, Huub, Marianne, Said, Barbara, Michelle, Lucienne, Joao, Hsiao-Yin, Frances, Mechteld, Jonneke, Angela, Sebastiaan, Laura, Jacqueline, Harrie, Yvonne, Dino, Tom, Tommy, Loek, Rhandy en Anika thank you for the amazing time in Utrecht.

Brenda, bedankt dat je altijd met een lach mijn onmogelijke verzoeken mogelijk hebt gemaakt!

Beste Tina, ik bewonder je rustige houding, zelfs wanneer er veel dingen mis gaan en de deadlines steeds dichterbij komen. Dankjewel voor de prettige samenwerking, onze vele discussies en je waardevolle input vanuit de chemische kant.

&

Best Wim, ondanks je vele grapjes kreeg ik altijd serieus en waardevol advies over de experimenten en de papers van Anna en mij, dankjewel hiervoor!

Ik wil ook iedereen van farmacie bedanken voor de gastvrijheid en hulp wanneer ik in jullie lab metingen kwam doen. Mies, dankjewel voor je hulp met de rheometer en de DMA. Ik waardeer het hoe je altijd meteen paraat stond als er problemen waren en ik heb genoten van onze 'roadtrip' naar Brussel voor de cursus van TA-instruments.

René, Janneke, Nikae, Stefan, Annemiek, Anna, Filipe en Saskia, bedankt voor de fijne samenwerking met diergeneeskunde. Jan, hartelijk bedankt voor het regelen van het slachthuismateriaal en de vele keren dat je voor me op en neer bent gereden om materiaal op te halen!

Also many thanks to Joaquin, Ramil, Caroline, Naveed, Jessica, Jordan, and Noel for you contribution to the work in this thesis. I really enjoyed supervising you all during your internships and learned a lot in the process.

Het Kippenhok; Ellen, Inge, Nadine en Marijke, hartelijk bedankt voor jullie steun en alle gezelligheid en lekkernijen! Dat we nog heel veel dagen zullen kakelen! ;)

Lieve familie en schoon familie, dankjewel voor jullie interesse en voor alle leuke feestjes, etentjes en uitjes. Ik hoop dat er nog veel zullen volgen!

Lieve pap en mam, hartelijk bedankt voor jullie onvoorwaardelijke steun en geloof in mij. Jullie hebben me geleerd om groots te durven dromen en nooit op te geven.

Lieve Emmy, ik heb veel van je geleerd als mijn oudere zus. Zeker gezien je het protmotie-traject voor mij hebt doorlopen, waardoor ik af en toe een beetje heb kunnen afkijken. Ik vind het heel fijn zoals je er altijd voor me bent als klankbord voor zowel persoonlijke als wetenschappelijke (vaak achteraf kleine) problemen. Dankjewel hiervoor!

Lieve Ian, dankjewel voor je nuchterheid en droge humor ook rondom mijn PhD stress. Ian en Kelly, ik waardeer het enorm zoals ik altijd bij jullie welkom ben, ook als hongerige, gestrande treinreiziger.

Lieve Ivo, ik ben ontzettend blij dat ik jou heb leren kennen. Je bent er altijd voor me en hebt me veel geholpen met dit proefschrift; door onze vele (felle) discussies over wetenschappelijke vraagstukken maar vooral door me moed in te spreken wanneer er iets spannends op de loer lag, me een schop onder de kont te geven wanneer ik er even geen zin meer in had en me af te remmen wanneer ik teveel in het werk opging, je houdt me in balans. Ik hoop dat we nog heel lang samen gelukkig zijn!

Addendum

Curriculum vitae

Vivian Mouser was born in Eindhoven, the Netherlands on the 17th of November 1988. She graduated in 2007 from high school (van Maerlantlyceum, Eindhoven), and obtained her Bachelor of Science in 2010, and her Master of Science in 2012, both in Biomedical Engineering at the University of Technology, Eindhoven. During her Master track she focused on the field of orthopaedic biomechanics and worked on the development of a bioreactor to culture nucleus pulposus tissue in vitro. After her Masters, Vivian started as a PhD candidate at the Utrecht Medical Center, department of orthopeadics, under supervision of Prof. dr. W. J. A. Dhert, Prof. dr. ir. J. Malda, Dr. ir. D. Gawlitta, and Dr. L. Levato. Her research focused on the development of bio-inks for 3D bioprinting of cartilage implants and on the development of an ex vivo osteochondral plug model. In March 2017, Vivian started as technical staff at the University of Technology, Eindhoven in the group of orthopaedic biomechanics.

&